Ontario Geological Survey
Miscellaneous Paper 125

Exploration Technology Development Program of the Board of Industrial Leadership and Development

Summary of Research 1984–1985

edited by
V.G. Milne and R.B. Barlow

Program Funded by the Board of Industrial Leadership and Development

1985

Ontario
Ministry of Northern Affairs and Mines

René Fontaine
Minister
George Tough
Deputy Minister

©1985 Government of Ontario
Printed in Ontario, Canada

ISSN 0704-2752 (series)
ISSN 0826-791X (subseries)

Publications of the Ontario Geological Survey, Ministry of Northern Affairs and Mines, are available from the following sources. Orders for publications should be accompanied by cheque or money order payable to the *Treasurer of Ontario*.

Reports, maps, and price lists (personal shopping or mail order):

Public Information Centre, Ministry of Natural Resources
Room 1640, Whitney Block, Queen's Park
Toronto, Ontario M7A 1W3

Reports and accompanying maps only (personal shopping):

Main Floor, 880 Bay Street
Toronto, Ontario

Reports and accompanying maps (mail order or telephone orders):

Publications Services Section, Ministry of Government Services
5th Floor, 880 Bay Street
Toronto, Ontario M7A 1N8
Telephone (local calls) 965-6015
Toll-free long distance 1-800-268-7540
Toll-free from Area Code 807 0-ZENITH-67200

The figures in this report are author prepared.

A project funded by the Board of Industrial Leadership and Development.

Every possible effort is made to ensure the accuracy of the information contained in this report, but the Ministry of Natural Resources and the Ministry of Northern Affairs and Mines do not assume any liability for errors that may occur. Source references are included in the report and users may wish to verify critical information.

Parts of this publication may be quoted if credit is given. It is recommended that reference to this report be made in the following form:

Rogozinski, A.
1985: Single Receiver, Frequency Scanning Fixed Source Electromagnetic System; Grant 039, p.2-5 *in* Exploration Technology Development Program of the Board of Industrial Leadership and Development, Summary of Research 1984-1985, edited by V.G. Milne and R.B. Barlow, Ontario Geological Survey, Miscellaneous Paper 125, 110p.

Scientific Editor: Guy Kendrick

1500-85-Thorn Press

Contents

Introductory Remarks iv

Grant 039 Single Receiver, Frequency Scanning Fixed Source Electromagnetic System
Andrew Rogozinski 2

Grant 048 Portable Intelligent Digital Graphic Recorder
Onorio Rocca 6

Grant 051 Development of a Field Portable Technique for the Analysis of the Magnetite, Hematite, and Ilmenite Content of Basal Tills
W.A. Morris 10

Grant 052 Production of a Seven-Frequency Helicopter Electromagnetic System
P.E. Wessler 14

Grant 059 Development of a Borehole Magnetic Properties Logging System
W.R. Thuma, Detlef Blohm, and M.T. Hamalainen 21

Grant 068 Isotope Ratios and Trace Elements in Gold and Base-Metal Occurrences in Ontario
E.J. Brooker and T.E. Eagles 23

Grant 072 A Microprocessor-based Digital Receiver Console for the DIGHEM$^{III/IV}$ System
S.J. Kilty 29

Grant 077 Development of a Field Portable Instrument for Semi-quantitative Mineral Determination in Geological Materials
M. Shats, D.R. Gladwell, and M. Dancziger 33

Grant 079 Seismic Full Waveform Logging and Seismic Geotomography
J. Wong 37

Grant 080 High Resolution EM Developments
Y. Lamontagne, J.C. Macnae, A.E. Wieckowski, and R. Huxter 45

Grant 081 Development of Interactive Software for the MAGLOG Small Diameter Borehole System
W.A. Morris and S.J. Balch 56

Grant 084 Helicopter Borne High Sensitivity Magnetometer Tridirectional Gradiometer Based on Overhauser Effect
Ivan Hrvoic 64

Grant 087 High Resolution Shallow Soundings Using Radar and Reflection Seismic Methods
J.L. Davis and A.P. Annan 68

Grant 089 Testing and Demonstration of Interpretation Software for Magnetic, EM, and Spectrometry Inversion
S.W. Reford and N.R. Paterson 80

Grant 090 The Application of Lake Sediment Surveying to Au Exploration in Ontario
J.S. Fox, T.E. Eagles, and E.J. Brooker 85

Grant 093 Software and Hardware Design of Controlled Source Audio-frequency Magneto-telluric (CSAMT) System and Test Survey
Mitsuru Yamashita 95

Introductory Remarks

EXPLORATION TECHNOLOGY DEVELOPMENT PROGRAM

Exploration in Ontario has reached a point where most mineral deposits located at or near the surface have been detected and tested for their economic viability. Therefore, future exploration must concentrate on locating mineral deposits at some depths below the surface. In order to resolve deeper deposits more effectively, new instrumentation must be developed. The Exploration Technology Development Program was created in late 1981 to facilitate this need for more precise instrumentation and techniques required in modern exploration programs.

With the establishment of the Ontario Geoscience Research Grants Program in the late 1970s, the Ontario Geological Survey developed a program to encourage geoscience research at Ontario universities. This program was viewed as the first step towards defining geological parameters and determining possible areas of high mineral potential in Ontario. The Exploration Technology Development Program was conceived as an important second step towards bringing these ideas and concepts to the private sector and ensuring the development of new technology through them.

The Exploration Technology Development Program was initiated to encourage the advancement of exploration geophysics and geochemistry by providing joint venture funding to Ontario companies leading to the development of innovative technology, specifically in those areas which support the mineral exploration industry in Ontario. The program supports applied research and development to seven areas of exploration activity:

1. mineral deposit and overburden, physical and chemical characterization studies
2. developoooment of new or modified airborne systems for improved detection of mineral deposits
3. development of new ground, equipment for better detection and dissemination of mineral deposits
4. development of concepts and techniques in exploration geochemisty
5. development of borehole logging systems and related drilling techniques
6. development or implementation of laboratory support equipment not presently available in Ontario for the purpose of offering improved analytical service to mineral exploration companies
7. development of data acquisition and signal processing hardware and software for real-time and part-time collection and interpretation of field data

Companies are eligible to receive grants for any one project for up to three years in duration, with the Ontario Government financing 60% of all activities to a maximum contribution for an individual project of $150 000 per year.

In order to receive funding support from the Program, companies are asked to submit project proposals to the Ontario Geological Survey by January 15. These proposals are reviewed and ranked by a Review Committee according to their scientific merit and relevance to the Program.

The members of the 1984-85 Committee included:

L.S. Collett, Chairman	Geological Survey of Canada
Dr. R.B. Band	Falconbridge Ltd.
R.B. Barlow	Ontario Geological Survey
J. Dowsett	Inco Limited
Dr. J.P. Greenhouse	University of Waterloo
G.E.M. Hall	Geological Survey of Canada
Dr. W.O. Karvinen	Karvinen and Associates
R.S. Middleton	R.S. Middleton Exploration Services Limited
Dr. I. Nichol	Queen's University
R.H. Pemberton	Noranda Mines Limited
L. Reed	Selco Division - BP Resources Canada Limited
Dr. D.H. Watkinson	Carleton University

During the 1984-85 year, 18 proposals were funded under this program. Of these, 8 were renewals to multiyear projects. Grant allocations in support of these 12 projects totaled $953 000.

The following research projects funded during 1984-85, will be published as Ontario Geological Survey Open File Reports:

Grant 014: New Digital Pulse EM Receiver; Crone Geophysics Limited.

Grant 039: Single Receiver, Frequency Scanning Fixed Source Electromagnetic System; Androtex Limited.

Grant 048: Development of Portable Digital Graphic Recorder; RMS Instruments Ltd.

Grant 051: Development of Field Portable Procedures for the Analysis of Magnetite, Hematite, and Ilmenite Content of Basal Tills; Morris Magnetics.

Grant 059: Development of a Borehole Magnetic Properties Logging System; IFG Company.

Grant 077: Development of a Field Portable Instrument for Semi-quantitative Mineral Determination in Geological Materials; Barringer Research Limited.

Grant 090: The Application of Lake Sediment Geochemical Surveying to Gold Exploration in Ontario; Teck Explorations Ltd. and X-Ray Assay Laboratories Limited.

Grant 091: The Development of a Pocket Digital - Reading Induced Polarization Resistivity Meter; EDA Instruments.

The undersigned would like to thank L.S. (Len) Collett, Chairman of the Program Review Committee, and the rest of the member and participating companies who gave freely of their time and made the whole program possible. As well, the efforts of the researchers are acknowledged. Thanks are also due to R.B. Watson who acted as Grants Administrator and Secretary to the Committee.

V.G. Milne

Director

Ontario Geological Survey

Conversion Factors for Measurements in Ontario Geological Survey Publications

If the reader wishes to convert imperial units to SI (metric) units or SI units to imperial units the following multipliers should be used:

CONVERSION FROM SI TO IMPERIAL			CONVERSION FROM IMPERIAL TO SI		
SI Unit	*Multiplied by*	*Gives*	*Imperial Unit*	*Multiplied by*	*Gives*
			LENGTH		
1 mm	0 039 37	inches	1 inch	**25.4**	mm
1 cm	0 393 70	inches	1 inch	**2.54**	cm
1 m	3 280 84	feet	1 foot	**0.304 8**	m
1 m	0 049 709 7	chains	1 chain	20 116 8	m
1 km	0 621 371	miles (statute)	1 mile (statute)	**1.609 344**	km
			AREA		
1 cm^2	0 155 0	square inches	1 square inch	**6.451 6**	cm^2
1 m^2	10 763 9	square feet	1 square foot	**0.092 903 04**	m^2
1 km^2	0 386 10	square miles	1 square mile	2 589 988	km^2
1 ha	2 471 054	acres	1 acre	0 404 685 6	ha
			VOLUME		
1 cm^3	0 061 02	cubic inches	1 cubic inch	**16.387 064**	cm^3
1 m^3	35 314 7	cubic feet	1 cubic foot	0 028 316 85	m^3
1 m^3	1 308 0	cubic yards	1 cubic yard	0 764 555	m^3
			CAPACITY		
1 L	1 759 755	pints	1 pint	0 568 261	L
1 L	0 879 877	quarts	1 quart	1 136 522	L
1 L	0 219 969	gallons	1 gallon	**4.546 090**	L
			MASS		
1 g	0 035 273 96	ounces (avdp)	1 ounce (avdp)	28 349 523	g
1 g	0 032 150 75	ounces (troy)	1 ounce (troy)	**31.103 476 8**	g
1 kg	2 204 62	pounds (avdp)	1 pound (avdp)	**0.453 592 37**	kg
1 kg	0 001 102 3	tons (short)	1 ton (short)	**907.184 74**	kg
1 t	1 102 311	tons (short)	1 ton (short)	**0.907 184 74**	t
1 kg	0 000 984 21	tons (long)	1 ton (long)	**1016.046 908 8**	kg
1 t	0 984 206 5	tons (long)	1 ton (long)	**1.016 046 908 8**	t
			CONCENTRATION		
1 g/t	0 029 166 6	ounce (troy)/ ton (short)	1 ounce (troy)/ ton (short)	34 285 714 2	g/t
1 g/t	0 583 333 33	pennyweights/ ton (short)	1 pennyweight/ ton (short)	1 714 285 7	g/t

OTHER USEFUL CONVERSION FACTORS

1 ounce (troy)/ton (short)	20 0	pennyweights/ton (short)
1 pennyweight/ton (short)	0 05	ounce (troy)/ton (short)

NOTE—Conversion factors which are in bold type are exact. The conversion factors have been taken from or have been derived from factors given in the Metric Practice Guide for the Canadian Mining and Metallurgical Industries published by The Mining Association of Canada in cooperation with the Coal Association of Canada.

Exploration Technology Development Program of the Board of Industrial Leadership and Development

Summary of Research 1984–1985

edited by
V.G. Milne[1] and R.B. Barlow[2]

[1]Director, Ontario Geological Survey, Toronto.
[2]Section Chief, Geophysics/Geochemistry Section, Ontario Geological Survey, Toronto.

Grant 039 Single Receiver, Frequency Scanning Fixed Source Electromagnetic System

A. Rogozinski

Androtex Limited, Mississauga

ABSTRACT

The development of a single sensor receiver is a new version of the Turam fixed source electromagnetic method, which is based on the automatic frequency scanning Elfast system. The project consists of three design phases:

1. high power transmitter with stabilized output current, programmable frequency pattern and cycle time synchronized with receiver
2. microprocessor-controlled digital receiver provided with solid state memory and serial port for transferring recorded data to the field computer
3. down hole logging attachment adapted to the receiver

The new system provides much better capabilities in terms of flexibility in the field and accuracy of measured parameters, as well as significant improvement in down hole logging surveys.

The measurement of the two parameters, amplitude and phase of the electromagnetic field can be made at any combination of five frequencies, 25, 75, 225, 675, and 2025 Hz. Due to automatic cycling time programmed individually for each frequency, internal data recording, simplicity of operation, and portability of the receiver, considerable improvement in productivity is possible.

Surveys with a new single sensor receiver Turam system can be carried out by one operator only, further increasing cost effectiveness.

INTRODUCTION

In the newly developed Turam system, based on advanced electronics, the receiver operates with single coil and memory, so that measurements at each frequency are directly compared with previous readings. Coherence is maintained by means of constant amplitude of an energizing electromagnetic field and a high stability of transmitted frequencies. This is achieved by a stabilized transmitting current-amplitude, and presynchronized temperature compensated crystal controlled frequency clocks in the transmitter and receiver-phase.

The accuracy of the measurements, particularly at large distances from source and lower frequencies, is improved due to the high power of a new transmitter as well as stable output current and frequencies. Furthermore, two-channel asymmetry in the receiver has been removed. The analogue input signal is transferred and processed in digital form, further improving the signal to noise ratio.

The single sensor Turam system in down hole surveys overcomes many problems that have, until now, beset frequency domain drillhole measurement, mainly due to the errors resulting from the variable distance and different conditions (temperature) between logging probe and reference sensor located at the surface; also, the large values of phase differences and amplitude ratios with increasing depth. A new system with single sensing coil receiver overcomes the above mentioned problems and, accurate amplitude as well as phase measurements are obtained, independent of depth.

INSTRUMENTATION

The design of the transmitter and receiver are based on an 8 bit low power CMOS microprocessor.

The transmitter, shown in Photo 039.1, consists of a power module with output current regulator and microprocessor controlled section for programming of output frequencies and cycle time, verifying standby battery voltage, internal protection circuits, digital display module, and communication with receiver during data transfer to the receiver.

Any combination of output frequencies can be pre-set at given times from 5 to 60 seconds in 5 second increments. Usually, lower frequencies will require a longer stacking time at the receiver due to the decrease in samples stacked and increased noise levels. A survey area with higher noise levels will also need longer transmission times.

The diagnostic values, which are input and output parameters, frequencies, and cycle time and faults indicated by protection circuits, are displayed on a 16 character LCD module, giving the operator a clear indication of the transmitter's operation.

A separate output "Sync" for connecting the receiver is provided to synchronize both clocks and transfer the timing and frequency pattern to the receiver. When both units are connected via the "Sync" cable (Photo 039.2), the transmitter will automatically turn on the receiver. After self test routines are completed, a 10 minute warm-up time for both oscillators is required, this is indicated by a countdown timer at the receiver.

When both units are fully synchronized, the frequencies and timing can be programmed via a keyboard at the transmitter. Data are transferred to the receiver in the serial mode, setting an identical program. After verifying data by the transmitter, the "Sync" cable can be disconnected. This procedure is indicated at the receiver's display. Further program change at the transmitter is disabled. In other words, programming of the transmitter and receiver is possible only when both units are connected via the "Sync" cable. Programming at the receiver is not available.

To ensure continuity of full synchronization with the receiver, when, for any reason, the motor generator stops operating, an internal standby rechargeable battery automatically takes over supply of all digital circuits; these are, crystal oscillator, programmer, and timer system. Thus, initial synchronization with the receiver is still valid and does not require corrections. Moreover, if the output power is turned off by a signal from the protection circuitry (overload,

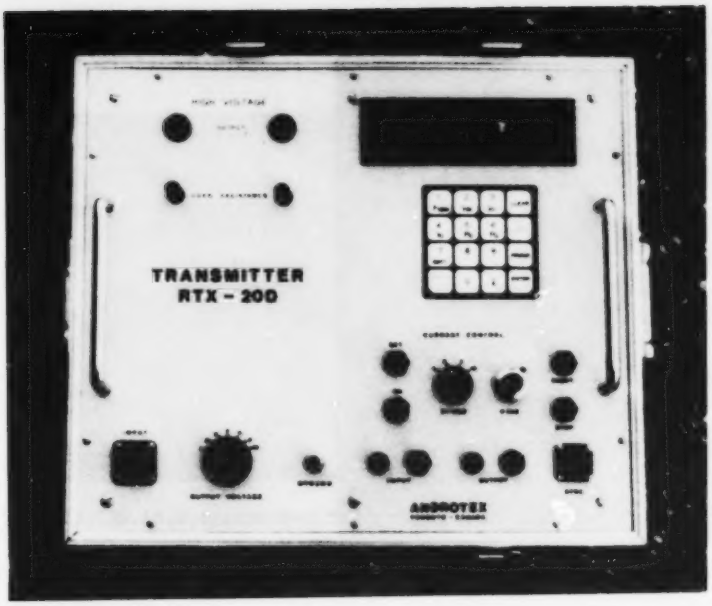

***Photo 039.1** Transmitter RTX-20D.*

open loop, etc.) no synchronization is required. After a period of approximately 2 1/2 hours, the timer disconnects the standby internal supply system and the transmitter's clock stops.

A new receiver, shown in Photo 039.3, retains its portability and low power consumption. The console consists of a rechargeable battery, as a power source, microprocessor unit with ROM memory, analogue to digital conversion and signal processing circuits, stacking module, RAM memory, as an internal data storage, and interface with the keyboard and display. A built-in serial port allows receiver communication with the transmitter during programming and data transfer to the portable field computer. Sensor frequency setting and sensitivity of the preamplifier are controlled in serial mode from the receiver console on the power supply cable.

The microprocessor system controls the overall receiver functions, operated via a 4 x 4 keyboard, the software routines minimize data entry. A dual 16 character LCD display is continuously communicating with the operator indicating "Present" and "Previous" results for verification. Amplitude in millivolts - mv and phase in degrees - d, at frequency C1 (25 Hz) are presented in Photos 039.4a and 039.4b.

Upon completion of measurements at one position, a station number is automatically advanced according to the preprogrammed "Step" station separation. The operator is also able to repeat measurements, erasing an existing record in the memory, return to the previous station, or change "Step" at any time.

"Recall" of stored readings at other frequencies is also possible. All these functions give an operator full control of field results as well as flexibility in terms of station separation.

A front panel of an HL-5D receiver is shown in Photo 039.5.

The downhole logging probe consists of sensing coil, preamplifier with variable gain stage, and digital transmission circuitry which also controls the frequency and sensitivity setting.

The probe is powered from the main receiver's battery and connected to the same input as the sensing coil used for surveys at the surface. Supply and signal is sent on two wire shielded cables with Kevlar reinforcement.

SPECIFICATIONS

Specifications of the new system were presented in Rogozinski (1984).

CONCLUSIONS

The single sensor version of the Turam fixed large source electromagnetic exploration system features better resolution and larger exploration depth due to increased accuracy of the measurements. In down hole logging surveys, the new instrument effectively provides consistent accuracy, independent of depth, based on the Turam frequency domain method.

Simplicity of operation and speed of execution make this system highly cost effective.

ACKNOWLEDGMENTS

The company is grateful to the Ontario Ministry of Natural Resources for its financial support which was made available for this development project through the ETDF program and the Ontario Geological Survey. Also, Androtex Limited would like to express their appreciation to Mr. John S. Dowsett from Inco Limited for his suggestions and ideas, which made a valuable contribution to the project.

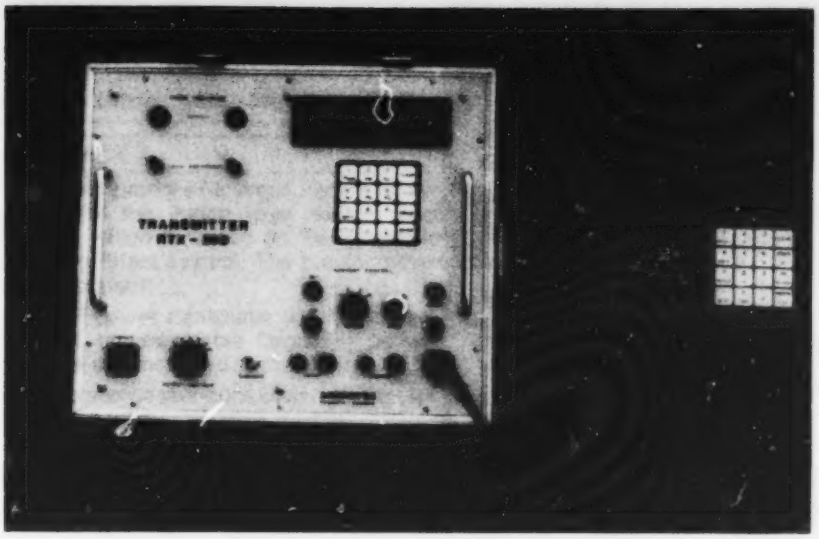

Photo 039.2 *Synchronizing receiver with transmitter.*

Photo 039.3 *Receiver HL-5D with sensor.*

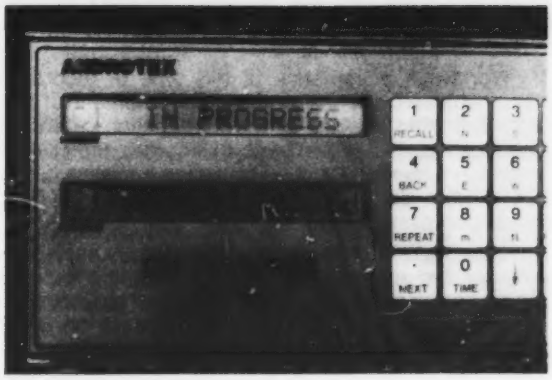

Photo 039.4a *Measurements in progress.*

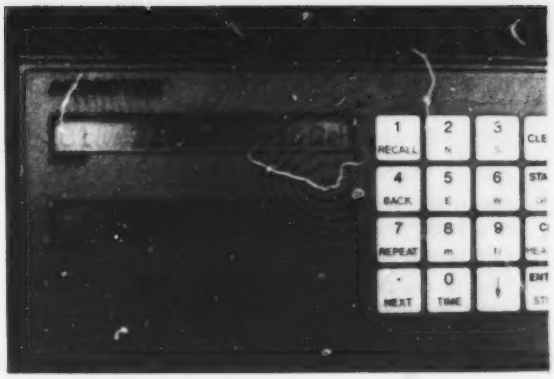

Photo 039.4b *Measurements completed.*

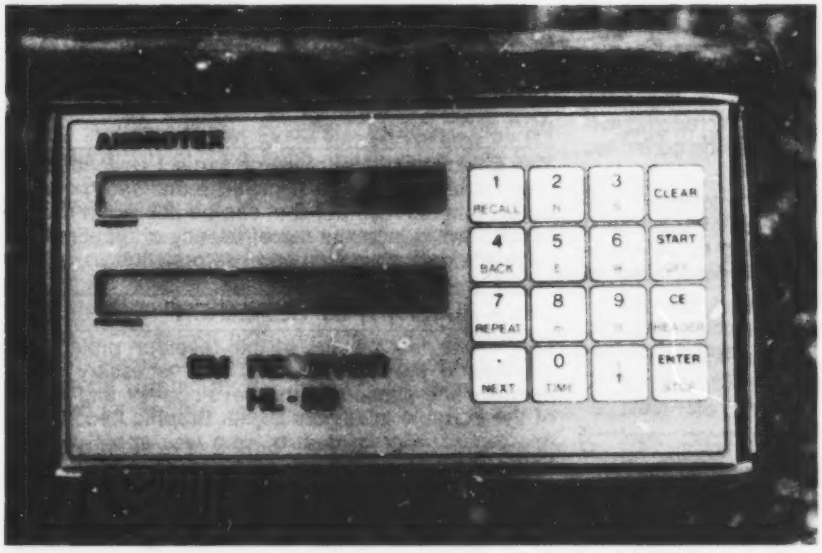

Photo 039.5 *Receiver front panel.*

REFERENCE

Rogozinski, Andrew
1984: Grant 039 Single Receiver, Frequency Scanning Fixed Source Electromagnetic System; p.61-65 *in* Exploration Technology Development Program of the Board of Industrial Leadership and Development, Summary of Research 1983-1984, edited by V.G. Milne and R.B. Barlow, Ontario Geological Survey, Miscellaneous Paper 120, 176p.

Grant 048 Portable Intelligent Digital Graphic Recorder

Onorio Rocca

RMS Instruments Limited, Mississauga

ABSTRACT

With the demise of the moving pen chart recorder and the development of microcomputer-based instruments, a number of disadvantages inherent with the old recorder have now been resolved:

1. capability of increased number of channels
2. interfacing to digital signals and instruments
3. alphanumeric annotation
4. operation may be monitored or controlled by microcomputer-based instruments.

The limitations imposed on the number of data channels available on the moving pen type recorder were determined by the number of pens used, normally 6 or 8 on the larger recorders.

Because digital inputs with the older type recorder were not provided, digital signals had to be converted to analog in order to be recorded.

Some of the pen recorders were capable of limited edge printing; however, most were unable to produce alphanumerics.

At the risk of operator error or omission, annotation of charts had to be dealt with in the field, whereas with the development of microcomputer-based instruments, chart annotation can be controlled by the recorder.

The development of the Portable Intelligent Digital Graphic Recorder will combine all of the above features as well as by being controlled by an external source, will increase the level of automation of the data acquisition process.

Automation resulting in reduced costs, improved reliability, and portability without the trade-off of features, will prove very attractive features to the geophysical survey industry in Canada.

INTRODUCTION

RMS Instruments Limited was established in 1980 with the development of the GR33 Graphic Recorder, the most advanced and versatile instrument for recording applications requiring high quality graphic records. This innovative, fully programmable recorder may be operated as a strip chart recorder with alphanumeric chart annotation, an alphanumeric line printer or, with a customer supplied computer, as a raster graphics printer, allowing production of hard copy such as custom graphics, contour maps, and FFT processed data.

The GR33 may be used as a stand-alone unit or be controlled by a computer, enabling the use of automated test sequences, extensive annotation of charts and rapid changes in set-up parameters for different interpretation of data. Plug-in interface modules are available for applications requiring direct input of analog or other data and will permit the recording of virtually any type of signal.

The GR33 is packaged in a standard 5.25 inch (133.4 mm) by 17 inch (432 mm) rackmount cabinet, making it ideal for airborne geophysical survey applications. Recorders are currently installed in helicopters, fixed-wing aircraft, and land vehicles for use in recording geophysical data.

Worldwide acceptance of this type of recording instrumentation and the ongoing development of the GR33 Recorder has led to the introduction of equipment such as the GR34 Graphic Recorder, the DGR33 Graphic Recorder/Data Acquisition system, the TCR12 Tape Cartridge Recorder, and the DAS8 Data Acquisition system.

The DGR33/DAS8 Data Acquisition systems are compact and rugged instruments following the same design approach used in the GR33 Graphic Recorder. The use of the same peripheral modules as the GR33 allows the further expansion of both systems by continuing the development of our line of slave processor based modules. Multiple packaging options allow minimization of system space requirements, as well as the initial system cost.

The Portable Intelligent Digital Graphic Recorder as proposed in this project, will expand on the knowledge and expertise gained in the development of our total line of data recording instrumentation.

PROJECT OBJECTIVES

The objective of the research project described below, is to manufacture a much demanded, portable, digital graphic recorder that can be utilized in mineral exploration to increase the efficiency of real-time and post-time data collection and interpretation.

BRIEF SUMMARY OF RESEARCH

One of the first phases of this research project was devoted to the acquisition of the necessary equipment for the support of the development and testing of the Portable Intelligent Digital Graphic Recorder. In this regard, a great deal of time was spent with our being familiarized with this equipment and its associated hardware and software.

Careful attention was directed to the choice of the printhead to be used in the recorder. As a result, the design will incorporate a high resolution (8 dots per mm), high speed (approximately 100 mm per second) printhead which will improve the accuracy of data recording. Previous problems encountered with the printhead temperature specifications have now been resolved. The fixed position, monolithic, thermal printhead with a 104 mm (4.09 inch) print span, will consist of a single row of 832 individual thermal printing elements spaced 0.125 mm apart. A microprocessor-based control circuit will create graphic images by controlling the energizing signals to the printhead as the thermal sensitive recording paper is advanced across the printing surface.

Input power to the recorder has now been defined as any DC voltage, 12V DC to 50V DC for use in portable, mobile, airborne, or laboratory applications. For AC power applications, there will be a separate module available.

The design of the Portable Intelligent Digital Graphic Recorder will incorporate the capability of recording any of the following data formats:

1. multiple channels of analog or digital information in a strip chart format with alphanumeric trace annotation and self generated grid patterns
2. alphanumeric text such as tabulated data or header messages
3. graphic images such as X-Y plots and bargraphs
4. alphanumeric messages printed while recording analog information without loss of data in the split mode of operation

An external instrument will be capable of monitoring and controlling operation of the recorder via one of several optional digital interfaces, such as RS232 serial, IEEE-488 instrument bus, parallel digital, etc.

Operating as a chart recorder, the instrument will be capable of recording up to 16 signal traces, with trace identification, programmable positions, sensitivities, etc. A virtually unlimited number of traces may be plotted with fixed spacing and no identification. Either approach allows internal grid generation.

An external instrument may provide alphanumeric messages for printing on the chart to annotate the record. Analog signals, input via an optional analog interface, may be recorded on the chart and may also be in digital format for further processing by an external instrument. Text, such as tabulated data and header messages, may be printed using the alphanumeric capabilities.

The graphics facility permits an external instrument to directly control the printing elements to create graphic images such as maps, profiles, bargraphs, etc. from the processed data.

The recorder will have provisions for expansion for high speed digitizing and storage of transient phenomena. (Refer to the following - High Speed Front End for Seismic Applications).

HIGH SPEED FRONT END FOR SEISMIC APPLICATIONS

BASIC CONVERTER ARCHITECTURE:

1. uses hybrid flash converter allowing either 8 bit resolution conversions with up to 1 million samples per second, or a hybrid conversion allowing considerably higher resolution at 100 kHz rate
2. (front end capable of better than 16 bits of resolution at rate ≅ 10 kHz). Hybrid conversion performs initial low resolution conversion using flash converter, increases gain then converts product of first conversion and real input.

FRONT END CONDITIONERS:

1. each signal channel has its own low noise differential amplifier with resistor programmable gain, followed by a sample and hold amplifier. Any number of signal channels may be handled by a unique addressing scheme
2. *all* signal channels may be sampled *simultaneously* (aperture uncertainty ≅ 100 nsec)
3. sample rate controlled by programmable counter/timer (no phase jitter in sample frequency)
4. each signal channel has its own selection circuitry allowing a mixture of single and multiple channel modules (multiple channel modules do not have separate instrumentation amp/signal)
5. sample rate programmable with 100 nsec resolution
6. up to 12 single channel inputs in basic unit
7. signal conditioners have anti-aliasing and RF filters (anti-aliasing assumes maximum sample rate) (filter characteristics may be altered)

STORAGE:

1. samples may be stored in expandable memory module until printing may be performed - 256K bytes (2.1 seconds of data at 10 kHz sample rate on all 12 channels)
2. memory may be partitioned for smaller samples (shorter events)
3. averaging may be performed if 128K byte sample memory sufficient
4. multiple events may be plotted together to create effect of larger number of geophones
5. filtering may be performed on sample memory prior to printing

TIMING:

1. external logic trigger or level sensitive trigger input
2. programmable sample length and trigger position
3. external sample input may be used instead of internal timing
4. if internal timers used, dither may be used on successive samples to effectively increase sampling rate
5. logic outputs may be used to trigger external equipment

OTHER:

1. external 'Black Box' front end may be slaved to main unit to expand channel capacity

FEATURES

1. event counters/frequency counters
2. event markers/chart on-off control
3. time markers or time dependent grid
4. real time clock (CMOS with data retention)
5. programmable grid plotting capability (including non-linear grids and partial or split grids)
6. chart speed 0 to 100 mm/sec
7. programmable signal identification labels
8. programmable filters
9. voltage and engineering units display and printing capability
10. programmable channel sensitivity

11. channel position anywhere on chart
12. different methods of plotting signals
13. individual signal programmable to wrap, ignore, or stop at boundaries, or wrap or stop at full width
14. programmable set points 'Hi-Lo' for each channel with alarm and message on chart
15. display message if fault occurs
16. able to control chart speed from an external frequency
17. programmable offset voltages
18. multiple set-up tables
19. header message configuration
20. parameter table printout
21. channel assignment displayed
22. capability to automatically separate all channels evenly on the chart
23. sampling rate up to 1 million samples per second and external sampling rate
24. chart speed control through analog source, using any analog channel
25. linearization capability programmable channel by channel
26. auto null programmable channel by channel
27. transient digitizer
28. programmable polarity
29. printhead test pattern
30. sample storage in memory (expandable sample memory)
31. FFT capability
32. 12 high speed inputs in basic unit
33. up to 128 pseudo-channels (created from successive events or from functions performed on sample data)
34. reporting capability

PRELIMINARY SPECIFICATIONS

RECORD

Size:

104 mm (4.1 inch) record on 113 mm (4.45 inch) paper

Resolution:

8 dots/mm (200 x 200 dots/inch)

Recording Method:

Fixed position monolithic thermal printhead consisting of a linear array of 832 individual printing elements

PAPER TRANSPORT

Paper Speed:

Up to 100 mm per second (3.9 inches per second). Paper speed may also be synchronized to an external frequency reference. Paper speed is controlled by an analog signal using one of the analog channels.

Drive Mechanism:

DC stepping motor, with an internal take-up spool

Paper Level Indicator:

Solid state level sensor

SERIAL DIGITAL INTERFACE

Signal:

EIA RS232C or 20mA current loop, 8 data bits and parity

Data Rate:

300 to 19.2 kb Baud

PARALLEL DIGITAL INTERFACE

Signals:

8 input lines, 8 output lines, active low or high input strobe, active low output strobe, active low and busy outputs, all TTL compatible

INSTALLATION

Size:

127 mm high x 177.8 mm wide x 355.6 mm long (5 inches high x 7 inches wide x 14 inches long)

Weight:

4 Kg (8.8 pounds) with no options installed

Power Requirements:

DC voltage from +12V DC to 50V DC range

AC power 115/220V AC optional

Temperature:

Not available at this time

Humidity:

10% to 80% non-condensing

ANALOG INPUT

Standard Inputs:

4 CHANNELS DIFFERENTIAL:

Rin:

1 Megohm in parallel with 20 pf to ground

Vin Max:

± 10 volts for linear operation

± 25 volts for continuous without damage

CMRR:

condition DC-60 Hz. 1K source imbalance 92 dB typical with sensitivity 10V to 100mV/inch 106 dB typical with sensitivity 100mV to 1mV/inch

Linearity:

0.007% (not considering printing resolution)

Accuracy:

0.07%

Optional Input Conditioners:

A number of different input configurations will be available for installation in the peripheral bus in the rear of the unit. The firmware will support a mixture of scan rates. Certain modules have their own sample and hold amplifiers. As a result, we have the capability of simultaneous sampling of as many as 12 channels. The sampling pulses are produced by programmable timers so there is very consistent timing with no jitter. The sampling may be externally controlled.

Resolution:

8 through 16 bit

Zero Suppression:

± 10 Volts (16 bit resolution)

Digitization Rate:

1M samples/second 8 bit conversions

10K samples/second 12 bit conversions

2K samples/second 16 bit conversions

Note: This is total regardless of number of channels. Mixtures of resolution and scan rates will alter maximum throughput.

Maximum Sensitivity:

Standard inputs 10mV/inch

Optional inputs 100uV/inch

Standard Event/Control Inputs:

6 event channels (TTL/CMOS dry-contact compatible)

Chart On/Off

Chart Speed Control

Sample Trigger Input

General Purpose Frequency Counter Input

Alarm Output (Open Collector)

Programmable Function Input (print voltages/header/marker, etc.)

CONCLUSIONS

RMS Instruments' commitment to design excellence, and our application of the best know-how in technology, will result in a product which will provide the most advanced state-of-the-art equipment available for the geophysical industry.

The Portable Intelligent Digital Graphic Recorder is expected to increase the efficiency, and thereby reduce the costs of geophysical data acquisition. This will be accomplished by improving the accuracy and quality of the displayed data, and by permitting further automation of data acquisition and interpretation. Availability of a versatile portable data recorder with digital interfacing capabilities is expected to encourage the development of other portable intelligent geophysical instruments.

ACKNOWLEDGMENTS

RMS Instruments Limited wishes to thank the Ontario Ministry of Natural Resources and the Ontario Geological Survey for their support.

Grant 051 Development of a Field Portable Technique for the Analysis of the Magnetite, Hematite, and Ilmenite Content of Basal Tills

W.A. Morris

Morris Magnetics Incorporated, RR#2, Lucan

ABSTRACT

The magnetic properties, acquisition coercive force, and saturation remanence, provide a method for mapping magnetic oxide variations in till. These properties are especially useful in situations where standard bulk susceptibility techniques fail to yield interpretable data, or when it is necessary to isolate the magnetic effects of hematite from magnetite. A previously reported example showed the value of this technique when it was applied to a uranium prospect located in the Northwest Territories. This study reports the results of tests made on an Au prospect from the Matachewan area of Ontario.

Silt and clay separates from B horizon soils were examined by saturation remanence techniques. These separates appear to contain only magnetite. A comparison between Au content and saturation remanence defines two distinct populations. A map of site mean remanence saturation values outlines two dispersal trains that closely resemble trains identified by the Au content. A third Au dispersal train is located in an area of high remanence saturation values.

INTRODUCTION

Measurement of the bulk magnetic susceptibility of a unit volume of till gives a direct estimate of the total magnetite content present in that sample. Experiments have shown a direct correlation between magnetite content and the concentration of specific elemental species. For example, Pulkkinnen *et al.* (1980) gave an example of the correlation between bulk magnetic susceptibility and the Mg, Cr, and Ni content of a till (Morris 1984). The basic assumption of this correlation is that upon transport of till over an ore zone in bedrock, minerals characteristic of the ore deposit are incorporated into the till. As the till is transported farther away, a dilution of the ore minerals is produced by the incorporation of more silicate particles. For orebodies which contain significant concentrations of magnetic oxides, the dispersal train down ice from the orebody will be marked by both elemental concentration of ore material detectable by chemical analysis, and magnetic oxides detectable by magnetic measurements.

The magnetic investigative technique used in this study is based on the acquisition coercive force and saturation remanence properties of magnetic oxides. This procedure is preferable to bulk susceptibility measurement because:

1. It is possible to use acquisition coercive force properties to differentiate the contributions of magnetite and hematite.
2. The separation of the silt-size fraction to obtain a more representative sample will enhance signal strength because the saturation remanence of a unit volume of silt-size magnetite is greater than for an equal volume of sand size magnetite.
3. The signal is always intensified by using high d.c. fields; there will never be a case where the signal is not detectable by available instrumentation.

A previous report documented the application of this saturation remanence technique to the study of a uranium prospect located in the Northwest Territories (Morris 1984). The source rock types for the soil samples in the RAD area are Precambrian sedimentary rocks. These specimens did not yield any meaningful data when standard bulk susceptibility methods were used to examine them. When the saturation remanence approach is used, it is possible to identify localized additions of magnetite and hematite which are associated with the uranium mineralization.

In this report, the authors examine the application of this technique to enhance the geological understanding of an Au prospect in the Matachewan area of Ontario. The study area is located between two former producing Au mines, the Matachewan Consolidated (MCM) and the Young-Davidson (Y-D) Mines. Details of the Quaternary geology of this area have been given by Stewart and van Hees (1984). A thin till sheet covers the area and ranges in thickness from 1 to 3 m, although a few deep pockets in excess of 5 m in thickness were measured. The overburden covers a typical suite of Abitibi greenstone rocks which consist of mafic volcanic flows and fragmental rocks with acidic intrusive rocks. The known Au deposits in the area are associated with two distinct rock types. These are "brick-red" syenite with Au occurring as inclusions in pyrite, and "carbonatized volcanic" rock in which Au occurs with pyrite. Less commonly, the gold occurs as free Au in quartz veins.

Samples of 2 to 5 kg were obtained either by backhoe, or by a 2-person gasoline engine auger. At each location, samples were obtained from the B soil horizon, and occasionally extra samples were also obtained from the underlying unoxidized till. From each sample, a silt plus clay fraction (-0.063 mm) was separated. The separate was used to prepare four specimens for each location. Each specimen was treated to incrementing applied fields of 25, 50, 75, 100, 250, 500, and 750 nT. After exposure to applied fields, the remanence acquired by the specimen was measured using a standard Schonstedt spinner magnetometer. All magnetite is considered saturated at 250 nT, any subsequent remanence increase acquired upon the application of higher d.c. fields is attributed to the presence of hematite in the specimens. The remanence saturation value quoted for each site is the mean of the logarithmic value of each specimen.

RESULTS

All the specimens examined in this study appear to contain only magnetite grains. None of the specimens exhibit any systematic remanence increase above 250 nT. On the basis of the magnetic data alone, hematite appears to be absent; even though one might speculate that the "brick-red" character of the syenite is related to the presence of hematite (Figure 051.1).

Gleeson *et al.* (1984) in a study of the control parameters for Au prospecting using till geochemistry emphasize the importance of comparing results from the same stratigraphic (B versus C) and lithologic (till versus glaciofluviatile) horizons. Data acquired in this survey further emphasize this point. While the normalized acquisition coercive force spectrum of the B and C soil horizons are identical (Figure 051.1), the magnitudes of the saturation remanence are quite different. In the three soil pairs examined in this study the C soil horizon has a saturation remanence which is consistently greater than 1.3 times that found in the overlying B soil horizon. Oxidation to produce the B horizon apparently involves the generation of a non-magnetic phase (again hematite appears absent). The comparison of saturation values from distinct lithotypes is even more misleading. For example, samples obtained from swamp muck give saturation values two orders of magnitude lower than anything found in the "B" soil horizons. It appears that saturation magnetic analysis most closely approximates to the heavy mineral separation of, or the chemical analysis for Au present in the -0.063 mm fraction.

Figures 051.2a and 051.2b respectively present the Au content of samples versus bulk magnetic susceptibility, and saturation remanence. These specimens have detectable susceptibility values because the sole oxide mineral is magnetite. Both figures suggest the presence of two distinct Au/magnetic mineral populations. Some specimens which were used for susceptibility measurements were not available for the remanence studies. The trends defined by the susceptibility data are more scattered than those defined by the saturation remanence measurements. There is a broad overlap between susceptibility values representative of the two populations, such that magnetic susceptibility cannot be used to map distribution of the areal two populations.

In contrast, the saturation remanence data (with three exceptions) define two quite distinct trends. For remanence saturation values below 10^{-2} emu/gm and Au contents of 100 ppb, the data define a gradual increase of Au content with a gradual increase of saturation remanence. Above the cut-off value of 10^{-1} emu/gm, the Au content of the till shows wide fluctuations from 250 ppb to over 900 ppb, while the saturation remanence values appear to be relatively constant. The first trend identifies a till type in which the Au content is directly related to the magnetite concentration. This possibly involves sedimentary sorting processes. The significance of the second

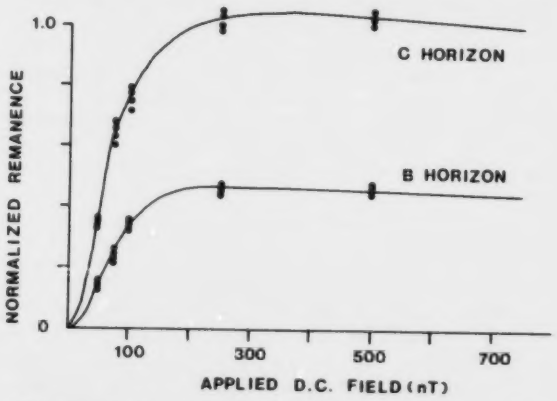

***Figure 051.1** Comparison of the remanence acquisition curve for B and C horizon samples from the same location. All individual specimen values are normalized to the intensity of the C horizon mean 750 nT value. Four specimens in each sample exhibit good internal consistency.*

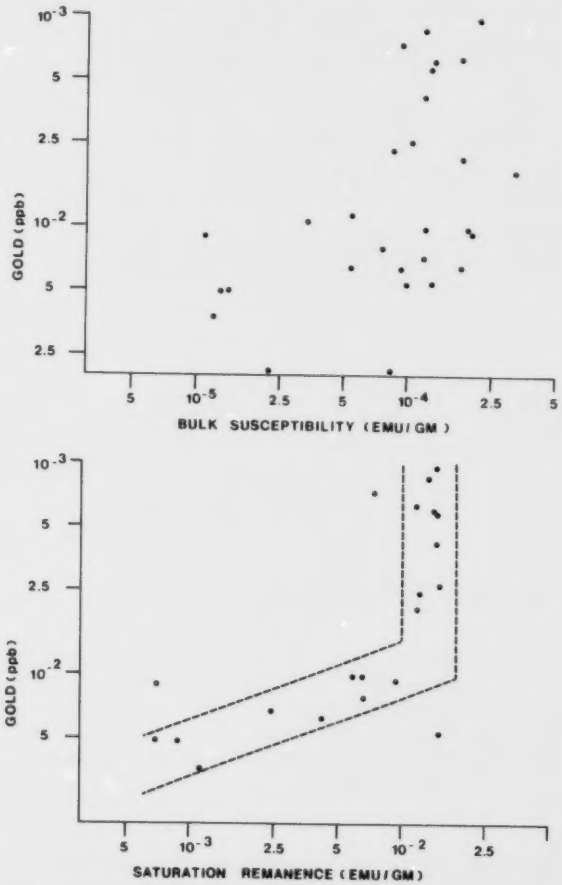

***Figure 051.2** Log-Log plots of the variations of Au content in -0.063 m separate versus a) bulk magnetic susceptibility, and b) 750 nT saturation remanence value.*

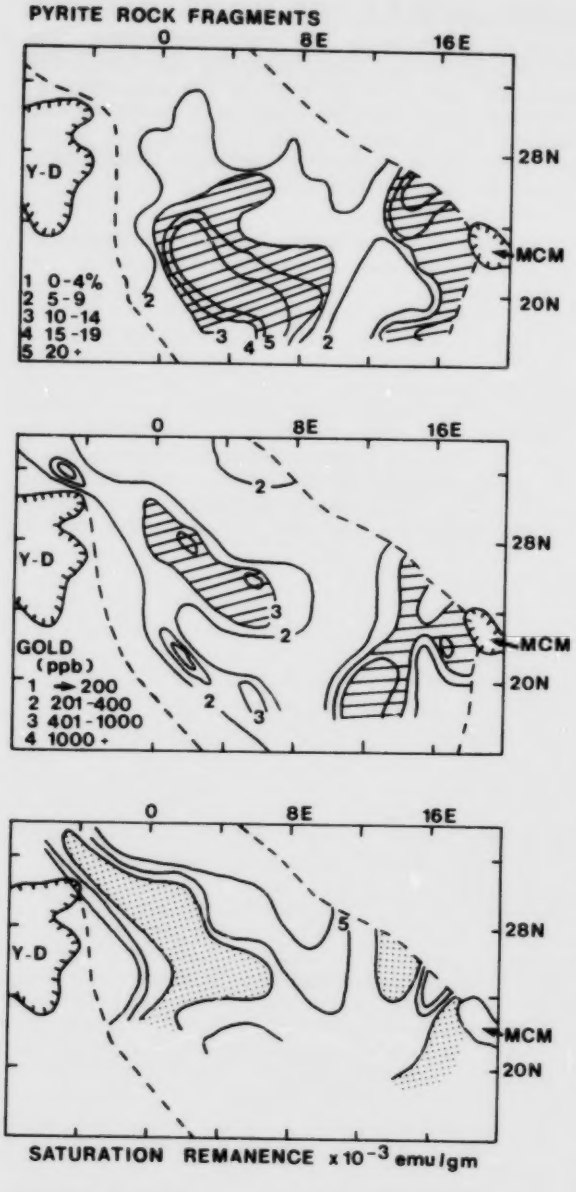

Figure 051.3 Contour plots of: a) the percentage of pyritic rock fragments in the intermediate heavy fraction of surficial sediment samples; b) Au in parts per billion; c) the log site mean saturation remanence of -0.063 m separate of surface samples.

trend is yet to be determined. The 10^{-2} emu/gm cut-off between the two populations provides a criterion for identifying the locus of zones of enhanced Au content.

Figures 051.3a, 051.3b, and 051.3c respectively present contour plots of the percentage of pyritic rock fragments, the Au content in surface samples (both taken from Stewart and van Hees 1984), and for comparison, the saturation remanence values of the area between the Matachewan Consolidated and the Young-Davidson Mines.

Stewart and van Hees (1984) recognized three trends in the pyrite data (Figure 051.3b):

1. An irregular linear belt having a northwest-southeast trend that is located on the southwest side of the grid.
2. A short blunt lobe trending north-northeast that is located in the northeast corner of the grid.
3. A small east-trending arcuate feature located in the southeastern corner of the belt.

Stewart and van Hees (1984) recognized two dispersal trains from their study of the Au data (Figure 051.3b):

1. The west Au dispersal train trending northwest-southeast is located on the west side of the sampling grid.
2. The east Au dispersal train is "tongue-shaped and trends almost due south from an area adjacent to the MCM open pit" [quote taken from Stewart and Van Hees (1984) report].

The saturation remanence map (Figure 051.3c) shows the same two trains as is shown by the Au content map. The west train, the most tightly constrained one, for the most part appears to have a well defined northwest-southeast trend. The train is not continuous across the whole study area, rather, it appears to come to an abrupt halt around the grid location 6E, 24N. There is a suggestion that this train may continue to the southwest, but this is poorly controlled. The east magnetic remanence train, like the Au content train trends approximately north-south and is abruptly terminated around 24 N just like the west train. Stewart and van Hees (1984) explained the termination of these dispersal trains by reference to the geomorphology of the sampling area. The sampled area is crossed from east to west by a broad bedrock ridge. The trains were formed in the lee of the ridge by deposition from the base of the glacier into a subglacial cavity. Termination of the dispersal trains occur at the point where the glacier reassumed contact with the underlying bedrock. The third dispersal train defined by pyrite concentrations is marked by a region of high remanence values. However, there are insufficient data to identify a trend.

CONCLUSIONS

1. Acquisition coercive force studies of B horizon samples from an Au prospect in the Matachewan area indicate that the dominant magnetic oxide is magnetite.
2. The difference between the B and C soil horizons at the same location corresponds to a change in the magnitude of the magnetite content. There does not appear to be any oxide compositional differences between the two lithologies.
3. Although bulk susceptibility data define two distinct populations of susceptibility/Au relationship,

it is not possible to use this information to locate areas of enhanced Au content.

4. Saturation remanence studies also define two populations of the magnetite/Au relationship. A criterion for separating the two populations was set at 10^{-2} emu/gm, and corresponds to a Au content of 100 pb.
5. A contour map of saturation remanence values identifies the same three trains as are recognized by geologists based on mineralogical (pyrite content) and geochemical (Au content) measurements.

This study provides a second example of a prospecting situation in which saturation remanence studies can be used to define economically important dispersal trains. In both these cases, standard magnetic susceptibility measurements failed to give interpretable data. In the uranium example, all samples had susceptibilities below instrument detection limits, while in the Au example, it was not possible to separate individual populations. Application of the saturation remanence technique overcame these problems in both cases, and yielded results which closely agree with those given by other geological investigative methods.

ACKNOWLEDGMENTS

The authors would like to thank Ed van Hees of Pamour Porcupine Mines for supplying these samples, and for permission to publish this data. Bob Stewart of Iowa State University is to be thanked for providing help with field sampling, geological mapping, and the interpretation of Quaternary geology. Finally, this research would not have been possible without the financial support of the Exploration Technology Development Fund (ETDF), the authors are gratefully appreciative of this support.

REFERENCES

Gleeson, C.F., Rampton, V.N., Thomas, R.D., and Paradis, S.
1984: Grant 065 Development and Adaptation of Geochemical Techniques to Au Exploration in Glacial Drift; p.129-150 *in* Exploration Technology Development Program of the Board of Industrial Leadership and Development, Summary of Research 1983-1984, edited by V.G. Milne and R.B. Barlow, Ontario Geological Survey, Miscellaneous Paper 120, 176p.

Morris, W.A.
1984: Grant 051 Development of Field Portable Apparatus for the Analysis of the Magnetite, Hematite, and Ilmenite Content of Basal Tills; p.77-84 *in* Exploration Technology Development Program of the Board of Industrial Leadership and Development, Summary of Research 1983-1984, edited by V.G. Milne and R.B. Barlow, Ontario Geological Survey, Miscellaneous Paper 120, 176p.

Pulkinnen, E., Puranen, R., and Lehmuspelto, P.
1980: Interpretation of Geochemical Anomalies in Glacial Drift of Finnish Lapland with the Aid of Magnetic Susceptibility Data; Geological Survey of Finland, Report of Investigation, Number 47, p.39.

Stewart, R.A., and van Hees, E.H.
1984: Evaluation of Past Producing Gold Mine Properties by Drift Prospecting: An Example from Matachewan, Ontario, Canada; *in* Tills and Related Deposits, edited by E.B. Evenson, C. Schluchter, and J. Rabassa, 1983, A.A. Balkema, Rotterdam, Netherlands, Proceeding of INQUA Symposia on the Genesis and Lithology of Quaternary Deposits, p.179-194.

Grant 052 Production of a Seven-Frequency Helicopter Electromagnetic System

P.E. Wessler

Geotech Ltd., Markham

ABSTRACT

During 1984-1985, Geotech Ltd. has continued to refine the EMEX-2 seven-frequency system. Numerous design parameters have been revised since work was originally begun in late 1983, resulting in totally new printed circuit boards and an improved system performance. Limited test flying has been done to date.

In keeping with the advancement of EM technology, Geotech Ltd. is continuing to expand on the capabilities of the seven-frequency system by incorporating the latest techniques developed by Geotech Ltd. for other projects. Original design frequencies covered the range from 190 Hz to 12 kHz transmitted on three coil geometries. During 1985, Geotech Ltd. has successfully demonstrated the ability to further extend this frequency range from 95 Hz to 16 kHz. A prototype bird has been flown with an upper frequency of 32 kHz producing acceptable noise levels. A corresponding bird weight increase occurs as one lowers the transmitter frequency.

A laser altimeter and bird motion monitors have been successfully installed and tested in a four-frequency EMEX bird. Testing done to date indicates that it is feasible to incorporate these ancillary devices internal to the seven-frequency system. Qualitative measurements of bird motion and accurate sensor terrain clearance information are thus available for the first time to aid in post-flight data processing.

The addition of an accurate bird sensor height measurement extends the usefulness of the HEM system into areas of groundwater exploration in arid areas as well as airborne bathymetry over coastal waters. The seven-frequency system with its three coil geometries and broad frequency spectrum will be ideally suited for areas of complex geology typical of many of the gold-bearing areas of Ontario.

***Photo 052.1** EMEX bird flying with ASTAR 350D Helicopter.*

INTRODUCTION

In 1981, Geotech Ltd. began development of a "state-of-the-art" helicopter-towed Electromagnetic Exploration System. This work culminated the following year in the successful field trials of the system. The EMEX-1 four-frequency system is currently being flown in Canada by independent contractors serving the mining community. Photo 052.1 shows an EMEX bird flying with an ASTAR 350D helicopter. Geotech Ltd. expects the seven-frequency EMEX-2 System to be part of the final phase in the evolution of Helicopter EM systems.

The seven frequencies have been arranged to provide widely spaced frequency transmission on three independent coaxially coupled coils, two horizontal coplanar coils (whaletail), and two vertical coplanar coils (fishtail). All coils are maintained with an 8 m coil separation, although other coil separations are possible on special order. The removable transmitter and receiver modules are contained in a 9 m Kevlar composite shell. Geotech Ltd. has produced its own custom designed mandrel for the production of these bird shells in order to maintain a consistent mechanical integrity. The unique construction of the 9 m shell has been tested to demonstrate adequate strength and dimensional stability while at the same time providing weight savings that are critical in helicopter work. Tolerances in the construction can be maintained well enough to allow interchange of removable structures from one bird to another. This is important from a spareparts or maintenance viewpoint. Hook load, which, for the EMEX-2 System will be about 300 kg depending on transmitter frequencies, is within the load capacity of most small helicopters such as the ASTAR 350, and will allow the addition of ancillary sensors to the system without decreasing the fuel load. A preliminary EMEX-2 specification sheet is included in this report.

Photo 052.2 *Nine metre EMEX-2 bird on ground transport supports.*

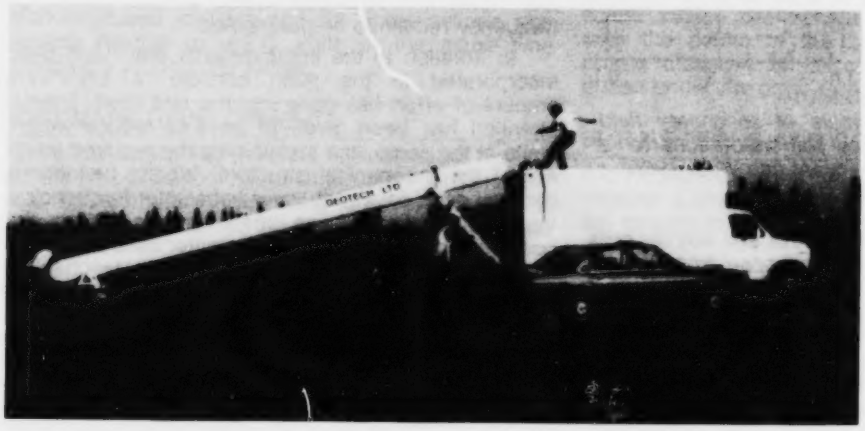

Photo 052.3 *EMEX-2 bird being loaded on Geotech cube van.*

The following nominal frequencies are incorporated into the standard system (upper frequency available to 32 kHz):

1. 190 Hz horizontal coplanar (whaletail)
2. 870 Hz horizontal coplanar (whaletail)
3. 380 Hz vertical coaxial
4. 918 Hz vertical coaxial
5. 2200 Hz vertical coaxial
6. 5000 Hz vertical coplanar (fishtail)
7. 12000 Hz vertical coplanar (fishtail)

Note that the selection of coil orientation allows for three coaxial geometries that can be nominally tuned for any frequency within the range of 190 Hz to 12 kHz. This also applies to the whaletail and fishtail configurations. As an example of the versatile nature of the design, the whaletail coils could be configured with operating frequencies of 190 Hz and 5000 Hz. The only restriction on the final selection of the frequencies is that the harmonic relationship between transmitter frequencies must be considered for coils having similar geometries.

Thus, 14 channels of geophysical information are provided by the EMEX-2 System, along with power line monitors for each frequency should it be required. This configuration of frequencies and coil orientations should provide specific information in areas where the geology was previously unknown. Post-flight processing of this large amount of data can accomplish overburden stripping, multi-layered earth interpretation, and resistivity mapping, along with dip and strike interpretations. Optional are laser altimeter and bird motion detectors.

Photo 052.2 shows the 9 m EMEX-2 prototype bird on its ground transport supports. Photo 052.3 shows the 9 m EMEX bird being loaded on top of the Geotech cube van after initial flight trials. A custom engineered bird lifting device was developed in order to allow the 210 kg bird to be elevated and rolled onto the roof of the cube van. A maximum of two EMEX birds can be readily transported in this fashion.

In Figure 052.1, the effect of coil geometry, coil separation, and flying height are shown for a horizontal sheet. At a flying height of 30 m, the absolute value of the response for the whaletail pair is twice that for the coaxial or the fishtail pair. It should be

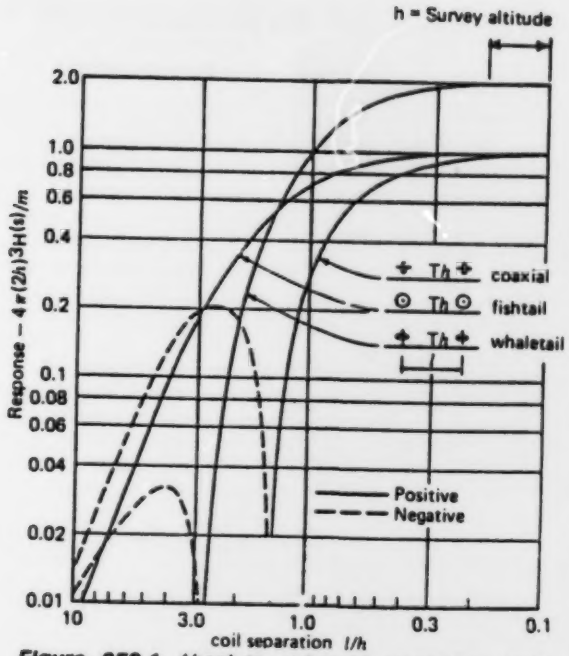

Figure 052.1 *Absolute value of secondary field responses of the three coil orientations for a horizontal sheet (after Grant and West 1965).*

noted here that although the fishtail and coaxial coils produce a similar secondary response from a horizontal sheet, in absolute terms, the number of ppm recorded by the system for the coaxial coils is half that of the fishtail coils. This is because the primary field seen by the coaxial coils is twice that seen by the coplanar coils; it is the ratio of secondary to primary field that is measured by the EMEX-2 system. The simultaneous acquisition of this information should provide additional interpretive information to the end user.

Figure 052.2 is an unretouched copy of actual airborne flying showing the integration of the laser altimeter and bird motion detectors with a four-frequency bird. Geotech Ltd. has elected to carry on the seven-frequency development by varying the parameters and installing new devices utilizing EMEX-2 electronics coupled with standard EMEX-1 mechanics in order to reduce variables in the debugging process. In this example, we see the upper transmitter frequency extended to 16 kHz. Please note that the activity on the 16 kHz coplanar coil is increased compared to the 527 Hz coplanar coil. Pitch and roll sensor activity is related to laser altimeter readings. Corrections may be applied to the laser readings to compensate for apparent elevation changes caused by bird pitch and roll. Flying conditions for this flight were 'moderately' turbulent over rolling terrain. A Urtec Limited UDAS-100 Data Acquisition System was used to record EM data in both analog and digital form. A detailed analysis of the field data obtained is currently underway to determine the merits of the integration of the laser altimeter and bird motion detectors. At the time of writing, Geotech Ltd. is confident that there have been no deleterious effects on the EM system performance due to the addition of these extra components within the EMEX bird. The cost effectiveness to benefits ratio remains to be ascertained.

INSTRUMENTATION DEVELOPMENT

Client feedback has demonstrated the need for a wider range of transmitted frequencies. The recent emphasis on gold exploration and structure delineation has produced the need for higher frequencies than were previously available. In keeping with this need, Geotech Ltd. has embarked on a program to provide a range of frequencies that should suit most geophysical applications, and has been successful in producing a transmitter design that allows the efficient transmission of frequencies from 95 Hz to an upper limit of about 16 kHz. The possibility also exists to produce a transmitter coil system that can produce the required dipole moment at frequencies well beyond the current 16 kHz upper limit. A 32 kHz transmitting system was produced and successfully test flown in 1985. The merits of this ultra high frequency remain to be determined.

In addition to the improvements that have been incorporated in the main console, a significant amount of effort has gone into the bird itself. Special attention has been given to ways to reduce weight while at the same time maintaining the required integrity of the mechanical structure. Weight restrictions become quite severe at lower transmitter frequencies. Various techniques have been used to reduce the possibility of motion of the transmitter coils relative to the receiver coils and the bucking coils. Mechanical design for an EM system requires rigid coupling between the receiver and transmitter coils. A 1 ppm change in coil separation will result in a 3 ppm change in signal amplitude. Temperature gradients in excess of 10° Celsius can be encountered from the start to the end of a typical survey flight, thus the temperature coefficients of materials become important to the airborne performance of the system. Geotech's attention to detail in all aspects of bird design should result in improved performance. Additional airborne testing is required before the benefits of this effort can be finally categorized. It has been observed that the base line drift is somewhat dependent on the actual transmitter frequency as well as the coil geometry.

Figure 052.3 shows a block diagram of the EMEX-2 main console; there are four external front panel adjustments on each of the EMEX-2 modules. During 1985, an optional "Spherics Monitor" has been added to the main system console; up to four of these monitors may be added to the system. Therefore, a total of 28 front panel controls are available to the field operator. Due to the nature of the electronic design, a minimum amount of operator intervention will be required in actual practice. Ground calibration and alignment will be done prior to takeoff with essentially no operator adjustments required when airborne. Refinement of calibration procedures occurred in 1985. There is the strong possibility that the system will eventually be manufactured under microprocessor control and all the required adjustments and alignment would be done under software control

in real time. In this vein, Geotech Ltd. has continued to investigate requirements for converting this system to a digital design. This conversion will gradually take place concurrent with the current program, and possibly in a future phase of the project. Geotech Ltd. anticipates a very rapid transition to the digital receiver after complete debugging of the analog system has been done.

In keeping with the stringent temperature range that the EM system must operate within (-40°C to +50°C), Geotech Ltd. has recently acquired a used environmental chamber. This chamber will be used for temperature cycling of the various system components. It is hoped that Geotech Ltd. can offer the use of this environmental chamber to other small companies within the geophysical community.

Only recently has Geotech Ltd. received the custom designed tow cable and special connectors required for the seven-frequency system. Final assembly of the required tow cable is underway now and we expect to be flying the complete EMEX-2 system in the third quarter [of 1985]. This tow cable has been produced to Geotech Ltd. specifications and remains flexible to -65°C while at the same time providing a tough outer jacket.

SOFTWARE DEVELOPMENT

As well as continuing to refine an automated method for the interpretation of multifrequency airborne EM data, Geotech Ltd. is continuing to develop a suite of interpretational aids for the EMEX-2 System. A suite of phasor diagrams for all three coil configurations will be produced. These diagrams would take into account dipping plates of various sizes, spheres of various sizes, orientations, and so on. Also to be developed is an overburden stripping program for the various coil orientations. Included will be such items as dip estimation, consideration of conductive host rock, and estimation of body extent using profile information for all three coil geometries. These interpretation aids will be invaluable to the end user of the EMEX-2 System.

Figures 052.4 to 052.7 are computer-generated phasor diagrams representative of a horizontal coplanar coil geometry with a 6.45 m separation. Figure 052.4 represents the response to a 20 m sphere. Note that the estimated depths are to the centre of the sphere. Figure 052.5 shows the in-phase and quadrature response expected for a half space, while Figure 052.6 shows the response to a horizontal thin sheet. Figure 052.7 is representative of a response to a vertical plate at 90° to the flight line as the HEM System traverses over the plate. Note that the absolute values of in-phase and quadrature are not over the centre of the body. A complete suite of phasor diagrams for all coil geometries will be produced under the grant extension.

FUTURE PLANS AND CONCLUSIONS

It is hoped that as part of Grant 052, Geotech Ltd. will execute a small airborne survey over known geological targets in Ontario. This flying project would be

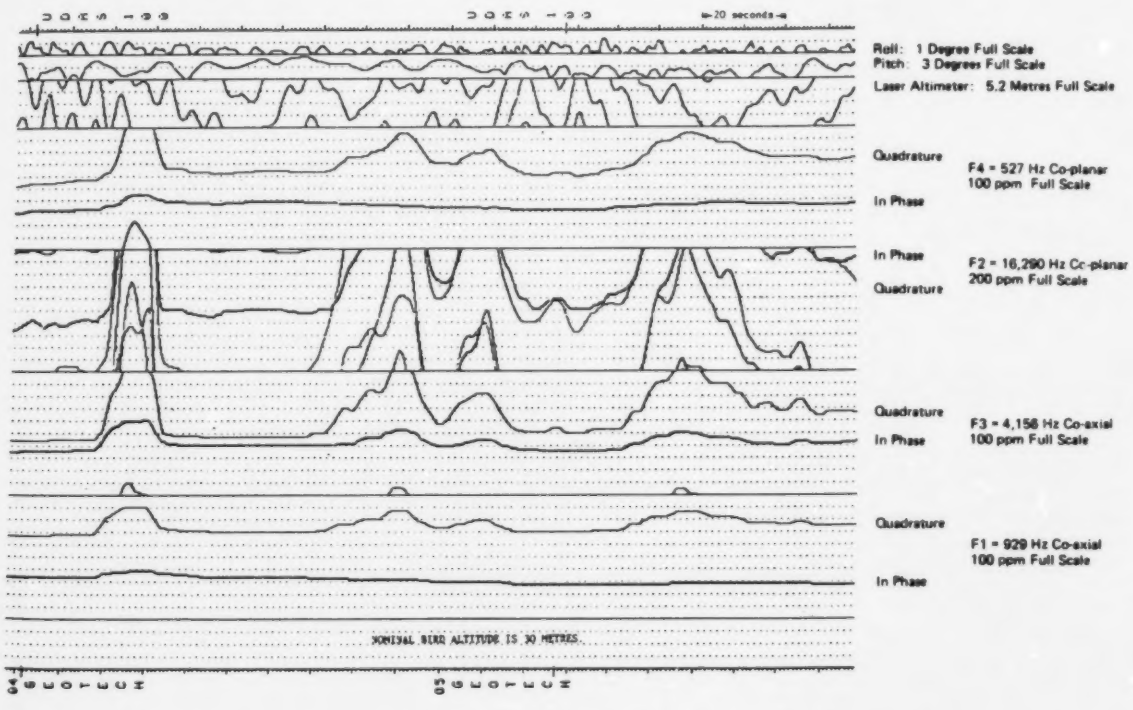

***Figure 052.2** Airborne example of integration laser altimeter and bird motion monitors with EMEX system. Note 16.29 kHz activity.*

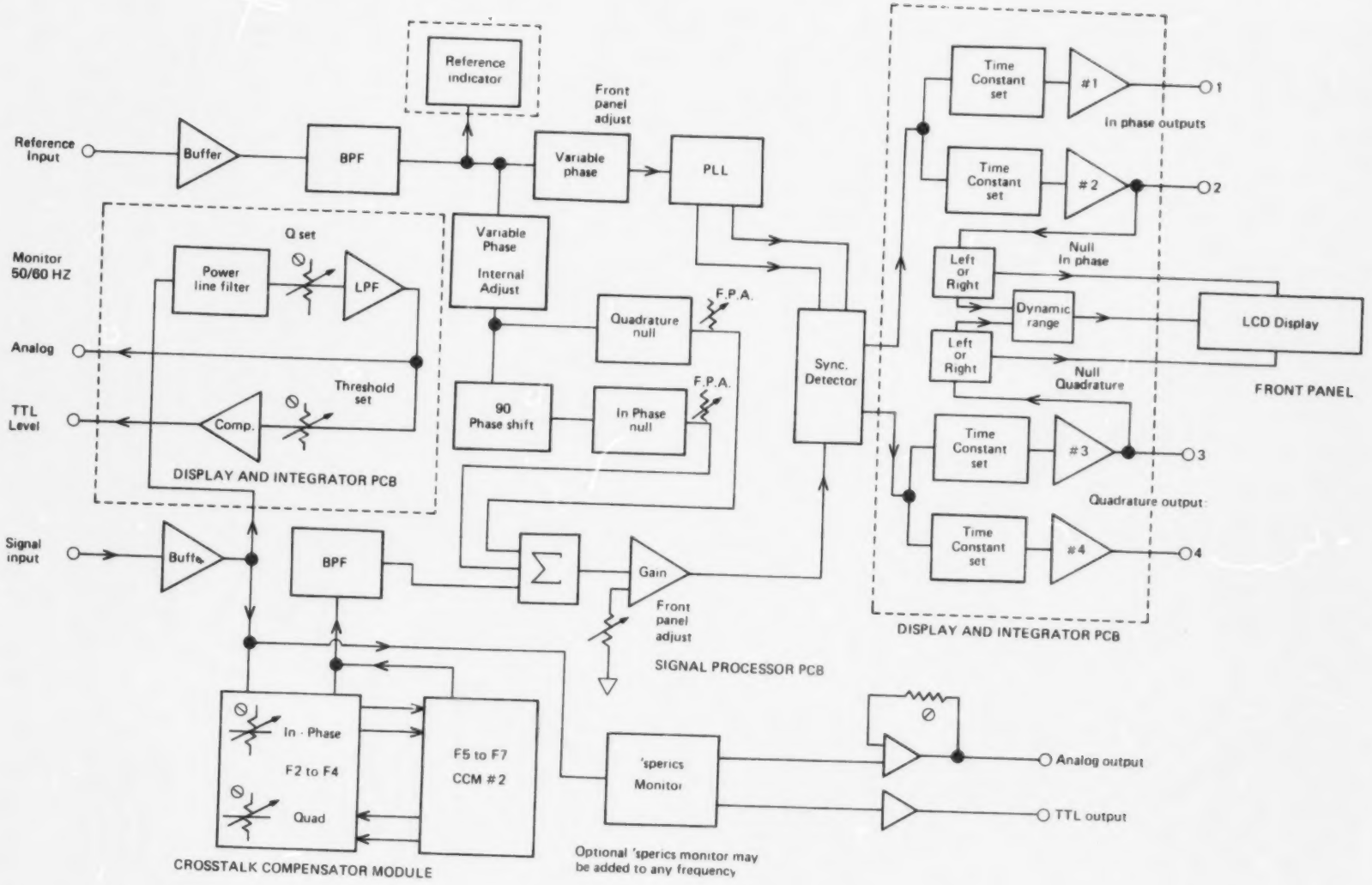

***Figure 052.3** Block diagram of EMEX-2 receiver module.*

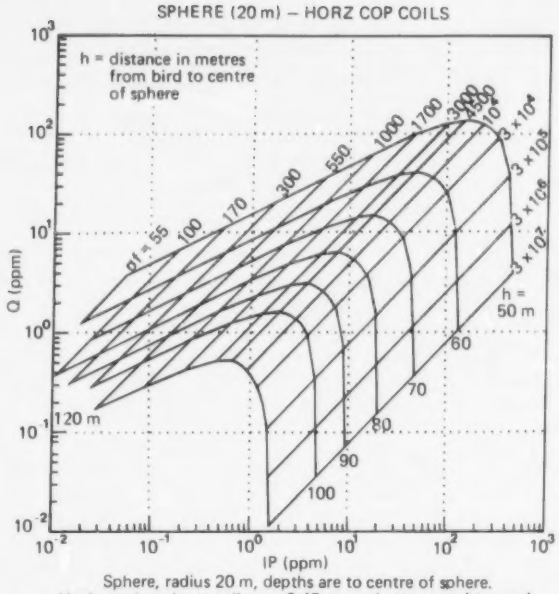

Sphere, radius 20 m, depths are to centre of sphere.
Horizontal coplanar coils, sep 6.45 m, peak response data used.

***Figure 052.4** Computer-generated phasor diagram, representing the response to a 20 m sphere.*

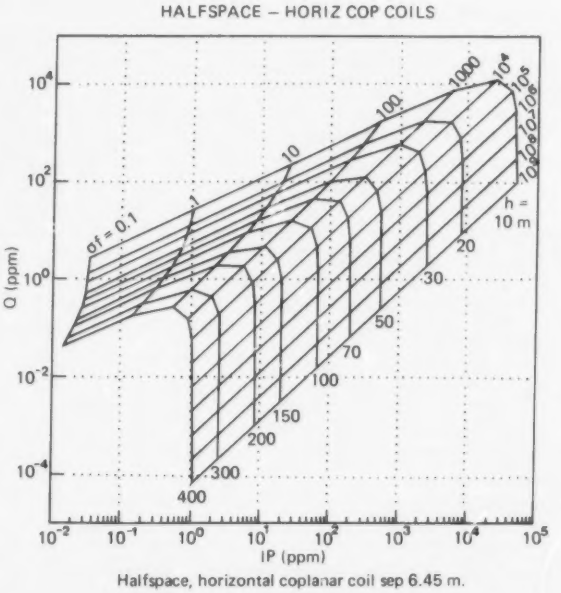

Halfspace, horizontal coplanar coil sep 6.45 m.

***Figure 052.5** Computer-generated phasor diagram, showing the in-phase and quadrature response expected for a half space.*

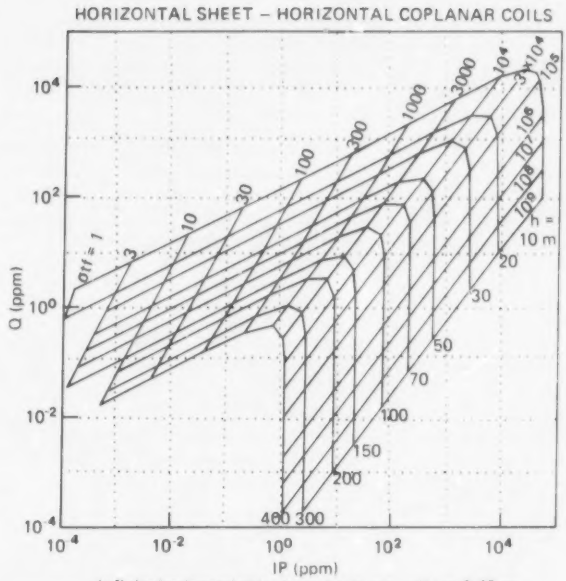

Infinite horizontal thin sheet, horiz.cop coil sep 6.45 m.

***Figure 052.6** Computer-generated phasor diagram, showing the response to a horizontal thin sheet.*

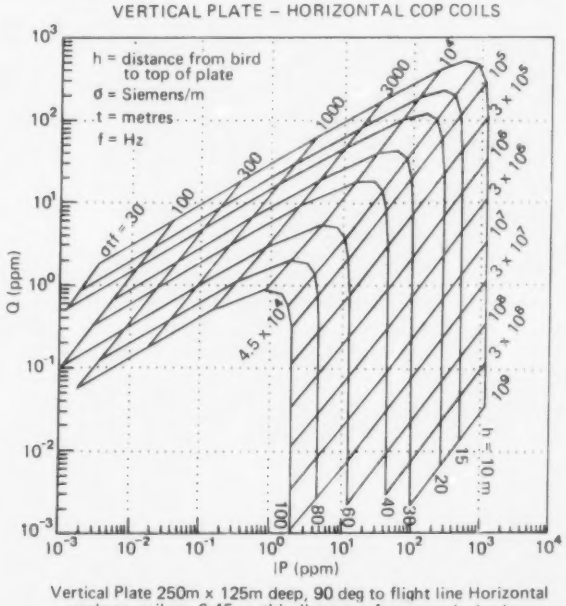

Vertical Plate 250m x 125m deep, 90 deg to flight line Horizontal coplanar coil sep 6.45 m, this diagram refers to peak absolute amplitudes of IP and Q, NOT over centre of body!

***Figure 052.7** Computer-generated phasor diagram, representing the response to a vertical plate at 90° to the flight line as the HEM System traverses over the plate.*

established and conducted with input from the Ontario Geological Survey. Interpretation aids previously developed would be used to produce the final maps from this small test survey and comparisons made with previous data.

The EMEX-2 System will be completely documented, and detailed manuals produced. Attention will be paid to the total HEM survey package including such items as data acquisition systems, radar altimeters, and electronic navigation system integration.

It is hoped that this analog version of the EMEX-2 seven-frequency helicopter electromagnetic system will find immediate application in Earth Science applications that extend beyond the more traditional mineral exploration surveys for which the system was originally designed. Geotech Ltd. will continue to attempt to advance and expand the variety of engineering applications of helicopter-borne survey systems.

ACKNOWLEDGMENTS

Geotech Ltd. would like to thank Mr. George McDonald of the Canadian Hydrographic Survey for allowing the company to borrow various pieces of instrumentation for system testing. Geotech Ltd. is especially grateful for the cooperation and financial assistance made available for this development through the ETDF program and the Ontario Geological Survey.

REFERENCE CITED

Grant, F.S., and West, G.F.
1965: Interpretation Theory in Applied Geophysics; New York, McGraw-Hill Book Company Incorporated, p.456, 501, 526, 571.

GENERAL REFERENCES

Fraser, D.C.
1979: The Multicoil II Airborne Electromagnetic System; Geophysics, Volume 44, p.1367-1394.

Frischknect, F.C.
1967: Fields About an Oscillating Magnetic Dipole Over a Two-layer Earth; Colorado School of Mines, Volume 62, Number 1.

Lodha, G.S., and West, F.G.
1976: Practical Airborne EM Interpretation Using a Sphere Model; Geophysics, Volume 41, p.1157-1169.

Morrison, E.B.
1983: Grant 018 Development of a Four Frequency Helicopter Electromagnetic System; p.77-81 *in* Exploration Technology Development Program of the Board of Industrial Leadership and Development, Summary of Research 1981-1983, edited by E.G. Pye and R.B. Barlow, Ontario Geological Survey, Miscellaneous Paper 115, 135p.

Paterson, N.R.
1971: Airborne Electromagnetic Methods as Applied to the Search for Sulphide Deposits; Canadian Institute of Mining Bulletin, January, p.29-38.

Pemberton, R.H.
1962: Airborne EM in Review: Geophysics, Volume 27, p.691-713.

Sengpiel, K.
1983: Resistivity/Depth Mapping with Airborne Electromagnetic Survey Data; Geophysics, Volume 48, p.181-196.

Sinha, A.K.
1973: Comparison of Airborne EM Coil System Placed Over a Multilayer Conducting Earth; Geophysics, Volume 38, p.894-919.

Wessler, P.
1984: Grant 052 Development of a 7-Frequency Helicopter Electromagnetic System; p.84-94 *in* Exploration Technology Development Program of the Board of Industrial Leadership and Development, Summary of Research 1983-1984, edited by V.G. Milne and R.B. Barlow, Ontario Geological Survey, Miscellaneous Paper 120, 176p.

Grant 059 Development of a Borehole Magnetic Properties Logging System

W.R. Thuma[1], Detlef Blohm[1], and M.T. Hamalainen[2]

[1]IFG Corporation, Brampton

[2]Geoinstruments Ky, Helsinki, Finland

ABSTRACT

The practical application of fundamental magnetic properties logging in slimline boreholes has in the past been hampered by the inability to utilize conventional sensors in the limited space available. Further, the sensitivities and stability of earlier sensors made their application limited primarily to ore deposits with large magnetic fields and high susceptibilities. The development of stable ringcore fluxgate sensors by NASA for the MAGSAT program and improvements in both iron and air core susceptibility detectors in Finland have resulted in the potential for successfully developing a high sensitivity slimline probe under the control of a microprocessor. IFG in cooperation with Geoinstruments has been developing a portable multi-sensor borehole logging system based on this new technology since 1983 and 1984. When fully operational in late 1985, this system, referred to as the MAGLOG System, will offer new areas of geophysical interpretation to assist in mineral resource exploration.

INTRODUCTION

The use of both total and directional magnetic field intensity measurements made in the air and on the surface has been an important geophysical technique for the geophysical exploration of mineral and hydrocarbon resources and for geological mapping for decades. Nearly coincident with this has been the wide application of borehole logging using mainly electrical and nuclear methods to measure a variety of *in-situ* properties. The extension of these surface techniques to borehole applications has been restricted by physical and electronic constraints.

With the development of high sensitivity ringcore fluxgate sensors, primarily through the efforts of NASA's Goddard Space Flight Center during the MAGSAT project, it became possible to scale down directional magnetic field sensors to fit into smaller diameter probe shells. Further, by using more advanced low powered microprocessors and larger capacity A/D converters, it was possible to produce a device which would function over the full range of the field instead of being restricted to a role as a coarse variometer.

From a geophysical perspective, the necessity of including a susceptibility sensor into the probe was recognized from the beginning. The information derived from this is important in the full interpretation of the magnetic field data and would also yield fine detail on the lithology and structure in the near vicinity of the drillhole. Through a cooperative agreement with Geoinstruments Ky of Finland, IFG integrated their technology into the prototype design.

To further expand the applications of the MAGLOG System, and to take advantage of excess capacity of the microprocessor, it was decided to add the measurement of two other parameters, natural self potential and fluid temperature. These are relatively standard measurements in both softrock and hardrock logging and apart from adding additional interpretable data, would present a certain level of familiarity to the logs.

It was also possible to use the susceptibility sensor to measure the electrical conductivity of the surrounding media. Although this approach is not as indicative of apparent resistivity as normally measured by direct contact, particularly over the full range, it was considered interesting on a secondary level.

DESCRIPTION

The development of both the hardware and software has progressed according to the original plan though not on the original schedule. The hardware and most specifications are unchanged from those described in the previous annual report (*see* Thuma, Blohm, and Hamalainen 1984). The hardware consists of three basic components: 50 mm probe, portable surface console, and cable/winch assembly. The probe is slightly different than reported earlier, with an overall length of 1.8 m and two nearly equal length sections which may be dismantled for ease of shipment. The decision to transmit only digital data up the cable and only unregulated power down, led to the requirement to make the self potential measurement differential rather than single point which is common in analog-based logging systems. Therefore, two lead electrodes, separated by 16 inches (40.6 cm) are incorporated into the magnetometer section of the probe. The later addition of a pole-dipole ac resistivity measurement which uses this pair of electrodes is possible.

The miniaturization of the three-component fluxgate sensor was a major accomplishment of the MAGLOG development. This assembly is shown in Figure 059.1.

CURRENT STATUS

The system will undergo its first field test in June 1985 at Bells Corners, the Geological Survey of Canada's test site near Ottawa. Progress was hampered by the limitations of funds for the project and the unanticipated impact of other development and test projects. Production of the first system should be feasible in late 1985.

CONCLUSIONS

At this point, the MAGLOG development project has met all of the initial objectives set forth in the original ETDF proposal. Additions subsequent to that submission have expanded the scope and capabilities of the System, and it is expected that it will be a

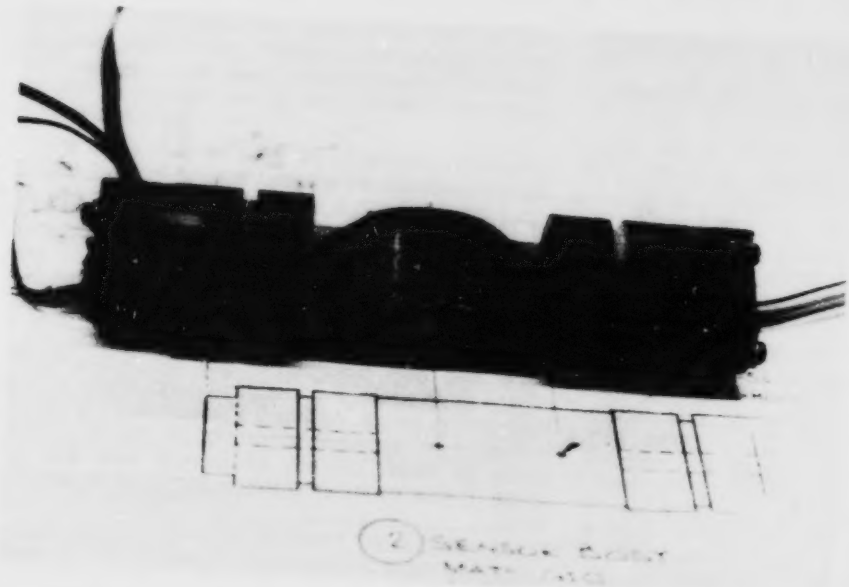

***Figure 059.1** Three component fluxgate sensor assembly.*

commercial success. Applications will include geothermal exploration, lithologic and structural identification, hydrocarbon exploration and evaluation, geohydrology, and basic geological research. Various technological and commercial spinoffs are anticipated as a result of this project and expansion of the System's capabilities is likely. These will largely be determined by feedback from field geophysicists and other market forces.

ACKNOWLEDGMENTS

The authors would like to thank Dr. William Morris of Morris Magnetics and Quentin Bristow and Pat Killeen of the Geological Survey of Canada. IFG is especially grateful for the continued support of the Ontario Geological Survey and the Exploration Technology Development Fund.

REFERENCE

Thuma, W.R., Blohm, Detlef, and Hamalainen, M.T. 1984: Grant 059 Development of a Borehole Magnetic Properties Logging System; p.115-119 *in* Exploration Technology Development Program of the Board of Industrial Leadership and Development, Summary of Research 1983-1984, edited by V.G. Milne and R.B. Barlow, Ontario Geological Survey, Miscellaneous Paper 120, 176p.

Grant 068 Isotope Ratios and Trace Elements in Gold and Base-Metal Occurrences in Ontario

E.J. Brooker and T.E. Eagles

X-Ray Assay Laboratories Limited, Don Mills

ABSTRACT

The plasma mass spectrometer has been referred to as the greatest advance in analytical spectroscopy since the introduction of inductively coupled plasma. In the late spring and early summer of 1984, the first commercial plasma mass spectrometers became available. The objective of this research program is to assess the potential of the plasma mass spectrometer for solving analytical problems relevant to exploration and mining activities in Ontario.

INTRODUCTION

Inductively coupled plasma/mass spectroscopy (ICP/MS) is frequently referred to as the offspring of the marriage between an inductively coupled plasma and a quadrupole mass spectrometer. ICP/MS provides the easy sample preparation and low detection limits characteristic of ICP and the simple spectra and isotope analysis characteristic of mass spectroscopy. The entire mass spectrum of all the elements totals less than 230 lines. The location of each of the lines in the mass spectrum is well documented, and with the exception of a few elements, such as Pb, the relative abundance of the isotopes is known to a number of significant figures. Thus, when isobaric interferences occur, very precise corrections can be made. With the exception of In, all of the elements have at least one interference free isotopic line in the mass spectrum. Indium has a Cd interference on one isotope and a Sn interference on the second isotope.

ICP/MS is not without its problems. The three most significant problems are the formation of molecular species, notably oxides, the formation of doubly-charged species, and matrix effects. The formation of doubly-charged species is not a serious problem, being limited to a few elements with a low second ionization potential, such as Br. The presence of molecular species is a far more serious problem. In particular, the formation of oxides results in secondary peaks at 16 mass units above the parent peak. Some consideration will be given to this problem in the discussion of rare earths in the experimental section of this report. Matrix effects usually result in reduced sensitivity. In our laboratory, the authors are trying to overcome matrix effects by using analytical procedures such as standard addition and isotope dilution.

In this report, our approach to a number of analytical problems using ICP/MS will be outlined. Some of these procedures have been proven as viable analytical methods; others, as will be pointed out, are still in the developmental stage.

INSTRUMENTATION

All experimental work was carried out on an ELAN 250 inductively coupled plasma mass spectrometer (SCIEX, Thornhill, Ontario, Canada). A schematic diagram of the instrument is shown in Figure 068.1. A detailed description of the instrument is given by Douglas *et al.* (1983).

EXPERIMENTS AND RESULTS

LEAD ISOTOPES ANALYSIS

Digestion of Galena Samples

A 20 mg sample of galena was weighed into a 100 ml volumetric flask. Ten ml of concentrated HCl (ULTREX brand) was added and the mixture was refluxed for 30 minutes. Then, 5 ml of concentrated HNO_3 (ULTREX brand) was added and the mixture was heated until complete digestion of the sample was achieved. The solution was then diluted to 100 ml with doubly distilled water. Then, 0.5 ml of this solution was further diluted to 50 ml. The final dilution factor was 500,000:1.

Digestion of Pyrite Samples

A 500 mg fraction of the sample was weighed into a beaker. Then, 3 ml of concentrated HNO_3 (ULTREX) was added and the mixture was digested on a hot plate for 30 minutes. Then, 3 ml of concentrated HCL (ULTREX) was added and the mixture was taken to dryness. The residue was dissolved in 5 ml 8 N HCl and was transferred to a 125 ml separatory funnel using an additional 5 ml 8 N HCl to carefully wash the beaker. The liquid in the separatory funnel was cooled under the cold water tap and then 10 ml of isopropyl ether was added. The solution was extracted for 1.5 minutes and the ether layer was discarded. The extraction was repeated a total of three

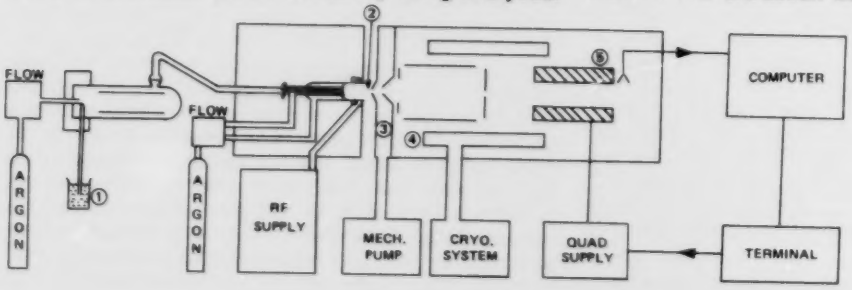

***Figure 068.1** ELAN 250 inductively coupled plasma mass spectrometer system schematic: (1) sample solution, (2) inductively coupled plasma, (3) differentially pumped interface, (4) helium cryopump, (5) quadrupole rods.*

TABLE 068.1 LEAD ISOTOPE RATIOS DETERMINED USING THE SCIEX ELAN 250

ISOTOPES ARE RATIOED AGAINST LEAD 206

		Raw Data			Corrected Using NBS-981		
Date	**Time**	**208**	**207**	**204**	**208**	**207**	**204**
Nov 8	12:00	1.981	0.7885	0.05134	1.968	0.7843	0.04893
Nov 9	12:00	1.948	0.7834	0.05335	1.965	0.7842	0.04961
Nov 12	13:00	1.956	0.7825	0.05008	1.963	0.7827	0.04934
Nov 14	12:40	2.012	0.7929	0.04903	1.992	0.7872	0.04822
Nov 16	17:00	1.951	0.7802	0.05038	1.955	0.7766	0.04980
Nov 17	10:40	1.988	0.7895	0.04980	1.961	0.7810	0.04964
Nov 17	11:10	1.988	0.7910	0.04941	1.961	0.7825	0.04925
Nov 17	11:25	1.989	0.7939	0.04959	1.962	0.7854	0.04943
Nov 17	11.40	1.992	0.7927	0.04943	1.965	0.7842	0.04927
Nov 17	11:55	1.993	0.7925	0.04949	1.966	0.7840	0.04933
Nov 19	11:45	1.989	0.7917	0.04965	1.966	0.7856	0.04945
Nov 20	13:45	1.996	0.7926	0.04941	1.959	0.7813	0.04943
Nov 21	12:30	1.947	0.7794	0.05126	1.948	0.7777	0.05003
Nov 22	12:45	2.013	0.7963	0.04920	1.954	0.7828	0.04987
Nov 23	12:00	2.015	0.7946	0.04922	1.955	0.7828	0.04913
Nov 26	10:40	1.990	0.7913	0.04993	1.965	0.7834	0.04981
Nov 27	9:50	2.006	0.7903	0.05011	1.962	0.7836	0.04972
Nov 28	13:15	1.887	0.7664	0.05538	1.945	0.7769	0.04828
Nov 29	12:20	1.877	0.7689	0.06033	1.968	0.7782	0.04557
Nov 30	9.50	1.955	0.7834	0.05096	1.949	0.7843	0.05002
MEAN		1.976	0.7878	0.05061	1.962	0.7825	0.04921
S.D.		0.035	0.0077	0.00254	0.009	0.0028	0.00090
R.S.D.		1.8%	0.98%	5.0%	0.46%	0.35%	1.8%

NOTES:
S.D. = Standard Deviation
R.S.D. = Relative Standard Deviation

times. The aqueous layer was then placed on a hot plate and brought to a gentle boil in order to remove the last traces of ether. The solution was diluted to 25 ml. The final dilution factor was 1:50.

Correction of Pb Isotopic Ratios

The Pb isotopic ratios obtained directly from the ELAN were normalized using the following procedure. The certified Pb standard NBS-981 was run at the beginning of the experiment and after every four samples. The certified values for NBS-981 and the ratios determined on the ELAN were used to determine a correction factor for each ratio which in turn was applied to the four samples. The data in Table 068.1 show the results of a study done to assess the potential of this procedure. In this study, a lab standard and a NBS-981 were run periodically for a period of three weeks. The first three columns of data give the raw data as it was reported by the ELAN. The next three columns give the adjusted ratios corrected using the NBS-981 reference materials. The last three lines of Table 068.I give the statistics over this period. The relative standard deviations of the ratios 208/206, 207/206, and 204/206 have been reduced by 1.8%, 0.98%, and 5.0% to 0.46%, 0.35%, and 1.8% respectively using the correction procedure.

In another study, samples which had been previously analyzed by thermal ionization procedures were analyzed using ICP/MS. The thermal ionization values were obtained primarily from the literature, and at least a few of these ratios are now considered to be suspect (R.Thorpe, personal communication, 1985). The ratio of the ICP/MS values to the reported thermal ionization values is given in Table 068.2. In general, the agreement is acceptable.

Case Study

A total of 42 samples from 13 mining camps in Ontario have been donated for this study. A preliminary report on the final group of these samples is given in Table 068.3. It should be noted that this data is indeed preliminary. Repeat digestions and analyses are currently taking place. The data is presented at this time for the sake of completeness.

PLATINUM METAL GROUP

The platinum metals were extracted from 25 gram samples using the nickel sulphide collection procedure described by Hoffman (1978). The sulphide precipitate thus obtained was digested in 10 ml of aqua regia. Standard addition spikes were made and the samples were diluted so that the final dilution factor was 1:1. Table 068.4 gives the analytical results obtained on synthetic samples which were analyzed using this procedure. Osmium was not analyzed because of the lack of a suitable standard. The results suggest the detection limits of 1 ppb are

TABLE 068.2 COMPARISON OF LEAD ISOTOPE RATIOS DETERMINED USING PLASMA MASS SPECTROSCOPY TO THOSE OBTAINED USING THERMAL IONIZATION

	P/MS RATIO DIVIDED BY THERMAL IONIZATION RATIO		
Sample Number	**208/206**	**207/206**	**204/206**
RF 63-19	0.9770	0.9939	1.1668
RF 63-195	1.0016	1.0073	0.9867
RF 63-511	0.9681	0.9831	1.1820
RFA 65-545	0.9915	0.9965	1.0156
LEA-MS-124	0.9980	1.0000	0.9957
TQ 82-180	0.9915	0.9926	1.0135
DY-2541	0.9936	1.0008	1.0072
SP-706	1.0062	1.0034	1.0164
RFA 64-417	0.9942	0.9987	0.9848
SP-1392B	0.9955	0.9989	0.9979
TQ 70-150	0.9898	0.9852	0.9968
TQ 65-14	0.9899	1.0005	1.0011
SP-1631 GN	0.9798	0.9922	1.0065
M27901	1.0024	0.9986	1.0064
M27901	1.0024	1.0009	0.9987
M14093	1.0067	1.0029	0.9922
M14093	0.9996	0.9973	0.9909

possible for all elements in this group. At this time, an extensive study of samples previously analyzed by neutron activation is being carried out. A suitable source of Os has been located and Os will be included in subsequent studies. The platinum metal group appears to lend itself to internal standard methods. This possibility will also be investigated.

Tl ANALYSIS

There are two isotopes of Tl Tl-203 and Tl-205 (relative abundance 29.5 and 70.5, respectively). Neither of these isotopes has a mass interference; however, high concentrations of Pb interfere with the 205 line. Samples were worked up using $HF/HClO_4$ digestion and diluted 100:1. There are very few certified reference materials for Tl. One that is available is NBS 1645 River Sediment. The certified value is 1.44 ppm. A concentration of 1.2 ppm was obtained using this procedure on NBS 1645.

BOROHYDRIDE GENERATION COUPLED WITH ICP/MS

The combination of borohydride generation with ICP/MS offers the potential of very low detection limits coupled with a multi-element analysis. For most geological materials, the existing procedures are more than adequate. The area where this combination should prove useful is for the analysis of materials such as pure metals where it is necessary to dilute the sample to avoid problems with interferences relating to the formation of the hydride. Experiments carried out by simply introducing the argon purge gas from the hydride generator into the nebilizer indicated that detection limits in solution of 50 parts per trillion are possible on Sn and Ge. The multi-element capability of the method is limited by the varying conditions required for each element in the hydride generator itself. It was found that the stability of the signal was greatly enhanced by mixing the purge gas with water or acid before introducing the gas into the spray chamber.

THE ANALYSIS OF RARE EARTHS

Every rare earth element has at least one interference free line in the mass spectrum. However, the spectrum is further complicated by the presence of oxide peaks. The ratio of oxide to parent peak is different for each rare earth. This ratio is of the order 0.02 - 0.03 and is relatively stable (±15%). The uncertainty in the oxide correction, however, can result in severe degradation of the detection limit when the element causing the oxide interference is present in much higher concentrations than the element being corrected. Despite these limitations, ICP/MS appears to be the first spectroscopic method with the potential of analyzing the entire rare earth group with a detection limit of 1 ppm. Because of the lack of interferences from matrix, the authors concentrated their efforts on analyzing samples without the use of elaborate matrix separation procedures.

Two sample preparation procedures were tried: namely, $HF/HClO_4$ digestion and $LiBO_4$ fusions. The $LiBO_4$ fusions were abandoned because the higher dissolved solids content of these digestions required an additional 10-fold dilution of the sample. Although $HF/HClO_4$ digestion is not a universal digestion procedure for material containing rare earth elements, this procedure will be used exclusively to develop the method. Other digestion procedures will be investigated once the analytical problems as they relate to the ICP/MS have been sorted out. The digestion procedure consisted of digesting 0.5 g of the sample with 10 ml of H_2O, 10 ml of HF, and 10 ml of $HClO_4$ in a teflon beaker. The digest was taken to dense fumes of $HClO_4$. The solution was then made up to volume with water. Aliquots of the digest were spiked for standard addition and were made up to volume.

TABLE 068.3 SAMPLES DONATED BY VARIOUS ONTARIO AND QUEBEC MINING COMPANIES

Sample Location and Separation Procedure	208/206	207/206	204/206
THIERRY MINE/UMEX-MAG	2.106	0.8503	0.05727
THIERRY MINE/UMEX 0.25 AMPS	2.145	0.8486	0.05531
THIERRY MINE/UMEX 0.50 AMPS	2.020	0.8193	0.05567
THIERRY MINE/UMEX 0.75 AMPS	2.013	0.8316	0.05776
THIERRY MINE/UMEX -200 MESH	2.062	0.8396	0.05806
THIERRY MINE/UMEX +3.32 -100 +200 C.P.	2.066	0.8704	0.06556
UMEX MAG	2.035	0.8309	0.05558
UMEX 0.25 AMPS	2.003	0.8092	0.05330
UMEX 0.75 AMPS	2.024	0.8167	0.05617
UMEX -200 MESH	2.002	0.8212	0.05993
UMEX +3.32 C.P.	2.025	0.8402	0.06131
SOUTH BAY MINE/SELCO PY	2.331	1.0256	0.07003
SOUTH BAY MINE/SELCO PY	2.311	1.0116	0.07001
SOUTH BAY MINE/SELCO -200	2.338	1.0315	0.07179
SOUTH BAY MINE/SELCO +3.32 -100 +200	2.424	1.0639	0.07286
SOUTH BAY MINE/SELCO -200 MESH	2.221	1.0705	0.07541
SOUTH BAY MINE/SELCO +3.32 -100 +200	2.105	1.0699	0.07723
DOME EXPLORATION -200 MESH	2.331	1.0213	0.06858
DOME EXPLORATION -200 MESH	2.310	1.0185	0.06948
DOME EXPLORATION +3.32 -100 +200	2.365	1.0349	0.07195
THIERRY MINE/UMEX 0.75 AMPS	2.007	0.6223	0.05763
UMEX 0.25 AMPS	2.005	0.8092	0.05481
DICKENSON RED LAKE GOLD MINES 0.05 AMP	2.133	0.8872	0.06335
DICKENSON RED LAKE GOLD MINES 0.25 AMP	2.128	0.8933	0.06004
DICKENSON RED LAKE GOLD MINES 0.5 AMPS	2.161	0.9086	0.06293
DICKENSON RED LAKE GOLD MINES 1.0 AMPS	2.146	0.8985	0.06033
DICKENSON RED LAKE GOLD MINES 1.8 AMPS	2.151	0.9049	0.06032
DICKENSON RED LAKE GOLD MINES -200 MESH	2.082	0.8687	0.05885
DICKENSON RED LAKE GOLD MINES +3.32 -1	2.065	0.8530	0.05482
DICKENSON RED LAKE GOLD MINES MAG	2.274	0.9965	0.07713
DICKENSON RED LAKE GOLD MINES -200 MESH	2.169	0.9177	0.06246
DICKENSON RED LAKE GOLD MINES -100 +200	2.155	0.9081	0.06285
KERR MINE/KERR ADDISON -200 MESH	1.995	0.8454	0.06891
KERR MINE/KERR ADDISON -100 +200	2.086	0.0884	0.06785
KERR MINE SMP-2 -150 MESH	2.207	0.9458	0.06591
CAMFLO MINES PORPHYRY PY	1.755	0.7682	0.06776
CAMFLO MINES ORE DIORITE-150 MESH	1.953	0.7846	0.04975
CAMFLO WASTE DIORITE PYRR+SILICATES	2.374	1.0474	0.08471
CAMFLO WASTE DIORITE PMS-17**	2.370	1.0350	0.08343
CAMFLO WASTE DIORITE PY X	2.343	1.0225	0.07747
THIERRY MINE/UMEX -200 MESH	1.996	0.8347	0.07186
UMEX-200 MESH	1.980	0.8030	0.06259
KERR MINE/KERR ADDISON -200 MESH	1.979	0.8224	0.06427
CAMFLO WASTE DIORITE PMS-17**	2.261	0.9901	0.07415

TABLE 068.4 Pt METAL ANALYSIS OF SYNTHETIC SAMPLES*

Element	1 ppb	2 ppb	5 ppb	10 ppb	20 ppb
Ru	0.2	3.8	5.3	9.2	19.8
Rh	1.0	2.4	4.0	10.5	20.3
Pd	1.0	2.0	3.7	7.3	20.2
Re	0.7	1.9	4.4	11.3	18.9
Os	-	-	-	-	-
Ir	1.1	2.1	4.0	10.1	19.9
Pt	0.5	1.4	7.7	9.2	19.0
Au	0.7	2.1	5.5	7.1	20.0

*Solutions correspond to 25 g sample treated using the NiS collection procedure. The NiS precipitate was digested in 25 ml of aqua regia. The digest was analyzed by standard addition methods.

The final dilution factor was 100:1. Because of the large number of isotope and oxide peaks in the region, it was necessary to analyze the rare earths in two groups in order to avoid spiking with interfering species. The elements and isotopes selected for analysis for group 1 were La-139, Ce-140, Pn-141, Nd-146, Eu-153, Dx-163, Ho-165, Er-167, Yb-174, and Lu-175. Group 2 consisted of Sm-147, Gd-157, Tb-159, and Tm-169. This work was ongoing at the time of writing.

ISOTOPE DILUTION ANALYSIS

The advantage of isotope dilution analysis is that no external calibration procedure is required. The sample is simply spiked with an isotope of the element, and the change in the ratio resulting from this spike is noted. The concentration of the element in the sample can then be calculated to the same precision as the ratio was determined to have. Only the ratio is used in the calculation; thus, one does not have to be concerned with dilution problems or with long term intensity variations. As was noted in the discussion of lead isotope ratios, the isotope ratio as determined on the ELAN varies from the true isotopic ratio. Therefore, it is necessary to experimentally determine the apparent isotope ratio and relative abundance. For real samples, this may not be a trivial chore, particularly for elements such as Sn and Cd which have a number of isotopes. Frequently, a large interference on one or more of the isotopes adds a great deal of uncertainty to the calculation.

The authors have adopted the following procedure to overcome this problem when analyzing elements such as Sn and Cd for which the relative abundance of the isotopes is not expected to change. The two isotopes are selected and the isotopic ratio is determined for the sample and for the spiked sample. The isotope dilution calculation is carried out using the relative abundance determined from the sample ratio. That is, for the purpose of the calculation, it is assumed that only two isotopes exist. The result of this calculation is the concentration of the two isotopes in the sample. This concentration number is then divided by the fraction these isotopes represent of the whole to give the actual concentration in the sample.

Os AND Re ISOTOPE ANALYSIS

Some work had been done on Os and Re isotopic ratios. The sensitivity of these elements is very good, but it is unlikely that the required precision of 0.1 to 0.2% can be achieved on the ELAN in the near future. The potential of this method as a screening procedure will have to be investigated.

I AND Br ANALYSIS IN WATERS

Well and surface water samples were analyzed for Br and I. The samples were treated using the method of standard additions. The detection limit for Br was 30 ppb, for I, 5 ppb. It was noted that there was a severe memory effect for both Br and I. The majority of the memory effect was traced to the tubing in the peristaltic pump.

DISCUSSION

In the past year, ICP/MS has been applied to a number of analytical problems with varying degrees of success. Some of the problems, such as the analysis of Br and I in water and the Pt metal group, yielded readily to the instrument; others such as Pb isotope ratio and rare earth analysis did not yield as readily. It has been demonstrated that ICP/MS can deliver the accuracy necessary for screening samples for Pb isotope geochemistry, but that the more precise work must still be left for thermal ionization methods. Similarly, samples for Rh and Os ratio studies can probably be screened by ICP/MS. The successful analysis of the entire rare earth group is possible, but until the oxide problem is reduced substantially, detection limits on some of the rare earths will be poor.

In general, ICP/MS is still in its infancy. The problems outlined above are not insurmountable. A lot of the problems will become better understood as more and more users introduce real samples into the machine.

One problem which has not been discussed in the experimental section of this report is matrix effects. This is probably the most serious problem for ICP/MS. Because the signal is so sensitive to matrix, it is virtually impossible to apply a concentration calibration directly to the signal except on very dilute samples. One possible solution to this problem is

careful selection of internal standards. If internal standards can be found which mirror the elements of interest in their response to matrix, then it may be possible to do concentration calibration type analysis. This would double or triple the productivity of the ELAN.

ACKNOWLEDGMENTS

X-Ray Assay Laboratories Limited wishes to thank the Ontario Ministry of Natural Resources and the Ontario Geological Survey for their support.

REFERENCES

Douglas, D.J., Quon, E.S.K., and Smith, R.G.
1983: Elemental Analysis with an Atmospheric Pressure Plasma (MIP, ICP)/Quadrupole Mass Spectrometer System. Spectrochima Acta 38B, No. 1/2. p.39-48.

Hoffman, E.L.
1978: Unpublished Ph.D. Thesis; Department of Geology, University of Toronto.

Grant 072 A Microprocessor-based Digital Receiver Console for the DIGHEM$^{III/IV}$ System

S.J. Kilty

Dighem Surveys and Processing Inc., Toronto

ABSTRACT

In 1980, Dighem embarked on a program to re-evaluate HEM technology in order to develop hardware that would extend the resistivity mapping capabilities of the DIGHEM^{II} system. New mining and engineering applications required the use of a much broader range of frequencies than previously employed. In order to meet this requirement, the DIGHEM^{III} and DIGHEM^{IV} systems were developed to meet these demands for operating frequencies between 90 to 56 000 Hz.

In December of 1983, the microprocessor-based digital receiver project was commenced. This has resulted in a high resolution system utilizing real time spheric and filter operators to compliment the earlier EM sensor improvements. When completed, this program will result in a reliable, spheric-free, high resolution system that can be used for mineral exploration and numerous engineering applications.

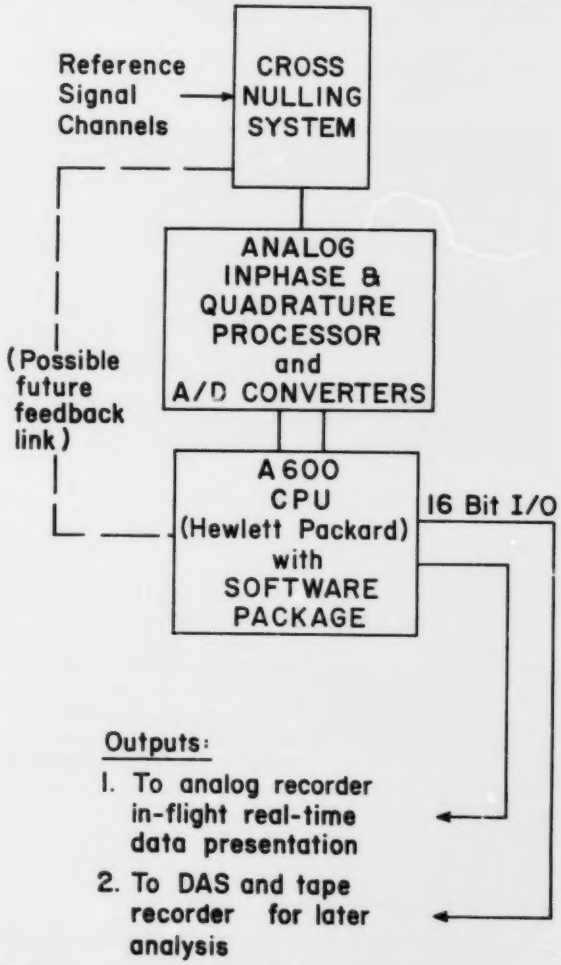
Reference Signal Channels
CROSS NULLING SYSTEM
ANALOG INPHASE & QUADRATURE PROCESSOR and A/D CONVERTERS
(Possible future feedback link)
A600 CPU (Hewlett Packard) with SOFTWARE PACKAGE
16 Bit I/O
Outputs:
1. To analog recorder in-flight real-time data presentation
2. To DAS and tape recorder for later analysis

***Figure 072.1** Receiver console package.*

INTRODUCTION

In December of 1983, Dighem commenced a research project to redesign the electronic processing section of the DIGHEM^{III} and DIGHEM^{IV} helicopter-borne electromagnetic systems. The benefits derived from this project were envisioned to be:

1. improved signal-to-noise ratio resulting in increased depth of exploration
2. increased resolution to allow the system response to be more interpretable in terms of conductor shape and orientation
3. improved ease of operation
4. increased reliability
5. increased system stability for better definition of zero levels

It was decided that the optimum means of providing these benefits was to design a digital receiver console which would perform a series of functions in real time to provide the desired benefits. The design consists of an analog front end, which performs basic signal processing, followed by a microprocessor providing real time data processing.

HARDWARE DESCRIPTION

Figure 072.1 illustrates the digital receiver configuration. The basic unit consists of an integrated analog processor/primary nulling system and a Hewlett-Packard 1000, A600 series microcomputer. The analog front end is a custom designed unit manufactured by Dighem and the A600 is readily available from Hewlett-Packard agents worldwide. This combination allows for easy servicing and repair of the hardware under field conditions.

ANALOG FRONT END

The analog section of the digital receiver project was designed in a modular fashion to allow for greater flexibility in a simplified design. The analog console contains an EM module for each frequency, a transmitter control unit, and a system monitor (Photo 072.1). This packaging provides a direct link between the bird signal and the processing module, thus eliminating any possibility of the signal being affected by electromagnetic radiation as it passes through intermediate buffering.

The EM modules (Photos 072.2 and 072.3) have been redesigned with extensive use of large scale integration technology, especially with regard to the frequency dependent components. Care was taken to ensure that the system would be reliable and easy to use over a long period of time under harsh field conditions.

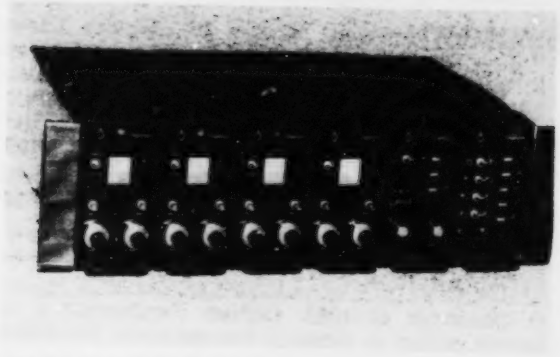

Photo 072.1 Analog console.

Photo 072.2 Analog module (front view).

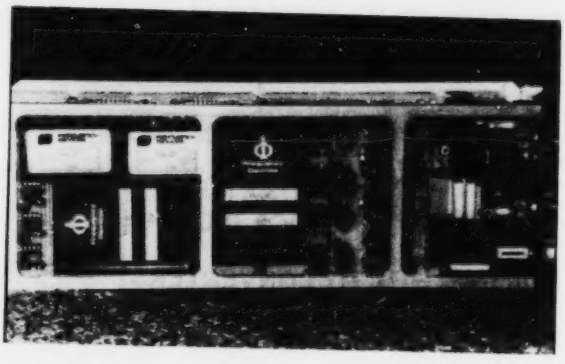

Photo 072.3 Analog module (side view).

The most important changes in this design involve the rise-time and the data output of the module.

Filtering within the module has been reduced from present industry rise-time standards of 0.1 to 0.5 seconds to 0.04 seconds. This rapid rise-time allows the resolution of short time events such as atmospherics and increases the definition of high frequency responses. This increased sensitivity provides improved resolution with regard to bedrock anomaly definition.

Output of the modules includes two additional channels to monitor gain and phase of the primary field. These are used for real time control of long term drift. The primary field signal gain at the transmitter is monitored to detect any changes in the dipole moment due to small changes in current in the transmitter coil. The phase signal is monitored to measure any possible phase drift. Control of both gain and phase provides a far more stable output allowing more accurate and reliable calculation of resistivity values.

THE DIGITAL PROCESSOR

All six outputs from each module are transferred directly to a Hewlett-Packard 1000 microprocessor (Photo 072.4) via a 16 bit A/D converter at a sample rate of 100 Hz.

The digital operations performed on the data can be broken into three basic modes: calibration, survey, and filter definition.

The first is the **calibration mode** where the electromagnetic base level and the system calibration (that is, millivolts-to-ppm conversion) is carried out. Also, during this time period, the processor provides statistical information on the amount of spheric activity.

In the **survey mode**, the receiver is acquiring and processing the raw inphase, quadrature, and primary field signals from the analog modules. At this point, several operators are applied to the data.

First, one second of incoming data from each of the 16 inputs is stored in a buffer for a total of 1600 data points. The eight basic EM channels (inphase and quadrature from four coil-pairs) are first examined for spheric activity. Figure 072.2 illustrates a typical spheric after passing through the analog module. The 100 Hz sample rate allows the seven millisecond wide pulse to be readily recognized and subsequently chopped. Following this, the EM channels are passed through an 81-point digital filter to remove unwanted high frequency content in the signal. Next, signal amplitudes are normalized relative to the primary field strength. This latter correction removes any long term drift caused by fluctuations in the dipole moment. Because the unwanted high frequency content is eliminated by the filter, the spheric-free data may be compressed. Compression of the 100 points per second yields an output of 5 points per second, and these are sent to the recording devices. This data is recorded on magnetic tape and also displayed on a digital graphics plotter. This output is the normal field product.

The **filter definition mode** allows modifications to the spheric rejection and filter operators. Here, it is possible to modify the real-time filtering. It is anticipated that some changes will be made to filter

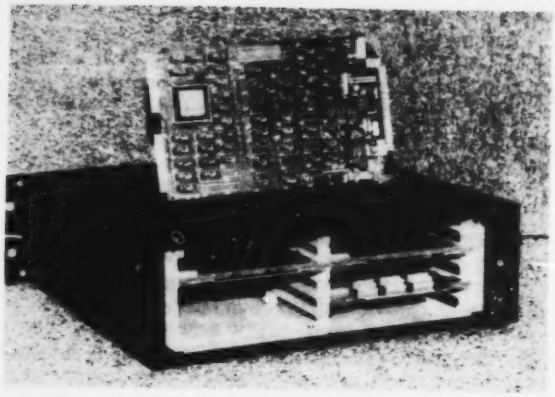

Photo 072.4 *The A600 microprocessor.*

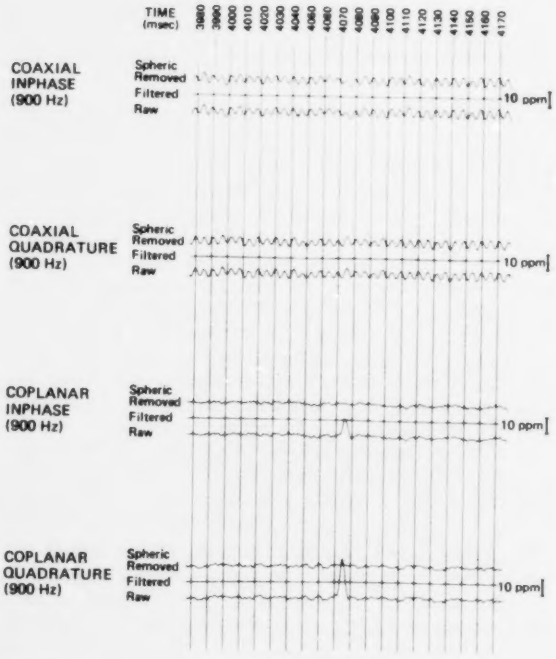
TIME (msec)
3980 3990 4000 4010 4020 4030 4040 4050 4060 4070 4080 4090 4100 4110 4120 4130 4140 4150 4160 4170
COAXIAL INPHASE (900 Hz)
COAXIAL QUADRATURE (900 Hz)
COPLANAR INPHASE (900 Hz)
COPLANAR QUADRATURE (900 Hz)
Spheric Removed
Filtered
Raw
10 ppm

Figure 072.2 *Spheric filtering.*

routines as experience is gained when utilizing the system under survey conditions.

NIGHT HAWK LAKE EXAMPLE

Figure 072.3 shows the output of the digital receiver over the Night Hawk Lake geophysical test site. Illustrated here are four of the eight EM channels of the DIGHEM[IV] system. These channels are the inphase and quadrature responses from the coaxial and coplanar coil-pairs operating at approximately 900 Hz. This profile shows the 100 Hz unfiltered raw data, the raw data with response from spherics clipped, and

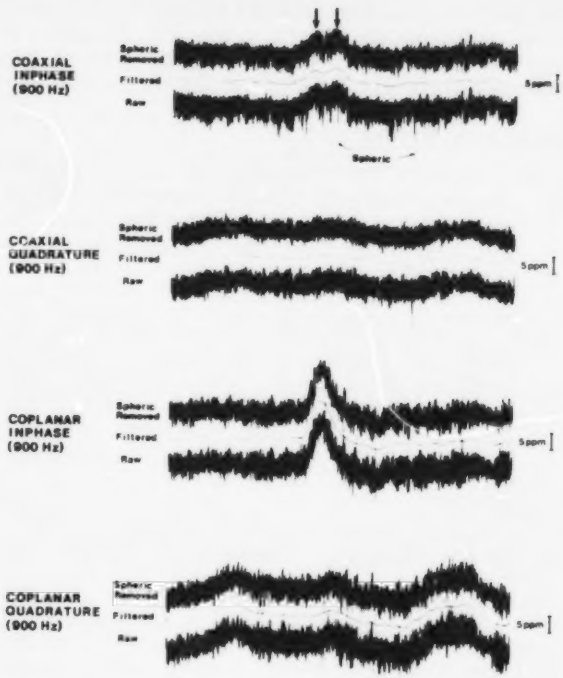

Figure 072.3 *Digital receiver response over the Night Hawk Lake test site.*

the final data after application of a filter operator for each of the four data channels.

The high frequency noise seen here is typical of EM data acquired with a fast rise-time, and includes beating at approximately 900 Hz on the two orthogonal coil-pairs. This noise is readily removed by digital filtering because its wavelength is considerably shorter than that of the desired signal. Of particular interest on this profile is the well defined double peak on the coaxial inphase channel over the Night Hawk Lake conductor and the ability to remove spherics without altering the shape of the anomaly.

DISCUSSION AND CONCLUSIONS

The majority of desired benefits expected to be derived from the digital receiver have been achieved. Figure 072.7 illustrates the improved signal-to-noise and increased resolution of the system. Improved ease of operation, reliability, and increased stability can only be judged after extensive experience with the system has been obtained.

Extensive field trials will be carried out over the summer of 1985 to ensure the integrity of the data and to provide examples of system response over a number of varying situations. If necessary, filter parameters will be altered utilizing the filter parameter mode. Data acquired during this process will be evaluated and, if necessary, modifications may be made to the processing hardware.

The DIGHEM digital receiver package is at present being evaluated by several foreign operators of HEM equipment. This will lead to export sales if they

decide to upgrade their present hardware to the new level of technology offered in this unit. In addition, Dighem expects to begin utilizing this system for commercial surveys in Canada in the fall of 1985.

ACKNOWLEDGMENTS

Dighem Surveys and Processing Inc. wishes to thank the Ontario Ministry of Natural Resources and the Ontario Geological Survey for their support.

SELECTED REFERENCES

Barlow, R.B.

1981: Night Hawk Geophysical Test Range Results Using Two Electromagnetic Systems, District of Cochrane; p.152-159 *in* Summary of Field Work, 1981, by the Ontario Geological Survey, edited by John Wood, O.L. White, R.B. Barlow, and A.C. Colvine, Ontario Geological Survey, Miscellaneous Paper 100, 225p.

Fraser, D.C.

1972: A New Multicoil Aerial Electromagnetic Prospecting System; Geophysics, Volume 27, p.518-537.

1973: Magnetite Ore Tonnage Estimates from an Aerial Electromagnetic Survey; Geoexploration, Volume 11, p.97-106.

1978: Resistivity Mapping with an Airborne Multicoil Electromagnetic System; Geophysics, Volume 43, p.144-172.

1979: The Multicoil II Airborne Electromagnetic System; Geophysics, Volume 44, p.1367-1394.

Kilty, S.J.

1983: Grant 025 The Development of an Omni-Directional Multi-Frequency Airborne EM System; p.99-105 *in* Exploration Technology Development Program of the Board of Industrial Leadership and Development, Summary of Research 1981-1983, edited by E.G. Pye and R.B. Barlow, Ontario Geological Survey, Miscellaneous Paper 115, 135p. Accompanied by 2 charts.

1984: Grant 072 Microprocessor-Based Digital Receiver Console for the DIGHEM$^{III/IV}$ Helicopter Airborne Electromagnetic System; p.173-176 *in* Exploration Technology Development Program of the Board of Industrial Leadership and Development, Summary of Research 1983-1984, edited by V.G. Milne and R.B. Barlow, Ontario Geological Survey, Miscellaneous Paper 120, 176p.

Grant 077 Development of a Field Portable Instrument for Semi-quantitative Mineral Determination in Geological Materials

M. Shats, D.R. Gladwell, and M. Danczlger

Barringer Research Limited, Rexdale

ABSTRACT

A compact, field portable system has been designed to determine abundances of clay minerals in geological materials based on the measurement of reflected light intensity. The system comprises a Barringer Hand Held Ratioing Radiometer (HHRR) interfaced with an EPSON HX-20 microcomputer which performs reflectance data acquisitions, manipulation, storage, and display of the final results. The interface also contains an analog to digital converter and an arithmetic processing unit (APU) necessary to rapidly perform calculations involved in the deconvolution of clay mineral spectra. Tests of the deconvolution algorithm software on reflectance data generated from rock samples from an Au deposit have demonstrated that variations in clay alteration mineral content can be detected and mapped.

INTRODUCTION

In 1982, a research project was initiated by Barringer Magenta to investigate the potential of reflectance radiometry as a rapid, semi-quantitative method for alteration mineral analysis. This technique is based on recognizing overtone and fundamental Al-O-H molecular vibrational absorption features characteristic of clay minerals (kaolinite, montmorillonite, illite, muscovite, chlorite, biotite) in the 2.2 and 2.65 to 2.8 micron region of the spectrum. During preliminary investigations (Gladwell 1984), the intensity of clay diagnostic absorption features was measured using narrow band interference filters installed in the Barringer Hand Held Ratioing Radiometer (HHRR) and also with a prototype scanning spectrometer comprising the Barringer HHRR as a detector and a modified Jarrell-Ash monochromator.

Following a series of tests with these instruments to establish instrumental error, effects of sample humidity, and effects of interfering minerals, an algorithm was developed to deconvolute component spectra of clay minerals based on reflectance measurements at 1.86, 1.9, 2.65, 2.68, 2.71, 2.73, 2.75, and 2.77 microns. The deconvolution algorithm involved firstly, mathematical matching of mixed pure mineral spectra with sample spectra; secondly, the selection of best fit spectra (minimum of five) and calculation of weighted averages of those minerals producing the mixed spectra; and thirdly, adjustment of the first estimates of mineral composition using empirical selection rules to minimize known spectral interferences. The selection rules decided whether smectite, illite, muscovite, or a mixed layer illite - smectite is present in a sample with either kaolinite or biotite and/or chlorite. Analysis of 53 rock and soil samples by the technique demonstrated a good comparison between results obtained by the reflectance method and data generated using quantitative x-ray diffraction. Samples containing >10% (XRD measured) of the mineral groups: (a) kaolinite / biotite, (b) smectite, muscovite, illite, and (c) chlorite were correctly classified in 94% of determinations. The mean error of mineral abundance estimation was <30% absolute. Errors in the technique were attributed to variations in calibration and sample mineral spectra caused by differences in sample matrix, measurement errors (generally <4%), errors in X-ray diffraction data (especially where HHRR modal percent values are compared to XRD weight percent values), changes in ambient humidity, and errors in background spectra.

PROJECT OBJECTIVE

The object of the program is to interface a Barringer Hand Held Ratioing Radiometer (HHRR) to a portable battery powered microcomputer (the EPSON HX-20) for the purpose of reflectance data recording and calculation of clay mineral (kaolinite, muscovite, smectite, illite, chlorite) content of geological materials using an algorithm developed by a previous ETDF project conducted by Barringer Research's sister company, Barringer Magenta.

REFLECTANCE MEASUREMENTS UNDER FIELD CONDITIONS

Before the conceptual design of the HHRR-EPSON HX-20 system was initiated, the performance of the HHRR in the 2.6 to 2.8 micrometer region was tested.

The HHRR is not normally used in this spectral region and the previous ETDF grant obtained results using a laboratory, modified version of the HHRR which utilizes two diffraction gratings to obtain reflectance data. The first part of the research, therefore, compared flux and noise levels obtained under field conditions and using optical interference filters with those obtained under laboratory conditions.

The objective of these field tests was to ensure that measurable reflectance data values may be obtained using an HHRR with suitable fore optics, a 10 volt tungsten halogen light source, and optical interference filters in the 1.8 and 2.7 micrometer wavelength regions. Definition of expected noise levels under these conditions was also an important part of the experiment. The experiment consisted of measuring radiance data at 1.86, 1.9, 2.65, 2.71, 2.73, 2.75, and 2.77 micrometers on clay mineral reference standards illuminated with a 10 v, 250 w, quartz envelope, tungsten halogen source. Results for montmorillonite (STX-1) and kaolinite (KGa-2) are presented in Table 077.1. The results show that adequate signals are obtained under field conditions in the above wavelength range. The noise at these wavelengths varied from 0.001 to 0.005 volts, values which are comparable to those obtained under laboratory conditions.

TABLE 077.1 RADIANCE (VOLTS) DATA OBTAINED UNDER FIELD CONDITIONS WITH TUNGSTEN HALOGEN LIGHT SOURCE ON MONTMORILLONITE (STX-1) AND KAOLINITE (KGa-2)

Centre Wavelength (micrometers)	Bandpass (nm)	Radiance *(volts) for: STX-1	KGa-2
1.86	30	.435	.507
1.90	30	.476	.753
2.65	25	.105	.086
2.71	25	.042	.018
2.73	25	.029	.015
2.75	25	.029	.017
2.77	25	.030	.022

* HHRR gain setting at lowest integral value (1)

SYSTEM DESIGN AND DEVELOPMENT

System components are shown in Figure 077.1 and in Photo 077.1. Illuminating radiation reflected from the target is accepted by the Hand Held Ratioing Radiometer (HHRR Mk II) which measures the target's reflectance at wavelengths in the 1.86 to 1.9 and 2.65 to 2.8 micron wavelength region using appropriate interference filters. Analog values proportional to each of the reflectances are converted into the corresponding digital signals in the analog to digital converter (A/D) and stored in the memory of the EPSON HX-20 microcomputer. From these data, six ratios are processed through an algorithm which outputs deconvoluted mineral ratios. The deconvoluted mineral ratios are proportional to the modal percent of each mineral present in the sample. Final results indicating percentage of each mineral in the sample are stored on the magnetic tape and printed out.

The basic instrument for the reflectance measurement is the Barringer Hand Held Reflectance Radiometer previously described in detail by Daubner *et al.* (1981) and Gladwell (1984). Modifications to the instrument have been carried out in the areas of opto-mechanics and signal processing electronics to enable: a) efficient operation in the 2.6 to 2.82 micron region; b) measurement of relatively small samples (such as drill cores) at short distances; c) digital recording of data; d) real-time processing and printing of results. A removable optical attachment for the front optics of HHRR which will collect reflected radiation from targets about 15 mm in diameter has been designed and fabricated. Furthermore, the ratio range of HHRR signal processing electronics has been extended by 10-fold in order to reliably process weak signals in the 2.6 to 2.82 micron region obtained with narrow band pass optical filters.

Spectral data acquisition, manipulation, storage, and transmission is performed by the EPSON HX-20 microcomputer via an analog to digital converter and additional expansion adapter, containing a floating point arithmetic processor. An operator interface feature allows rapid and simple data collection.

The EPSON HX-20 is a CMOS portable computer featuring built-in rechargeable batteries, file and data storage facilities, and a liquid crystal display. An interface to enable transfer of signals from the HHRR to the EPSON HX-20 and an Arithmetic Processing Unit (APU) was designed and a prototype was manufactured.

The purpose of the APU is to rapidly perform arithmetic calculations that would take significantly longer to perform on the HX-20 computer itself. The algorithm involves performing approximately 18 000 additions, 19 000 subtractions, and 27 000 multiplications. Tests were done with the HX-20 computer and its floating point software routines. Following a review of specifications of available APU's, an Advanced Micro Device's AM 9511 A APU was selected and obtained. This APU was found to be the only device capable of the high speed arithmetic necessary for efficient data processing. The AM 9511 A, operating at 3 MHz, is capable of performing all of the required calculations significantly faster than the HX-20 alone. An expansion unit obtained for the HX-20 provides additional memory and a physical location for the APU and analog-to-digital converter (ADC) necessary to input raw reflectance data from the HHRR to the EPSON HX-20. In addition to the construction of the prototype electronic components, instrument packaging and peripheral components (core viewing attachment, light source), 6301 assembly language software has been coded for the ADC and APU controllers using an Osborne microcomputer with a 6301 cross assembler. Coding of the clay mineral algorithm itself into assembly language, loading of the coded algorithm onto an integrated circuit, and development of BASIC software for the operator interface was still in progress at the end of the project period.

Actual operation of the completed system would involve initial selection of appropriate filter pairs on the HHRR for reflectance measurements. The operator would press a key on the EPSON HX-20 to signal that data was ready and when all five sample ratios have been acquired, the computer would start execution of the clay mineral composition algorithm. When the algorithm concludes, execution control would be passed to BASIC which would be responsible for all data formatting and storage.

For each acquisition cycle, a data record would be written on magnetic tape in the following format:

DATE TIME RAW RATIOS ANALYSIS RESULTS

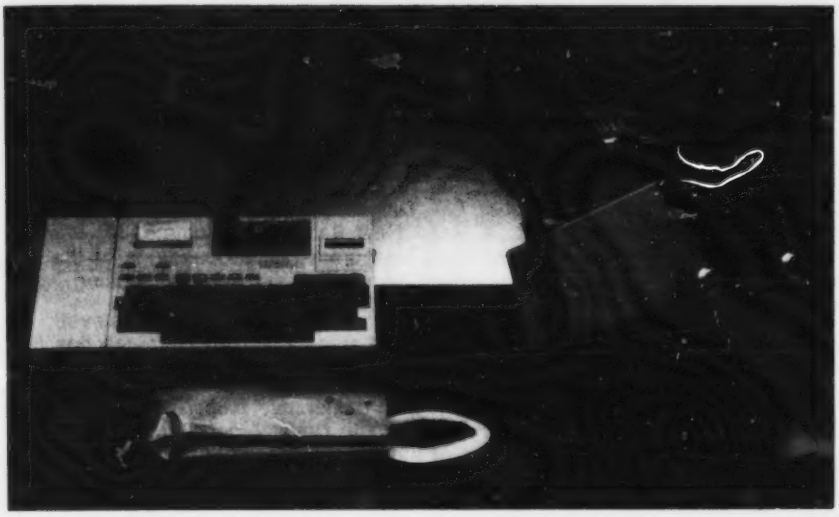

Photo 077.1 *Field portable instrument.*

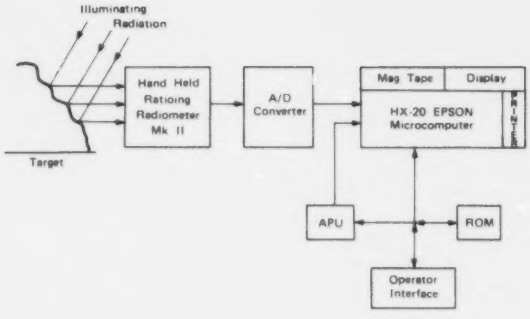

Figure 077.1 *System block diagram.*

All or part of the data could be optionally listed on the printer. Data on the tape could be played back for further analysis and/or transmission to another (larger) computer system for further processing or long term storage.

SOFTWARE APPLICATIONS TESTING

Preliminary tests designed to test the application of the clay mineral composition software are described by Gladwell (1984). A detailed study has also been made of clay mineral variations in a suite of rocks from the Horse Canyon, Nevada, epigenetic Au deposit (Gladwell *et al.* 1985). At Horse Canyon, micron-sized Au grains are associated with clay altered rocks of the Roberts Mountain thrust in contact with the Ordovician Vinini Formation and the Devonian Wenban limestone. Rock samples from locations over the thrust zone above the main ore zone were analyzed for clay mineral content by the reflectance technique and by x-ray diffraction. Samples were also analyzed for aluminium and calcium oxide by HF - HNO_3 - $HClO_4$ acid digestion - inductively coupled argon plasma emission spectroscopy. High reflectance ratios and contents of Al and Ca over fault zones (Figure 077.2) suggest the development of clay alteration minerals associated with these structures. Illite/muscovite and kaolinite abundances calculated from the raw reflectance data by the algorithm demonstrate higher clay mineral content in the thrust zone compared to values beyond the limits of the zone (Figure 077.3). Muscovite / illite demonstrate a significant increase over the ore zone, whereas kaolinite / biotite show a slight increase within the thrust zone, but outside the ore zone. The XRD data correlate with abundances determined by the clay mineral algorithm and indicate that illite is the primary clay mineral present.

CONCLUSIONS AND FUTURE PLANS

During the program, all hardware and the majority of software components necessary to implement the clay mineral analytical system based on reflectance analysis were completed. Several tests designed to compare semiquantitative data generated by both reflectance and XRD techniques have been successfully carried out and these have demonstrated significant variations of alteration minerals across one Au deposit. However, further software development will be necessary before the system is fully operational.

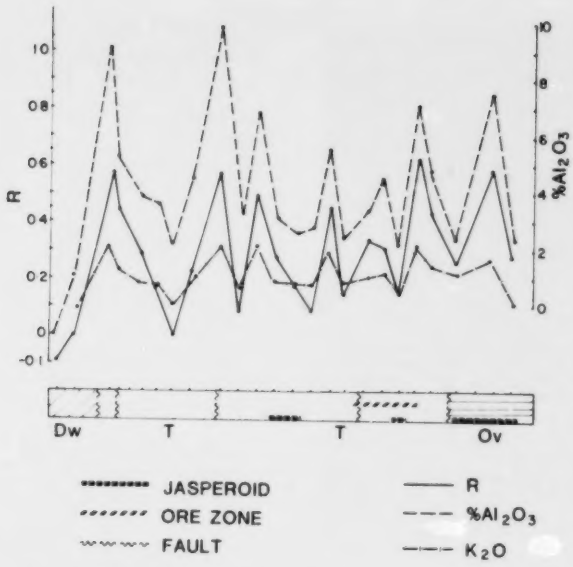

Figure 077.2 *Horse Canyon, comparison of the reflectance ratio 2.65/2.75 micrometers (R) with Al_2O_3 geochemistry.*

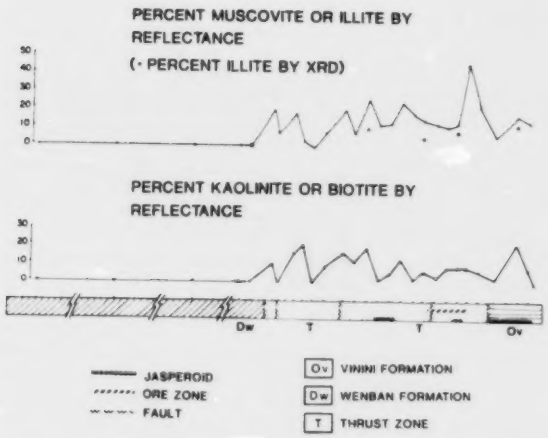

Figure 077.3 *Horse Canyon, distribution of reflectance determined illite/muscovite and kaolinite/biotite.*

ACKNOWLEDGMENTS

The authors are grateful to the Ontario Ministry of Natural Resources for financial support during this project and to Placer Development for assistance in sample collection and data acquisition.

REFERENCES

Daubner, L.R., Davies, J.H., and Goetz, A.
1981: A Hand Held Ratioing Radiometer for Remote Radiance Measurements; Proceedings of the 7th Canadian Symposium on Remote Sensing, Winnipeg, p.423-428.

Gladwell, D.R.
1984: The Application of Reflectance Radiometry of Semiquantitative Alteration Mineral Determination in Geological Materials; p.69-76 *in* Exploration and Technology Development Program of the Board of Industrial Leadership and Development, Summary of Research 1983-1984, edited by V.G. Milne and R.B. Barlow, Ontario Geological Survey, Miscellaneous Paper 120, 176p.

Gladwell, D.R., Lawrence, P., and Dancziger, M.
1985: The Application of Rapid, Semi-quantitative Clay Mineral Determination at the Cortez Gold Mine, Nevada; Society of Mining Engineers of AIME, Preprint No. 85.5.

Grant 079 Seismic Full Waveform Logging and Seismic Geotomography

J. Wong

JODEX Applied Geoscience Limited, Toronto

ABSTRACT

Seismic geotomography is a method for imaging subsurface geology using seismic data obtained in a borehole-to-borehole configuration. Practical implementation of the technique involves several major tasks:

1. developing reliable technology for transmitting and detecting seismic signals between boreholes 100 to 300 m apart
2. devising computer algorithms for efficiently condensing and displaying the information contained in crosshole seismic scans
3. performing case studies with the method in order to explore the potentialities as well as the limitations of its use in assisting detailed subsurface mapping

To meet the above objectives, two related seismic systems are being developed. The first is a crosshole seismic scanner consisting of a high-power transmitter and a multi-detector seismic receiver. This system will use continuous-wave transmission and cross-correlation to enable recording of high-frequency seismograms between deep boreholes with separations of at least 100 m. The second system is a full-waveform seismic logger, the purpose of which is to enable observation of both P and S waves in rock in the immediate vicinity of a single borehole. The P and S velocities (or related parameters such as the dynamic elastic moduli) can be compared to core logs, providing fundamental information on rock elastic properties on which to assess the geological significance of crosshole seismic data. In addition to the hardware development, computer software is being coded both for instrumentation control and for imaging and displaying maps of subsurface seismic properties. The imaging algorithms will be based on well-founded principles used in medical tomography. Once the hardware and software developments are completed to the point of being usable for surveying, test cases will be done in a variety of exploration and engineering environments in order to thoroughly evaluate seismic geotomography as a useful and economically viable geophysical technique.

INTRODUCTION

Core logging and standard geophysical logging of boreholes provide information regarding lithologies and structural features deep within a rock mass. However, they both have the limitation of restricted zones of investigation so that the rock more than a few metres from the boreholes is largely unsampled. Recently, electromagnetic and electrical techniques have been developed using surface and downhole instrumentation to greatly extend the radius of investigation in the search for conductive massive orebodies when there are significant conductivity contrasts between the target and host rock. In many other geological situations, such conductivity contrasts do not exist, and variations in some other physical property must be exploited for remote assessment of geological conditions. A highly suitable alternative is the variation in elastic and mechanical properties of rock as indicated by the velocities and attenuation of seismic waves.

Seismic reflection techniques have been used with great success in hydrocarbon mineral exploration, where the interesting geological features lie in deep, stratified sedimentary sequences. Penetration of seismic energy thousands of metres into the earth is made possible by using low-frequency (1 to 30 Hz) seismic waves, which, despite their long wavelengths, can adequately resolve oil and gas traps hundreds of metres in scale. In mining exploration or engineering projects in crystalline rock, the important geological details may lie within 300 m of the surface where resolution of features tens of metres in size is often required. Such resolution means that the seismic waves must have frequencies of hundreds of Hertz or higher. Unfortunately, these high frequencies are strongly dissipated by the top 50 m or so of severely weathered and altered rock. In addition, stratification is not a dominant condition in crystalline rock, so that one is never sure that coherent reflection and refraction from deep-seated targets will occur. These factors act against the technical and economic effectiveness in hardrock environments of traditional surface seismic techniques, which consequently have never been widely used for base-metal exploration.

However, a crosshole seismic method, shown schematically in Figure 079.1, which scans the rock between two boreholes could overcome most of the limitations associated with surface techniques. A seismic transmitter is fixed at a given depth in one borehole, and seismograms are recorded for many positions of seismic detectors in a second borehole. This procedure results in a fan of seismograms, and if many such fans are generated with different transmitter positions, the section of rock between the two boreholes would be scanned systematically by a dense network of many seismic raypaths. Crosshole seismic scanning operates in the transmission mode, and does not depend on coherent reflections or refractions for useful results. It operates beneath the overburden and weathered zone, so that high-frequency (up to 2 kHz) seismic waves having sharp resolving power can be used without complete loss of signal through attenuation.

The rationale for scanning a section of rock between two boreholes as depicted in Figure 079.1 is quite simple. If the rock is relatively homogeneous, then both the travel times and amplitudes of the first arrivals will be predictable and systematic. Suppose, however, that there is a structure such as an orebody, a fracture, or an alteration zone with a significant difference in seismic impedance compared to the host rock. Such seismic impedance contrasts can

be caused by large differences in density, mechanical strength, or seismic velocities. The crosshole seismic scans should indicate the existence of these differences (even though neither borehole intersects the structure) through unexpected variations in arrival times. As well, unexpected decreases in signal amplitudes will occur because only a fraction of the seismic energy incident on a boundary of seismic impedance will penetrate through to reach the detectors. Thus, a seismic inhomogeneity will cast a "seismic shadow". Not only will the existence of a seismic inhomogeneity be revealed by the crosshole data, but also, under favourable conditions, its location within the rock section can be determined fairly accurately.

The interpretation of travel times and amplitudes for a crosshole scan of many rays is best done by tomographic imaging techniques. Computer assisted tomography (CAT) has been used extensively in medical biophysics to obtain images of the internal structure of various parts of the human body (Brooks and Di Chiro 1976; Herman and Rowland 1973). The mathematical concepts and numerical algorithms for image reconstruction have been adapted to process geophysical data scans (Bois *et al.* 1972; Lytle and Dines 1980; Daily *et al.* 1982; Wong *et al.* 1983, 1984). Thus, it is possible to create images or maps of the geological structure between two boreholes via CAT processing of first arrival times or amplitudes from a crosshole seismic scan. The procedure beginning with crosshole seismic surveying in the field and ending with image reconstruction using CAT algorithms may be called seismic geotomography.

Because of its importance to the hydrocarbon industry, there exists a great deal of theoretical and experimental information regarding the seismic properties of sedimentary rocks. On the other hand, a paucity of data exists on the seismic properties of crystalline rocks and ores related to geological engineering and base-metal exploration. In those relatively rare instances where laboratory measurements of seismic velocities or attenuation coefficients are made on cored samples, the small physical sizes of cores dictate that ultrasonic frequencies tens of kiloHertz and higher must be used. These frequencies are far beyond practical seismic frequencies, so that some question exists about the validity of relating the laboratory measurements directly to survey observations. Fundamental information concerning the seismic properties of rocks are essential for the proper geological interpretation of seismic geotomographs, but the measurement of these properties should be made using audiofrequencies and without drastic stress relief in the rocks being studied.

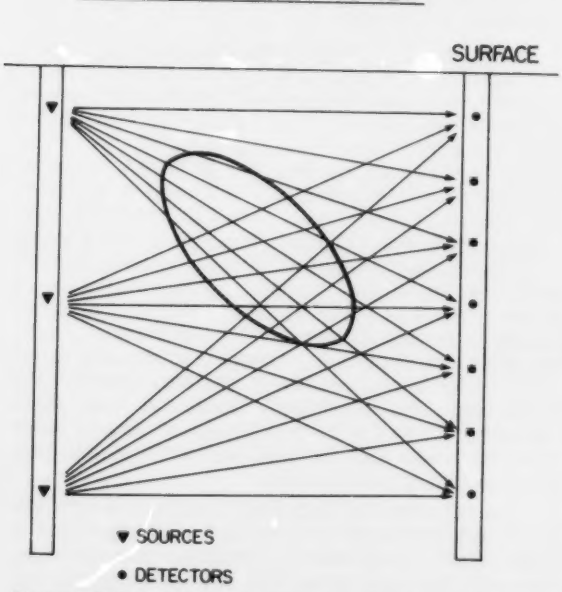

***Figure 079.1** Schematic diagram showing field procedure for crosshole seismic scanning between two boreholes.*

The most convenient way of doing this is to obtain the seismic properties within existing boreholes, where the proper frequencies can be used, the rock is relatively undisturbed, and correlations with other parameters, both physical and geological, can be drawn. For this purpose, a full waveform seismic logger is being developed for operation in 36 mm or larger diameter holes to provide *in situ* seismic properties. Unlike the common sonic logger, a full waveform logging device has the capability of yielding S wave as well as P wave velocities. Cycle skipping is not a problem because the full waveform of a seismic train is digitized and recorded. The full waveform seismic logs would be a valuable addition to standard geophysical logs, and they would provide the rock properties data required for reliable geological assessment of seismic geotomographs. The P and S wave velocities obtained from full waveform logs can be used to infer the dynamic elastic moduli of the rock along boreholes. These apparent elastic moduli have geological significance since they are related to rock strength, alteration, or degree of microfracturing. Paillet and White (1982) have described the use of full waveform logging in investigations of fracturing in crystalline rock, and Asten (1983) has reported on the geotechnical applications to coal deposit development of elastic moduli estimated from sonic logs.

DESCRIPTION OF INSTRUMENTATION

CROSSHOLE SEISMIC SCANNER

Design concepts for a prototype crosshole seismic scanner were defined in a research project carried out at the University of Toronto Department of Physics Geophysics Laboratory (Wong *et al.* 1983). The present ETDF project uses extensions and modifications of these concepts, and is orientated towards producing an optimized system suitable for commercial purposes.

Figure 079.2 shows the seismic scanner under development. The system consists of a transmitting sonde and up to eight detector sondes together with uphole and downhole electronics modules, cables, winches, motor generators, and a digital data acquisition subsystem based on a desktop computer. For good resolving power, the operating seismic frequen-

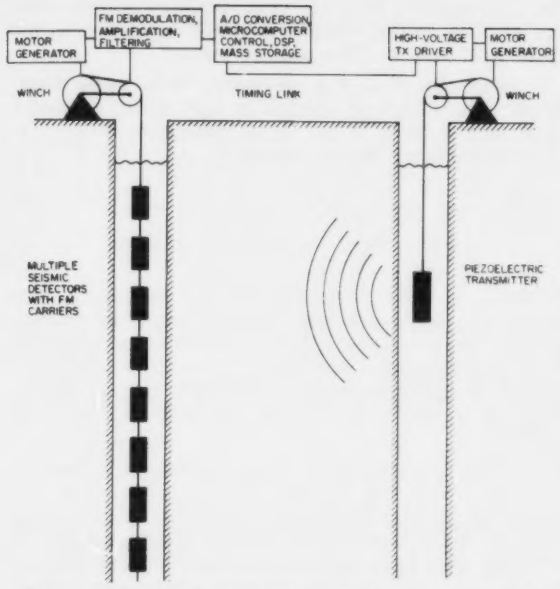

Figure 079.2 Function blocks and component subsystems of the crosshole seismic scanner.

cies will be relatively high, in the range of 500 to 2000 Hz. With these frequencies, the scanner is expected to give good seismograms for crosshole distances of 100 to 300 m depending on the rock quality. The downhole probes are designed to enter 76 mm or larger diameter boreholes, with operating depths initially targeted to be up to 500 m in water-filled holes. The uphole instrumentation and support equipment will require a semi-controlled environment such as a covered truck or a tent.

Both the transmitter and the detectors employ piezoelectric ceramics to generate and detect seismic waves because they are easily controlled, acoustically well-matched to solid rock, and are fairly efficient in converting electrical energy to mechanical energy and *vice versa*.

The transmitter is a single downhole sonde on a four-conductor cable. It converts high-voltage pulses or time-varying signals into vibratory mechanical energy, that is, seismic waves. The receiver uses up to eight high-sensitivity hydrophone/accelerometer detectors on a single four-conductor cable. The multiple-detector configuration results in a large gain in operational efficiency during surveying. The spacing between detectors can vary, but the standard separation is 5 m. Each downhole detector sonde holds piezoelectric transducers coupled to a preamplifier whose output modulates an FM carrier in the 2 to 8 MHz range. With this FM multiplexing, all eight detector signals can be carried uphole using only a single conductor, thus decreasing cable weight and cost and increasing system portability. The carrier frequencies are separated by tuned circuits in the uphole electronics and then demodulated to yield the original audiofrequency seismic signals for each of the eight detector probes. After amplification and filtering, these are then digitized every 100 microseconds with 8-bit accuracy. Dynamic range and signal-to-noise ratios can be increased by stacking and averaging up to 1024 repeated waveforms. Synchronization for digitizing and stacking between the transmitter and the receiver is provided by a hardwire timing link.

A wide variety of waveforms can be used to drive the piezoelectric transmitter. However, we choose to drive the transmitter with swept-frequency chirps or pseudo-random binary sequences (PRBS) and obtain seismograms from the detected signals through cross-correlation in order to take advantage of the large gains in signal-to-noise ratios made possible by this method. The chirp and PRBS are continuous wave signals having the property that their autocorrelations are impulse-like functions. The impulse response of any linear system can be estimated by driving the system with a chirp or PRBS, and cross-correlating the output with the chirp or PRBS. This is a well-known method for studying the transfer functions of linear systems (Foster and Sloan 1972). For crosshole seismic scanning, the linear system under study is the rock between boreholes, while the impulse response functions are the seismograms (modified by the mechanical and electronic behaviour of the transmitter and receiver). The large enhancements of signal over noise resulting from cross-correlation makes it possible to keep the peak acoustic power being generated low enough to ensure no damage to boreholes and still obtain clear seismograms across transmitter-detector separations of 100 m and more.

In order to handle the large data volumes inherent in detailed seismic surveys and to perform computations such as stacking and cross-correlation, the crosshole seismic scanner must have fast digital computing power dedicated for its use. This is provided by interfacing a Tandy 2000 16-bit desktop computer to the receiver electronics. The computer has an operating frequency of 8 MHz and internal RAM of 256 kilobytes. Mass storage for data archiving is available on built-in hard and floppy disk drives. The computer is programmed to control the digitization, stacking, and storage of the raw, uncorrelated data. As well, machine-code software for cross-correlation immediately after data acquisition provides selected seismograms in CRT or hard copy graphical display for on-site monitoring of data quality during surveying. Configured in this way with the proper peripheral and software support, the desktop computer serves as a powerful self-contained data acquisition/processing/interpretation subsystem for the crosshole scanner. However, in many cases, it will be much more efficient to transfer the large volumes of raw data to faster mini- or mainframe computers for cross-correlation and other post-survey processing.

FULL WAVEFORM SEISMIC LOGGER

Figure 079.3 shows the components which make up the full waveform seismic logger being designed and built under the present project. The instrumentation consists of a piezoelectric transmitter and three detectors attached to a single multiconductor cable. When the string of probes is suspended in a water-

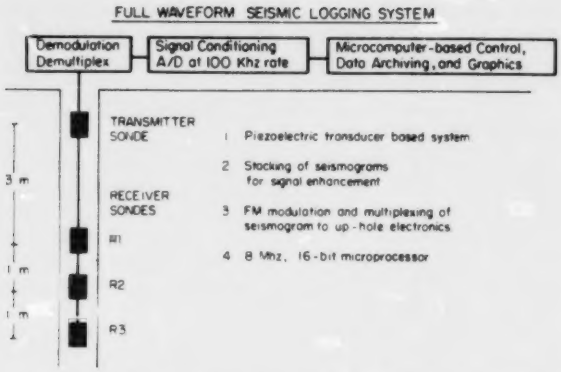

Figure 079.3 *Function blocks and component subsystems of the full waveform seismic logger.*

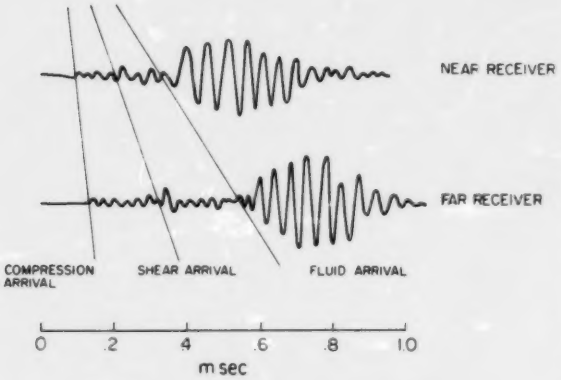

Figure 079.4 *Examples of multi-detector full waveform seismic log indicating the different moveout rates of P waves, S waves, and fluid arrivals such as guided modes or tube waves.*

filled borehole, the transmitter produces seismic pulses which penetrate into the rock as P and S waves. They propagate toward the detectors and arrive with times determined by the transmitter-detector separations and the wave velocities. The full waveforms of the seismic signals at the detectors are digitally recorded and plotted for many positions along the borehole. It is in principle possible to identify the P and S waves in each seismogram and determine the respective velocities from the travel times and probe separations. Identifying the P arrival poses no problem since it is the first energy reaching the detector. However, visual determination of the S arrival on the seismogram from a single detector may be difficult because of interference from other late arrivals such as guided modes and tube waves. This problem is alleviated when multiple detectors at different distances from the transmitter are used. When the seismograms from these detectors are plotted side by side in order, the different kinds of waves become separated in time because they have different velocities. Figure 079.4 shows this behaviour; the P, S, and guide/tube (shown as the fluid arrival) waves have different time moveouts as distance from the transmitter increases. Least-squares analysis can be applied to the multiple-detector data to give the best estimates for the various arrivals.

When the P and S velocities have been determined, they can be used with rock density (known from density logs or drill core measurements) to derive the dynamic elastic moduli:

$$G = V_s^2 \cdot \rho \quad \text{(shear modulus)},$$

$$E = G(3r^2-4)/(r^2-1) \quad \text{(Young's modulus)},$$

where ρ is the rock density, r is the ratio V_p/V_s, and V_p and V_s are the P and S wave velocities, respectively. These dynamic elastic moduli can be useful as estimates for the static moduli measured with traditional mechanical stressing methods, and as indicators of important mining factors such as rock rippability.

Since the maximum distance between transmitting and detecting sondes is only about 5 m, the detected seismic signal from driving the transmitter with a single sharp pulse will be strong enough so that we need not use the cross-correlation technique for signal enhancement. In most rocks, the arrival times at the detector nearest to the transmitter (R1 in Figure 079.3) will be from 0.5 to 1.0 milliseconds for P waves and 0.75 to 1.5 milliseconds for S waves. For sufficient precision in picking arrival times (to an accuracy of better than 2%), the transmitted seismic pulse must have reasonable energy in the 10 to 30 kHz frequency range. The detected signals are FM multiplexed so only one of the four conductors in the downhole cable is required to carry them to the surface. The remaining three conductors are used to supply DC power to the probes and to control the firing of the transmitter. In the surface electronics, tuned circuits separate the FM carriers and demodulate them to recover the seismic signals. After amplification and anti-aliasing filtering in the signal-conditioning circuits, the seismic waveforms are digitized by an 8-bit A-to-D converter at a rate of one sample every 10 microseconds. A complete seismogram consists of about 1000 digitized points. Synchronized stacking of waveforms from a series of transmitter pulses (fired every 12 milliseconds or so) is used to reduce both random and low-frequency noise. As in the crosshole system, a Tandy 2000 desktop computer interfaced to the receiver electronics is used to control the digitization, stacking, storage, and display (both CRT and hardcopy) of seismograms. The computer also runs programs which perform fast Fourier transforms and spectral analysis, providing a digital signal processing capability for the full waveform seismic logger. A major activity in the current project has been the development of software, both in machine code and in high-level languages, which enable the desktop computer to control the operation of the seismic instrumentation and to process, archive, and display the seismic data.

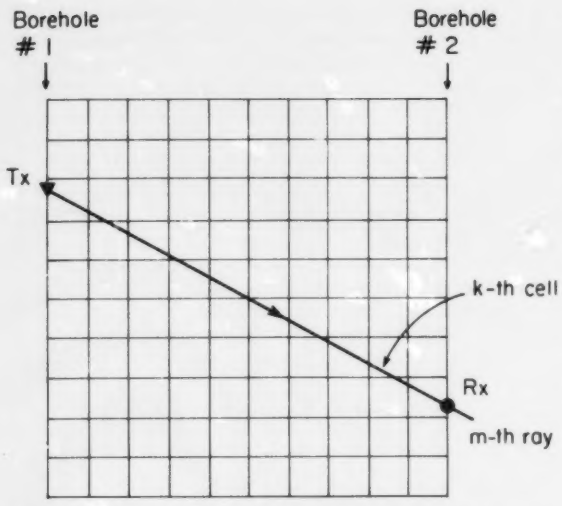

Figure 079.5 *Division of the rock section between two boreholes into a grid of rectangular cells in preparation for image reconstruction using crosshole seismic data.*

INTERPRETATION OF CROSSHOLE SEISMIC DATA: TOMOGRAPHIC RECONSTRUCTION

IMAGING USING BACK-PROJECTION AND ART

Figure 079.5 shows the essential features of a crosshole seismic experiment. A transmitter is placed in one borehole and a detector is placed in another. The transmitter generates a seismic wave which travels through the rock to the detector following the raypath labelled m. If many different depths are used for positioning both the transmitter (Tx) and receiver (Rx), then a seismic scan consisting of many raypaths across the rock section under study is produced. The problem is then to present the information contained in the scan (which may have on the order of 1000 seismograms) in a form easily comprehensible in geological terms.

A suitable presentation is a map showing the distribution of seismic properties in the rock section. For example, the travel times and signal amplitudes can be used to estimate seismic velocities and transparencies, and these can be related to subsurface geological conditions. The problem of information presentation becomes the following: given experimentally determined travel times and signal amplitudes from a seismic scan, estimate the velocity and transparency distributions within the rock section. To do this, we can use an imaging technique used in tomographic reconstruction called simple back-projection, the details of which we will now describe.

Mathematically, the travel time τ_m for the m-th ray can be written as

$$\tau_m = \int_0^{l_m} u(x,y)\, d\ell_m, \quad (1)$$

where u(x,y) is the spatially varying seismic slowness (= reciprocal of velocity), L_m is the length of the ray, and the integral is along the straight line joining Rx and Tx. As shown in Figure 079.5, the section of rock between the boreholes can be divided into a grid of rectangular cells or pixels. Within the n-th pixel, we assume that the slowness has a constant value u_n. By estimating the value u_n for each and every cell in such a way that the whole grid of values will be consistent (at least semi-quantitatively) with all the measured travel times, we will have "inverted" the experimental data to an image of the seismic slownesses in the rock section.

Note that in Figure 079.5, the m-th ray intersects a number of cells. The total travel time for the ray is the sum of the slowness values in the cells multiplied by the length of the ray within the corresponding cells. Thus, for each ray, the travel time changes from an integral to a ray sum:

$$\tau_m = \sum_k u_k \cdot l_{km}, \quad (2)$$

where l_{km} is the length within each pixel k intersected by the m-th ray. If we assume for the moment that u_k have the constant value u_m, then

$$\tau_m = u_m \cdot L_m,$$

where L_m is the distance between the receiver and the transmitter for that ray. Hence,

$$u_m = \tau_m / L_m. \quad (3)$$

The simple back-projection algorithm consists of the following steps. For each k-th cell intersected by the m-th ray, the value u_m is added to the cell sum S_k, and every time a value u_m is added to S_k, a counter N_k associated with that cell is increased by 1:

$$S_k = S_k + u_m, \quad (4)$$
$$N_k = N_k + 1.$$

Finally, when all the rays have been analyzed in this way, the estimate for the slowness within each cell which has a non-zero value counter N_k is

$$u_k = S_k / N_k, \quad (5)$$

and the velocity is $v_k = 1/u_k$. If N_k is zero, no ray has intersected the cell and therefore there is no direct estimate for the slowness within that cell. Once the grid of values has determined, contouring or interpolation and colour-coding can be done to produce a smooth visual display of the map.

There are alternative methods to simple back-projection for estimating the slowness distribution. When all the travel times are considered collectively as a set, equation (2) becomes a set of simultaneous linear equations. The unknown values are u_k, and we need to solve the system in order to obtain our map of seismic properties. In practice, the solution is es-

timated by trial and error in an iterative fashion using a class of reconstruction algorithms known as ART (algebraic reconstruction techniques; *see* Brooks and Di Chiro 1976). These trial and error techniques are potentially highly unstable, and can give artifacts in the image which have no relation to the actual target. Simple back-projection, however, has the advantage of always giving a stable image; as well, it is very fast and hence inexpensive in terms of computer resources. We must caution that strictly crosshole scanning is ineffective in resolving lateral variations in the geology, no matter what imaging algorithm is used.

The final image of course depends on how the rock section is divided up into a grid of pixels. Determining the number of cells in the vertical direction is straightforward; it can be set to be equal to the number of (equally spaced) transmitter or receiver positions. Assigning the number of cells in the horizontal direction is more of a problem. Strictly crosshole scanning is inherently poor at resolving lateral variations, and having too many cells in the horizontal direction is inefficient because they increase computational time without truly increasing lateral resolution. A useful rule of thumb is to define the numbers of vertical and horizontal cells so that the ratio of the vertical to horizontal dimensions of each cell is about half of the sine of the steepest angles in the rays. It is important that the size of each cell be large enough so that the majority of cells in the most interesting regions of the rock sections have several rays intersecting them.

The above remarks would indicate that crosshole seismic imaging is at best a semi-quantitative technique in its present state of development. Targets located near the upper and lower edges of the scan will generally be distorted, and laterally varying features may be poorly determined. However, targets which have a subhorizontal alignment or are near the centre of the network of intersecting rays will be imaged fairly well. In the future, new interpretation schemes incorporating as much geological input as possible and increased experience with crosshole as well as surface-to-hole scanning will make seismic imaging a much more reliable method for subsurface mapping. As well, improved interpretation will need to account for bending of seismic rays caused by refraction, a phenomenon not addressed by traditional tomographic algorithms.

IMAGING WITH SEISMIC AMPLITUDES

The above discussion on crosshole seismic imaging was based on using direct arrival times as the input data to obtain maps of seismic velocity. However, tomographic imaging is a general technique based on experimental data which is related to a physical property through a line integral of the form given in equation (1). As long as equation (1) is satisfied, it is immaterial to the mechanics of the imaging process what the particular data or physical property are. In this section, we show that the natural logarithms of seismic amplitudes can be formulated in terms of a line integral of attenuation coefficients or seismic transparency, so that amplitudes of direct arrivals can be used for imaging.

The amplitude of a seismic pulse arriving at a remote receiver from a point source can be written as

$$A(r,\theta,\phi) = A_0 \cdot R(\theta,\phi) \cdot \frac{e}{r}^{-\alpha r}, \quad (6)$$

where $R(\theta,\phi)$ is the radiation-reception pattern of the source-receiver configuration, A_0 is a known or assumed constant incorporating both source strength and receiver sensitivity, r is the distance while θ and ϕ are the angular displacements between the source and receiver, and α is the attenuation coefficient (which for the moment is assumed to be constant).

The amplitudes measured at the receiver may be corrected for the 1/r dependence (geometric spreading) and the radiation pattern ascertained from theoretical calculations:

$$A' = A(r,\theta,\phi) r / R(\theta,\phi) = A_0 e^{-\alpha r}. \quad (7)$$

Hence,

$$\log (A'/A_0) = -\alpha r = \int_0^r -\alpha \, d\ell \, .$$

If now α is generalized to be a function of position, we get

$$\log (A'/A_0) = \int_0^r -\alpha(x,y) \, d\ell, \quad (8)$$

Equation (8) is precisely the type of line integral used in tomographic imaging. Therefore, by using the experimental quantities $\log (A'/A_0)$ with standard tomographic reconstruction algorithms such as back-projection or ART, we can create images of seismic attenuation.

Sometimes it is difficult to determine what value the constant A_0 has. Incorrect values of A_0 used in equation (8) will result in incorrect absolute values for $\alpha(x,y)$. However, in most geophysical applications, it is much more important to determine changes with position or time of a particular parameter than it is to precisely measure its absolute value because, generally speaking, only variations are diagnostic of important or interesting changes in geological conditions. Since it is a constant, A_0 has only a small influence on the variations of $\alpha(x,y)$, and it is not critical in many geological applications to know its precise value in equation (8). Some measured amplitude at a fixed reference location near the transmitter can be used, or we can simply assume A_0 to be unity. Using this assumption, Equation (8) becomes

$$\log (A') = \int_0^r T(x,y) \, d\ell \, , \quad (9)$$

where we have substituted T(x,y) for $-\alpha(x,y)$ because, strictly speaking, by assuming $A_0 = 1$, we are no longer dealing with attenuation, so we change the notation to emphasize this fact. We call T(x,y) the seismic transparency, by which we mean an empirical quantity which describes the relative ability of a material medium to carry seismic energy without loss. Equation (9) says that T(x,y) can be imaged by tomographic processing of the logarithms of arrival amplitudes, or, equivalently, the amplitudes expressed in decibels.

The loss of seismic amplitude in excess of geometric spreading and radiation pattern effects may be due to microscopic frictional dissipation (classical anelastic attenuation), random Rayleigh and Mei scattering, or reflection and refraction on large boundaries of impedance mismatch. Each of these mechanisms is associated with a change in rock mechanical properties having some geological significance, but in practice it may be impossible to differentiate between mechanisms. By using the empirical transparency parameter, we bypass arguments concerning specific loss mechanisms, and concentrate on the geological interpretation for observed variations in amplitudes.

CONCLUSION

Crosshole seismic scanning and the interpretation of field results by tomographic imaging are relatively new concepts in applied geophysics, and there are not many published cases of its application to solution of geological problems. The few examples which do exist are the results of isolated research efforts rather than practical applications, but they have indicated that subsurface imaging through crosshole seismic scanning has considerable promise for increasing the value of boreholes by providing a means for investigating the geology between them. Thus, the potential capability of crosshole scans for detecting and locating targets not intersected by drilling is the most important factor in justifying efforts to make seismic geotomography a commercially viable geophysical technique. As with many geophysical techniques, crosshole seismic imaging has limitations, the chief of which are its inability to define detailed lateral variations and its tendency to distort geological features aligned nearly parallel to boreholes. These deficiencies are mitigated somewhat if data from surface-to-hole shooting can be obtained to add to the interpretation. The maps of seismic properties produced by seismic geotomography must be viewed with care in order to avoid false conclusions, but if due consideration is given to other geophysical data and known geological constraints, they will in many cases lead to a more detailed understanding of the lithology and structure between boreholes.

The current project is aimed at producing field instrumentation and computer-based interpretational packages which will be used for commercial applications of seismic geotomography. The instrumentation include a crosshole seismic scanner and a full waveform seismic logger. We have presented the technological considerations and theoretical ideas behind the equipment design. As well, we have explained in some detail how tomographic imaging algorithms can be used to produce maps of subsurface seismic properties from crosshole seismic data. Construction of the scanning and logging equipment has advanced satisfactorily, and coding of interpretational software has been initiated. By the time this report is published, we will have field-tested the instrumentation and conducted the first crosshole seismic survey with it in boreholes maintained by the Geological Survey of Canada at the CANMET Centre near Nepean, Ontario. The project will continue with modification and optimization of both hardware and software to correct shortcomings of the system revealed by the field-testing.

ACKNOWLEDGMENTS

The development of borehole seismic instrumentation described in this report is funded in part by the Ontario Geological Survey through the Exploration Technology Development Program. Jodex thanks Dr. G.F. West of the University of Toronto for technical advice, and the Geological Survey of Canada for access to test boreholes.

REFERENCES

Asten, M.E.
1983: Borehole Log Analysis Using an Interactive Computer; Bulletin of the Australian Society of Exploration Geophysicists, Volume 14, p.3-11.

Bois, P., Laporte, M., Lavergne, M., and Thomas, G.
1972: Well-to-well Seismic Measurements; Geophysics, Volume 37, p.471-480.

Brooks, R.A., and Di Chiro, G.
1976: Principles of Computer Assisted Tomography (CAT) in Radiographic and Radioisotopic Imaging; Physics of Medical Biology, Volume 21, p.689-732.

Daily, W.D., Lytle, R.J., Laine, E.F., Okada, J.T., and Deadrick, F.J.
1982: Geotomography in Oil Shale; Journal of Geophysical Research, Volume 87, p.5507-5515.

Foster, M.R., and Sloan, R.W.
1972: The Use of Pseudo-noise Sequences to Code a Pulsed Neutron Logging Source; Geophysics, Volume 37, p.481-487.

Herman, G.T., and Rowland, S.
1973: Three Methods for Reconstructing Objects from X-rays; Computer Graphics and Image Processing, Volume 2, p.689-698.

Lytle, R.J., and Dines, K.A.
1980: Iterative Ray Tracing Between Boreholes for Underground Image Reconstruction; Institution of Electrical and Electronic Engineer, Transactions on Geoscience and Remote Sensing, Volume GE-18, p.234-240.

Paillet, F.L., and White, J.E.
1982: Acoustic Modes of Propagation and Their Relationship to Rock Properties; Geophysics, Volume 47, p.1215-1228.

Wong, J., Hurley, P., and West, G.F.
1983: Crosshole Seismology and Seismic Imaging in Crystalline Rocks; Geophysical Research Letters, Volume 10, p.686-689.
1984: Crosshole Audiofrequency Seismology in Granitic Rocks Using Piezoelectric Transducers as Sources and Detectors; Geoexploration, Volume 22, p.261-279.

Grant 080 High Resolution EM Developments

Y. Lamontagne, J.C. Macnae, A.E. Wieckowski, and R. Huxter

Lamontagne Geophysics Ltd., Toronto

ABSTRACT

Developments on two main fronts are needed to improve the resolution of complex structures, and particularly deep targets using EM measurements: instrumentation developments to improve the definition of the response, and research into interpretation tools to facilitate the interpretation of the often complex data. This project includes contributions to these two comp'ementary aspects in the form of a high power high efficiency EM source, and processing algorithms to transform the measured data to approximate images of the conductivity structure. The developed transmitter was designed after a careful study of the configuration which would be the most effective for deep EM exploration. The main characteristics of this transmitter are its high output voltage, high bandwidth, precise current regulation, and its programmable waveform. A prototype suitable for field operation is being built and bench tested. Two distinct data processing algorithms are being developed: one called *Depth Image Processing* is usable for sounding data and is based on representation of the response by a distribution of images of the source; the other process, *Matched Filter Processing*, will be suitable for the detection, and approximate characterization of discrete and laterally varying conductive structures by combining optimum pattern recognition techniques and empirical interpretation rules.

INTRODUCTION

Electromagnetic survey methods are being increasingly applied to problems which stretch the limits of the available apparatus and data interpretation techniques. Deep sounding applications, where the conductivity structure of a quasi-layered earth must be determined to depths of up to several kilometres, have been of considerable importance in recent years.

In more conventional uses for mineral exploration, new advanced EM tools are most often used to search for deposits at depths which were unheard of only a few years ago. In areas where deep targets are sought, the volume of rocks which must be searched may often contain other conductive structures such as overburden, thick sedimentary cover, or shallow mineralized zones. In the vicinity of mining installations, EM surveying also has to contend with high electromagnetic noise levels, and a variety of cultural responses.

Developments along two general avenues of research are needed to deal more effectively with these problems. One set of developments should aim at achieving a more accurate, quantitative definition of the response by improving signal source strength and system fidelity. Another set of developments should improve our ability to make use of the measured data.

This research project is tackling developments which will contribute to both of these avenues:

1. The development of an effective high power EM source suitable for practical, deep, large scale exploration and sounding.
2. Computer-based interpretation tools using a *data processing* approach to give a more pictorial view of the data.

The objectives of these two subprojects, and the results obtained so far will be presented in two separate sections.

HIGH POWER TRANSMITTER

The purpose of this project is to develop an effective practical high power EM source suitable for deep large scale exploration. *High power* means a source producing a high *measurable response signal strength*, rather than one that only dissipates a lot of power in the load. The authors conducted an extensive study of the factors influencing the effectiveness of a high power EM source during the initial planning of this project, and during its development when design specifications were reconsidered. This study can be summarized by a review of four main considerations.

FIELD STRENGTH

For a transmitter loop enclosing an area A and driven by a current I, its effectiveness in producing a strong primary field is often quantified in the form of its dipole moment D:

$$D = IA \quad (1)$$

This parameter is useful because at large distances from the loop (compared to its size), the primary field approaches that of a dipole with the same dipole moment. The authors have considered the loop to be only resistive, and have quantified the relationship between dipole moment D, output power P, the total wire mass M, and loop size S as follows:

$$D = (PMS^2/C)^{1/2} \quad (2)$$

In this formula, C is a constant dependent on the wire material conductivity σ, its density d, and on the ratio r of loop perimeter to the side of a square loop with the same area:

$$C = 1000\sigma dr^2 \quad (3)$$

Formula 2 shows the importance of using a loop as large as is geophysically possible. If, for example, the loop size is reduced by a factor of two, the product of transmitter power and the loop wire mass must be increased by four to compensate. If one considers the greater effort involved in making a large loop, which may be expressed as

$$E = MS \text{ (loop laying effort)} \quad (4)$$

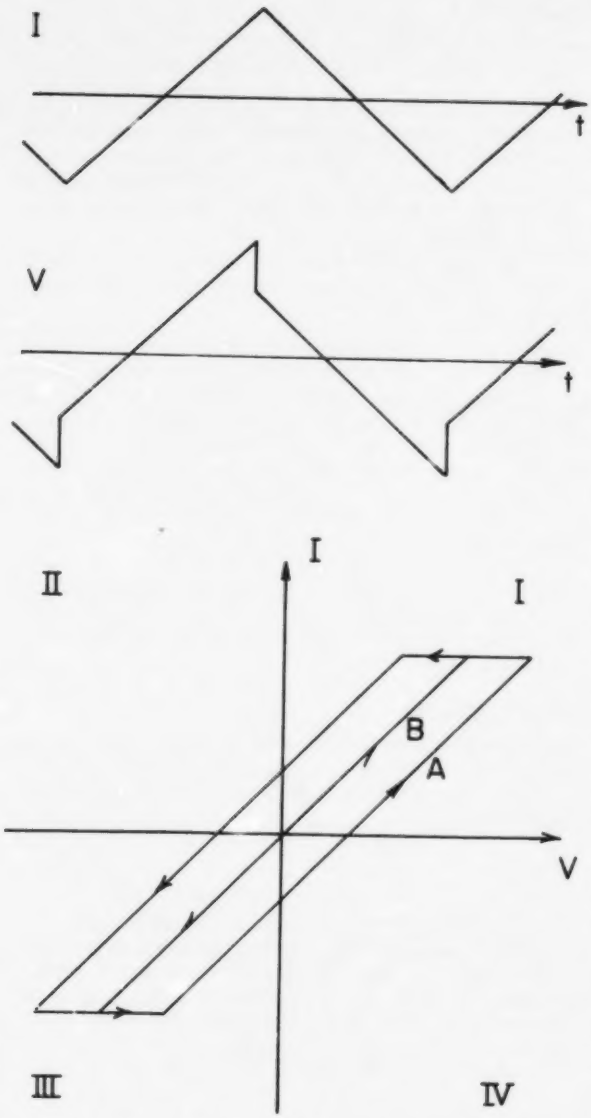

Figure 080.1 *Sketch of the voltage applied across an inductive (and resistive) loop for a regulated ramp waveform and the resulting I versus V plot for an inductive loop (A), compared with a purely resistive load (B).*

there is still an advantage in using a loop as large as possible to produce a large dipole moment, as is shown by substituting MS in formula (2):

$$D = (PES/C)^{1/2} \quad (5)$$

However, the transmitter must have sufficient output voltage capability to exert its full power on a large high resistance loop. The maximum dipole moment attainable is actually critically dependent on the output voltage capability of the transmitter (V) according to the relation:

$$D = \left[\frac{PVE^2}{C^2}\right]^{1/3} \quad (6)$$

The maximum dipole moment would then be for a loop of size:

$$S = \left[\frac{MV^2}{CP}\right]^{1/2} \quad (7)$$

In defining the signal strength from an EM source, the dipole moment is not the only factor to consider. For survey effectiveness, the preferable source is probably the one which will produce a given field strength over the largest possible area, or perhaps over the largest possible volume if deep targets are sought. These considerations emphasize the importance of having a source capable of driving a large loop. This means that the source is capable of a high voltage output.

EFFECT OF LOOP INDUCTANCE

One problem in using large loop sources is that they are difficult to drive because of their high self-inductance. This problem is caused by inductive energy U_L which is stored in the magnetic field of the source. The peak energy occurring at maximum current is:

$$U_L = I^2L/2 \quad (8)$$

where I is the peak current, and L is the self-inductance of the loop.

This energy must be removed by the transmitter when the current is turned off. This is illustrated in the case of a ramp waveform in Figure 080.1. If the I-V plane is divided in the four quadrants shown, the load trajectory of an inductive load (a) goes through all four quadrants, whereas for resistive loads (b), the trajectory is contained in quadrants I and III only. In quadrants I and III, the transmitter is supplying a net amount of energy to the load, whereas in quadrants II and IV, it is absorbing energy.

The higher the inductance, the higher this magnetic energy transfer will be. The peak rate of this energy transfer (absorbed peak power) can be very large depending on the waveform. This absorbed power can be very damaging for the transmitter since it manifests itself in the form of a back emf which resists any decrease in current. This emf can increase almost without limit if the transmitter attempts to switch off the current instantaneously.

Since the inductance increases linearly with loop size, there may be a temptation to keep the loop to a rather small size, but in order to produce the same dipole moment, the inductive energy stored in a smaller loop is even greater as can be seen by comparing relations (1) and (8).

In the high power source under development, this problem is attacked using two approaches:

1. Full wave current regulation such that the current turns on or turns off on continuously.
2. Regenerative *four quadrant operation* in which the stored inductive loop energy is transferred back to the transmitter power supply, rather than be instantaneously dissipated in the output devices of the transmitter.

CURRENT WAVEFORM AND SIGNAL EFFICIENCY

Signal efficiency is a measure of how much response a system can produce for a given peak primary field strength, and of how well it can use this response. The two main choices in this respect are systems with continuous duty cycle requiring precise current regulation, and those with discontinuous duty cycle, and only *off-time* measurements having a much lower current regulation requirement. The main factors relevant to this complex topic are:

1. *The signal efficiency of the transmitted waveform.* In general, precise current regulation entails some loss in signal efficiency because the regulating device must have some excess gain and voltage capacity. Therefore, the device must operate at less than its maximum output limit. The complex regulation process causes inevitable power losses. If regulation is achieved by linear devices, this power loss can even be greater than the output power.
2. *The efficiency of the whole system in using the waveform.* A current regulated source makes it possible to sample the whole response waveform produced by the source. An unregulated transmitter allows measurements to be made only in the *off-time* periods, but the response occurs mostly in the *on-time*. As a result, only a small fraction of the excited response is actually sampled. The efficiency of off-time measurements is worse for slow decaying responses.
3. *The geophysical application of the system.* Certain critical EM applications require exceptional characteristics. Two extremes are the detection of very small shallow poor conductors versus the sounding for very deep highly conductive layers. In the first case, the anomalies may have very short time constants, and be smaller than the error of regulation of any feasible full wave system. In the second case, the response is almost completely in the on-time of any on-off transmitted waveform unless it is operating at a much lower frequency than a comparable full wave system.

A comparison of these factors is a difficult task which is best done with reference to specific models. The conclusion of our analysis was that for the detection of *good conductors*, for *very deep soundings* where the long delay response is most important, a full wave current controlled transmitter is more effective than an unregulated one many times more powerful.

PROGRAMMABLE WAVEFORM

This is a highly desirable feature which can be implemented in a current regulated transmitter. The main advantage is that a waveform can be chosen that produces a better signal-to-noise for the same output (Macnae *et al.* 1984) and that facilitates interpretation of the data.

In particular, the pre-emphasis technique described in Macnae *et al.* (1984) can be expanded to include a much greater class of waveforms. One such expansion, which is particularly promising, is the use of a superposition of pre-emphasized periodic waveforms of different periods such that the peak signal is not increased, but the waveform is much more active. This possibility may make possible measurements to very long time delays without the usual extreme reduction of short delay time precision.

DESCRIPTION OF THE PROTOTYPE TRANSMITTER

The above discussion showed that deciding on the design of an effective powerful EM source is not a simple task. Significant additional constraints for a practical system are the size of the power source (motor generator set) required to drive the transmitter and the amount of heavy wire which must be used.

The main trade-offs for deep exploration are between the horrendous complexity of an efficient current regulated device, and the extreme power levels needed for an equally effective "brute force" unregulated transmitter. Consideration of the large gain in effectiveness which can be realized, led the authors to opt for a design which takes advantage of presently available technology to maximize exploration effectiveness.

The transmitter under development is a high power (15 kW), high voltage (up to 1000 V), current regulated device with programmable waveform. To achieve a high efficiency and reduce the cooling requirements, high frequency switching techniques are used. Using these *switch-mode regulation* techniques, internal power dissipation is kept to <10% of the output power, and the high output voltages can be produced from normal power sources using small efficient high frequency transformers. Special circuitry is included to allow regenerative *four quadrant* operation, by which the energy inductively stored in the load, is transferred back to the power supply by the output regulator. The high level of regulation, and the facility to program the output waveform are achieved using two high speed digital signal processors working in tandem.

Block Diagram

Figure 080.2 shows a functional block diagram of the transmitter. All signals shown except the power and output paths are digital signals or groups of signals. The signal paths to and from the waveform measuring module (5), which is floating at the high voltage of the output, are optical links.

The main high speed low precision regulation loop follows the path 2- 3-4-5- 7-8-6. The input signal enters the waveform measuring module (5) through an optical port (10). An error signal generated within

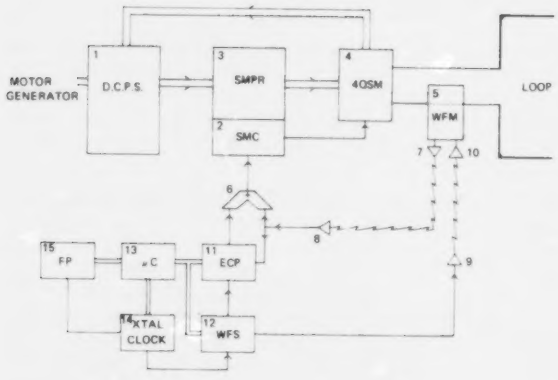

Figure 080.2 *Block diagram of the prototype transmitter:*

1. *DCPS—D.C. power supply*
2. *SMC—Switch-mode controller*
3. *SMPR—Switch-mode preregulator*
4. *4QSM—Four quadrant switch mode regenerative regulator*
5. *WFM—Waveform measuring module*
6. *High speed digital adder*
7,8,9,10. *Optical transducers*
11. *ECP—Error correction processor*
12. *WFS—Waveform synthesizer*
13. *μC—Microcomputer circuit*
14. *Precision crystal controlled clock*
15. *FP—Front panel*

the WFM exits through optical port 7 and is routed to the input of the switch-mode controller (2) through a high speed digital adder (6). The switch-mode controller modulates a phase controlled differential output switch-mode preregulator which does most of the power regulation under normal use. A series four quadrant switch-mode amplifiers (4) does the final regulation of the output by extracting power from the SMPR or by feeding power to the D.C. power supply (1). The switch-mode regulators operate at a switching frequency of 180 kHz to provide useful regulation with a bandwidth of 25 kHz.

An error correction processor (11) examines the current waveform error and calculates for each point of the waveform the mean correction to add to the error and applies this correction iteratively to the adder. This function is implemented by a high speed 32 bit signal processor. The error correction filter implemented by the ECP is adaptive and is based on the closed loop response of the switch-mode system including the effect of the load which is calculated by the ECP.

The waveform synthesizer (12) calculates the waveform from a table of values stored in the memory, applying to the waveform a pre-emphasis filter. For example, for the initial waveform programmed, which is the standard UTEM 3 waveform, it pre-emphasizes and integrates the digital representation of a square wave. This function is implemented by a second high speed signal processor using timing information from a high stability crystal controlled clock similar to that used in the UTEM 3 time bases.

A general purpose microcomputer circuit (13) controls the two signal processors by downloading programs and data tables to them, and provides user interfaces through front panel mounted keyboard, display, and external port (15).

SPECIFICATIONS AND PROJECT STATUS

Table 080.1 shows the objective specifications set at the beginning of this project and the progress achieved so far. The regulation shown in the table is that obtained without the aid of the ECP which is being programmed and tested separately. The gap between this and the objective regulation level shows how essential the digital correction loop is to the success of such a switch-mode design. The specifications of the *present status* are only temporary as the different components are being debugged and tested to increasing power levels. However, the presently achieved output voltage level may remain at this derated level until suitable higher voltage semiconductors are available.

CONCLUSIONS

An effective high power EM source needs to have a number of characteristics such as high output voltage, inductive load tolerance, and precise current regulation over a wide bandwidth. These characteristics can multiply the effectiveness of an EM source by a large factor for deep exploration, but this is at the expense of greatly increased circuit complexity.

A power efficient transmitter having these characteristics is under development using a combination of high frequency switch-mode power control, signal processing, and fibre optic technology. This new development promises to open new applications to EM exploration such as deep base-metal exploration in noisy environments and deep sounding for hydrocarbon-bearing structures. The possibility of programming almost any waveform also opens the possibility of using the same transmitter with other geophysical systems requiring a well regulated high power current source.

EM DATA PROCESSING TECHNIQUES

The data processing developments of this project aim to make EM data more amenable to interpretation by transforming them to more visual graphical representations.

Two types of processing have been considered, one suitable for EM sounding data measured over quasi-layered terrains, and another suited best to the location of local conductors and lateral conductivity changes. The first type of processing, named *depth image processing*, has now been developed to the stage where it can be applied to UTEM sounding field data; and the second, *matched filter processing*, is still in the software development stage.

TABLE 080.1 HIGH POWER TRANSMITTER SPECIFICATIONS

Specification	Objective	Present Status
Peak output power	15 kW	12 kW
Peak output voltage	1000 V	800 V
Peak output current	32 A	32 A
Current regulation bandwidth	20 kHz	20 kHz
Long term current regulation	<0.1%	3%
Regenerative power handling	2500 W	under test
Waveform	Programmable	fixed

MATCHED FILTER PROCESSING

The automatic interpretation of measured anomalies in terms of three-dimensional conductivity structures is the ultimate goal of any computerized interpretation system. This exact inversion procedure is only a distant dream at the present since the forward problem of computing the EM response of an arbitrary conductivity structure is itself an almost untractable problem.

What is sought in this research is a forward data transformation inspired by theory and interpretational experience which produces results more amenable to interpretation than the original data. In particular, the processing should isolate anomalies and indicate at least approximately the location, depth, size, and quality of simple causative structures.

If the shape of the anomalies sought is known, the process needed is one of pattern recognition, but in cases where the conductive structure is complex, a more suitable initial process would be one of transforming the response to distributed sources within the earth. A number of techniques which appear very promising for combining these two functions can be grouped under the general name of *matched filter* processing.

Applications of *matched filters* in geophysics (for example Clay *et al.* 1974; Wood *et al.* 1978) and electrical engineering (Turin 1960) have been mostly confined to problems where the input data are only functions of time. Optimum multi-channel velocity filters used in seismic processing are examples of multivariate matched filters.

As illustrated in Figure 080.3, each matched filter is actually a detector for a given pattern to be matched, and its output is not a filtered function but a single correlation number. In the example shown, an array of matched filters is used to define the correlation as a function of two parameters which could be, for example, the depth and x position of the source producing the pattern to be matched. Each matched filter would be designed to be an *optimum detector* for the corresponding pattern to be matched under certain conditions. In many applications where events of a given shape are to be located in a large domain and a matched filter is used for each possible position, adjacent matched filters are almost identical in shape but shifted relative to each other, such that the overall effect of applying a series of filters may be similar to a true filtering operation. This will be the approach used here for some parameters.

The first step in the process is to transform the data to a correlation density function as a function of the parameters defining a source pattern to be matched. The parameters are x,y,z position of the source, time constant, and other parameters defining the source geometry. As a second step, with the use of physical insight and scaling relations, secondary processing can be devised to transform this multivariate distribution into an approximate conductivity distribution.

The first sources which the authors have considered are dipoles, which in simple cases are thought to be caused by elementary spheres (if higher multipoles are neglected). Because of the nature of EM induction, the response of a conductivity structure is generally much different from the sum of responses of the parts. The method of anomaly representation which is chosen must, therefore, be capable to at least grossly account for this effect. With the

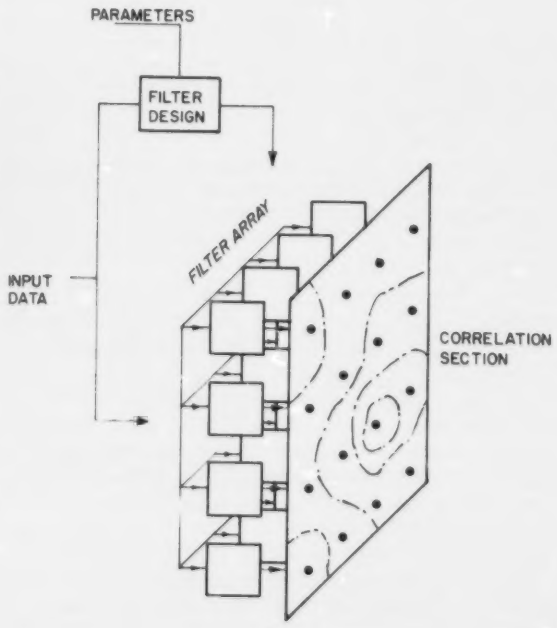

Figure 080.3 *Block diagram showing a 2-D array of matched filters used in producing a correlation section.*

matched filter formalism, there is flexibility to introduce any additional parameters to our elementary *sphere* model such as size, ellipticity, orientation, and time decay to effect a physically meaningful conversion.

Matched Filter Formulation

A matched filter can be defined as a least square optimum detection function for the pattern to be matched. In the general case, if D is the complete set of field data that could be measured; M, the actually measured data; and T, the test functions, and the covariances C_{DD}, C_{MT}, and C_{TT} can be estimated as a function of the parameters, then, using matrix notation for the covariances, the result of match filtering can be formally expressed as:

$$R = C_{MT}/C_{DD} \quad (9)$$

In this notation, C_{MT} can be considered a vector with each element corresponding to a point considered in parameter space, C_{DD}, a matrix expressing the covariance as a function of any two such points. The division represents a multiplication by the inverse matrix. The result R is a function of the parameters. This matrix formulation, therefore, denotes the application of a whole array of matched filters, that is, one for each parameter combination.

By comparison, the deterministic fitting of the data by a sum of functions T would have a solution:

$$U = C_{MT}/C_{TT} \quad (10)$$

The difference between the two processes is that U would represent the amplitude distribution of sources fitting the data, whereas R is the "likeliness" that a source with the given fixed amplitude T exists for the given parameter set.

The field D can be thought to be the sum of desirable responses T and noise N (error of fit) which is uncorrelated to T. In this case

$$C_{DD} = C_{TT} + C_{NN} \quad (11)$$

where C_{NN} is the covariance of the noise. If these assumptions are true, and C_{DD} is well estimated, then R should be ≤ 1.

If there is an incomplete set of parameters, or a poor estimate of C_{DD} is used, R can be >1, or otherwise be scaled improperly. Another complamentary process exists which is useful in such cases:

$$S^2 = C_{MT} \times C_{MT}/C_{DD} \times C_{TT} \quad (12)$$

S is related to the *similarity* or *coherence* function of Neidell and Taner (1971). It has a maximum value of 1 for a function M fitting a model T perfectly. The ratio of R and S is an amplitude estimate which is used to define the effective sphere size relative to the test model size.

The most subjective part of the matched filter process lies in the estimate of C_{DD}. This is usually estimated as the autocorrelation matrix of a set of input data, which in the least square derivation is only valid for parameters related to the variable of measurements in the T function as in a linear filter, that is,

$$T = T(x_1 - p_1, x_2 - p_2, \ldots) \quad (13)$$

Under such assumptions, there is a perfect discrimination as a function of parameters when the input is made up of purely one function T with no noise. For parameters with no such relationship, the same formulation is commonly used, but the results are more damped even in the absence of noise.

The estimate of C_{DD} also entails the use of a suitable portion of the input data, with due *windowing* in calculating the autocorrelation matrix and in choosing the number of lags to use in the process.

Parameters of the Elementary Dipole Model

The initial parameters considered for the elementary dipole model are:

x_m, y_m, z_m: location of dipole
τ_m: logarithm of time constant
d_m: dip angle of dipole

With this choice, the function T has the form:

$$T(x,y,\tau;x_m,y_m,z_m,\tau_m,d_m) = T'(x-x_m, y-y_m, \tau-\tau_m; z_m, d_m)$$

Thus, C_{DD} can be easily estimated for parameters x_m, y_m, and τ_m. The effective radius of the equivalent sphere model is chosen to be equal to $z_m/4$ in the design of the T functions, such that the maximum amplitudes are all almost equal in the near uniform field of a large loop.

Block Diagram of the Process

Figure 080.4 shows the flow diagram of the algorithm which is being implemented in the case of the R process. The covariance in x_m, y_m, and τ_m becomes a three-dimensional autocorrelation and conceptually the autocorrelation matrix C_{DD} has six dimensions, but for the purpose of the matrix inversion it is considered to be a square matrix as a function of two sets of (x,y,τ) points.

The difficulties in the implementation of the algorithm lie in the size of matrix C_{DD}. This matrix could be up to 2500 x 2500 in size in a typical case:

k = 25 stations x 10 lines x 10 channels

In fact, to stabilize the process, experiments with one dimension indicate that the autocorrelation should be limited to roughly one third of this range using a tapered window resulting in a sparse matrix which is easier to invert. Further reductions in computations can be obtained by compressing the sparse 6-D matrix in a suitable manner and then stretching the inverse. This time saving process is now being validated on scaled down matrices with a similar struc-

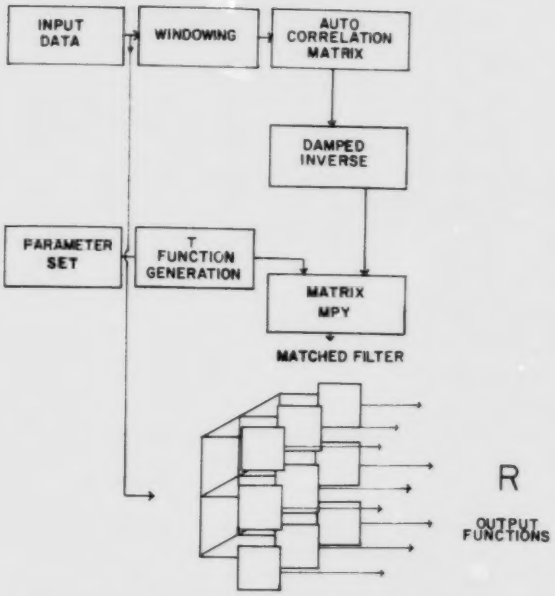

Figure 080.4 Block diagram of the algorithm used for the "R" matched filter processing. In the actual program, there are five parameters rather than the two illustrated.

ture. Another point receiving special attention is the treatment of end effects in the estimation of both C_{DD} and C_{MT}. For consistency with the least square assumptions, the test functions T must be truncated, whereas the data used in C_{DD} must be smoothly continued near the boundaries.

Computing Cost

Anticipating the completion of the full-scale algorithm, the result in R and S would be density functions of the five initial parameters. In the present algorithm, there are 60 000 different parameter points considered:

20 x_m values
10 z_m values
5 y_m values
10 τ_m values
6 d_m values

For a data set of 2500 (x,y,τ) points, and a single component, the estimated processing time including filter design is extrapolated to be 150 minutes for each of R and S on a VAX 11/750. This estimate is assuming that a satisfactory approximation of the inverse matrices can be made in compressed form.

Secondary Processing

This processing will be necessary to be able to display the result in a more condensed, and geophysically meaningful manner. The outline of the secondary processing now planned is:

1. Use the ratio of R and S as an amplitude factor from which an effective size parameter (sphere radius) is to be derived.
2. Obtain an estimated *ellipticity* from the variation of R with d_m and primary field orientation for the loop positions available.
3. Calculate a mean τ_m value (time constant) for each set of other parameters, and use the results of 1 and 2 to estimate an apparent conductivity.
4. On x-z sections, sum the correlation coefficients over the respectively determined elliptical *areas of influence* for each point conductivity class to produce a modified correlation density section for each conductivity class.

Display of Results

The data presentation planned is in the form of coloured sections where the colour will represent the conductivity, and areas of poor total correlation (poor resolution) will be indicated by adding a white component.

DEPTH IMAGE PROCESSING

Time domain EM soundings measurements have customarily been made using a single centre loop measurement for each transmitter loop. Survey practice with the UTEM system has indicated that there are great advantages in survey efficiency and model resolution in using multiple measuring stations for each loop position. This practice in effect combines both geometrical and time sounding for each loop, and makes it possible to use multiple loop positions for each receiver station to optimize model resolution.

The *depth image* process has been developed particularly to reduce the data obtained from such surveys, but can also be used to great advantage in centre loop surveys.

Induced Currents in a Layered Earth

It is possible to calculate the secondary fields produced in a layered earth by a step change in a primary magnetic field. Nabighian (1979) showed that in the case of a uniform half-space, secondary current flow consists of a "smoke ring" which expands out and down from the source. Maxwell (1892) showed that if the only conductor present is an infinite thin sheet, although the induced currents are confined to the sheet and expand horizontally, the secondary field at any point on the earth surface could be calculated at any given time by a single image of the source, the location of which is a simple function of the sheet conductance and the time delay.

Inspired by these concepts, the authors have attempted to devise a means of keeping track of the induced currents as a function of time. The method chosen was to numerically find the discrete distribution of vertical images of the source that would precisely fit the calculated secondary fields at a series of test points distributed over the observation plane. Figure 080.5 illustrates this concept. Initially, the half-space response was used in these numerical experiments (Figure 080.6), but it was later found that

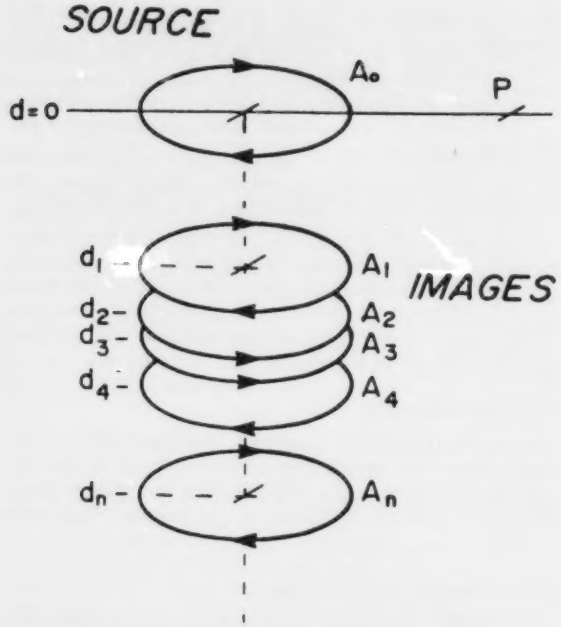

Figure 080.5 The concept of using a sum of discrete vertically distributed source images to fit the response of a layered earth at all points on surface. A theoretical requirement is that the sum of the amplitudes of the image current = source current.

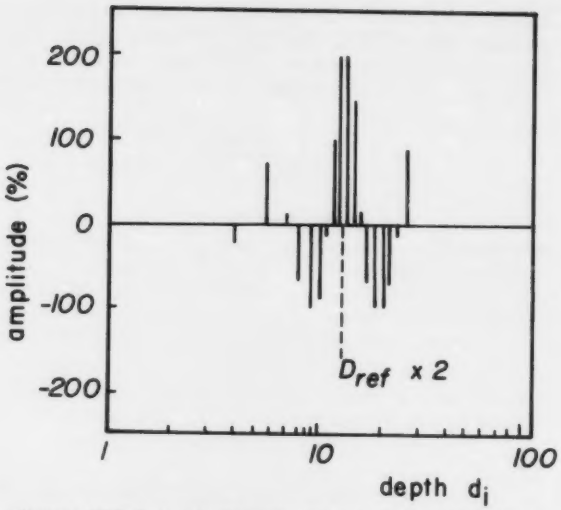

Figure 080.6 A 14 discrete image distribution that fits a half-space response to within 0.3%. The reference depth Dref is used to keep track of the depth of the induced currents within the earth. By compressing or expanding the width of this distribution, and allowing Dref to vary as a function of time, a wide range of layered earth responses can be fitted by a distribution of this shape.

in practice, any layered earth response can be fitted by image distributions, and this was also verified on the wavenumber formulation of the EM step response.

Basis of the Depth Image Fitting Algorithm

Furthermore, it was found that the shapes of the fitting distributions are all very similar, resembling sync. functions, i.e. sin x / x, in logarithmic depth, and that the main differences between the distributions of different models are in the manner in which the centre depths and, to a lesser extent, the widths of the distributions vary with delay time. Since the image response is only weakly dependent on the distribution width, a method was found to iteratively determine the centre depths and widths, assuming initially a single image (i.e. - a very narrow width). This process uses an empirical relation, by which the width of the best fitting distribution can be estimated from the manner in which the centre depths vary as a function of delay time. It thus appears that, although the correct width as well as centre depth must be used to fit a layered response precisely, there is little independent information in the width function. Essentially, this means that after a response is fitted, virtually all the information pertaining to it is contained in the variation of the centre depth as a function of time.

In transforming field data, an average of all or many stations is used to initially determine the best fitting distribution width ratios, and then individual data points are transformed to an apparent centre depth in the last iteration. If the earth is truly layered locally, all stations measured would give the same depth time function, regardless of its position with respect to the loop. But the resolution in determining this function is better for a given depth range for particular station positions relative to the source. Resolution functions are calculated by the DIP program, and these are used to stack together the depth functions obtained with different loop-receiver configurations, and thus produce a well resolved function at all depths. The most usual type of stacking done is the common receiver stacking of the data of different loops.

Slowness and Integrated Conductance

One of the most stable parameters of any layered earth section that can be determined by inversion of EM magnetic field data is the integrated total conductance down to a depth (Fullagar and Oldenburg 1984). Guided by this concept and dimensional analysis, it was anticipated that the slowness (inverse velocity) of the diffusion process should be directly proportional to the integrated conductance provided that "reflections" are not significant. By reflections, is meant upward travelling energy, as opposed to the measured quasi-static magnetic field which may be present everywhere without energy transfer.

Figure 080.7 shows how this hypothesis was tested for a suite of three-layer models with variable second and third layers. The results show a remarkable similarity between the integrated model conductance and the slowness calculated from the fitted centre depths divided by two. In fact, the slowness

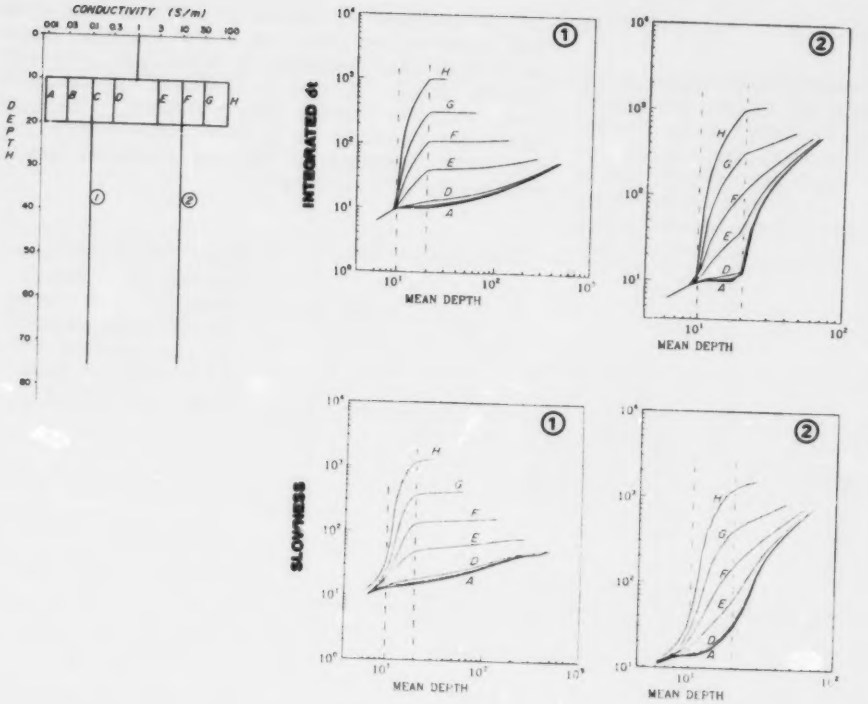

Figure 080.7
Conductivity structure of a three layer model with variable second layer, and two different third layers (series 1 and 2). The upper curves are the integrated conductance (note the log-log scales), whereas the lower curves are the slownesses obtained using the apparent depths h (matching Dref) determined by the DIP program and scaled by μ_0.

curves give slightly smoothed estimates of the true conductances except for a constant factor of $\sqrt{2\mu_0}$. The smoothing is more pronounced for poorly resolved models, that is, those with very resistive imbedded layers.

Conductivity Calculation

It follows from the similarity between slowness and conductance that the conductivity can be estimated by differentiating the slowness with respect to depth. Thus, the apparent resistivity can be expressed in terms of the depth versus time function as:

$$\sigma_a = \frac{1}{\sqrt{2\mu_0}} \frac{d^2 t}{d h^2}$$

Figure 080.8 shows the slowness derived apparent conductivity versus apparent depth for six models scaled to a top layer with unit conductivity. For comparison, the true conductivity section is also shown. As expected, very resistive and deep layers are more poorly resolved.

The calculation of apparent conductivity has now been incorporated in the DIP processing. Since the second derivative is with respect to the dependent variable h (determined from the data), this operation is highly non-linear in h. As a result, a discrete estimate of the second derivative is usually inconsistent with the data; i.e. assuming steps, or a linear interpolation, the discretely determined values do not integrate back to the true sampling times. This problem was solved by using a seventh degree spline to fit the t = f(h) function, such that t and its first three derivatives are continuous, and that the fourth derivative is minimum. The second derivative is then estimated by analytic differentiation of the spline formula. In essence, this well behaved process determines one of the smoothest σ_a functions consistent with the data.

Field Example

Figure 080.9 shows part of one line of data obtained in a sounding survey in sedimentary terrain. The loop size was 400 m, and each station was measured with three loop positions as shown by the staggering of the data sections. The apparent depths obtained from the transformation of the measured data are shown below the data sections. The horizontal datum lines are the averages of each channel for the whole line, and two types of shading emphasize the difference between the determined depth and this mean: heavy shading for greater depths, and light shading for shallower depths. In general, the conductivity of the section is greater where the depth of penetration is shallower and vice-versa, but a given conductive layer would have a greater effect when located at a shallower depth.

The computed slowness derived apparent conductiveness are displayed in Figure 080.10 as continuous profiles versus depth as calculated by differentiating the spline formulae. The scale is logarithmic with resistivity increasing towards the right. The base lines represent a resistivity of 30 ohm-m (shale), and the spacing between lines, a factor of ten. The heavily shaded area in the right-hand part of the section is a resistive feature (300 Ωm) which has been identified by a borehole near station 13000. The conductive feature centred around station 12000

(<3 Ωm) is thought to be a brine saturated zone within porous rocks.

The regularity of the results illustrates the power of this processing technique for imaging the ground conductivity structure in quasi-layered areas. The authors' experience with the process has showed that an essential condition to obtain such regular results is that the measurements must provide uniform resolution at all depths and stations. It was found that this can be achieved in practice by using at least three loop positions per station as in this example. Experience with data measured in areas with prominent shallow lateral changes has shown, on the other hand, that the method fails completely with such cases, but that it can be of some value in identifying the subtle response of discrete structures deeply buried within a layered earth.

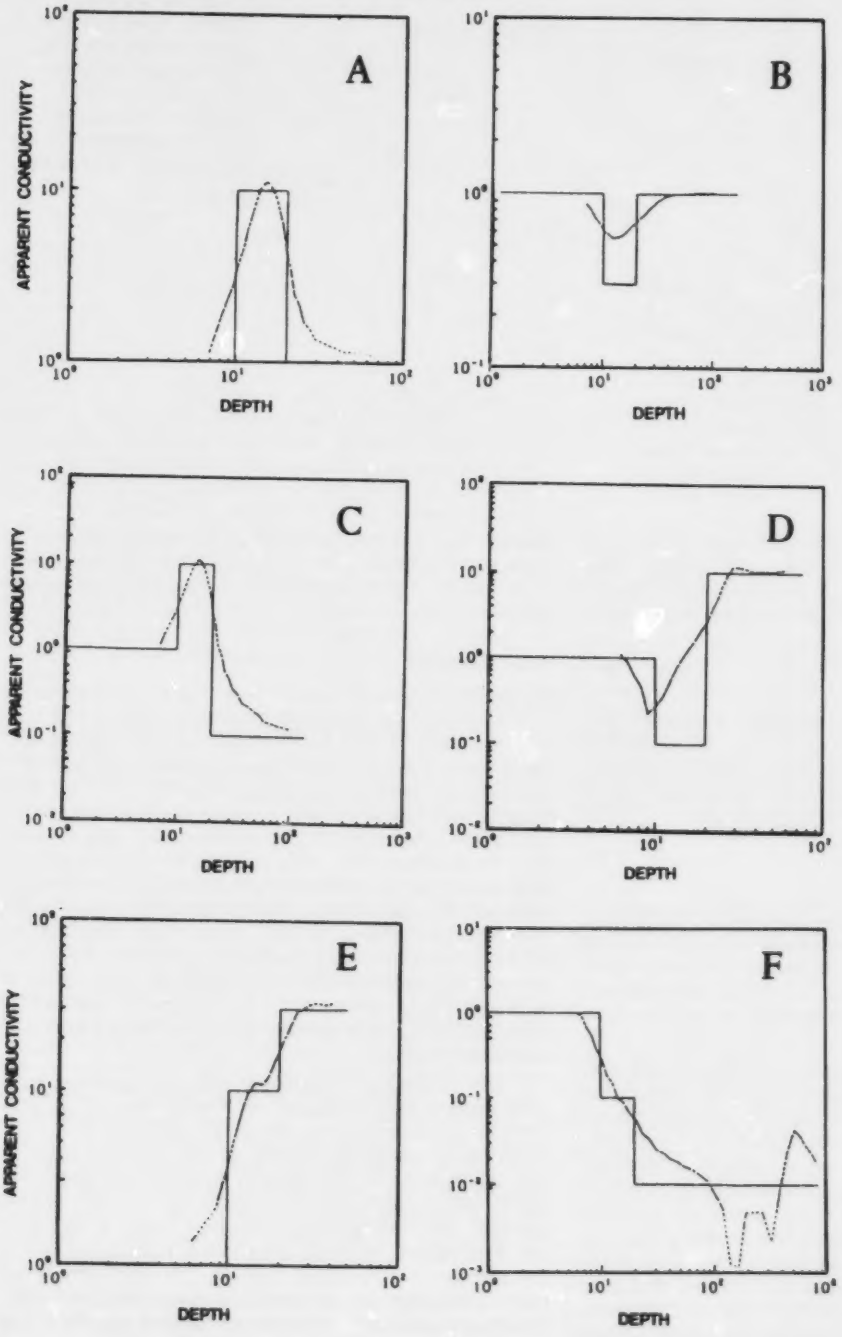

Figure 080.8 *Calculated conductivities versus apparent source depth (dashed), compared to the true conductivities for six representative three-layer models.*

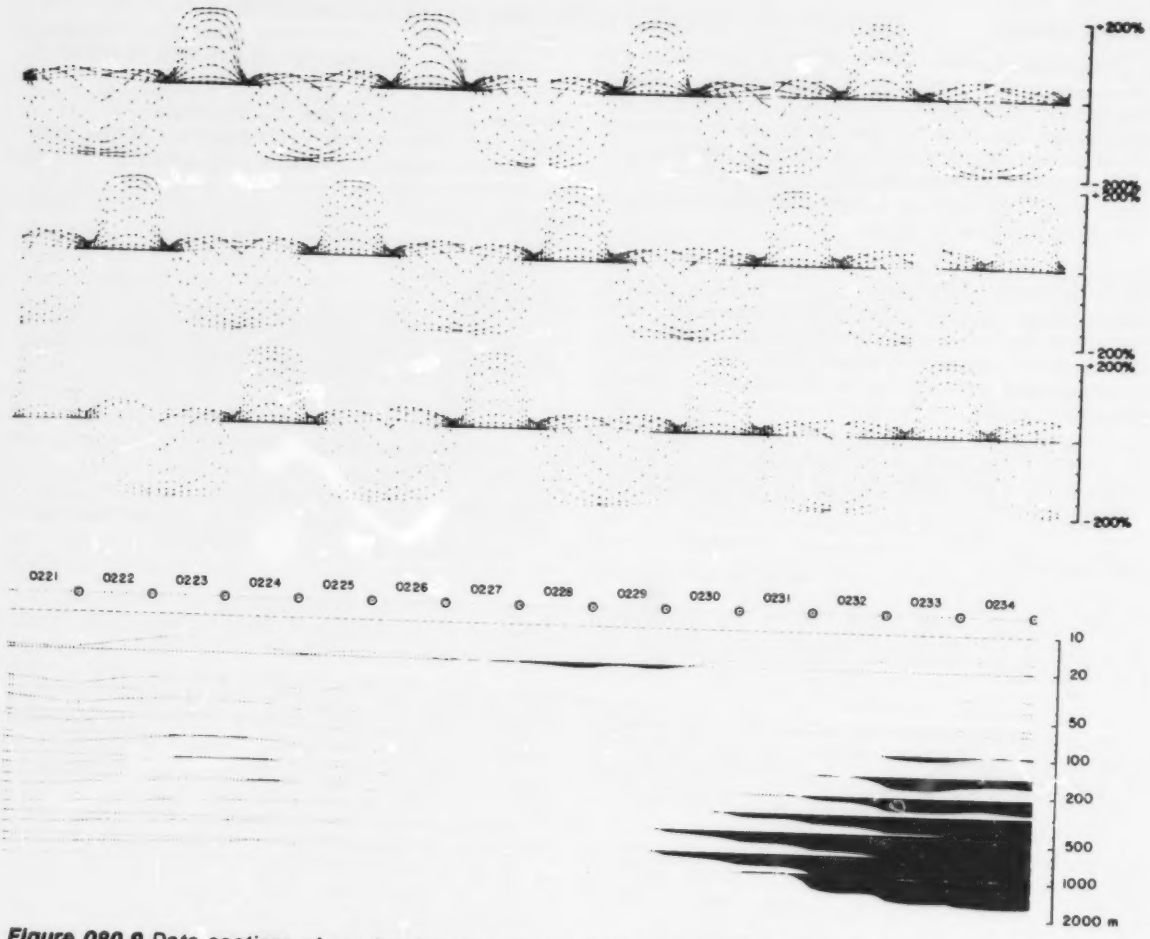

Figure 080.9 *Data sections of overlapping traverses with 15 loop locations covering a segment of a survey line, and the stacked apparent depths produced by the DIP program.*

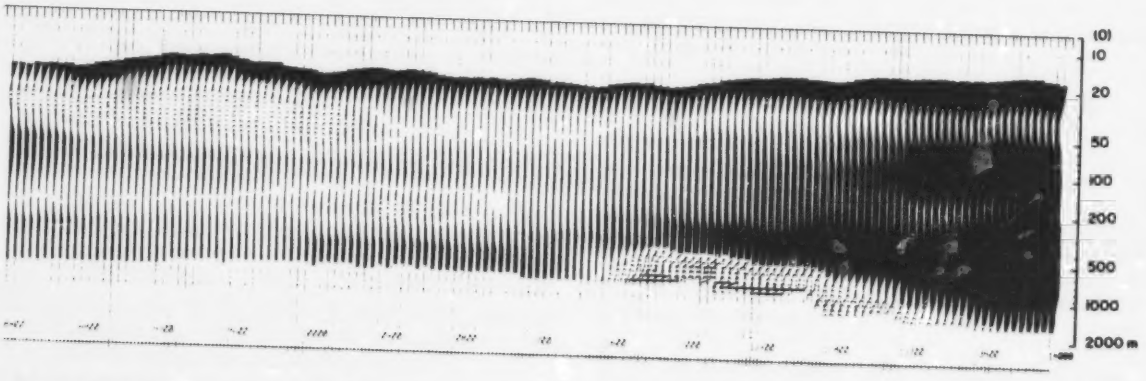

Figure 080.10 *Calculated minimum curvature slowness derived apparent conductivity obtained by taking the second derivative of spline functions. There is a vertical trace every 40 m. The base line of each trace is the 30 Ωm line, and the spacing between lines is a factor of ten. Resistivities higher than 30 Ωm are heavily shaded.*

CONCLUSIONS

A processing system - Depth Image Processing - was developed which produces an approximate image of the ground conductivity structure in horizontally layered areas. For more complex situations where three-dimensional conductive structures are present, it is hoped that an alternate imaging process being developed which is based on pattern matching techniques will serve a similar purpose.

ACKNOWLEDGMENTS

The authors thank BP Exploration Canada and Sohio Petroleum for their support in the initial development of the Depth Image Processing. The DIP field data examples are reproduced by permission of BP Exploration Canada.

The authors also wish to thank the partial funding of this project by the Ontario Geological Survey through the Exploration Technology and Development Program.

REFERENCES

Clay, C.S., Greischar, L.L., and Kan, T.K.
1974: Matched Filter Detection of Electromagnetic Transient Reflections; Geophysics, Volume 39, p.683-691.

Fullagar, P.K., and Oldenburg, D.W.
1984: Inversion of Horizontal Loop Electromagnetic Frequency Soundings; Geophysics, Volume 49, p.150-164.

Macnae, J.C., Lamontagne, Y., and West, G.F.
1984: Noise Processing Techniques for Time-Domain Electromagnetic Systems; Geophysics, Volume 49, p.934-948.

Maxwell, J.C.
1892: A Treatise on Electricity and Magnetism; Dover, New York.

Nabighian, M.
1979: Quasi-static Transient Response of a Conducting Half-Space - An Approximate Representation; Geophysics, Volume 44, p.1700-1705.

Neidell, N.S., and Taner, M.T.
1971: Semblance and Other Coherency Measures for Multichannel Data; Geophysics, Volume 36, p.482-497.

Turin, G.L.
1960: An Introduction to Matched Filters; Institute of Radio Engineers Trans. Information Theory, IT6, p.311-329.

Wood, L.C., Heiser, R.C., Treitel, S., and Riley, P.L.
1978: The Debubbling of Marine Source Signatures; Geophysics, Volume 43, p.715-729.

Grant 081 Development of Interactive Software for the MAGLOG Small Diameter Borehole System

W.A. Morris and S.J. Balch

Morris Magnetics Incorporated, RR#2, Lucan

ABSTRACT

Software has been developed to assist in the interpretation of data acquired by the MAGLOG slimline borehole logging system. Examples are given of the use of these programs for total magnetic field and bulk susceptibility data. Analysis of the total field data permits more accurate resolution of the dip and depth extent of anomalous magnetic bodies. Numerical interpretation of the bulk susceptibility data identifies a suite of susceptibility populations which corresponds to differing geological states, for example; the alteration grade of a granite, or the decomposition of pyrite in sulphide-rich tailings. Work is continuing on the development of programs for the interpretation of fluid temperature and self potential gradient data.

INTRODUCTION

Instrumentation for the acquisition, and algorithms for the interpretation of surface total magnetic field data have been available for many years. Total magnetic field surveys provide distinctive responses in a wide spectrum of geological situations. Examples include lithological contacts, fault boundaries, fracture/alteration zones, and perhaps most importantly, the detection of magnetic oxide concentrations associated with economically important mineral deposits. Bulk magnetic susceptibility measurements also provide diagnostic responses in similar geological situations. While the susceptibility readings provide information on the surface in immediate contact with the detector, interpretation of total field surveys involves a numerical estimation of the geometry of the causative body. As these surveys are conventionally performed at, or above, the Earth's surface, the least well constrained of the model parameters are those associated with the dip and depth extent of the causative bodies. Information provided by the MAGLOG slimline borehole magnetic properties logging system can overcome these problems. However, the interpretation of this data requires the development of a new suite of data processing and interpretational software.

Software development required for the MAGLOG system falls into three categories:

1. Interpretive algorithms for each of the four physical properties measured by the probe: i) total magnetic field, ii) bulk magnetic susceptibility, iii) fluid temperature, and iv) self-potential gradient.
2. A database management system which will permit selective and easy access to segments of the total database for use in interpretation.
3. An interface routine which will allow transfer of data from the MAGLOG field data storage medium to the database of the interpretive microcomputer system.

PART 1: INTERPRETIVE ALGORITHMS

TOTAL MAGNETIC FIELD

Typically, the observed magnetic field is approximated by a geometric model with specified magnetic property characteristics. In forward modelling, fixed model parameters are used to produce a theoretical curve which is then compared to the observed field curve. Inverse modelling allows the model parameters to vary iteratively until the theoretical and observed fields converge to within some acceptable limit. To achieve the objective of developing algorithms which are adaptable to a wide variety of geological geometries, programs have been developed around two general three-dimensional bodies; the finite prism, and the n-sided polygon.

Operational Programs

1. PRISMT calculates the theoretical total field at any point above or below the surface of a finite dipping prism of uniform magnetization, and variable strike and dip (Hjelt 1972).

2. PRISMV calculates the theoretical total field at any point above or below the surface of a finite vertical prism of uniform magnetization which is striking north-south (Hjelt 1972).

3. PRISMB is a routine for forward modelling the anomaly associated with up to five prisms of varying model geometry and magnetic characterstic.

4. POLYG calculates the theoretical total field of a magnetized n-sided polygon at any point P (x,y,z) (Plouff 1976).

5. GUPTA calculates the total field variations produced by topographic changes along a surface profile (Gupta and Fitzpatrick 1971).

6. OPTSVA provides inverse modelling of the total field due to the prism model defined by PRISMT or POLYG. A non-linear least squares optimization is performed using a singular value analysis of the sensitivity matrix. The N x M matrix contains the M partial derivatives of each parameter (numerically approximated) multiplied by the N observed field values and indicates how sensitive the observed field values are to small changes in each parameter (Lawson and Hanson 1974).

7. OPTMAR provides inverse modelling with a prism model where the non-linear least squares optimization is achieved using Marquardt's algorithm (Marquardt 1963).

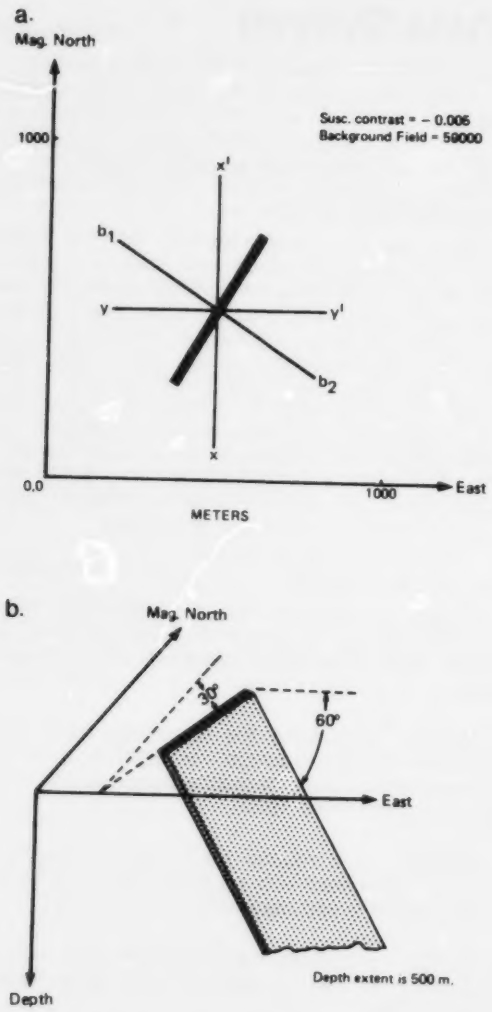

Figure 081.1 *a) Plan view of the surface outcrop of alteration zone (thick bar), the surface total magnetic field traverses X-X' and Y-Y' and the boreholes B1 and B2; b) Perspective view of dipping prism.*

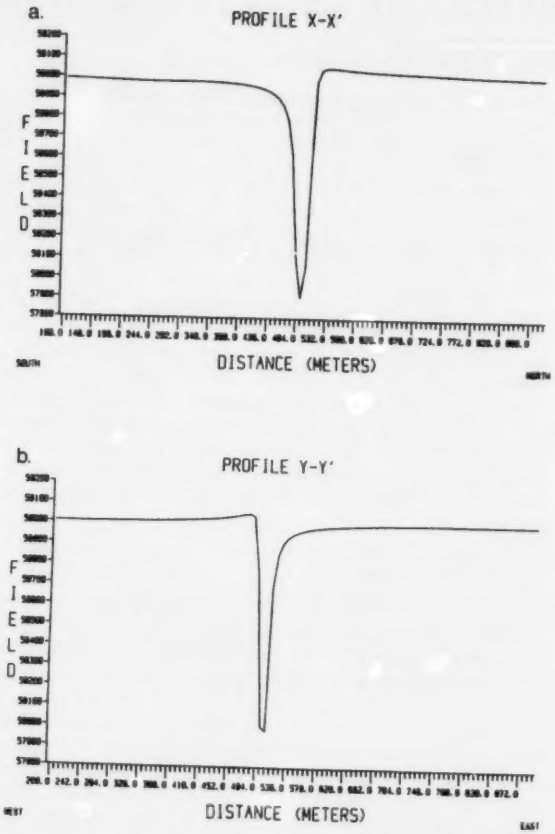

Figure 081.2 *Profiles of total magnetic field (gammas) along surface profiles X-X' and Y-Y'.*

Examples

To exemplify the use of these routines, the reader should consider the geological situation portrayed in Figure 081.1; a dipping alteration zone with negative susceptibility contrast relative to the surrounding country rock. Two orthogonal surface surveys over the body X-X' and Y-Y' give the total magnetic field profiles shown in Figures 081.2a and 081.2b. While it is quite apparent from these profiles that the body dips to the southeast, the exact value of the dip and the depth extent of the body are poorly constrained by the surface magnetic data. Total field profiles down boreholes at locations B1 and B2 resolve this problem. The log of borehole B1 (Figure 081.3a) shows very little sign of any anomaly, while in borehole B2 (Figure 081.3b) the anomaly is strongly developed. The crossover point defines the depth extent of the body and the exact dip of the body can be calculated from the borehole and the surface data.

As noted above, the model geometries used in the optimization routines have the form of finite prisms and n-sided polygons. Upon completion of the interpretation of any single anomaly, the log profile and its interpretation will be presented in the form given in Figure 081.4. The three parts of the diagram show, respectively: a) a three-dimensional perspective plot of the anomalous body, b) a listing of the geometrical and physical properties of the body, and c) a plot of the observed and the optimized model data.

BULK MAGNETIC SUSCEPTIBILITY

Magnetic susceptibility variations are caused by changes in the character of the magnetic oxides present in a volume of rock. Factors controlling the susceptibility are magnetic oxide grain size, composition, and content. As a result, susceptibility logs provide a means for detecting features such as lithological boundaries, the presence of mineralization concentrations, and alteration zones.

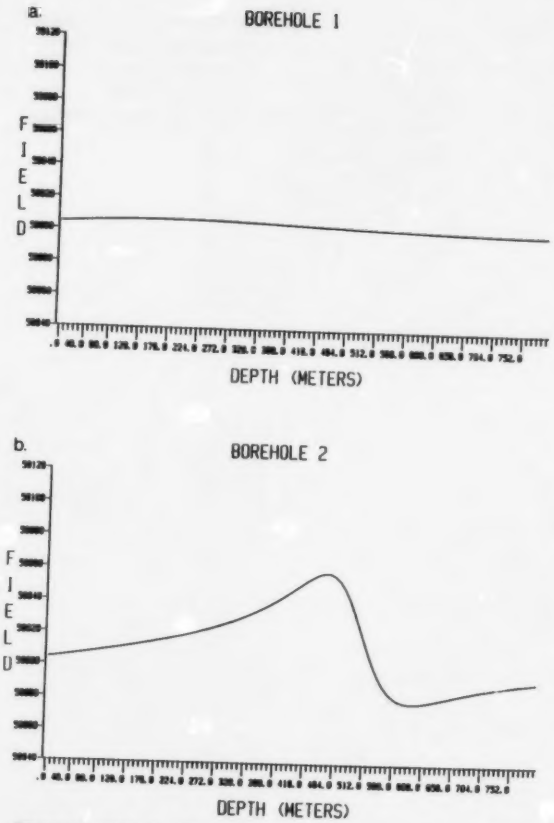

***Figure 081.3** Profiles of total magnetic field (gammas) along boreholes B1 and B2.*

Magnetic susceptibility is characterized by a $\log_{10}$ - normal distribution. The separate populations characteristic of the different geological states present in a core log, can be derived by using routines for the non-linear least squares decomposition of mixtures of normal distributions. Plots of cumulative frequency plotted on log-normal probability axes are the basis of these routines.

Operational Programs

1. HISTO produces a histogram of a set of data and calculates the cumulative frequency.

2. DISPOP separates the individual $\log_{10}$ - normal populations in a given data set, and calculates the boundary value between individual populations.

3. WALSHB identifies boundaries based on transformation of the data into the Walsh domain (Lanning and Johnson 1983).

4. IDENB identifies boundaries between zones of uniform susceptibility levels based on the short- and long-term averages of the susceptibility well-log (Chan 1984).

Examples

Bulk susceptibility core logs have been measured on a wide range of rock types. On cores from Archean and Paleozoic granites, susceptibility logs have been used to identify the location and significance of fracture/alteration zones. On cores from the tar sands, bulk susceptibility logs have been used to locate lithological boundaries and to deduce lithostratigraphic correlations. On cores obtained from uranium tailings, bulk susceptibility logs provided a method for the rapid location of the pyrite alteration front related to surface water migration.

The Archean Eye-Dashwa Pluton located near Atikokan, Ontario, has been examined by Atomic Energy of Canada Limited (AECL) as one of a number of test areas for concept verification as part of the Canadian Nuclear Fuel Waste Management Program. A number of cores drilled in this pluton have been logged at 10 cm intervals by a bulk susceptibility bridge. In the vicinity of the boreholes, the granite has an extremely uniform lithology; hence, any significant change in susceptibility level can generally be attributed to alteration. Figure 081.5 presents cumulative frequency plots of the susceptibility data from boreholes ATK1 and ATK5. Note that both these logs have very similar susceptibility populations. The unaltered granite corresponds to the susceptibility population between 14 and 20 x 10^{-3} S.I. The populations below this level correspond to progressive levels of alteration of the granite. ATK5 has an additional high susceptibility population that is not present in ATK1. After reference to the geological log, it is apparent that this corresponds to a granodiorite unit that is only found in ATK5. By inverting these probability plots, it is possible to develop the pseudo-lithology plots as shown in Figure 081.6. The different shadings correspond to different susceptibility populations, extensions of this type of SUSLOG are susceptibility based geological cross-sections.

An example of the use of IDENB is given by using data from another AECL study area, the Gabbro-anorthosite intrusion at East Bull Lake near Massey, Ontario. Figure 081.7a presents the raw susceptibility data from borehole EBL3. Even cursory examination reveals this core contains both lithological and alteration related susceptibility level changes. Figure 081.7b compares the boundary picks identified by IDENB (the lines) and the real lithological boundaries (the arrows) as identified by geologists.

SELF POTENTIAL GRADIENT

Self potential studies involve the measurement of naturally occurring potential differences usually caused by electrochemical or mechanical subsurface activity. Within the oil/gas industry, this technique has received a lot of attention as a means for studying such features as: depositional environment, stratigraphic correlation, structural mapping, shaliness mapping for permeability traps, and water salinity. Quantitative interpretation of self potential measurements in terms of mineral exploration appears less well developed. Bolviken *et al.* (1973) have presented experimental results which indicate that significant self potential anomalies are often associated with

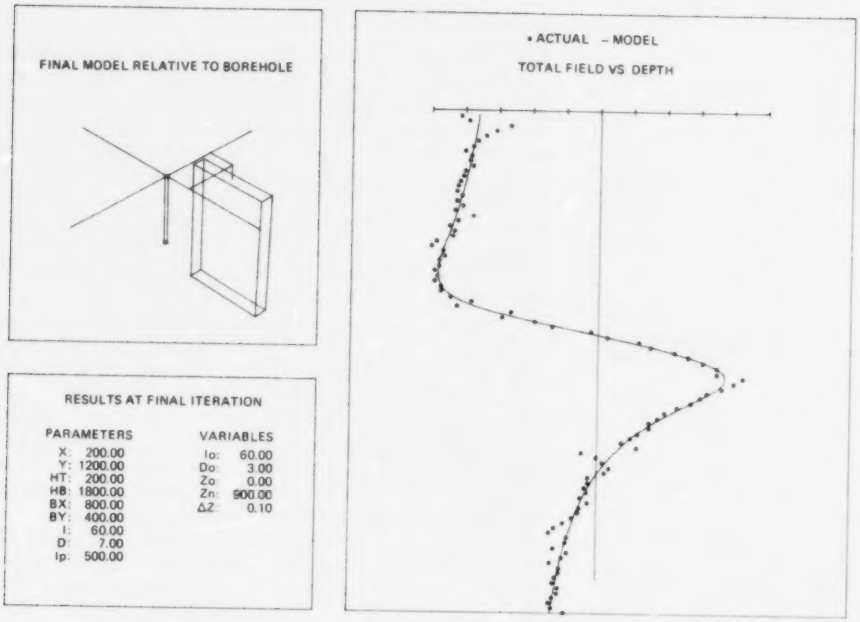

Figure 081.4 *Example of the output from the interpretation of a downhole total magnetic field anomaly.*

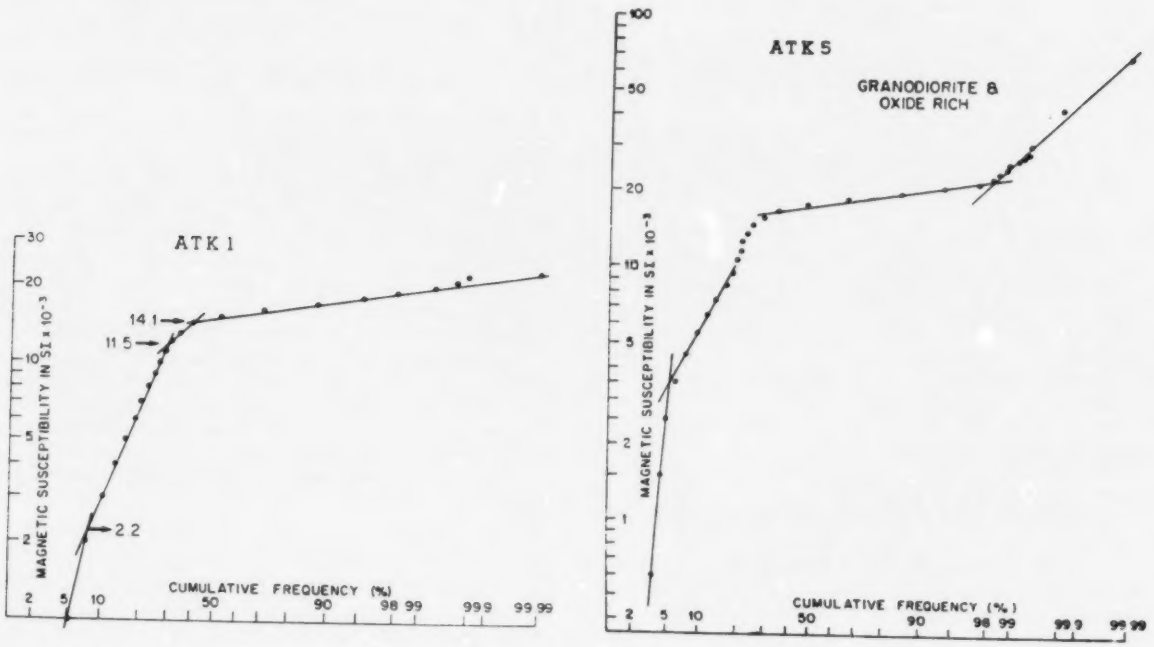

Figure 081.5 *Log_{10} - normal cumulative frequency plots of bulk susceptibility data acquired from ATK1 (a) and ATK5 (b) from the Atikokan research area of Atomic Energy of Canada Limited.*

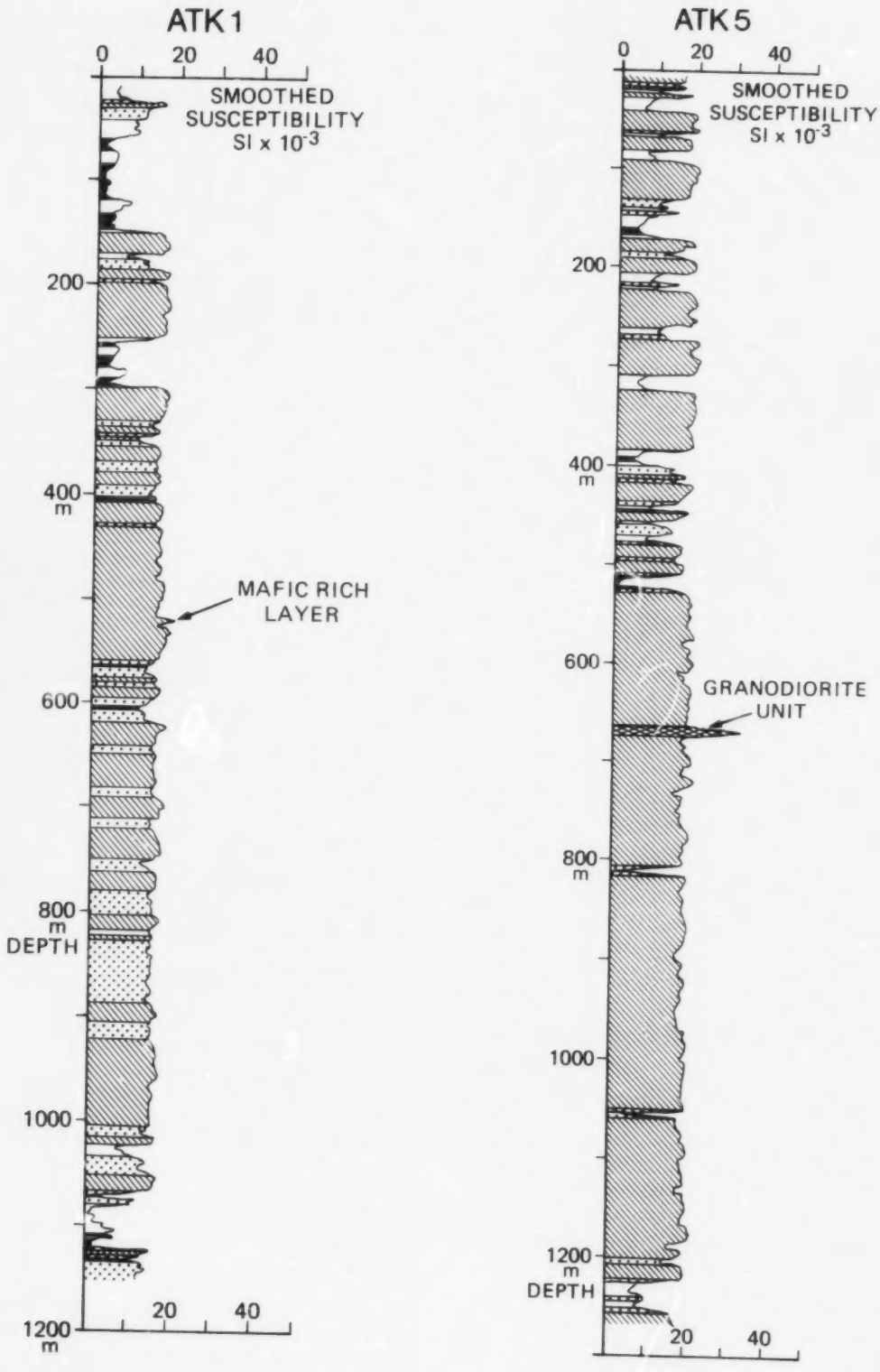

Figure 081.6 *Pseudo-lithology plots from boreholes ATK1 (a) and ATK5 (b) derived from the bulk susceptibility logs.*

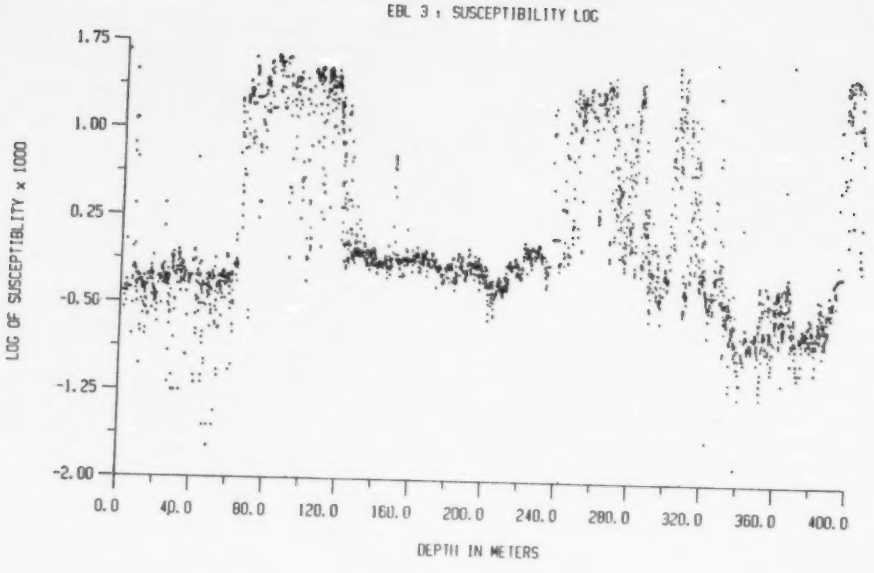

Figure 081.7a *Plot of the raw bulk susceptibility data from EBL3 in the East Bull Lake gabbro - anorthosite.*

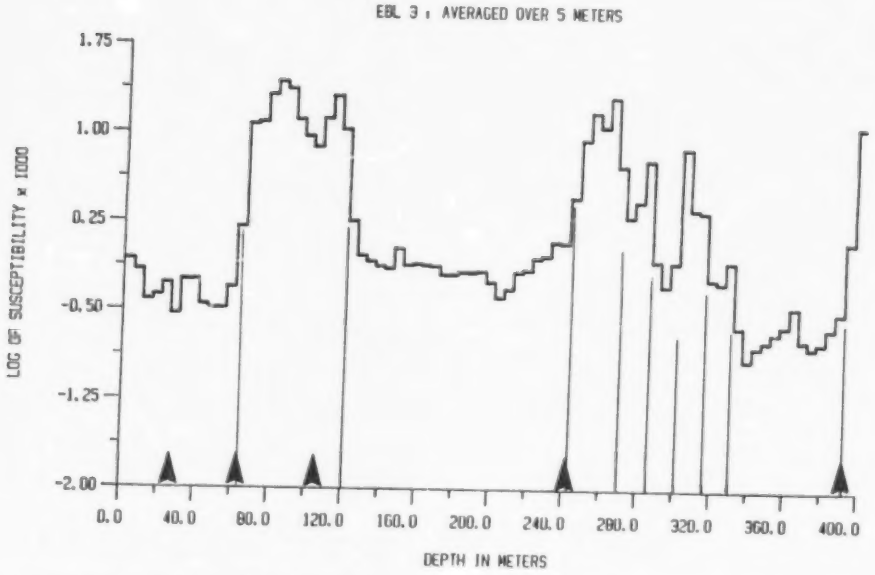

Figure 081.7b *Comparison of the boundaries picked by IDENB (thin lines) versus the lithological boundaries mapped by geologists.*

concentrations of sulphide, magnetite, and graphite. More recently (Society of Exploration Geophysicists, Atlanta, 1984), a number of companies have shown an interest in surface self potential measurements for mineral exploration and for geotechnical site surveys.

At the present time, no programs have been developed for this part of the MAGLOG data. These are to be the subject of the 1985-1986 project year.

TEMPERATURE

The temperature logging system will serve two purposes. First, it will be used in reducing the data gathered from the other logs to a constant temperature. This for example is important in the case of water salinity calculations based on the self potential measurements. Second, temperature logs will be used for detecting water seepage zones, and the preparation of temperature gradient logs for mapping lithological detail (Conaway and Beck 1977; Kayal 1981).

No programs have been developed at the present time. These are to be the subject of the 1985-1986 project year.

UTILITY ROUTINES

A number of routines have been written that can be used with any of the above physical parameters. The utilities perform tasks which aid in data processing.

1. PLOT2D program for producing a linear - linear x-y plot on a HP7470A.

2. MOVAG calculates the moving average of a data file.

3. CROSSCOR, AUTOCOR to perform cross-correlation and auto-correlation between logs from separate boreholes.

4. SPLINE to perform a spline interpolation of a data set at some specified spacing interval.

5. POLYFIT a program to fit a Nth order polynomial to a data log.

6. FILTER a program which uses an optimum bilateral exponential smoothing model for separating signal from background noise.

7. GOLAY a program which uses a least squares polynomial line fitting routine for the smoothing and differentiation of borehole logs.

PART 2: CONSTRUCTION OF A DATABASE FORMAT

In operation, the MAGLOG system (or any other borehole system for that matter) produces a stream of data which contains a record of the sequential variations of each individual parameter measured by the probe. The authors anticipate that each record will contain at least seven fields of data. The objective of the database program will be to develop a system whereby it will be possible to:

1. access selected segments of the data from various files and route them to the desired interpretation package
2. permit simple editing of the data file
3. permit efficient storage and retrieval of information produced by either of the procedures above

With the aid of commercially available software tools, work on a general database program has begun. The authors expect completion of the program by late summer 1985.

PART 3: THE INTERFACE

The MAGLOG system (or any other logging tool) generates a field data record on a magnetic tape or cartridge. To make this information accessible to their computer system requires that the authors develop a program which will transfer the field data onto a medium compatible with their system. This will probably require the conversion of field data from a high density cartridge to a nine track tape, or hard disc system.

The interface, in the form of software, will not be developed until the MAGLOG system becomes operational which is currently expected to be during the spring of 1985.

ACKNOWLEDGMENTS

Morris Magnetics is grateful to the Ontario Ministry of Natural Resources for its financial assistance through the Exploration Technology Development Fund; without this assistance, this research would not have been possible.

The authors wish to thank Atomic Energy of Canada Limited for permission to publish examples from studies made at the East Bull Lake and Atikokan research areas.

Pierre Lapointe of Earth Physics Branch, Energy, Mines and Resources, Canada, Bil Thuma of Geotech, and Detlef Bluhn of IFG are all thanked for their many contributions to this project.

REFERENCES

Bolviken, A., Logn, O., Breen, A., and Uddu, O.
1973: Instrument for In Situ Measurements of Eh, pH, and Self Potentials in Diamond-Drill Holes; Geochemical Exploration 1972, edited by M.J.J. Jones, Proceedings Symposium Geochemical Exploration 4th London 1972, p.415-420.

Chan, D.S.K.
1984: Discussion of Lanning and Johnson (1983); Geophysics, Volume 49, p.1801-1802.

Conaway, J.G., and Beck, A.E.
1977: Fine Scale Correlation Between Temperature Gradient Logs and Lithology; Geophysics, Volume 42, Number 7, p.1401-1410.

Gupta, V.K., and Fitzpatrick, N.M.
1971: Evaluation of Terrain Effects in Ground Magnetic Surveys; Geophysics, Volume 36, p.582-589.

Hjelt, S.E.
1972: Magnetostatic Anomalies of Dipping Prisms; Geoexploration, Volume 10, p.239-254.

Kayal, J.R.
1981: Correlation of T-log with E-log in Coal Bearing Formations; Pageoph, Volume 119, p.349-355.

Lanning, E.N., and Johnson, D.M.
1983: Automated Identification of Rock Boundaries; Geophysics, Volume 48, p.197-205.

Lawson, C.L., and Hanson, R.J.
1974: Solving Least Squares Problems; Prentice Hall Inc.

Marquardt, D.W.
1963: An Algorithm for Least Squares Estimation of Non-Linear Parameters; Journal of the Society of Industrial Applied Mathematicians, Volume 11, p.341-441.

Plouff, D.
1976: Gravity and Magnetic Fields of Polygonal Prisms and Application to Magnetic Terrain Corrections; Geophysics, Volume 41, Number 4, p.727-741.

Society of Exploration Geophysicists
1985: Engineering and Groundwater Applications of the Self Potential Method; p.152-168 *in* Abstracts of 1984 Annual General Meeting of the Society of Exploration Geophysicists held in Atlanta, 302p.

Grant 084 Helicopter Borne High Sensitivity Magnetometer Tridirectional Gradiometer Based on Overhauser Effect

Ivan Hrvoic

GEM Systems, Inc., Toronto

ABSTRACT

GEM Systems has recently developed a broadband continuous source of proton precession frequency based on the Overhauser effect. "Proton Oscillator" model GSM-11A has many features of a standard proton precession magnetometer, such as high absolute accuracy, almost non-existent drift, plus increased sensitivity approaching sensitivities of alkali vapour magnetometers. Four proton oscillators have been installed in a special "bird" with two fins at the tips of the imaginary tetrahedron to allow for measurement of absolute magnetic field and the gradients in three directions: vertical, along, and across the track, with a noise envelope of 0.025 nT/m for two readings per second. Elaborate signal processing provides also a measure of noise (fourth difference) for all channels, direct gradients between any pair of sensors, and convenient interfacing to analog recorders and data acquisition systems.

INTRODUCTION

Over the past three years, GEM Systems Inc. has developed a source of continuous proton precession signals, model GSM-11A Proton Oscillator (Photo 084.1), based on Overhauser Effect (Abragam 1961; Pomerantsev *et al.* 1968). The Overhauser Effect can be evoked in assemblies of interacting dissimilar spins such as protons and free electrons in liquids.

The effect is used in other areas of research in chemistry, physics, biology, and so on. In Weak Field Magnetometry, it serves to increase proton polarization above thermal equilibrium. The increase is proportional to the ratio of precession frequencies of electrons and protons. Special "free radicals" have been developed that have a free electron dwell in a local magnetic field of the nitrogen atom. The field is about 16 Gauss and the free electrons' precession frequency about 45 times above the normal level of the Earth's magnetic field. The precession frequency of the free radical used is 62 MHz compared with 2.1 kHz proton precession frequency in a 0.5 Gauss magnetic field.

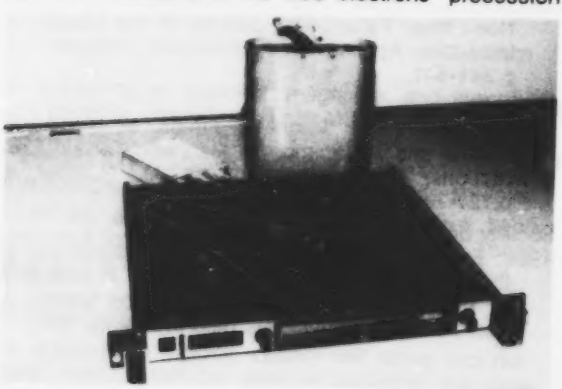

***Photo 084.1** High Sensitivity Airborne Proton (Overhauser) Magnetometer.*

By saturating electron spin resonance lines at 62 MHz, proton polarization of the sensor liquid is increased by some 5000 times over the thermal equilibrium in the Earth's magnetic field. This polarization is steady as long as electron spin resonance lines stay saturated.

To generate the proton precession signal, a proton magnetization vector must be deflected into a plane of precession at right angles to the applied magnetic field. This is done by placing the sensor liquid in a set of coils in bridge configuration, and applying the "excitation current" to its input. The excitation current generates the excitation magnetic field which in turn deflects the proton magnetization vector into the plane of precession. The precessing proton magnetization vector generates voltages at the output of the bridge, while the induced voltage of the originally applied excitation field is highly suppressed at the output. The proton precession signal is further amplified and fed back to the input of the filter, to generate spontaneous proton oscillations. The oscillator generates a continuous proton precession signal as long as the electron spin resonance line of the free radical stays saturated.

A sensor of the proton oscillator contains about 1 L of liquid and the electronic circuitry, including the RF source takes only a modest space of about 10 by 15 by 5 cm. Power required is only about 6 to 8 Watts to produce a sufficiently clean proton precession signal for 0.01 nT/s resolution, or 0.1 nT per 0.2 second interval. The proton oscillator is a wideband, untuned system, simple and convenient to operate. Ground tests in a quiet environment showed a noise envelope below 0.1 nT for 5 readings per second. Two magnetometers have been tested in the same area, and the difference in readings observed was calculated in order to eliminate the influence of diurnal variations.

Airborne tests in a helicopter borne vertical gradiometer configuration showed the noise envelope of the difference in readings of <0.1 nT for two readings per second. With 3 m spacing between the sensors, this sensitivity is about at the level required for federal-provincial surveys (0.025 nT/m).

GRADIOMETER CONFIGURATION

Four proton oscillators are used in a special configuration, shown in Photo 084.2, to measure tridirectional gradients. The sensors are placed in the back end of the bird shell and in the tips of three fins, 3 to 4 m apart from each other. Average periods of the four precession frequencies are measured by a special

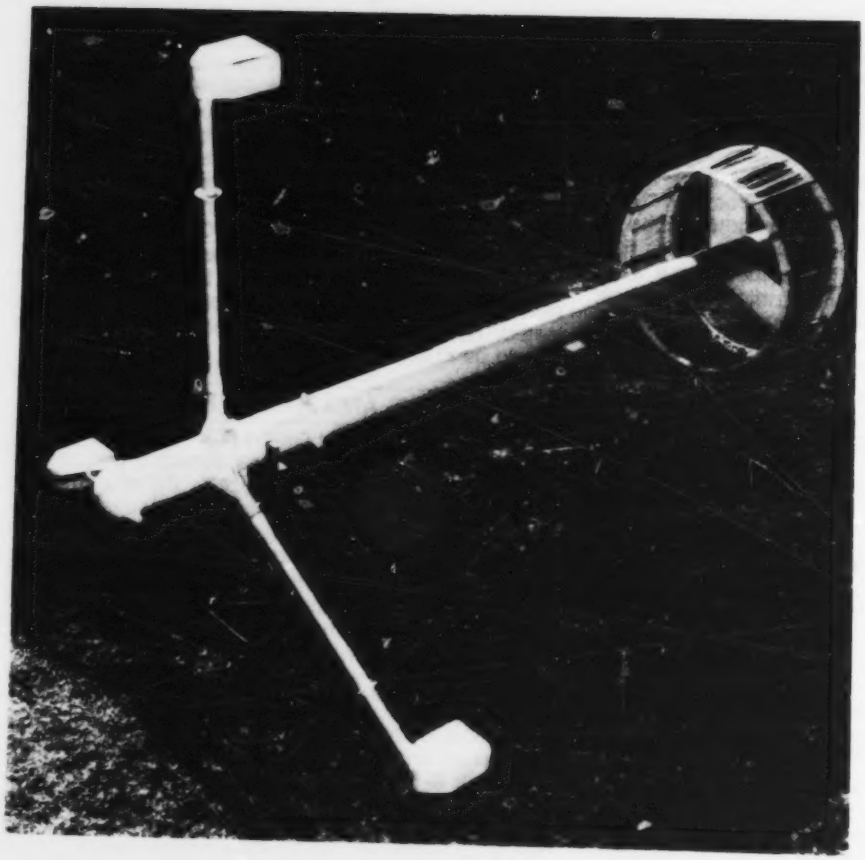

Photo 084.2 *Special configuration of four proton oscillators used to measure tridirectional gradients.*

computerized frequency meter (Photo 084.3) and converted into magnetic field units. The differences in readings are taken and divided by the sensor spacings. Horizontal across track gradient is measured directly from the readings of the two lower (horizontal) sensors; the vertical is determined from the average field measured by horizontal sensor and the sensor in the vertical fin. Horizontal along the track gradient is based on the average field from the three sensors placed in the fins and the bird-end sensor. Fourth differences are calculated for all three gradients as well as four absolute values of magnetic field.

THE BIRD

Traditional design criteria for EM birds were observed when the bird was designed. The bird is shown in Photo 084.2.

Requirements for rigidity are very much relaxed in comparison with EM birds. It is sufficient to measure gradients with 0.1% accuracy (up to 25 nT/m and beyond) compared with EM measurements of some parts per million. The bird's shell was, therefore, designed of sufficient diameter and wall thickness to accept the magnetometer sensor and support weight of sensors, fins, skirt, and its own weight with <0.1% change of relative sensor positions due to shell flexing.

The fins are spaced at 120 degrees to allow for simple calculation of gradients in all three directions: the average magnetic field of the two lower fins fall beneath the upper fin sensor to allow for vertical gradient determination; the average field of all three sensors falls in the centre of the bird shell to allow for simple determination of along-track gradient.

All three fins are 2.0 m long to achieve a spacing for the vertical gradiometer equal to 3.0 m. Horizontal across and along the track gradients are based on a sensor spacing of 3.46 and 3.76 m, respectively, although the sensor in the bird shell can be moved along the shell to suit any potential requirements for different along-track configurations.

The bird skirt is designed to allow for variable drag in order to experimentally optimize the bird stability and flight characteristics.

In order to improve the distribution of weight along the bird shell, the fins are placed in front to somewhat overweigh the skirt and to make the front end somewhat heavier in a stationary state. This ensures a downward pressure on the skirt when flying, and a stable towing of the bird. Pick-up points are selected close to Euler minimum flexing points, although rigidity is not critical.

SIGNAL PROCESSING

The Overhauser magnetometer supplies a continuous precession frequency to the processor for precise measurement and conversion into magnetic field units.

In our case, the frequency of about 2.4 kHz has to be measured to within 3 mHz, or close to 1 ppm within 0.5 second intervals. The average period of the precession frequency is determined, and the field calculated by reciprocation. This method has a weak point in relatively limited synchronization of readings: plus or minus one quarter of precession period is the maximum uncertainty, since the authors measure all zero crossings of the precession frequency. Synchronization becomes important when the magnetic field varies sharply with relatively low gradient changes. For example, if a magnetic field changes by 1000 nT/s, synchronization within 100 usec may result in a false difference reading of 0.1 nT or a gradient of 33 pT/m.

A signal processor has been designed and made in cooperation with Urtec Ltd of Toronto. Model GSM-11GH4 measures four channels of magnetic field, calculates appropriate differences and fourth differences as a measure of noise. Various speeds of measurement are selectable as well as bandwidths. Higher order digital filters are used to limit the bandwidth of measurement and prevent aliasing. Relatively wideband phase-lock loops are used in each channel as tracking bandpass filters.

Elaborate interfacing with analog recorders and data acquisition systems is provided as well as selection of internal or external triggering. The signal processor supplies power for the Proton Oscillators.

RESULTS

Considerable work has been done on Proton Oscillators. Reliability and signal-to-noise ratio has been significantly improved and RF source optimized for power consumption. A new, improved free radical has been procured and sensors have been prepared and tested. Packaging of the sensors has been completed. The bird has been designed and manufactured. Its total weight is about 100 kg (220 pounds). As the distribution of weight is favourable, no additional weights will be required for balancing. The signal processor has been completed, and partially tested. By the end of the fiscal year, the system should be in a bench test state.

CONCLUSIONS AND FUTURE PLANS

The gradiometer, Model GSM-11GH4, has exceptional features such as high absolute accuracy and resolution with negligible long term drift. By now, the authors are certain its performance will satisfy specifications set forth for the federal-provincial program of gradiometer surveys. Additional data provided by the tridirectional gradiometer will help improve the quality of contour maps. It will also offer a better means of determinating the parameters of the sources of secondary fields. The usage and the interpretation of data will be the subject of continuing research.

At this point, there is a considerable amount of work to be completed. One remaining problem to be solved is a precise in-flight positioning of the bird and its orientation in space. It is not obvious how critical the positioning parameters are and some theoretical work will be needed before opting for the most effective practical solution.

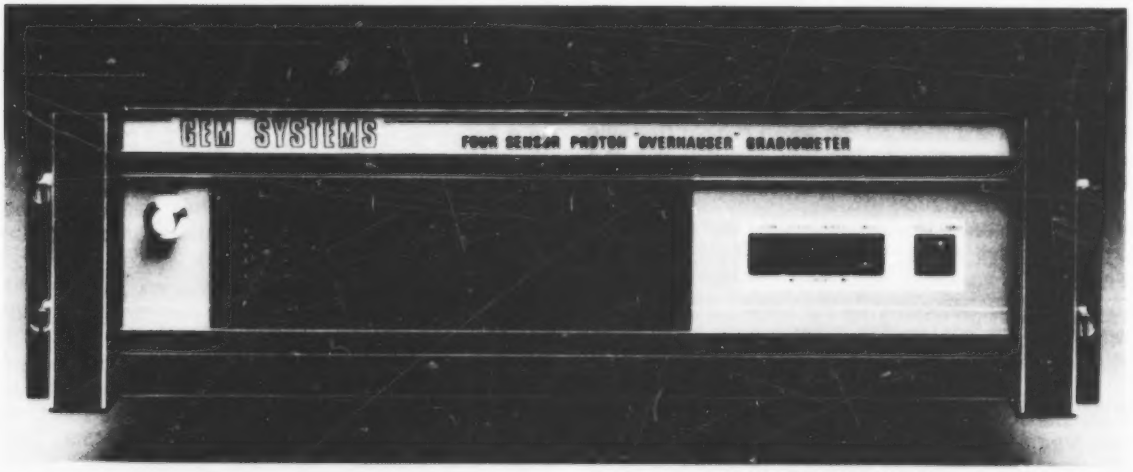

Photo 084.3 *Special computerized frequency meter used to measure the average periods of the four precession frequencies.*

ACKNOWLEDGMENTS

The author wishes to thank the Ontario Ministry of Natural Resources and the Ontario Geological Survey for their help. S. Washkurak and L.J. Kornick of the Geological Survey of Canada are thanked for their helpful discussions and suggestions.

REFERENCES

Abragam, A.
1961: Principles of Nuclear Magnetism; Oxford University Press.

Pomerantsev, N.M., Ryzhkov, V.M., and Skrotskiy, G.V.
1968: Geofizicheskaya Apparatura, Number 33, 1967, p.13-94; published *in* Quantum Magnetometry, Joint Publications Research Service, JPRS 46444.

Grant 087 High Resolution Shallow Soundings Using Radar and Reflection Seismic Methods

J.L. Davis and A.P. Annan

A-Cubed Inc., Mississauga

ABSTRACT

Radar and seismic methods are complimentary geophysical techniques that offer the highest resolution sounding methods available. The seismic method can sound to greater depths than radar, but the radar provides higher resolution soundings more economically.

High resolution mapping is required by geomorphologists, geochemists, and hydrogeologists who require detailed information on bedrock topography and soil strata. The bedrock topography has a major influence on the groundwater flow patterns and thus on the deposition of heavy metals and contaminants. The bedrock topography is also a major factor for the interpretation of other geophysical and geochemical surveys. Mining and geotechnical site investigations require high resolution mapping. Mapping the extent of economically extractable sands and gravels is also a major concern in Ontario. Radar and seismic methods are well suited for all these mapping applications especially when used with borehole logging. Current radar instrumentation can sound to 30 m depth in resistive geological materials and shallow seismic reflection is most successful at depths >30 m.

This paper describes the radar and seismic methods and presents three case histories that illustrate how the radar and seismic methods extend the borehole data, and also how radar and seismic data can be used together to identify and map the bedrock topography when no borehole data are available.

BACKGROUND

There are a large number of applications where high resolution shallow soundings are required. Some of the applications include overburden mapping to delineate the bedrock interface, soil strata and, in coarse-grained soils, the water table. The bedrock topography is often the controlling factor affecting groundwater flow and exploration for placer deposits.

In areas of deep overburden cover, the bedrock topography can be a major factor in the interpretation of other geophysical data. Furthermore, the data for this work can also be used to design geochemical surveys, especially basal till sampling programs. Stratigraphic mapping is significant in the exploration for placer gold deposits. High resolution mapping is also required in the evaluation of peat and coal deposits in the Hudson Bay Lowlands, and also for the evaluation of the sand and gravel reserves. These are major concerns in Ontario.

Geotechnical site evaluations also require high resolution subsurface mapping. The economic viability of many mineral deposits is controlled by the cost of mine development. Open-pit mining and tunnel development are controlled by the overburden thickness and stability. Radar and reflection seismic are two methods well suited for these applications.

Radar has very high resolution characteristics and often can resolve features that are only a few cm thick with depth accuracies of a few tens of cm. The shallow reflection seismic method can map stratigraphy to much greater depths but with lower resolution than the radar method. Typically, the reflection seismic soundings are only practical at present at depths >30 m. Geological Survey of Canada personnel (Hunter *et al.* 1984) are developing methods to make the seismic reflection method practical to shallower depths. A-Cubed Inc. is currently developing a radar instrumentation and techniques that will yield greater depth penetration. The effective depth of exploration ranges of the two methods will soon overlap.

Ground probing radar and reflection seismic methods offer the highest resolution geophysical sounding methods available. The two methods are complimentary with seismic having the ability to sound to greater depths in terrain where radar penetration is limited, whereas radar provides higher resolution sounding at a more economical cost.

In general, no single geophysical technique can uniquely determine geologic stratigraphy without other correlative information such as borehole data. In some instances, two sets of geophysical data can be used to uniquely identify the geologic source of a response. For example, seismic refraction can often be used in conjunction with the radar to uniquely identify the depth to bedrock.

In this paper, descriptions of the principles underlying ground probing radar and shallow seismic methods, the equipment used, the field survey procedure, and the field data obtained are presented. Field examples illustrate how radar data can be used to extend the borehole data and how radar and seismic soundings can be used to identify the bedrock interface. In addition, data from a new radar instrument presently under development are compared with results from an earlier generation of equipment.

BASIC PRINCIPLES AND METHODOLOGIES

The radar and seismic techniques are very similar both in principle and survey method. The seismic method uses an acoustic energy source to generate sound waves which propagate into the ground. The radar method uses electrical energy to generate electromagnetic (radio) waves which are radiated into the ground.

SEISMIC

The seismic methods map subsurface structure by detecting sound waves which are reflected and/or refracted at changes in acoustic impedance. Seismic stratigraphy maps subsurface changes in acoustic wave propagation properties. Correlation of seismic

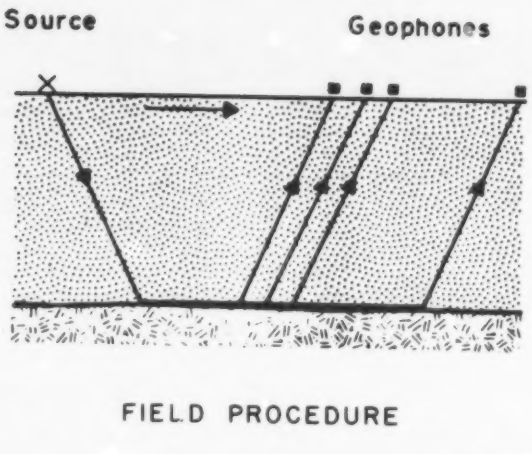

Figure 087.1 Schematic representation of a seismic refraction sounding and data collected from the shot. Arrows represent acoustic wave paths through the overburden and along the overburden-refractor interface. A fully interpreted refraction spread yields refractor depth beneath each geophone location.

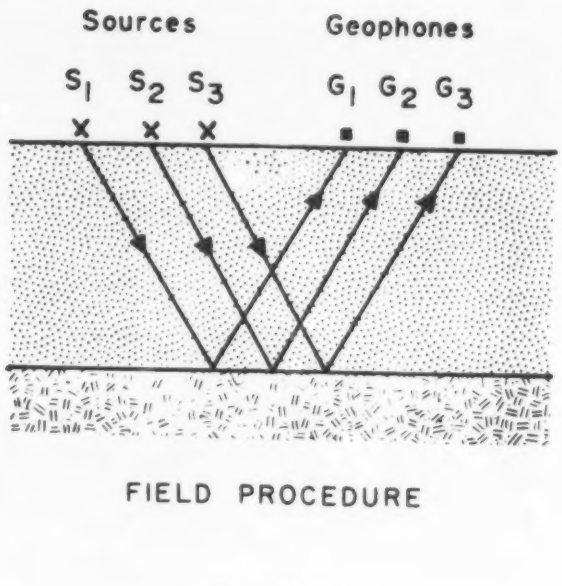

Figure 087.2 Schematic representation of common offset seismic reflection profiling. Data is obtained for the midpoint position of each source geophone pair producing a representative cross-sectional view of the subsurface.

stratigraphy with geologic control information permits extrapolation of geologic stratigraphy. Seismic methods are divided into two main classes, namely, refraction and reflection methods.

The seismic refraction and reflection methods are conceptually illustrated in Figures 087.1 and 087.2. Typical data outputs are shown beside the sketch of each method. The seismic refraction method is most effective when it is used for shallow sounding. Refraction surveys are most often useful for determining the depth to bedrock because there is usually a large velocity increase at the overburden bedrock contact. Weathered bedrock surfaces can be difficult to map with the refraction method since the velocity contrast may be reduced and will be gradational.

Seismic reflection methods are preferable to refraction techniques for mapping purposes. A number of practical acoustic and equipment properties limit the application of seismic reflection to depths usually in excess of 30 m. The seismic reflection method is well developed for petroleum exploration. The shallow reflection seismic method is becoming more common with the advent of portable, multichannel seismographs. The technique is being further developed at the Geological Survey of Canada; Hunter *et al.* (1984) gave excellent examples of shallow reflection seismic data.

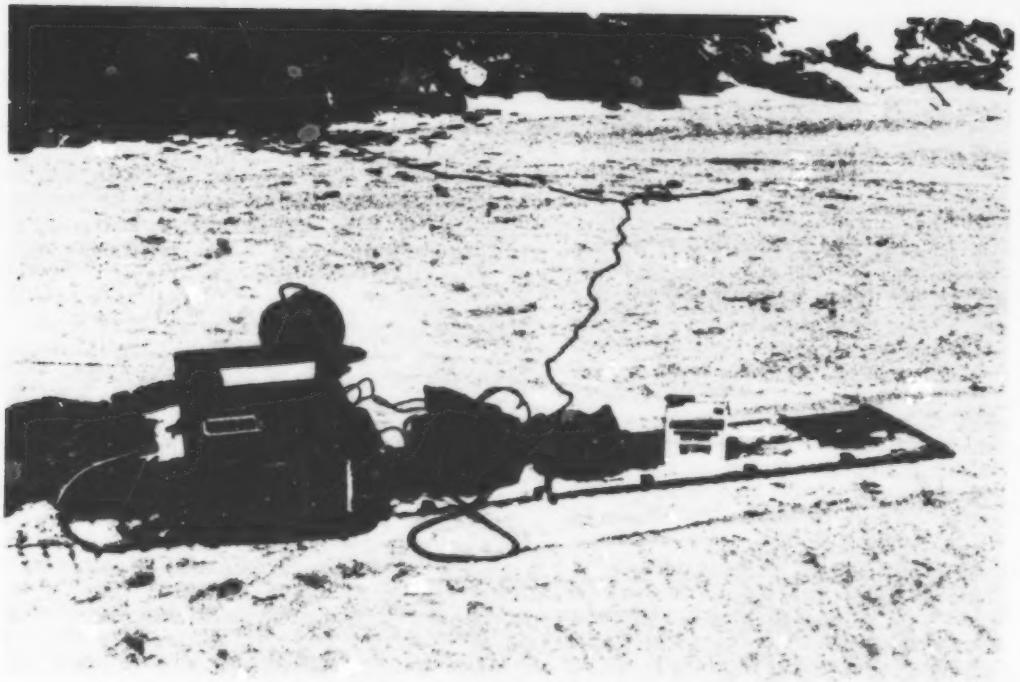

Photo 087.1 Portable seismograph in field operation.

Photo 087.1 shows a portable 12-channel enhancement seismograph. There are a number of such units commercially available and they are all similar in size and capability. A hammer, a shotgun shell, or dynamite can be used for the seismic source depending on the depth and material to be sounded. The geophones are spaced depending on the depth range and resolution required.

RADAR

In the radar method, a short burst of high frequency electromagnetic energy is transmitted into the ground. Transmission of the radar signal depends upon the high frequency electrical properties of the ground which are primarily controlled by the water content of the soil. There is usually a large contrast between the electrical properties of wet soils and bedrock. Variations in grain size distribution in soils usually are associated with changes in porosity, which in turn give rise to radar reflections.

Radar surveys are carried out in a similar manner to seismic surveys. Figure 087.3 shows a typical setup for radar wide angle reflection and refraction (WARR) sounding, while Figure 087.4 shows the reflection profiling mode. The WARR sounding is the electromagnetic equivalent of seismic refraction. Typical data outputs are shown beside the sketches of each procedure. The radar reflection profiling mode is used for high resolution mapping of lateral changes. WARR soundings are used to estimate velocity versus depth to aid interpretation of the data collected in the reflection profiling mode.

The radar technique is analogous to the seismic technique, but there are major functional differences between the techniques. The basic principles of the radar method are given in Morey (1974) and Annan and Davis (1976). The radar system transmits and receives signals many thousands of times a second and physical contact with the ground is not necessary. As a result, radar survey data can be collected very quickly.

Radar is usually used in the reflection mode where the spacing between the antennas is kept fixed while the antennas are moved over the ground. The spacing between the antennas is determined by the exploration depth and resolution desired just as the geophone spacing is determined for seismic sounding. In rough forested terrain, which is typical of much of Ontario, the antennas can be moved in discrete steps. This allows the antennas to be manipulated through the trees and over rough terrain, and permits maximum signal coupling into the ground. A-Cubed Inc. has developed portable and robust equipment as well as data handling techniques for this type of radar survey. Photo 087.2 shows the radar unit, cassette tape recorder, and antennas that are used in typical placer environments. In rough terrain, up to 3 to 4 line km can be surveyed using 3 m step intervals in a day. Greater distances can be covered if the terrain is flat and in open country.

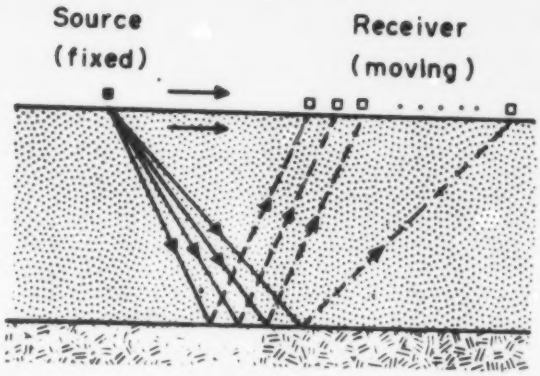

Figure 087.3 Schematic representation of a radar wide angle reflection and refraction sounding and collected data. Arrows indicate direct travel paths of electromagnetic waves through air and overburden and reflected paths from a buried interface. Corresponding events are labelled on the data sketch.

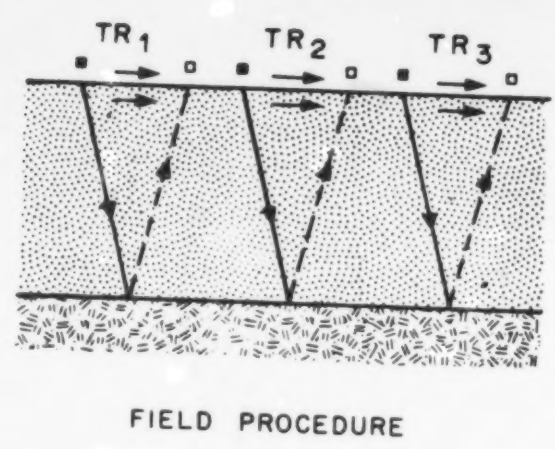

Figure 087.4 Schematic representation of radar reflection profiling and data. As the transmitting and receiving antennas are moved, data is obtained from each location. Arrivals are identified on the data sketch.

DATA REDUCTION AND INTERPRETATION

The data from both the seismic and radar methods can be displayed either in the field at the time of data acquisition or at the end of the survey day. The amount and type of data processing depends upon the quality of the field data obtained and the end use of the data. The ideal situation is one in which the geology is simple and the quality of the field data is sufficient to give a two-dimensional representation of the bedrock topography and soil strata such as that shown on the radar record in Figure 087.5. In this record, the bedrock is the reflector occurring at a delay time of about 400 ns which is equivalent to about 15 m depth. There are a number of reflections in the overburden which can provide a wealth of information to geomorphologists.

Usually the data are not as clear and simple as those shown in Figure 087.5. Additional information and effort are needed to obtain a satisfactory interpretation. Corrections for varying propagation velocities in the ground and for topographic effects are necessary. Considerable experience is needed to select the reflections that are of greatest interest to the user. Seismic reflection data needs these corrections before interpretation can be attempted. Figure 087.6 is an example of a common offset reflection seismic section that was obtained using a 7 kg hammer. The data was static corrected and filtered to enhance the particular events of interest. The depth scale for this

Photo 087.2 Portable radar system in field operation.

section is based on a velocity model obtained from the interpretation of the wide angle reflection and refraction soundings. In this case, a velocity model consisting of 6 m of 400 m/s material overlying a variable thickness of 2100 m/s material is adopted.

The reflection labelled 1 at 40 m depth is from a layer identified from boreholes as the upper/lower till boundary. The strong reflection labelled 2 at 60 m is from the bedrock surface which agrees well with the depth to refusal of 60 m and 80 m in boreholes about 150 m off the ends of the line. Further processing of this data was not warranted since it provided the basic information required for the application.

CASE HISTORY EXAMPLES

Three case history examples are offered in summary form to show how the radar and seismic techniques are used to obtain detailed information about the bedrock topography and the soil strata in the overburden. The first example demonstrates that the standard radar unit can be used to extend existing borehole data. In this example, a bedrock high which was not detected by the boreholes was found using

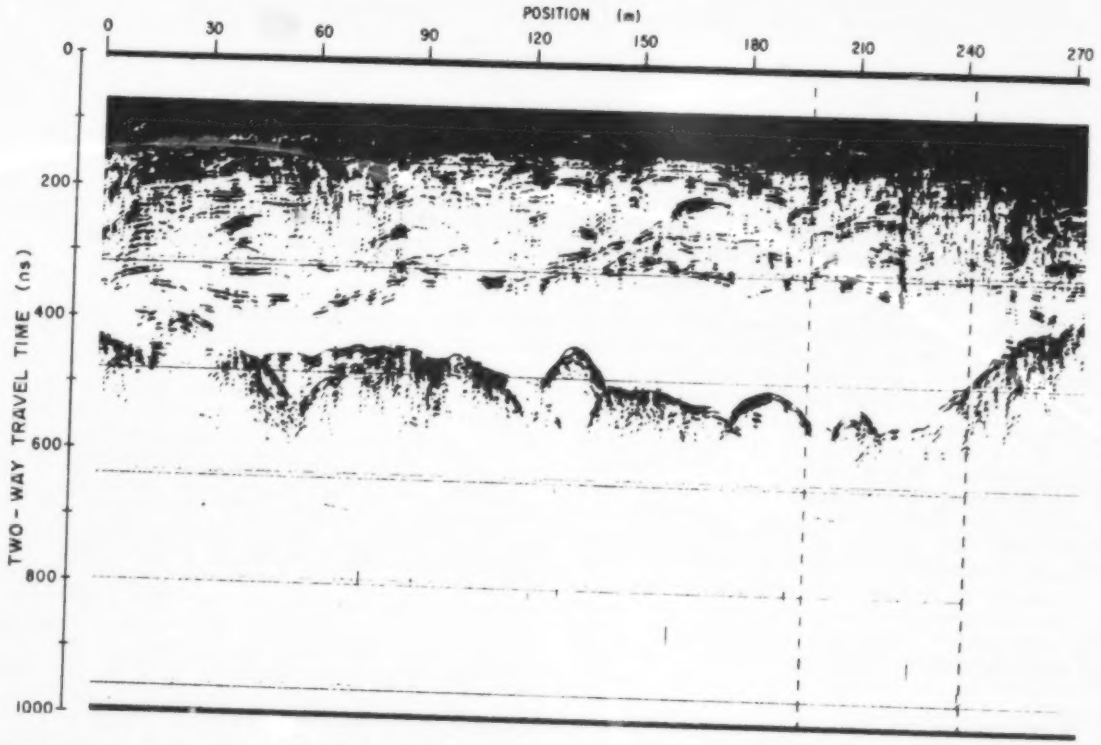

Figure 087.5 *An example of high quality radar profiling record. The reflections are presented on a grey scale burned paper recorder where the signal amplitude is proportional to darkness. Acquisition of many traces per second produces a continuous cross-section of the subsurface.*

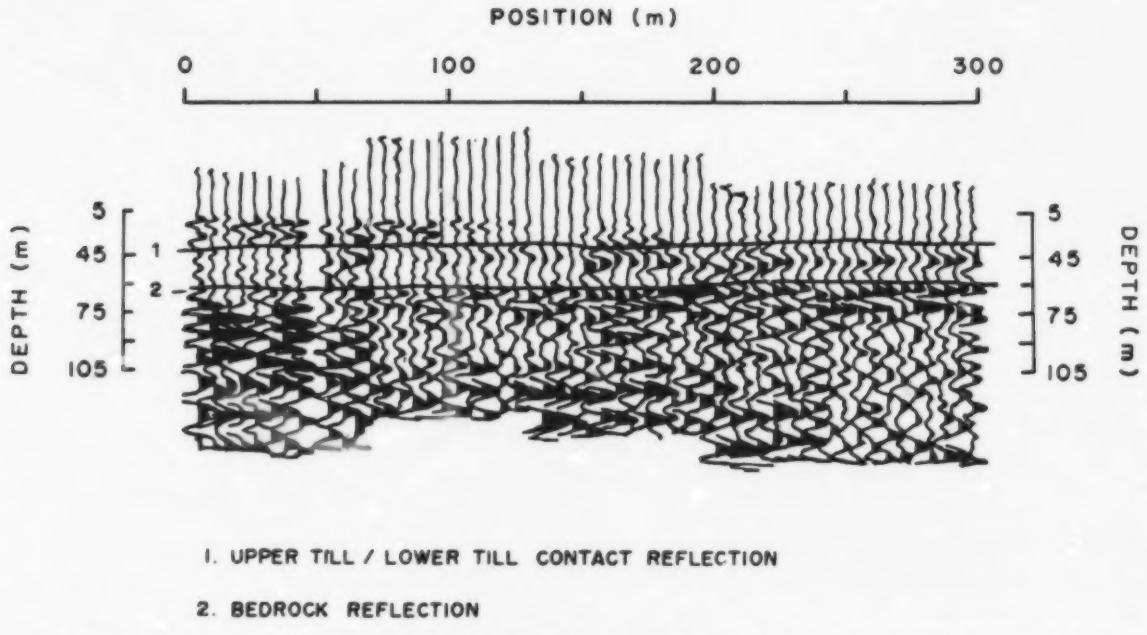

Figure 087.6 *An example of common offset seismic reflection profiling data obtained with the unit in Photo 087.1. Reflectors have been identified as the upper and lower till interface and the top of bedrock.*

the radar. This bedrock high significantly affected the groundwater flow in the area. The second example shows how the radar and seismic methods can be used to compliment one another especially since the cost of drilling is very high in the remote area where the surveys were carried out. An inferred paleochannel was mapped using the radar and seismic methods, and is of special interest in exploring for heavy metal deposits. The third case history example shows the results of a new radar system developed to extend the penetration range in geological materials especially in fine-grained soils. This new development will extend the range over which radar and seismic methods can be used to obtain high resolution maps of the subsurface.

EXAMPLE 1

Figure 087.7 shows a radar record along 0.5 km of line. The horizontal axis represents the distance along the survey line and the vertical scale represents the depth to the reflectors. The black banding on the radar record are reflections from bedrock and overburden strata. The reflections are not as clear in this record as in the record shown in Figure 087.5. The geology exhibits more variation and antenna coupling with the ground was degraded by deep snow conditions at the time of survey.

Figure 087.8 displays the interpreted radar reflectors combined with borehole information along the same cross-section. The solid lines denote subsurface features defined by both the radar data and the stratigraphic contacts defined in the borehole logs. Long dashed lines denote stratigraphic features that can be defined with confidence from the borehole information, although no clearly defined radar reflection was observed. Short dashed lines represent radar reflections that were not correlated with stratigraphic features visually observed in core samples.

The radar provided excellent resolution of the bedrock surface. The radar time range was set to 500 ns for the initial survey. In areas where bedrock reflection two-way travel time exceeded 500 ns, the lines were reprofiled with the range set to 1000 ns. A shallow and strong radar reflector is correlated with the upper surface of the interstratified very fine sand and silt unit. In the western half of the section, there is good agreement between the upper and lower contacts of the garnetiferous sand and radar reflections. Figure 087.9 displays the interpreted geologic section which has been inferred from all the available data sets of the combined borehole and radar data. Low density, high water content gyttja fills the deeper parts of the lake. The interstratified fine sand and silt unit is shown as thickening to the east. It may in fact underlie the lake, but the strong water/soil reflection at the lake bottom masked weaker reflectors from under the lake. Garnetiferous sands define the contact between aeolian and fluvial sands.

The bedrock surface was clearly and accurately resolved to a depth of 25 m. The prominent bedrock high beneath the lake shown on Figure 087.9 is part of a ridge trending just east of north. This bedrock high was not expected from the drilling. Overburden stratigraphy was clearly controlled by bedrock topography in many areas. This information has proven invaluable to geomorphologists synthesizing a depositional history in the survey area.

A refraction seismic survey in the area also was used to map the depth to bedrock, but with substan-

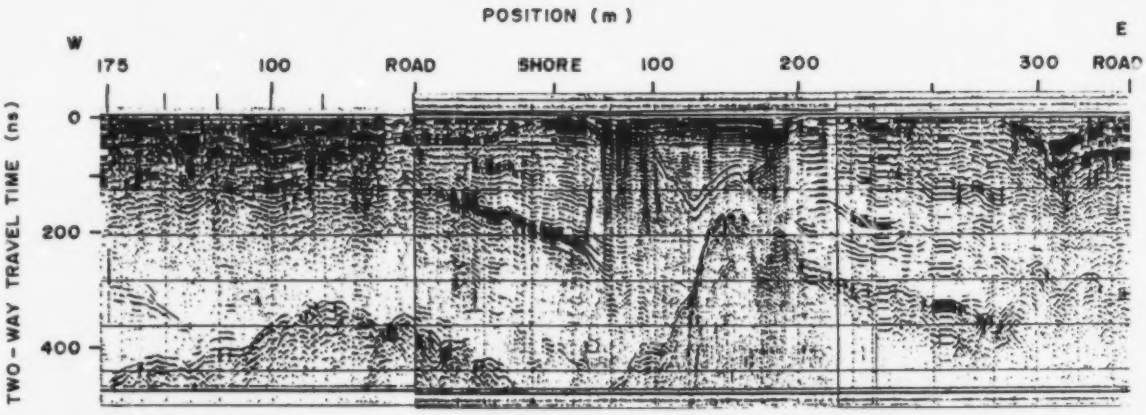

Figure 087.7 *Radar reflection section in an area of aeolian and fluvial sands overlying a granitic bedrock. Stratification within the overburden is evident.*

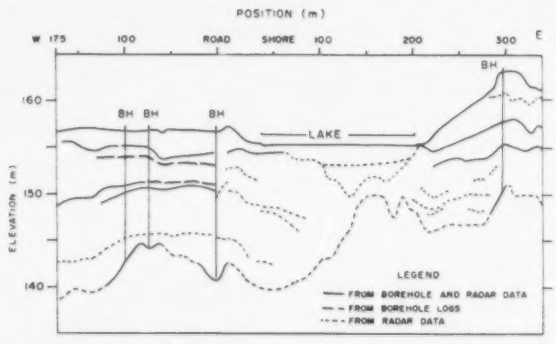

Figure 087.8 *Reduced radar section of the data of Figure 087.7. Radar reflections have been corrected for topography, variable surface profiling rate, and velocity versus depth. Available borehole data has been added to indicate the degree of correlation between radar and borehole logs.*

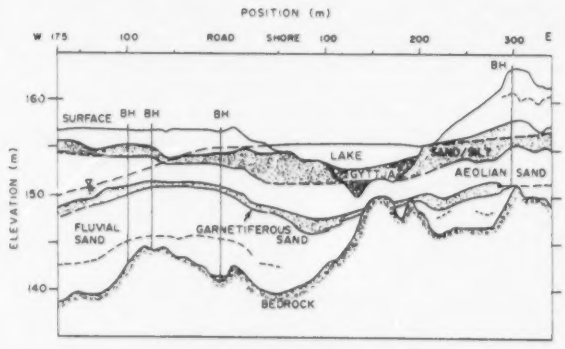

Figure 087.9 *The radar and borehole data were used to generate an inferred geologic section of the data of Figures 087.7 and 087.8. Detailed stratigraphic information is essential to Quaternary geologists in order to identify likely placer deposits.*

tially less resolution both vertically and horizontally. The overburden was too thin to apply the reflection seismic method. The high quality of radar data and the short time available for the field survey dictated that the radar method be used as the primary investigation technique.

EXAMPLE 2

This example is from an area which is part of a major glacial flow channel at the upper end of a major river system. Very little is known about the nature of the bedrock in the area. Exposures of bedrock are observable north of the survey area, but no outcrop was visible in the survey area itself. Overburden consists of coarse gravel and cobble beds derived from glacial deposition. The near surface overburden material is a very fine sand.

Figure 087.10 shows a radar reflection record obtained using reflection profiling. The record is composed of individual wiggle traces obtained at station spacings of 2.5 m. The discrete mode of survey operation allows the antennas to be maneuvered through the bush and to be placed on the ground for maximum signal coupling into the ground. This record as it stands is difficult to interpret. A computerized routine has been used to compensate for topographic variations and the resulting data are shown in Figure 087.11. It is much easier to follow features through the subsurface over long distances. The reflection at about 10 m depth is a good example of this improvement. The depth to this reflection is inferred from propagation velocity estimates obtained from a number of radar refraction soundings. What is not derivable from the current type of radar data is the source of this reflection. Possible sources included the bedrock surface, the water table, or a sand-till contact.

A comprehensive seismic refraction survey was also carried out along this line. Figure 087.12 shows the interpretation of the seismic survey. The velocities in the overburden ranged from 400 to 600 m/s. The refractor velocity was usually >4000 m/s indicat-

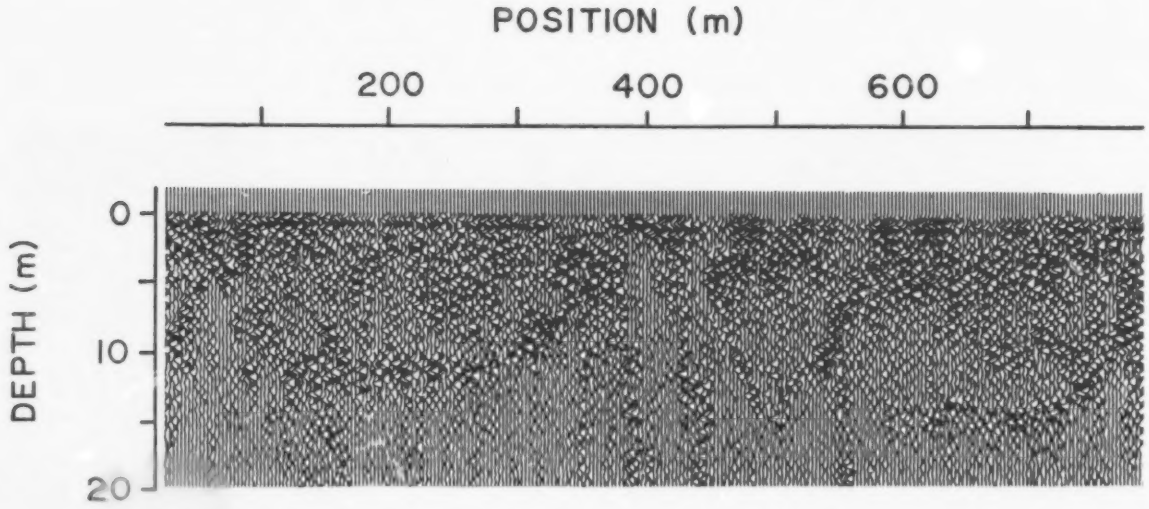

Figure 087.10 *An example of radar reflection profiling data collected on a placer property by moving the antennas at discrete intervals along the surface. Each variable area trace represents a sounding location. A velocity model has been applied to convert travel time to depth.*

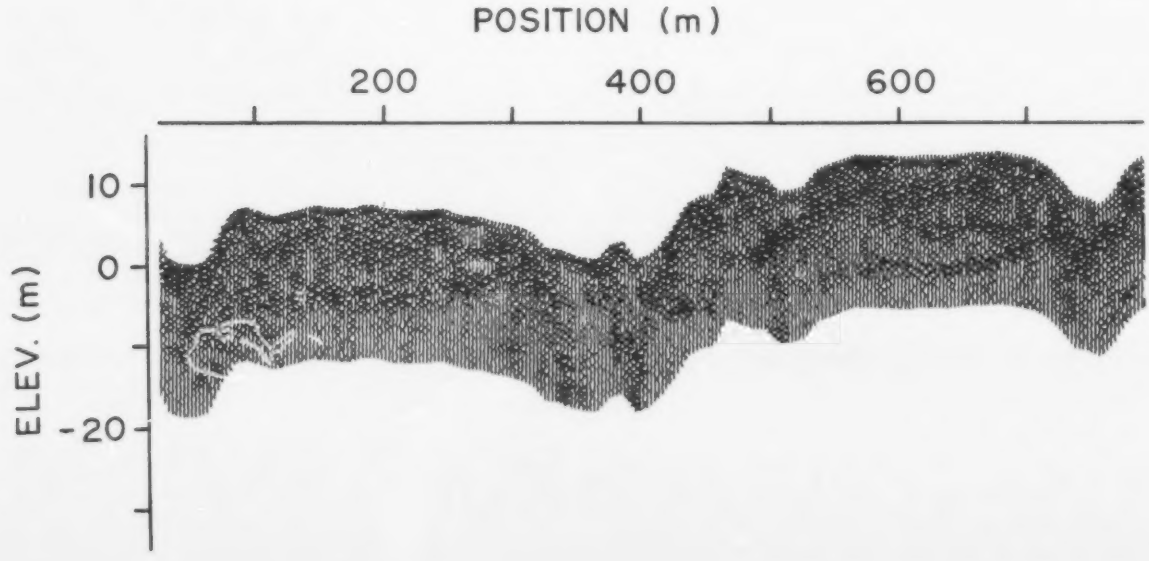

Figure 087.11 *The data presented in Figure 087.10 after compensation for topography. Reflection events have become easier to trace through the section.*

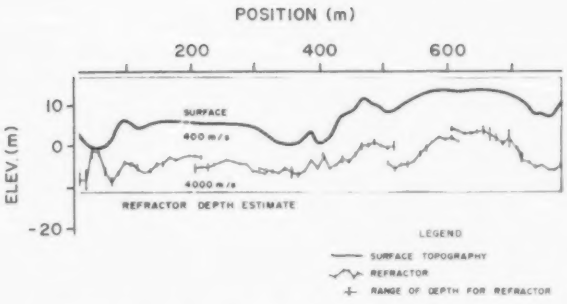

Figure 087.12 *Seismic refraction section for the line of Figure 087.10. A simple layer over bedrock model has been adopted.*

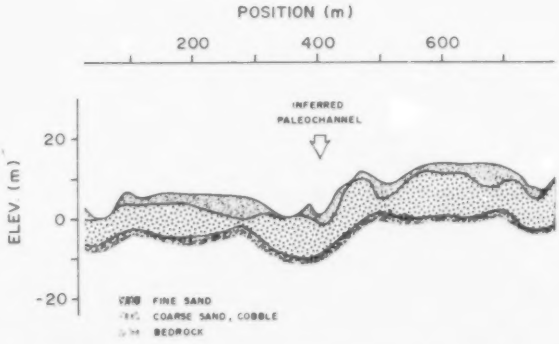

Figure 087.13 *Simplified interpretation of the geology along the same line as Figure 087.10. An inferred paleochannel has been labelled and will present a target for drilling and test pitting programs.*

ing that it was bedrock. The refractor depth is about 10 m and correlates well with the depth to a major radar reflection at the same depth. The bedrock profile derived from the seismic and radar results is shown in Figure 087.13 combined with the inferred geological section of the overburden.

This example is an excellent demonstration of how the radar and seismic methods can be used in a complimentary fashion. When the radar works well, larger spacings can be used between the seismic refraction spreads. Using the seismic and radar in this way saves money, time, and effort while obtaining a high resolution map of the bedrock topography. In clay and silt overburden, the current radar instrumentation would not have penetrated more than a few m and a comprehensive seismic refraction survey as shown in Figure 087.12 would have been essential. There is no doubt about the depth to bedrock in the survey area. Drilling data has still not been obtained in the survey area because of the remote nature of the site.

EXAMPLE 3

This example shows the results obtained in a comparison study of A-Cubed Inc.'s new 30 MHz radar and GSSI's 100 MHz radar. Figure 087.14 shows the radar data using the 30 MHz radar and Figure 087.15 shows the radar data using the standard 100 MHz radar system. The radar data clearly demonstrates the increased penetration of the new A-Cubed radar compared to the GSSI radar, especially between distances 100 and 600 m along the road. It is significant that the 30 MHz radar mapped the bedrock even under the two 1 m thick clay layers in the fine sand, whereas the GSSI radar only mapped down to these layers. It should be noted that the increased penetration is directly attributed to improved system performance.

The 100 MHz centre frequency is the lowest available frequency of operation with the GSSI radar, whereas the A-Cubed Inc. system will operate down to a few MHz.

Figure 087.16 shows the geologic section interpreted only from the continuous core logs from nine boreholes along the 0.7 km line. The reader should note the sketchy detail of the clay layers and the bedrock topography shown on the geologic section using only the borehole information compared to the continuous detail of the layers that is obtained using the radar with the borehole logs. The areas where the radar reflection gets a weak response from the clay layer such as at 550 m and 650 m may indicate that the clay layer is thinner than where the radar reflection is strong as observed at 450 m. Further study of the core logs will help to quantify the differences in the clay layer at these locations. The continuity of these layers strongly affects the hydrogeologic model used to predict the groundwater flow in the area.

The improved penetration range of the A-Cubed radar is attributable to the improved system fidelity and the use of digital signal acquisition in real time. An advantage of the digital radar is the superior variable area display commonly used in the petroleum seismic industry. Significantly more information can be determined from the variable area display than can be extracted from the standard intensity modulated, line scan recorder display used in the GSSI radar. A further advantage is that many of the processing techniques that have been developed by the seismic industry can easily be modified for the digital radar data.

CONCLUSIONS

Field work at several sites in Ontario has confirmed the effectiveness of high resolution radar and seismic survey methods for shallow high resolution soundings required for geotechnical and hydrological exploration programs. Conclusions to date are:

1. Radar provides the very high resolution needed for mapping subtle bedding in the overburden.
2. Seismic refraction is essential for defining shallow bedrock depths and for providing corroboration of radar reflection bedrock depth interpretations.

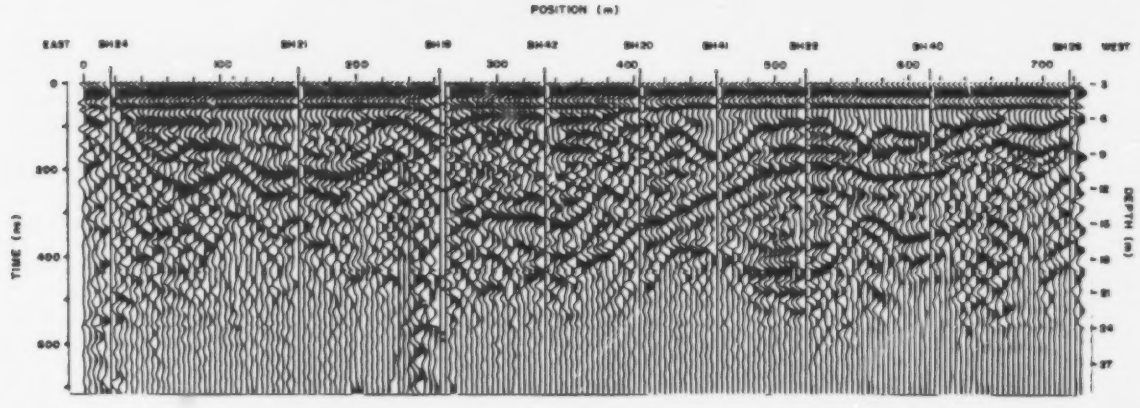

Figure 087.14 *Data from the new A-Cubed Inc. 30 MHz radar obtained along a road near Chalk River, Ontario.*

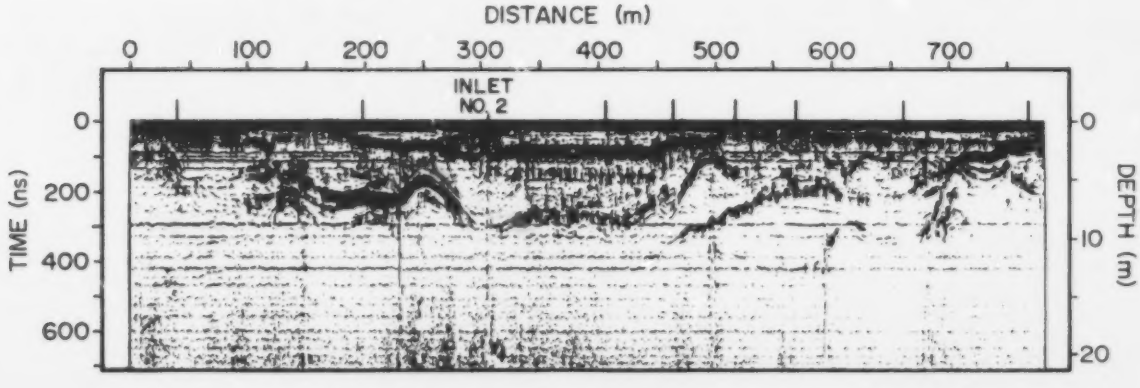

Figure 087.15 *Data from the standard GSSI 100 MHz radar obtained along the same survey line as that shown in Figure 087.14.*

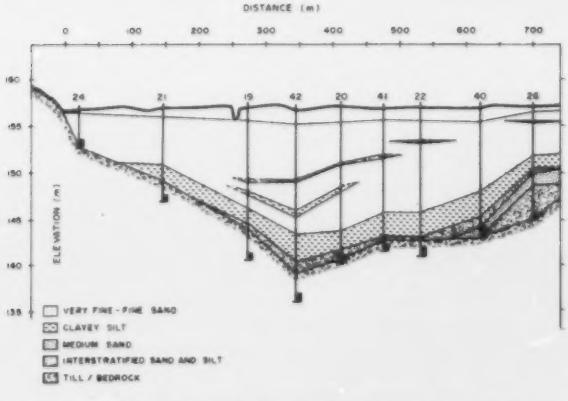

Figure 087.16 *Geologic section interpreted only from the continuous core logs from 9 boreholes along the same survey line shown in Figures 087.14 and 087.15.*

3. Seismic is currently the only technique to be used in environments where current radar instrumentation fails because of the high signal attenuation in silt and clay soil conditions.
4. A combination of radar and seismic soundings in conjunction with borehole logs can help to extend the horizontal extent of the borehole information.
5. A precise knowledge of bedrock topography and subsurface stratigraphy greatly improve effective placing of boreholes.
6. A sensible integrated program combining surficial geologic mapping, high resolution geophysical techniques, and drilling investigations provides the best manner for optimizing investigation programs.

The radar and seismic methods offer excellent cost effective means for economically mapping the bedrock and soil stratigraphy, especially when used in conjunction with drilling investigations. The field equipment, both radar and seismic, must be made more compact and rugged. The field data acquisition and data processing techniques must also be devel-

oped for cost effective data presentation. These developments will add finesse to an already powerful complimentary set of high resolution mapping techniques.

As part of this ETDF project, A-Cubed Inc. is establishing a number of standard test sites for radar and seismic instrumentation and methods. Further information on test areas is available from A-Cubed Inc.

ACKNOWLEDGMENTS

The authors wish to thank Len Collett of the Geological Survey of Canada, Jean Pilon of the Earth Physics Branch and the National Research Council, PILP program for their support for the development of the new radar. The support of the Ontario Geological Survey ETDF program which supported much of the field testing and data synthesis presented in this report is also acknowledged.

REFERENCES

Annan, A.P., and Davis, J.L.
1976: Impulse Radar Soundings in Permafrost; Radio Science, Volume 11, Number 4, p.383-394.

Hunter, J.A., Burns, R.A., Gagne, R.M., Good, R.L., MaCaulay, H.A., and Pullen, S.E.
1984: Field Experience with "Optimum Window" Hammer Seismic Reflection Technique; Society of Exploration Geophysicists, 52nd Annual Meeting, Abstracts, p.466-468.

Morey, R.M.
1974: Continuous Subsurface Profiling by Impulse Radar; Proceedings of Engineering Foundations Conference on Subsurface Explorations for Underground Excavation and Heavy Construction, Henniker, N.H., USA, p.213-232.

Grant 089 Testing and Demonstration of Interpretation Software for Magnetic, EM, and Spectrometry Inversion

S.W. Reford and N.R. Paterson

Paterson, Grant and Watson Limited, Toronto

ABSTRACT

Computer software has been developed to assist in the interpretation of airborne magnetometer, ground electromagnetometer (EM), and airborne spectrometer data. In addition, a suite of applications and general purpose software has been developed for the IBM Personal Computer. Emphasis has been placed on techniques of direct application to exploration problems in Ontario. Work is continuing to further develop these techniques and to test their applicability by means of data sets from a number of well-known areas. Documentation of some of the methods is complete; in other cases it is nearing completion. The development and application of the techniques are being presented to the mineral exploration community through publications, case histories, conference presentations, and marketing.

OBJECTIVES

Several geophysical interpretation software programs were developed from 1981 to 1984 with the aid of Exploration Technology Development Fund (ETDF) Grant 011. The overall objective of the current project is to evaluate and demonstrate the effectiveness of these programs by rigorously testing the methods on data sets in areas where the physical properties and geology are adequately known. After necessary modifications to the programs, final interpretations will be prepared and published in the form of case histories.

The three essential elements to the project are: testing and evaluation; modifications and final development; final application and publication. All three phases are considered essential if these interpretation tools are to be accepted by the mineral exploration industry and applied effectively to exploration in Ontario.

FIELDS OF STUDY

MAGNETIC INVERSION (SUSCEPTIBILITY MAPPING)

The SUSMAP technique was introduced and developed under our previous ETDF grant (Paterson *et al.* 1983). It is a spatial domain procedure that permits a depth-to-magnetic-source to be assigned to each grid point of an X-Y gridded dataset. The magnetic susceptibility is varied iteratively at each point until the calculated field on the surface of measurement is equal to the measured field (total field or vertical gradient). The result is a map of apparent susceptibility that is more easily and accurately interpretable. The program will also calculate a magnetic field whose source is specified by a grid of susceptibility values. This will allow, for example, the calculation of simulated drape-flown aeromagnetic data from a magnetic field measured by a barometric-flown survey, or vice-versa.

Significant improvements were incorporated in the method during the past fiscal year. The efficiency of the software has been upgraded, leading to cheaper processing costs. The need for creating an initial grid of susceptibility values by Fourier-domain processing has been eliminated. Starting susceptibility values are now calculated by the SUSMAP program. This was made possible by removing the problems of processing magnetic data not measured at high magnetic latitudes (near the poles).

The vertical-sided prism is a difficult source to model in areas of low magnetic inclination. However, by first reducing such data to the magnetic pole, the problem is essentially eliminated. The method was tested on a dataset measured near the magnetic equator and was quite successful in producing a good quality susceptibility map. For data measured at medium magnetic latitudes, an option has been added to the SUSMAP software whereby compensation is provided for the peak response of a particular prism not being centred over the prism itself. The main effect of these improvements is that the large expense of initial Fourier-domain processing has been removed.

After some delay, the high sensitivity total field and gradiometer survey in the area of Clarendon Township, southeastern Ontario, was acquired in digital form (Barlow 1983). Study of the newly published maps was initiated in preparation for testing of the SUSMAP method. Under our previous grant, several ground magnetic and vertical gradient traverses were measured in the area, coincident with the airborne survey profiles, as well as corresponding *in-situ* and laboratory measurements of magnetic rock properties. The comprehensive ground truth studies and accurate aeromagnetic and altimetry data will lead to an excellent case history, to be prepared during the next fiscal year.

A paper was presented at the 54th Annual Meeting of the Society of Exploration Geophysicists in December 1984 that summarized the SUSMAP technique and gave examples of its applications (Misener, Grant, and Walker 1984). By July 1985 in Lausanne, Switzerland, N.R. Paterson will have presented a paper on aeromagnetics at the Symposium on Geophysics in Rugged Terrain. The paper will have had included in it a discussion and examples of the SUSMAP method with particular reference to the removal of terrain effects from aeromagnetic data and the continuation of data between arbitrary surfaces (for example from a barometric to a drape-flown observation plane).

A study is underway to determine whether it would be useful to replace the current iterative method of fitting the data by some form of matrix inversion. The authors would hope to achieve improved efficiency, convergence, and accuracy of the SUSMAP method.

MAGNETIC INVERSION (MAGNETIC MODELLING)

Under our previous ETDF grant, the venerable MAGMOD program for inversion of discrete magnetic anomalies was adapted to accommodate vertical gradient as well as total field data. The method utilizes the well-known Marquardt least-squares optimization of the source parameters to provide a geological model for the observed magnetic response.

Much of the work during the past year focussed on the application of singular value decomposition (SVD) to the MAGMOD method. SVD has a proven record (for example Paterson *et al.* 1983) in the determination of the contribution and accuracy of the various fitted parameters to a model. A significant weakness of the Marquardt method is its inability to provide this information. To date, the required theory has been developed and verified and the inversion algorithm has been completed. This has included the development of a forward formula for a six-sided prismatic magnetic body and the 11 partial derivatives required for the inversion. As well as providing new information on the source parameters, the application of SVD will lead to a greater variety of model shapes, inversion to multiple magnetic bodies, and the ability to joinily invert multiple data sets, such as total field and vertical gradient.

A remanent magnetic vector has been added as a fixed model parameter for MAGMOD inversion. This will allow the geophysicist to account for magnetic remanence in areas where it has been measured. It is also possible to create forward models and determine the effect of remanence for a particular case or to test the effect of varying remanence on measured field data.

It is expected that testing and documentation of the new SVD version of MAGMOD will be completed during the coming year. It may be of interest to the reader to note that the current version of MAGMOD was recently downloaded for PC operation.

EM AND RESISTIVITY INVERSION

The GEMINV method for inversion of frequency-domain EM data to an n-layer earth model was developed under our previous ETDF grant (Reford *et al.* 1984). This followed the successful development of the AEMINV method for inversion of airborne EM data to a two-layered or halfspace earth model. Both methods employ singular value decomposition (SVD) as an aid to the determination of the model parameters (layer resistivities, magnetic permeabilities, and thicknesses for GEMINV).

During the past year, the GEMINV software was upgraded to model data measured by tilt angle ellipticity systems as well as the more common secondary field inphase and quadrature systems. The software was first checked and verified against forward solutions to two- and three-layer earth models that had previously been derived for the GEM-8 system (an 8-frequency tilt angle ellipticity system manufactured by McPhar Geophysics). It was then tested on real data acquired on a GEM-8 survey in the Alfred Township area.

The EM sounding survey in the Alfred Township area was conducted over a multi-layered earth that varies widely in layer conductivities and thicknesses. At least four distinct layers have previously been confirmed by extensive geological mapping and borehole information. The area has been used as a research and test site for a number of airborne EM, ground EM, and electrical systems. Soundings were measured at ten locations using all eight of the GEM-8 frequencies (41 Hz to 5248 Hz) and usually three coil separations (100 m, 200 m, and 300 m), all in the horizontal loop transmitter mode. Soundings at three locations were also conducted with a MAXMIN II system for comparison of results with the GEM-8.

The GEM-8 data was processed with the GEMINV software, which was quite successful in delineating two or three distinct layers at various sounding sites. Figures 089.1 and 089.2 show the results of inversion at one of the sites. A separate inversion was conducted for each of the four transmitter-receiver separations, covering the full range of eight frequencies (that is, the data was treated as a series of parametric soundings). One can see how SVD analysis of the resultant layer parameters is important. As the separation increases from 100 to 400 m, SVD shows that the layer parameters are better determined. This is also demonstrated by the data, where the second layer becomes well defined at 200 and 300 m, and the third layer becomes apparent at 400 m. Note the effect on the calculated resistivity value of layer 2 as the layer is transformed from a halfspace to a discrete layer at 400 m separation. Note also that the first layer looses some definition at the 400 m separation. The final model was interpreted from the four inversion results and correlated with the known geology in the area.

During the next fiscal year, a case history will be prepared focussing on the GEMINV results (both GEM-8 and MAXMIN II) obtained from the Alfred Township survey. Comparisons will be drawn with the extensive geological and geophysical knowledge available for the area through geological mapping, borehole information, and electrical and EM survey analyses (for example, Schlumberger and EM-34 soundings, TRIDEM data). This study will be submitted for publication to a respected journal such as Geophysics or Geophysical Prospecting.

The extended technical abstract for a paper entitled, "Inversion and SVD Analysis of Frequency-domain EM Data", was submitted to the Society of Exploration Geophysicists for presentation at its 1985 annual meeting. The paper discusses both the GEMINV and AEMINV (for inversion of airborne EM data) methods, developed under this, and our previous ETDF grant. The authors are S.W. Reford, N.R. Paterson, and R.N. Edwards.

Development and testing of GEMINV will continue, particularly with data measured by new EM systems, including large loop transmitter configurations.

The main limitation of the GEMINV method appears to be in the physics of the problem: the inability to separate thickness from conductivity when the conductive layer is small in comparison with the coil separation. On the other hand, the layer conductance is usually well determined. To rectify this problem, the authors are studying the problem of joint inver-

INVERSION OF GEM-8 SOUNDING DATA

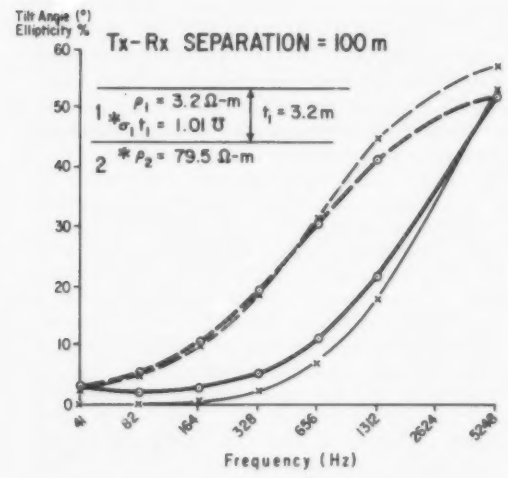

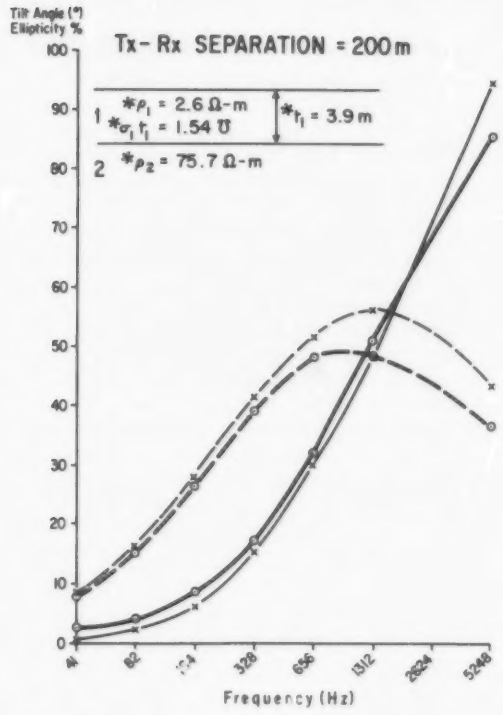

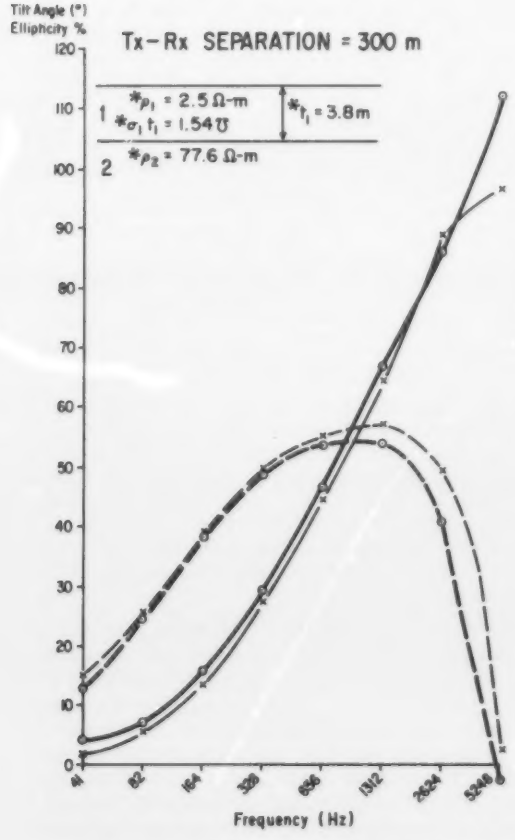

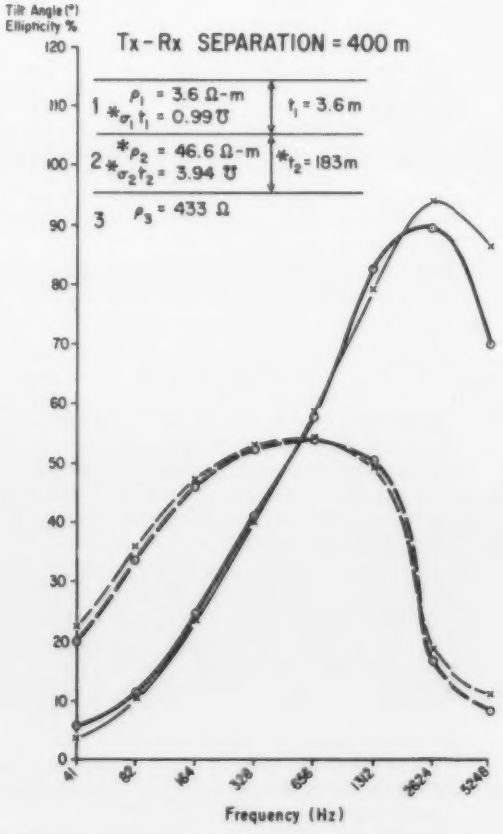

***Figure 089.1** Example of inversion of GEM-8 sounding data, Alfred Township, Ontario (see Figure 089.2 for legend and interpretation).*

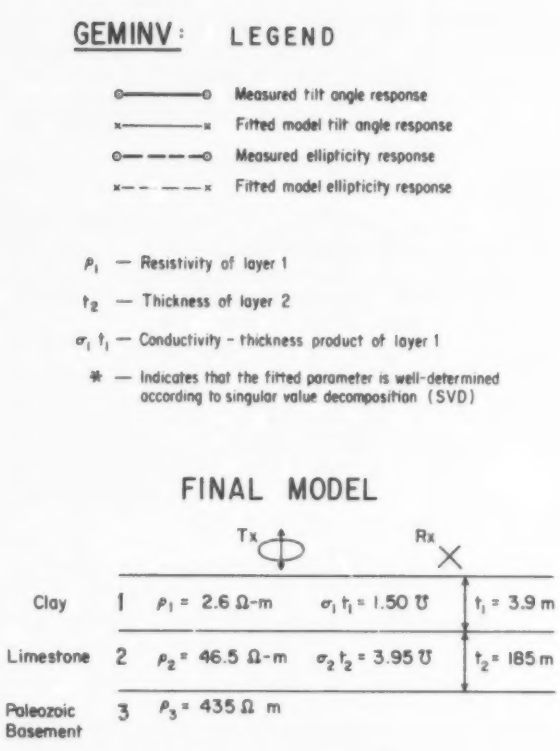
GEMINV: LEGEND
Measured tilt angle response
Fitted model tilt angle response
Measured ellipticity response
Fitted model ellipticity response
ρ_1 — Resistivity of layer 1
t_2 — Thickness of layer 2
$\sigma_1 t_1$ — Conductivity - thickness product of layer 1
* — Indicates that the fitted parameter is well-determined according to singular value decomposition (SVD)
FINAL MODEL
Tx
Rx
Clay
1 ρ_1 = 2.6 Ω-m $\sigma_1 t_1$ = 1.50 ℧ t_1 = 3.9 m
Limestone
2 ρ_2 = 46.5 Ω-m $\sigma_2 t_2$ = 3.95 ℧ t_2 = 185 m
Paleozoic Basement
3 ρ_3 = 435 Ω m

***Figure 089.2** Legend and interpretation for the example (Figure 089.1).*

sion of both ground EM and DC resistivity data along identical profiles. If successful, the conductivity and thickness parameters of the layered earth model will be more accurately determined with the addition of resistivity data to the inversion.

INVERSION OF GAMMA-RAY SPECTROMETRY

The SPECMAP method was developed under our previous grant (Reford *et al.* 1984) to plot three radioelement gamma-ray spectrometer data on a single colour map. It overcomes the pitfalls of the traditional method of having to geologically zone a number of maps simultaneously. A chart showing examples of SPECMAP processing in colour accompanied our report in the previous volume.

The method continues to be applied on a production basis to the regional interpretation of spectrometer data. At the same time, improvements to the method are being implemented. During the past year, the input and output have been streamlined to the advantage of the user. An extensive executive report is now provided which allows the user to determine whether a particular plot will make the desired use of the plotter's available colours before going to the expense of generating a colour plot.

The SPECMAP software has been modified so that the particular coding scheme of any plotter on the market may be accommodated. A program was added to the package, courtesy of Dataplotting Services Inc., to create the final plot file of the colour coded map for submission directly to an Applicon colour plotter.

The software was originally developed in cooperation with Dataplotting Services Inc., who, at the same time, developed their own approach to the technique. In accordance with a strategy for joint marketing of the SPECMAP software, the two versions will be integrated to provide a more flexible package for the user.

During the past year, a set of "user notes" was prepared for the operation of SPECMAP. Complete documentation of the software will be prepared in the coming year. This will include the development of a legend for the final colour map so that both the user and casual observer can correlate the various colours with the actual numerical values of the three radioelement responses. It is envisioned that a ternary diagram will be plotted with scales showing the relative distributions (in percent) of the three radioelements for the various colours. In addition, vertical scale bars, one for each radioelement, will attach a numerical response value to each level of colour intensity. Neither of these two scales will be linear when the two exponential factors are used to enhance the colour and intensity variation of the plot. Further refinement and testing of the SPECMAP method will proceed using good quality Ontario datasets.

A paper was presented at the 54th Annual Meeting of the Society of Exploration Geophysicists in December 1984 that summarized the SPECMAP technique and gave examples of its applications (Misener *et al.* 1984).

PERSONAL COMPUTER SOFTWARE

The company has been applying the IBM Personal Computer (and compatible systems) to geophysical problems for the past three years, particularly for forward modelling and general processing of ground geophysical data. Some of the software was developed under our previous ETDF grant (Reford *et al.* 1984). It is written for the general manipulation of geophysical line data. Testing and documentation of the software was completed during the past year and it is now being successfully marketed under the trademark GEOSOFT. All of the software was written to accommodate data in a very simple standard text-file format so that any typical text-file editor may be employed. This ensures compatibility between applications and utilities software, such as that for line plotting or filtering. All the software is now written in PASCAL.

Six packages for the manipulation and presentation of geophysical data have been developed under the current ETDF program. XYPLOT is a program for the plotting of data on the line printer. PLOTLINE is a flexible plotting package for use on a six-pen colour plotter, colour monitor, and line printer. MGMDPLOT will take the results of a MAGMOD magnetic inversion and plot them with the fitted model on the colour plotter. PASGRAPH is an extensive PASCAL graphics language that is now used as the basis for programs such as the previously described PLOTLINE. LINEPROC is a package for the handling and manipulation of profile data stored in the GEOSOFT line database format. It has been incorporated into a wide

variety of applications software. GRAPHED is a program with extensive capabilities for the manipulation and processing of profile data, including a number of filtering and splining options. The application of any option may be viewed on-screen. The program can also incorporate point-by-point editing.

FUTURE PLANS

The current ETDF grant has been renewed for the next fiscal year. The work will continue as outlined above by our objectives and as described in our fields of study.

ACKNOWLEDGMENTS

The company is grateful to the Ontario Ministry of Natural Resources for its financial assistance, and for the cooperation of the staff of the Ontario Geological Survey in various aspects of the work, including the provision of test field data.

The authors acknowledge the important contribution of Dataplotting Services Inc. in the development of the SPECMAP program.

The following also made valuable contributions to the work described in this paper: R.N. Edwards, R.C. Bailey, Peter Walker, Charles Broughton, D.J. Misener, F.S. Grant, Elizabeth Baranyi, R.B. Hearst, and Michael Sahib.

REFERENCES

Barlow, R.B.
1983: Test Surveys and Developments in Aeromagnetic Gradiometry; p.142-144 *in* Summary of Field Work, 1983, by the Ontario Geological Survey, edited by John Wood, Owen L. White, R.B. Barlow, and A.C. Colvine, Ontario Geological Survey, Miscellaneous Paper 116, 313p.

Misener, D.J., Grant, F.S., and Walker, P.
1984: Variable Depth Space Domain Susceptibility Mapping; p.237-239 *in* Expanded Abstracts of the Technical Program with Authors' Biographies, 54th Annual Meeting of the Society of Exploration Geophysicists, 914p.

Misener, D.J., Reford, S.W., Bailey, R.C., and Holroyd, M.
1984: Ternary Colour Plotting of Three Radioelement Spectrometer Data; p.750-751 *in* Expanded Abstracts of the Technical Program with Authors' Biographies, 54th Annual Meeting of the Society of Exploration Geophysicists, 914p.

Paterson, N.R., Grant, F.S., and Misener, D.J.
1983: Grant 011 Development of Computer Software for Geophysical Interpretation; p.53-61 *in* Exploration Technology Development Program of the Board of Industrial Leadership and Development, Summary of Research 1981-1983, edited by E.G. Pye and R.B. Barlow, Ontario Geological Survey, Miscellaneous Paper 115, 135p.

Reford, S.W., and Paterson, N.R.
1984, 1985: Testing and Demonstration of Interpretation Software for Magnetic, EM and Spectrometry Inversion; Progress Reports, Paterson, Grant and Watson Limited, July 1984, October 1984, February 1985, April 1985.

Reford, S.W., Paterson, N.R., and Misener, D.J.
1984: Grant 011 Development of Computer Software for Geophysical Interpretation; p.44-51 *in* Exploration Technology Development Program of the Board of Industrial Leadership and Development, Summary of Research 1983-1984, edited by V.G. Milne and R.B. Barlow, Ontario Geological Survey, Miscellaneous Paper 120, 176p.

Grant 090 The Application of Lake Sediment Surveying to Au Exploration in Ontario

J.S. Fox[1], T.E. Eagles[2], and E.J. Brooker[2]

[1]Teck Explorations Ltd., Toronto

[2]X-Ray Assay Laboratories Limited, Don Mills

ABSTRACT

Coker *et al.* (1982) have shown that the sampling of organic lake sediments offers some potential for reconnaissance Au exploration in the Shield. The objective of Grant 090 is to further refine techniques developed by these authors by developing additional Au dispersion case histories, developing software suitable for the multivariate statistical treatment of lake sediment data, researching the nature of Au mobilization and deposition in the natural environment, and by developing analytical techniques for Au at the ppt level.

Orientation studies carried out at a number of Au showings during the first year of the grant have confirmed that dispersion halos of up to 300 m can be detected in organic lake sediments by means of neutron activation analysis. A preliminary examination of sample homogeneity suggests that these halos are a result of chemical rather than mechanical dispersion. Further work is under way, using highly sensitive radiochemical techniques, in order to determine if dispersion can be detected over even greater distances.

A preconcentration technique has been developed for analyzing the Au content of water at the 5 to 10 ppt level. Preliminary results using this technique around a number of mineralized bodies suggest that surprisingly large amounts of Au can be dissolved in groundwater in nature (up to 450 ppt was found in water flowing over an undisturbed, mineralized quartz vein at the Golden Rose Mine). This, along with the information on sample homogeneity, indicates that hydromorphic dispersion of Au can occur, and that the phenomenon can be used as a valuable tool in Au exploration.

INTRODUCTION

Recent developments in the Hemlo area have emphasized the importance of Au to the provincial economy generally, and to the local mining industry in particular. Although the Hemlo discoveries have generated extensive exploration, most of it has been in the vicinity of old showings, in regions that are geologically well known, and has involved conventional evaluation techniques.

Grassroots Au exploration in some of the less well known regions of the Province has not been pursued, despite the potential of these regions for large tonnage deposits (for example Lupin-type mineralization in the Superior Province sedimentary paragneiss belts). To a large extent, this has been due to an absence of remote sensing technology appropriate for regional scale Au exploration.

Most known Au occurrences respond poorly to existing geophysical techniques. New remote sensing technology is, therefore, likely to evolve along geochemical lines. Moreover, any new approach should involve direct sensing for Au since experience has revealed limitations in the use of geochemical "path finders".

Au dispersion in lake sediments in Canada was investigated by Coker *et al.* (1982) who reported a high degree of within-sample homogeneity ($R=0.82$, $R^2=0.68$) in replicate samples from Saskatchewan lakes.

From this, and from their preliminary selective extraction studies, Coker *et al.* inferred that Au had been hydromorphically transported over unexpectedly large distances. These authors concluded that lake sediment surveying, using direct Au determinations, was a viable reconnaissance-scale exploration technique.

PROJECT OBJECTIVES

The objective of ETDF Grant 090 is to firmly establish the reliability and cost-effectiveness of the technique, and to refine the required sampling and analytical methods by:

1. developing additional lake sediment survey case histories
2. researching the chemistry of Au in the natural environment with respect to its mobilization and transport
3. developing software suitable for the treatment of lake sediment Au data
4. optimizing analytical methods for Au detection in lake sediments at the ppt-ppb level
5. optimizing field techniques for following up lake sediment Au anomalies

INITIAL RESULTS

Au DISPERSION IN LAKE SEDIMENTS

Orientation lake sediment grids were established near a number of bedrock sources in 1984, including showings at Lovell Lake near Goudreau, Ontario, Arsenic Lake near Temagami, Ontario, and Pap and Sulphide Lakes in Saskatchewan. All of the lakes involved are characterized by organic bottom sediments, and by an apparent lack of human contamination (for example tailings, drill sludge, and so on). Samples were taken with a Hornbrook bomb sampler, and lake bottom water Eh, pH, conductivity, and temperature were obtained at every two to three sample sites. Eight gram briquettes were obtained from each dried organic lake sample, and were analyzed using standard neutron activation techniques.

The results indicate that strong Au dispersion in organic lake sediments, in the order of 200 to 300 m, is associated with the Galena showing and the new "camp" discovery on Sulphide Lake, and with the numerous occurrences at Pap Lake. Weak dispersion, of two to three times the regional mean, is apparent

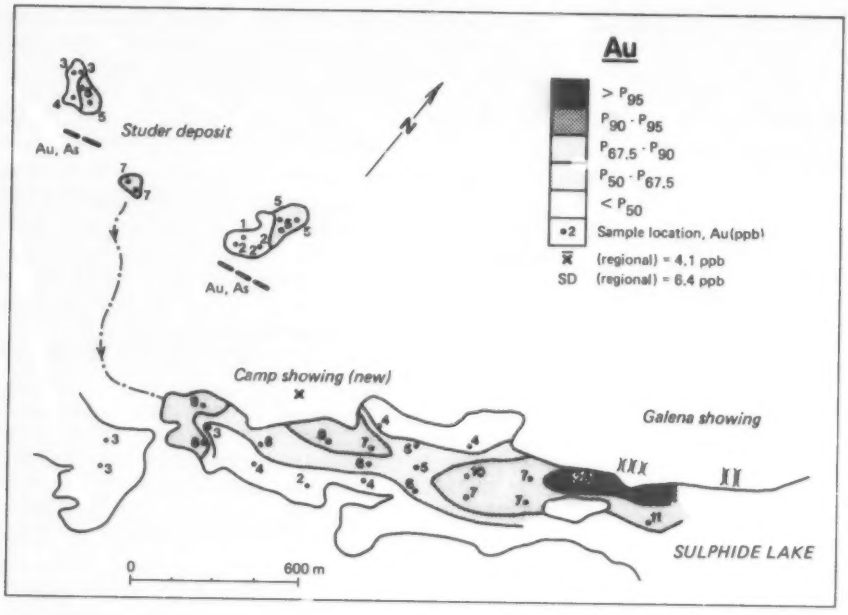

Figure 090.1 Au content of organic lake sediments at Sulphide Lake, Saskatchewan. Percentile values were calculated from assays obtained during an earlier regional survey.

over a similar distance at Lovell Lake, and in association with the Studer showing north of Sulphide Lake (Figures 090.1, 090.2, and 090.5). No systematic Au dispersion was observed at Arsenic Lake (not shown), despite the presence of a significant bedrock source - the Little Dan "mine".

It should be noted that Au dispersion at Pap and Sulphide Lakes may in fact be greater than is shown. The recent, straight-forward neutron activation analyzes have been combined with older, less accurate fire-assay/neutron activation analyses in order to calculate the percentiles shown in Figures 090.1 to 090.4.

Complete data is now available for Pap Lake, which shows an excellent correlation between Au and As, as might be expected from the nature of the bedrock mineralization. A correlation between lake bottom-water pH and Au may also be present (Figures 090.2 to 090.4), but no relationship with any other variable is observed. No relationship between Au, pH, Eh, T, or depth was observed at Sulphide or Lovell Lakes.

SOFTWARE DEVELOPMENT

A multivariate statistical package, containing regression, factor, and discriminant analyses was constructed, largely by modification and elaboration of software obtained from the Kansas State Geological Survey. Until now, packages such as this could be leased at considerable cost. The package was used on reconnaissance lake sediment data recently collected in a northern Ontario area, in order to determine its ability to distinguish truly anomalous metal values from geochemical variations caused by such environmental parameters as local geology, physiography, and lake bottom character.

A much stronger correlation exists in this area between Au and such variables as Fe and Mn than is the case, for example, around Sulphide Lake, Saskatchewan (Figure 090.6). As a result, a dramatic "signal to noise" enchancement with respect to Au was obtained by using the package's regression-based normalization procedure. It is interesting to note that a new Au occurrence was found as a result of the ground follow-up of the normalized data (Figure 090.7).

PROCEDURES FOR ANALYZING THE Au CONTENT OF WATER

The ability to analyze Au in water to a level of 5 to 10 ppt is crucial to our study of Au mobilization. In this regard, two analytical procedures have been tested. The first makes use of activated charcoal, and is similar to the method described by Hamilton *et al.* (1982, 1983). The second procedure uses a reducing resin, Amborane-344, developed by the Rohm and Haas Company, of Philadelphia.

In the case of the resin technique, water samples were passed through a 1.2μ filter, and an aliquot of filtrate (UE1 - Table 090.1) was obtained. The water sample bag was lightly washed, and saved for analysis (BAG). The Amborane beads were washed into a second filter and then carefully scraped off for analysis (EX1), while the second filtrate was saved. Both filter, and any non-Amborane residue, were saved for a later analysis (PRT).

Secondary extractions were done on both the resin and charcoal samples in order to determine the efficiency of a single extraction. For the resin technique, the Amborane beads were powdered, mixed with the filtrate from EX1, filtered again and the powered amborane and filter were then saved for analysis (EX2), along with the re-used filtrate (UE2). For the second charcoal-based extract, paper pulp rather than new charcoal was used as the second adsorption medium.

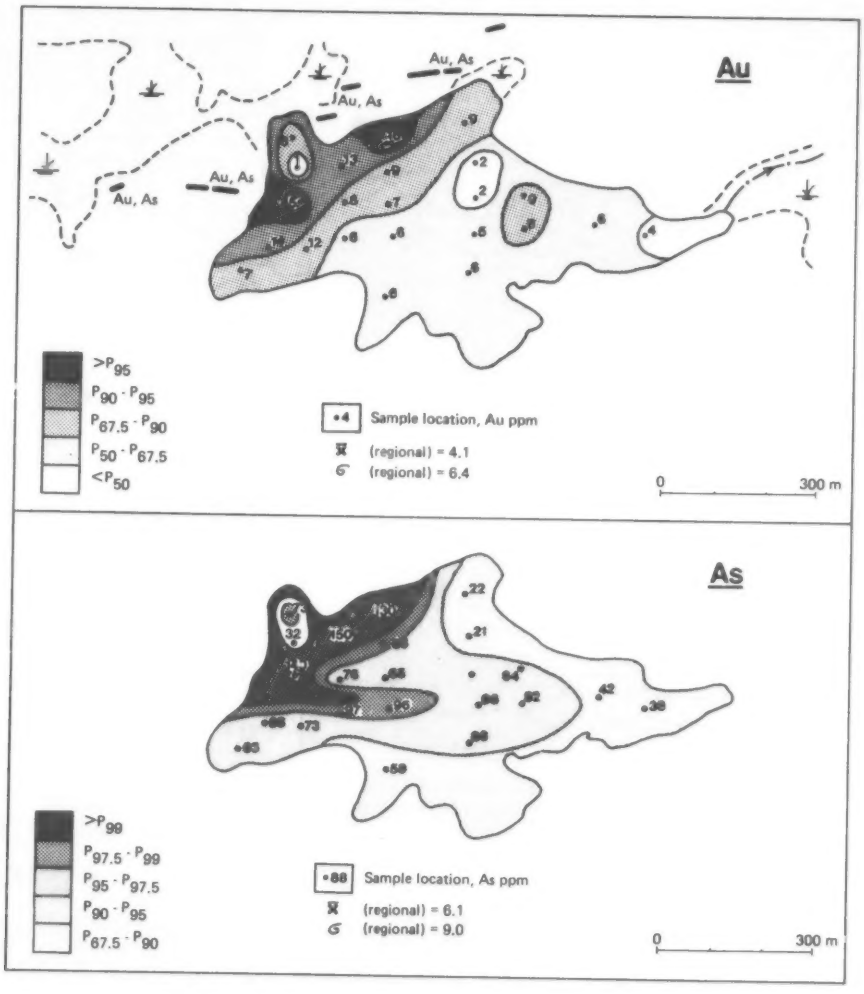

Figure 090.2 *Au and As contents of organic lake sediments at Pap Lake, Saskatchewan. Percentile values were calculated from assays obtained during an earlier regional survey.*

Laboratory solutions in the range of 5 to 350 ppt Au were prepared in order to calibrate the two methods of extraction. Our results show that the resin extracted about 20% of the Au from the solutions and that good correlation was found to exist between the Au in solution and the Au extracted by the resin. Similar studies using activated charcoal were equally promising, with about 40% of the Au being extracted. The calibration curves for both extraction media are shown in Figure 090.8.

It was found that the coarser Amborane particles could easily be filtered from solution, while the activated charcoal tended to plug the filters. Amborane was also preferred from the point of view of neutron activation because it did not get as "hot" as charcoal upon irradiation, implying better detection limits. The Amborane preconcentration involved a greater extraction time, but the samples could be extracted in bulk using a rotating extractor, which constantly mixed the samples. This, coupled with faster filtering times, was found to outweigh the extraction time disadvantage.

In the laboratory experiments, and in field sampling, water was collected in plastic sample bottles, lined with "Glad" freezer bags. To our surprise, it was found that the liner bags proved to be more efficient in extracting Au from solution than either the resin or charcoal. In fact, when natural waters were sampled, it was found that the bags extracted up to 10 times as much Au as the Amborane or the charcoal. Research into this phenomenon is continuing.

Au CONTENT OF NATURAL WATERS

Orientation ground water and lake water samples were taken near the Matachewan Consolidated, Majestic, Emerald Lake, Cordova, and Pamour Mines, and at Arsenic Lake, and various localities near Timmins. Although the data from these natural waters is more erratic than was the case with the synthetic samples, concrete new information was obtained. Values of between 70 and 450 ppt Au were measured at the above sites (Table 090.1) which compares with the 20 ppt Au "background" found in Toronto tap water. These results compare favourably with the 1 to 100 ppt Au range of dissolved Au reported by Hamilton *et al.* (1983), using the ac-

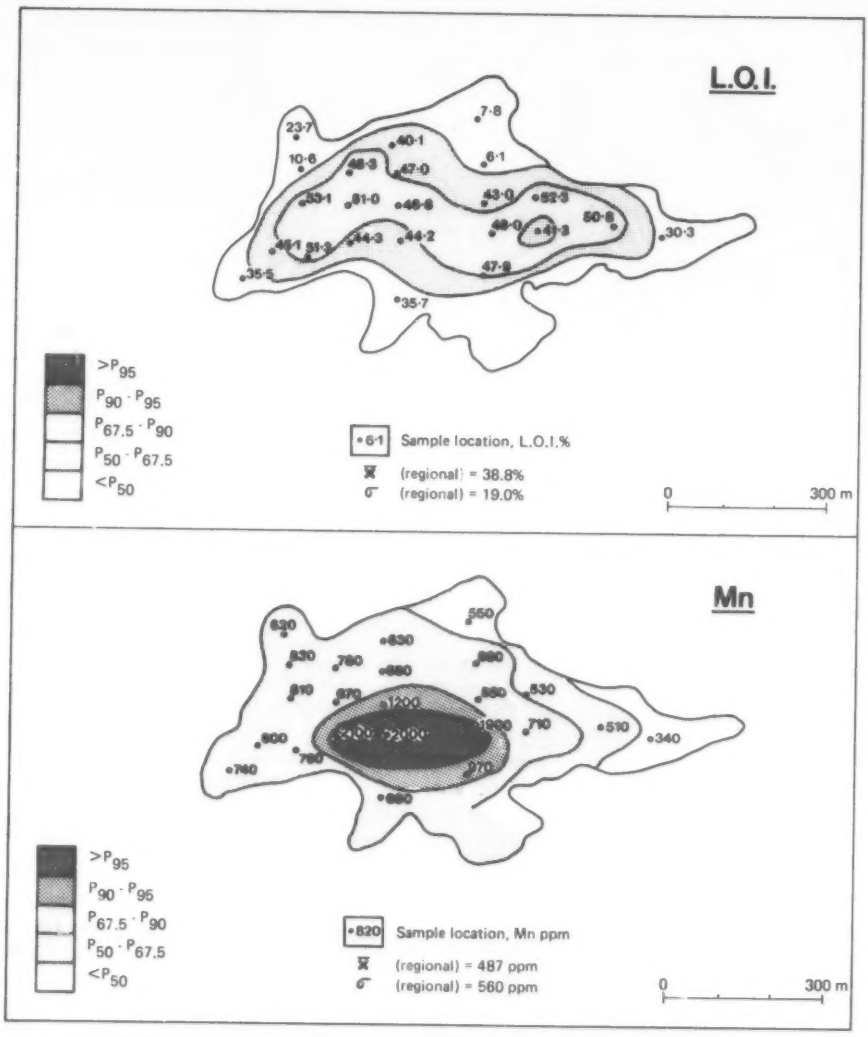

Figure 090.3 *Loss on ignition and manganese contents of organic lake sediments at Pap Lake, Saskatchewan. Percentile values were calculated from assays obtained during an earlier regional survey. Note the lack of correlation between these variables and Au.*

tivated charcoal preconcentration technique, near mineralization in Australia.

All of the data shown in Table 090.1 relate to groundwater flowing over, or stagnant on mineralized bedrock, or else lake water near the bedrock showing. We have yet to explain the variations in water Au content from one deposit to another (no relation to Eh, pH, etc. is evident), and obviously more background data is required, but there can be no doubt about the relatively high solubility of Au in natural waters, and the feasibility of transport of Au into nearby lakes.

OPTIMUM Au ANALYTICAL TECHNIQUES FOR ORGANIC LAKE SEDIMENTS

Lake sediment samples containing a range of Au contents have been analyzed with four standard techniques in order to select the one most suitable. A number of 8 g briquettes from each sample were initially analyzed by means of neutron activation. After a suitable "cooling off" period, the radioactive samples were then subjected to fire assay collection, and the resulting beads were then counted for radioactive Au. After this conventional radiochemical analysis, the same beads were re-irradiated for fire assay-neutron activation analysis, and finally digested and analyzed by means of D.C. plasma. F.A./N.A. and F.A./D.C.P. are methods commonly used in the analysis of Au in other media (for example soils), although 20 g samples are usually used.

The initial results are shown in Table 090.2. Significant reproduceability with N.A. and radiochemistry is evident for three of the four samples analyzed. The lack of reproduceability in EDT 18X is reflected in both techniques and suggests sample inhomogeneity.

The results from samples EDT 202X and EDT 65X suggest slightly better radiochemical reproduceability than is the case for straight-forward neutron activation. Reproduceability is worst, and mean Au contents are highest for the two methods which use fire assay

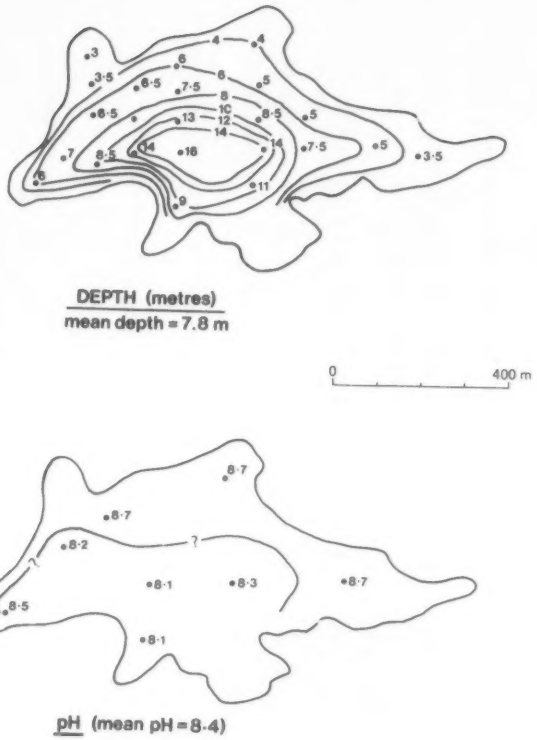

Figure 090.4 Depth and pH at Pap Lake, Saskatchewan. A possible correlation between bottom water pH and Au is evident.

collection, and this probably reflects a significant background Au value for the litharge present.

Additional analyses, over a wider range of Au concentrations, are clearly required, and are currently underway. At this point, however, little difference is apparent between standard neutron activation and radiochemical techniques, although both are clearly better than F.A./N.A. and F.A./D.C.P. in terms of the analysis of auriferous organic lake sediments. However, it should be noted that the greater accuracy of radiochemistry at the detection limits of straightforward neutron activation could be important in terms of broadening weak lake sediment dispersion halos.

Au SPECIATION IN ORGANIC LAKE SEDIMENTS

Statistical considerations as well as selective extraction analysis carried out on auriferous organic lake sediments lead Coker *et al.* (1982) to infer chemical rather than mechanical transport of Au for their study area. Statistical analysis of duplicate samples taken from the regional lake sediment survey in northern Ontario ($R = 0.95$, $R^2 = 0.90$ - Figure 090.8) leads to the same inference.

The internal homogeneity of samples EDT 65, 163X and 202X (Table 090.2) as well as the demonstrated ability of natural waters to dissolve surprisingly large amounts of Au (Table 090.1) is additional evidence for the hydromorphic transport and chemical fixation of this metal in organic lake sediments. The apparent inhomogeneity of sample EDT 18X remains to be explained, but may reflect the sort of Au crystal nucleation described by Watterson *et al.* (1984).

The determination of the nature of Au speciation in organic lake sediments is an important objective of Grant 090. The application of Au speciation in organic media to exploration has been discussed by Roslyokov (1984). A method of humic and fluvic acid isolation from organic material suitable for a relatively sophisticated speciation analysis has been described by Chin *et al.* (1978), but results to date using this method have been inconclusive.

DISCUSSION

Significant Au dispersion in organic lake sediments has been demonstrated around a number of showings in Ontario and Saskatchewan. It has also been demonstrated that natural waters can show a surprising degree of Au solubility (up to 450 ppt in groundwater dripping over an undisturbed auriferous quartz vein at the Golden Rose Mine, Temagami). From this, and from the relatively high degree of chemical homogeneity of organic lake sediments at low Au concentrations, it is concluded that chemical transport and precipitation of Au in the lacustrine environment occurs to a greater degree than previously expected. This phenomenon has been used, along with computerized geochemical "noise" filtering techniques, to find new mineralization in Northern Ontario by means of reconnaissance lake sediment sampling.

So far, hydromorphic Au dispersion distances of 200 to 300 m have been demonstrated using standard neutron activation analytical techniques. Larger dispersion halos may be detectable, and larger reconnaissance sampling grids may be possible, using radiochemical analysis which has lower detection limits (in the range 100 to 1000 ppt). This possibility is being investigated by the authors.

Work in progress includes the detailed analysis of 1 m in stratigraphic samples collected from anomalous and background lakes in Northern Ontario. It is hoped that an understanding of the relationships between Au content, changing forest cover, forest burn, and paleo pH (diatom inferred) in organic lake sediments will be obtained. Also underway, is additional speciation analysis.

Au dispersion is curiously weak or absent at two sample localities, namely the ponds found immediately up-drainage from the Studer deposit at Sulphide Lake (Figure 090.1), and at Arsenic Lake. Additional dispersion case histories over as broad a range of geological and physiographic conditions as possible, as well as integrated chemical studies of groundwater, lake water, soils, and bedrock at these and other localities, should be carried out to determine the variables affecting the suppression of hydromorphic Au transport here, and its enhancement elsewhere.

TABLE 090.1 GOLD CONCENTRATION (PPT) OF WATER SAMPLES TAKEN IN THE TIMMINS AREA, AND IN THE VICINITY OF THE CORDOVA, GOLDEN ROSE, AND MATACHEWAN CONSOLIDATED GOLD MINES

RESIN							CHARCOAL								
TOT	PRT	EX1	BAG	UE1	EX2	UE2	TOT	PRT	UE0	EX1	BAG	UE1	EX2	UE2	DESCRIPTION/LOCATION
Cordova Mine Area															
58	5	2	24	27	0	27	72	2	62	3	15	46	0	46	Drain S.E. Cordova Mine
69	8	1	26	34	0	34	55	2	22	8	14	46	0	46	Upstream from mine
127	9	36	18	64	0	64	63	3	36	31	13	29	0	29	Cordova Mine, puddle in tailings
48	4	5	14	25	0	25	80	1	57	7	5	85	0	85	Large pond west end tailings
69	3	16	15	35	0	35	100	1	94	14	8	73	0	73	Narrow trench west of tailings
38	4	3	11	21	0	21	41	1	33	4	6	33	0	33	Stream above tailings
87	3	5	35	44	0	44	46	-1	46	4	5	33	0	33	Roadside stream County Rd. 44, background
71	8	2	25	36	0	36	56	1	39	7	7	51	0	51	Small lake off County Rd. 44, background
Timmins Area															
207	14	9	83	89	30	83	174	12	98	54	43	67	11	95	Trench 6"H_2O, Denton #1, 5' from sulphide showing
210	34	8	43	150	14	86	333	21	100	58	190	51	12	110	Trench 4"H_2O, near 1-2 oz, Au Denton #1
164	18	64	45	57	13	3	152	9	63	25	66	55	8	69	Denton #4, pit 0.01-0.03 oz, half water gone this time
135	14	5	53	70	12	44	133	5	54	17	60	38	35	58	Denton #4, Trench 3' water, 0.8 oz Au from Grab sample
148	7	4	41	92	23	76	173	9	80	47	56	110	11	57	Pamour Mine area, stream flow north Bob's Lake
1811	29	1500	160	100	44	100	751	11	620	670	50	70	9	100	Carshaw water pumped from 1st level of mine in iron formation
241	23	12	79	160	25	69	194	34	130	22	52	61	9	58	Small creek running through valley near Carshaw Mine site
149	14	8	45	72	11	80	240	32	160	34	75	53	20	69	Small creek S of Croesus Mine Beaver Dam

TABLE 090.1 (CONTINUED)

RESIN							CHARCOAL								
TOT	PRT	EX1	BAG	UE1	EX2	UE2	TOT	PRT	UE0	EX1	BAG	UE1	EX2	UE2	DESCRIPTION/LOCATION
Golden Rose and Little Dan Area, Temagami Region															
450	31	59	190	96	94	150	173	8	120	19	31	79	26	150	Groundwater dripping from exposed quartz vein over main adit, Emerald Lake Mine
290	19	29	97	170	20	100	248	18	140	19	39	240	15	190	Groundwater seep into pool dug in humus 50'S of adit, Emerald Lake
337	46	79	99	100	45	81	339	160	65	41	85	78	20	66	Groundwaster seep into pool dug in humus 50'N of adit, Emerald Lake
241	7	4	35	97	32	260	222	18	250	14	35	59	12	75	Water, bottom rock trench over sulphide-bearing quartz vein, Emerald Lake
155	12	11	85	76	10	8	96	7	46	9	25	60	10	77	Lake water 75' N of adit, Emerald Lake
183	12	10	73	66	22	88	237	21	140	37	71	79	26	120	Lake water, foot of dump with Au-bearing rubble, Little Dan Mine
239	33	17	85	120	20	67	297	120	130	18	50	78	22	110	Swamp water 100'E of Dump, Little Dan Mine
138	5	5	37	59	22	100	0	0	0	0	0	0	0	0	Run off from swamp into Lake 20' N of Little Dan Mine dump
Matachewan Consolidated Mine Area															
150	7	5	82	50	13	48	164	6	110	16	54	80	14	69	Lake water S. shore Otisse Lake
361	5	14	52	520	23	36	148	7	84	25	29	59	12	160	Open stope water N of #2 Shaft
276	82	16	56	160	24	60	133	8	55	17	44	72	9	100	E side of open stope W of #1 shaft
102	8	9	26	65	9	44	174	3	35	10	110	46	8	100	W side of open stope W of #1 shaft
98	6	3	42	33	11	51	104	21	62	9	16	50	10	66	Pond water N of #1 shaft open stope
281	110	9	93	62	19	57	394	230	49	51	76	73	12	65	Run off puddle on tailings E end of property
137	7	4	40	110	15	46	156	9	160	15	15	72	31	75	Groundwater seep at shore line

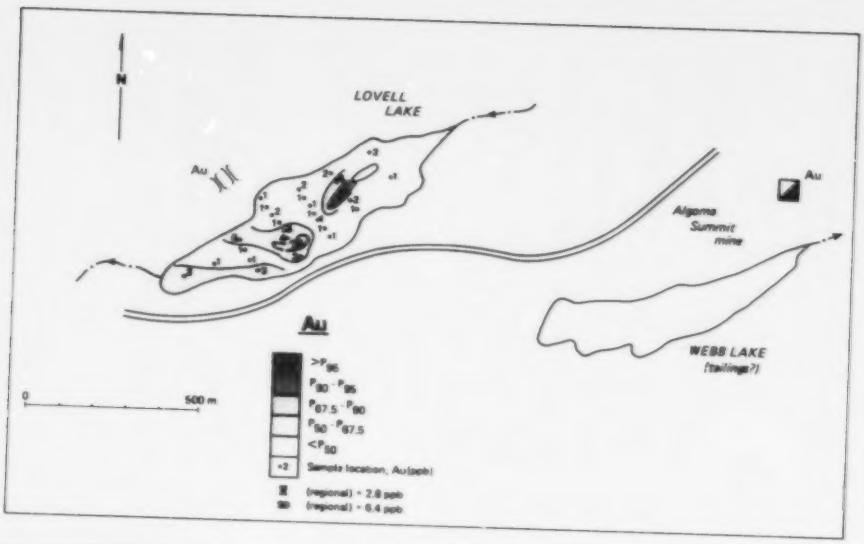

Figure 090.5 *Au content of organic lake sediments at Lovell Lake, Ontario. Percentile values were calculated from assays obtained during an earlier regional survey.*

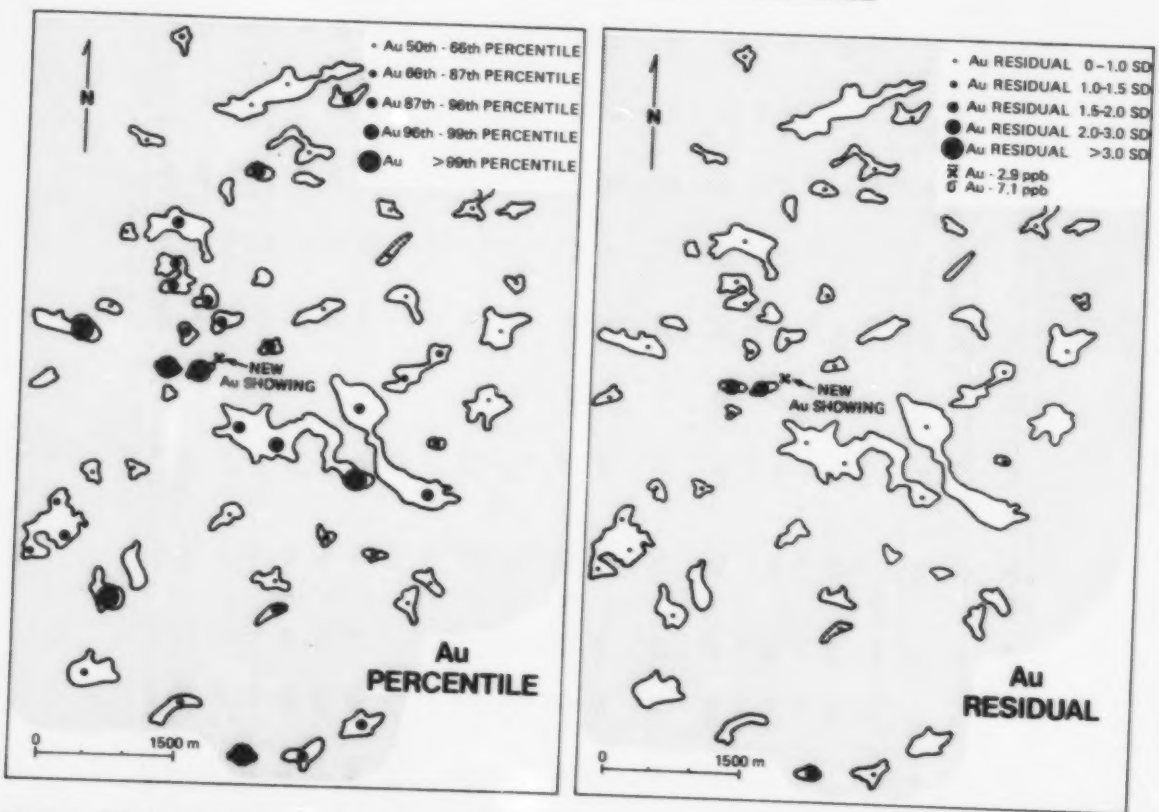

Figure 090.6 *Normalized (residual) and non-normalized (percentile) Au lake sediment values from a reconnaissance survey in northern Ontario. Residual values were obtained from the raw Au data by means of regression analysis.*

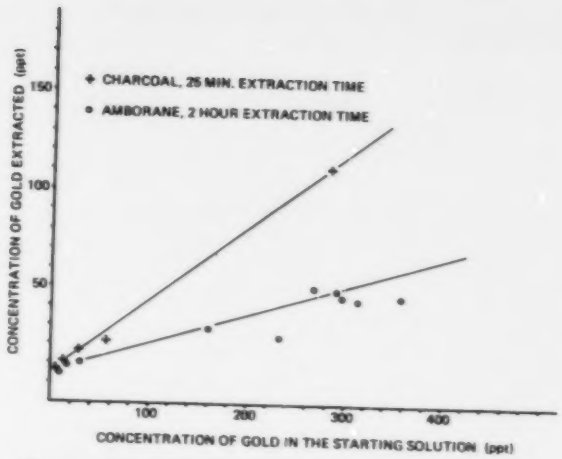

Figure 090.7 Extraction of Au by Amborane resin and by activated charcoal from synthetic solutions.

N. ONTARIO REGIONAL SURVEY

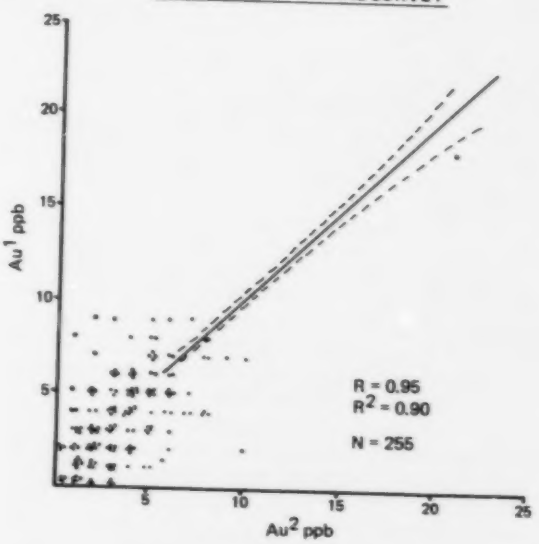

CORRELATION MATRIX

	Au	As	Zn	Cu	Mn	Fe	LOI
LOI	-.17	-.05	-.03	.13	-.25	-.23	
Fe	.41	.35	.88	.31	.89		
Mn	.22	.20	.83	.19			
Cu	.14	.28	.47				
Zn	.22	.40					
As	.08						
Au							

SULPHIDE L. REGION, SASKATCHEWAN

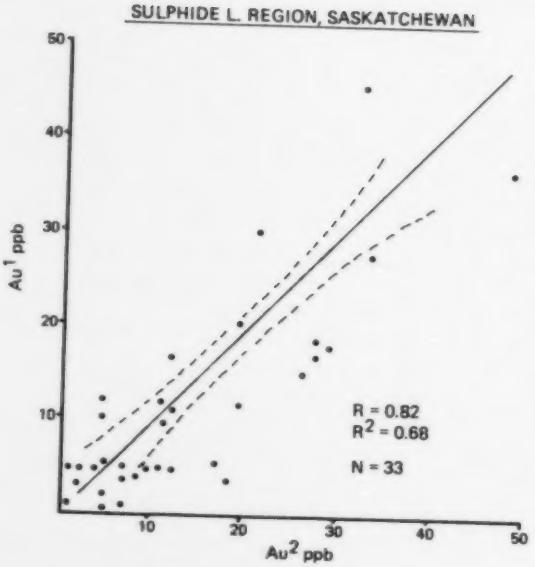

CORRELATION MATRIX

	Au	As	Zn	Cu	Mn	Fe	LOI
LOI	-.07	.06	.32	.43	.05	-.21	
Fe	-.07	.00	.50	.07	.29		
Mn	-.03	.03	.34	.03			
Cu	-.04	-.02	.44				
Zn	-.13	-.06					
As	.13						
Au							

Figure 090.8 Statistical analysis of duplicate samples taken from the Sulphide Lake region, Saskatchewan, and from a survey area in northern Ontario. Dashed lines are 95% confidence bands.

TABLE 090.2 COMPARISON BETWEEN VARIOUS INSTRUMENTAL TECHNIQUES FOR THE ANALYSIS OF GOLD IN ORGANIC LAKE SEDIMENTS

Sample No.	Date	Au, ppm Neutron Activation	Au, ppm F.A.neutron act.	Au, ppm Radiochem.	Au, ppm DCP/MS.
EDT 18X	10/84	d.1			
	4/85	3	11	4.4	17
	4/85	3	12	4.4	13
	4/85	9	18	10.4	21
	4/85	3	4	4.3	6
	4/85	3	8	3.6	13
	4/85	6	8	8.4	8
EDT 65	10/84	4			
	4/85	3	d.1	4.0	d.1
	4/85	4	d.1	4.4	d.1
	4/85	6	3	4.2	3
	4/85	4	3	3.7	2
EDT 163X	10/84	1			
	4/85	d.1	d.1	1.8	3
	4/85	d.1	d.1	2.0	d.1
	4/85	d.1	d.1	2.6	d.1
	4/85	d.1	d.1	2.1	d.1
	4/85	d.1	d.1	2.3	d.1
EDT 202X	10/84	3			
	10/84	2			
	4/85	3	-	3.7	-
	4/85	3	5	3.8	2
	4/85	4	4	4.8	11
	4/85	4	20	3.8	15
	4/85	2	d.1	3.7	d.1

ACKNOWLEDGMENTS

X-Ray Assay Laboratories Limited wishes to thank the Ontario Ministry of Natural Resources and the Ontario Geological Survey for their support.

REFERENCES

Chin, Y., Scnesi, N., and Schnitzer, M.
1978: Chemical and Physical Characteristics of Humic and Fulvic Acids Extracted From Soils of the Mediterranean Region; Geoderma, Volume 20, p.87-104.

Coker. W.B., Fox, J.S., and Sopuck, V.J.
1982: Organic Centre - Lake Sediments - Application in the Geochemical Exploration for Gold in the Canadian Shield of Saskatchewan; p.267-280 *in* Geology of Canadian Gold Deposits, edited by W. Petruk and R.W. Hodder, Canadian Institute of Mining and Metallurgy, Special Volume 24.

Roslyokov, N.A.
1983: Zoning of Forms of Gold in the Surficial Environment as a Criterion for Buried Gold Deposits (Abstract); Tenth International Geochemical Exploration Symposium, Helsinki, p.66-67.

Watterson, J.R., Nishi, J.M., and Botinelly, T.
1984: Evidence That Gold Crystals Can Nucleate on Spores of *Bacillus Cerus*; United States Geological Survey, Open File 84-487.

Hamilton, T.W., Ellis, J., and Florence, T.M.,
1982: Determination of Gold in Fresh Waters by Neutron Activation Analysis After Preconcentration on Activated Charcoal; Analytical Chimica Acta, Volume 148, p.225-235.

Hamilton, T.W., Ellis, J., Florence, T.M., and Fardy, J.J.
1983: Analysis of Gold in Surface Waters in Australia: An Investigation Into Direct Hydrogeochemical Prospecting for Gold; Economic Geology, Volume 78, p.1335-1341.

Grant 093 Software and Hardware Design of Controlled Source Audio-frequency Magneto-telluric (CSAMT) System and Test Survey

Mitsuru Yamashita

Phoenix Geophysics Limited, Willowdale

ABSTRACT

A Controlled Source Audio-frequency Magneto-telluric (CSAMT) system has been successfully developed utilizing, initially a Phoenix 6-channel IPV-3 spectral IP receiver and IPT-1 (AC3003 model) transmitter. The CSAMT System presently manufactured by Phoenix Geophysics Limited comprises the microprocessor controlled V4 8-channel receiver with magnetic sensor coil and IPT-1 (AC3004) model) DC-10 kHz transmitter. The system was successfully used in several test surveys.

In standard operation, six E-field magnitudes and one H-field magnitude are simultaneously measured at 16 binary related frequencies (0.25 to 8192 Hz). The controlled signal source is the IPT-1 transmitter, which drives current through a grounded long-wire dipole. This generates an electromagnetic field at the same frequencies. The transmitter dipole is located several km from the area to be surveyed. A large trapezoidal survey area on either side of the transmitter dipole can be covered from a single transmitter setting. This makes the CSAMT technique very cost-effective for mapping.

Apparent resistivities are calculated in real time for the six E-dipole sounding locations at the 16 frequencies. All the measured and calculated data are stored in RAM memory, listed on a pocket printer through a parallel I/O and/or transferred to a mass storage device through a RS232 serial I/O at the measuring site. Phase, E-field, H-field, and the standard deviations are also measured and stored.

Later in a field base camp, the data are dumped into a field computer and processed automatically to generate an apparent resistivity pseudo-section plot. A near-field correction is also applied. A 1-D inversion program has also been developed for the field computer.

INTRODUCTION

The CSAMT method was introduced by Goldstein (1971) and Goldstein and Strangway (1975) to overcome problems encountered by the Audio Magnetotelluric (AMT) and MT methods.

The MT method is a well known exploration technique, used widely in hydrocarbon and geothermal exploration. The MT method measures fluctuations in the earth's natural electric and magnetic fields, in a broad range of frequencies between about 0.0001 and 100 Hz. When the measurements are made in the audio-frequency range (10 to 20 kHz), the method is known as Audio-frequency Magnetotellurics (AMT). Neither MT nor AMT requires a man-made power source. However, these advantages are often negated by the low magnitude and variability of the natural signals.

The advantages of the controlled source method are several:

1. Signals are stronger, therefore, the receiving equipment does not need to be as sensitive as that for MT or AMT.
2. Because of the coherent signal, the usual signal processing and enhancement techniques are far more effective.
3. Thus, CSAMT surveys can be much faster than AMT surveys.

One disadvantage with respect to the natural field mode is the closeness of the signal source. In the natural field methods, the signal source is, in effect, infinitely distant. This "plane wave" assumption simplifies both the mathematics and the interpretation of AMT/MT data. When a controlled scurce is used, the "plane wave" assumption is no longer true (at least close to the transmitter), and the calculated apparent resistivity must be corrected for the "near-field" effect.

This project fully utilized the multi-channel, multi-frequency, microprocessor control instrumentation technology developed by Phoenix Geophysics Limited, resulting in swift achievement as well as producing a CSAMT System that has improved further on the above CSAMT advantages.

SYSTEM CONCEPTS

CSAMT PARAMETERS MEASURED AND CALCULATED

Both electric field (E-field) and magnetic field (H-field), are measured at the frequency transmitted from the remote transmitter dipole source. The magnitudes of both the E-field and H-field are determined, as well as their relative phases. The measured data are digitally stacked, filtered, and processed in real-time, calculating apparent resistivity. This is done using the following Cagniard equation and the phase difference.

$$\rho_a \simeq \frac{1}{5f}\left|\frac{Ex}{Hy}\right|^2 \quad (1)$$

$$\phi = \phi_E - \phi_H$$

where ρ_a is apparent resistivity in ohm-m; f is frequency in Hz; Ex is the E-field magnitude, in mv/km, parallel to the transmitter dipole; Hy is H-field magnitude perpendicular to the E-dipole in gammas; ϕ is phase difference in radians; ϕ_E is E-field phase and ϕ_H is H-field phase.

In addition to the parameters mentioned above, the standard deviations of each parameter, |Ex|, |Hy|, ρ_a, ϕ_E and ϕ, are calculated for signal verification.

RECEIVER SYSTEM

The CSAMT Receiver System consists of the V4 receiver console, a magnetic sensor coil, and peripherals. Photo 093.1 shows a V4 eight-channel universal receiver which can be used for spectral IP, conventional IP in time or frequency domain, and CSAMT. Photo 093.2 shows a magnetic sensor coil to measure H-field. Non-polarizable electrodes are usually employed for E-dipoles to measure the E-field.

The main features of the V4 receiver are:

1. simultaneous measurement of eight input channels
2. microprocessor-controlled real-time filtering, signal stacking, and averaging
3. data logging in solid state non-volatile memory
4. two standard output ports (parallel and serial) for a vest pocket printer and data transfer to a microcomputer
5. automatic gain control and self-potential (SP) cancellation
6. frequency range from 0.25 to 8192 Hz for CSAMT operation
7. real-time calculation of apparent resistivity, phase, mean, and standard deviation of measured parameters
8. continuous monitoring of any measured and calculated parameters on 4 lines x 16 character LCD display
9. comprehensive keyboard-and-prompt operation

TRANSMITTER SYSTEM

The CSAMT transmitter system consists of a transmitter console, a frequency control device, a motor generator, and peripherals. Photo 093.3 shows an IPT-1 transmitter console. For the transmitter dipole, a long magnet wire is laid on the ground in an approximate straight line. Both ends are grounded.

The main features of the transmitter system for the CSAMT operation are:

1. frequency range from 0.25 to 8192 Hz, with a binary step
2. output voltage of up to 800 volts
3. maximum continuous output power of 3KW with MG-3 motor generator
4. regulated current up to 10 amperes
5. automatic turn-off protection if the current exceeds 150% full scale or if it is <5% full scale

The transmitter system is portable. Furthermore, the transmitter system can be situated at one location to cover a large survey area. There are more powerful transmitter systems available from Phoenix Geophysics Limited for applications where portability is not the most important factor.

Photo 093.1 The Phoenix V4 multichannel universal receiver console.

Photo 093.2 The CSAMT magnetic sensor coil.

SURVEY CONFIGURATION AND GRID

Figure 093.1 illustrates the survey configuration and grid. The standard configuration performs six (or seven) Ex-field and one Hy-field measurements at 16 frequencies (0.25 to 8192 Hz). As illustrated, the E-fields are measured with a dipole using non-polarizable electrodes in the same way as IP measurements. The survey traverse line for the series of equally spaced E-dipoles is parallel to the transmitter dipole. The dipole length is determined by the desired scale of the survey; this may also be influenced by the E-field signal strength, which is in turn determined by the transmitter - receiver distance, the transmitter dipole current, and the earth resistivity. The receiver dipole length may be in the range from 10 to 20 m.

A horizontal magnetic sensor coil is placed on the ground approximately at the centre of the series of E-dipoles. The coil axis is oriented perpendicular to the E-dipoles. It must be placed several m away from the E-dipole line and the receiver console to avoid interference, as well as to reduce inductive coupling due to operator movement. Only one H-field measurement is required for each group of six E-field measurements; the justification for this will be discussed later.

The transmitter (powered by a motor generator) sends current into a long wire, grounded dipole. The length of the dipole may be varied from several hundred m to several km, depending upon signal strength requirement. This will also be discussed later, as will the transmitter - receiver distance and the survey area to be covered with one transmitter dipole location.

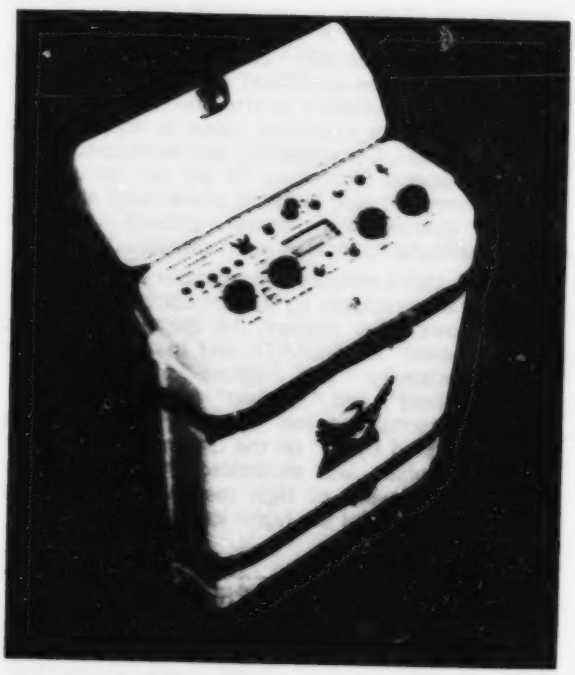

***Photo 093.3** The Phoenix IPT-1 multi-purpose transmitter.*

CSAMT SIGNALS AND PARAMETERS

FIELD STRENGTH

At a given receiver location, the field strength depends upon various factors: location of measuring point (relative to Tx dipole), transmitter dipole length, current in the dipole, earth resistivity and measuring frequency. It is important to know the approximate expected field strength in order to plan the survey grid and the transmitter location properly to give the optimum survey results.

Figures 093.2a and 093.2b show examples of contours of the Hy-field and Ex-field strength at 1024 Hz over a homogeneous earth of 1000 ohm-m based on the parameters indicated above. The heavy dashed contours indicate the region in which the field becomes minimal.

APPARENT RESISTIVITY

The apparent resistivity is calculated from the ratio of the electric field and magnetic field magnitudes using the well known Cagniard equation (1) for MT. It should be noted that this Cagniard equation is valid only in the plane wave region of the electromagnetic field; that is, when the distance between transmitter signal source and receiving location is sufficiently large.

Figure 093.2c indicates the apparent resistivity, calculated by the Cagniard equation over a homogeneous earth of 1000 ohm-m referring to the field strength magnitudes shown in Figures 093.2a and 093.2b. It should be observed that the valid area for the application of the equation is indicated by the calculated apparent resistivity value of approximately 1000 ohm-m. The dashed line depicts the plane of the minimal field previously mentioned and measurements in this area should be avoided.

The effective survey area, a trapezoidal shape, indicated in Figure 093.2 is thus optimized by the maximum possible field strengths and by avoiding areas that are too close to the transmitter dipole.

FAR-FIELD AND NEAR-FIELD

In a CSAMT survey, the distance between the transmitter and receiver locations is constrained in general by the requirement that the magnetic and electric field be strong enough to permit useful measurements. The paradox is that where the "plane-wave" assumption is valid, the signal may be weak; and where the signal is strongest (near the transmitter), the "plane-wave" assumption is no longer true.

At some distance from the transmitter dipole, where the transmitted electromagnetic field becomes a "plane-wave", it is called "far-field". The Cagniard equation is valid in the "far-field" situation to calculate the apparent resistivity. The "far-field" distance, Lf, is approximately given by the following equation:

$$Lf > 3 \times \text{skin depth} \cong 1509 \sqrt{\rho / f}$$

where Lf is in m, ρ is resistivity of the homogeneous earth in ohm-m, and f is frequency in Hz.

If the distance between transmitter and receiver is much less than Lf, the transmitted field is not "plane-wave" in character; it is referred to as the "near-field". In the "near-field", the Cagniard equation overestimates the actual resistivity. Figure 093.3a shows the apparent resistivity curve, using the Cagniard equation with theoretically calculated Ex and Hy values, over a homogeneous earth. The apparent resistivity curve in the "near-field" is characterized by a slope of 45°, meaning that the apparent resistivity value is doubled by each binary frequency step. The area of the gradual change from "far-field" to "near-field" is called "transition-zone" or "transition-field".

Figure 093.4a shows Hy-field versus frequency over a homogeneous earth, for various resistivity and transmitter - receiver distances. The Hy-field can be expressed by the following equations:

in "far-field"; $Hy \sim 1/(\sqrt{\sigma f} r^3)$ (2)

in "near-field": $Hy \sim 1/r^2$ (3)

where $\sigma = 1/\rho$ is conductivity in mhos/m.

Figure 093.4b shows Ex-field versus frequency in the same way as Figure 093.7.

The Ex-field can be expressed by the following equations:

in "far-field"; $Ex \sim 1/(\sigma r^3)$ (4)

in "near-field"; $Ex \sim 1/(\sigma r^3)$ (5)

For "far-field", from equation (2) and equation (4);

$$\frac{Ex}{Hy} \sim \left[\frac{1}{\sigma r^3}\right] \Big/ \left[\frac{1}{\sqrt{\sigma f} \cdot r^3}\right] = \sqrt{\frac{f}{\sigma}}$$

therefore,

$$\rho_a \sim \frac{1}{f} \left|\frac{Ex}{Hy}\right|^2$$

introducing factor, Kf/5,

$$\rho_a = \frac{Kf}{5f} \left|\frac{Ex}{Hy}\right|^2 \quad (6)$$

For 'near-field', from the equation (3) and the equation (5),

$$\frac{Ex}{Hy} \sim \left[\frac{1}{\sigma r^3}\right] \Big/ \left[\frac{1}{r^3}\right] = \frac{1}{\sigma r}$$

therefore,

$$\rho_a \sim r \left|\frac{Ex}{Hy}\right|$$

introducing 'near-field' factor Kn,

$$\rho_a = Kn \cdot r \left|\frac{Ex}{Hy}\right| \quad (7)$$

FIRST ORDER "NEAR-FIELD" AND "TRANSITION-FIELD" CORRECTION

Figure 093.4c shows the Kf and Kn factors versus fr|E/H| over a homogeneous earth for the entire resistivity, transmitter - receiver distance, and frequency ranges. It should be noted that the Kn is constant, 0.63, in the "near-field" and Kf is constant, 1.0, in the "far-field" indicating that equation (6) is the same as the Cagniard equation. From the known values of f (frequency), r (transmitter receiver distance), and |E/H| (measured), it is possible to categorize a field situation as "far-field", "transition-field", or "near-field".

The corrected apparent resistivity, now, can be calculated using: the Cagniard equation if it is in the "far-field"; equation (7) if it is in the "near-field"; and equation (6) or equation (7) using proper Kf or Kn values if it is in the "transition-field".

If a correct "near-field" and "transition-field" correction is performed on CSAMT data ,to obtain apparent resistivity equivalent to the "far-field" situation, then the apparent resistivity value is equivalent to that of MT/AMT. Consequently, well-developed existing interpretation techniques for MT can be utilized. Proper correction also prevents some false and dangerous interpretation errors caused by the "near-field" and "transition-field" effects.

Figure 093.5 indicates an example of the method executed automatically by a microcomputer. The example shows three profiles: the Cagniard equation, the "near-field" equation (7), and the corrected apparent resistivity. The regions of "near-field", "transition-field", and "far-field" are also indicated. After corrections, the low resistivity portion of the curve, designed by "A" on the uncorrected Cagniard resistivity profiles, was eliminated; the data indicate perhaps two layers of high resistivity over a low resistivity, instead of the high - low - high layered geometry.

DATA PROCESSING AND PRESENTATION

Survey data are measured, the parameters are calculated, stored in the RAM of the receiver unit, and transferred into permanent mass storage media (such as a cassette tape) at the end of each day in the field base camp. The data can then be immediately processed by microcomputer. The field presentation of the results is in the form of a contoured apparent

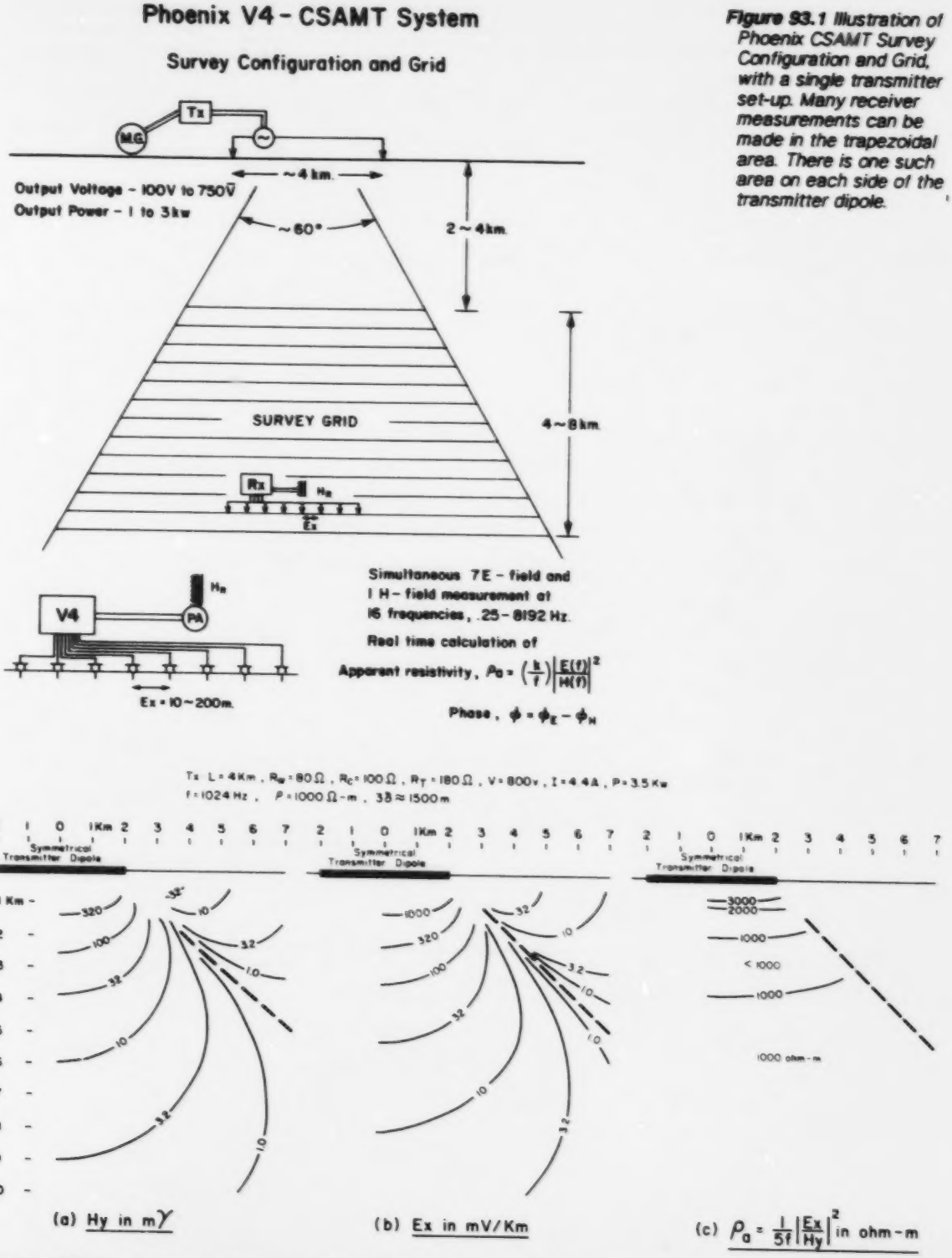

Figure 93.1 Illustration of Phoenix CSAMT Survey Configuration and Grid, with a single transmitter set-up. Many receiver measurements can be made in the trapezoidal area. There is one such area on each side of the transmitter dipole.

Figure 093.2 An example of calculated Hy-field, Ex-field, and apparent resistivity over homogeneous earth based on the parameter indicated above, where R_w is wire resistance, R_c is contact resistance, and R_T is total resistance of the dipole.

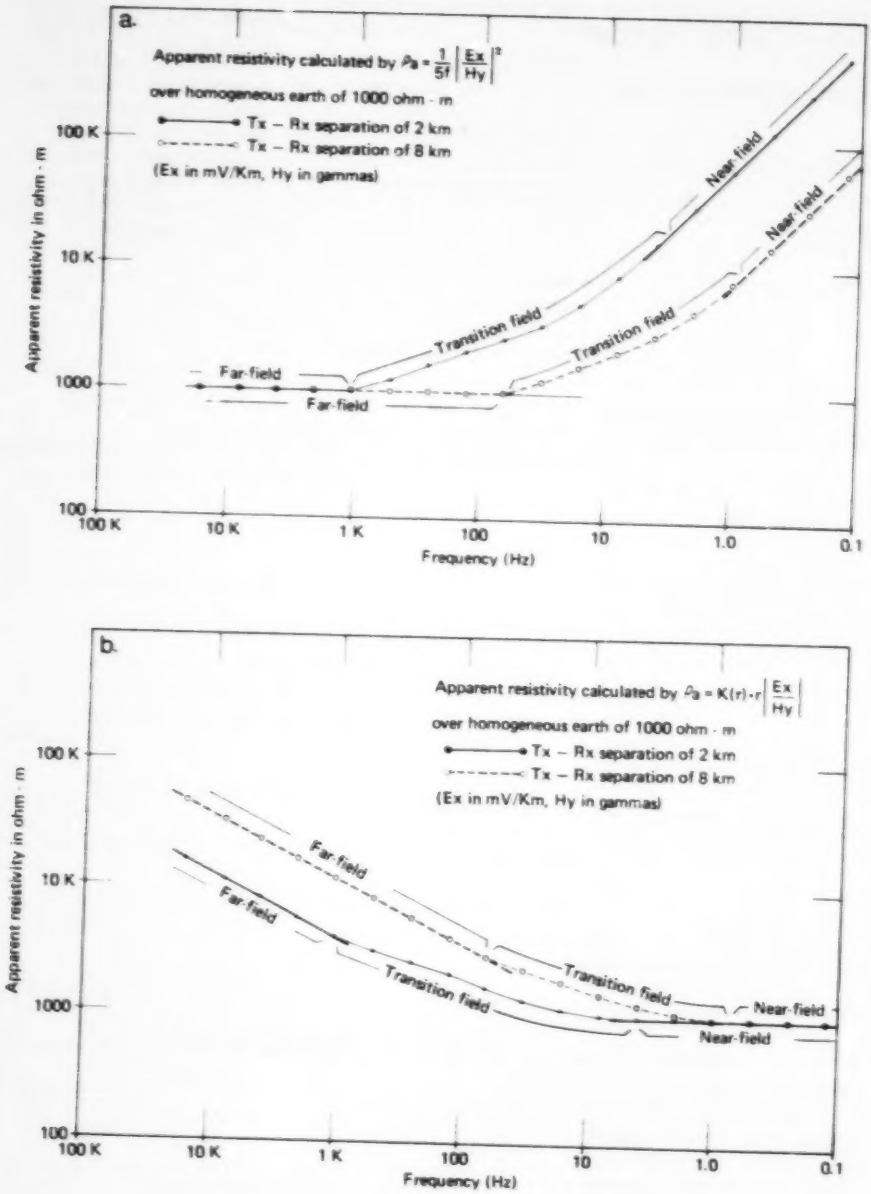

Figure 083.3 *Apparent resistivity versus frequency calculated using Cagniard equation (a) and "near-field" equation (b) over homogeneous earth of 1000 ohm-m.*

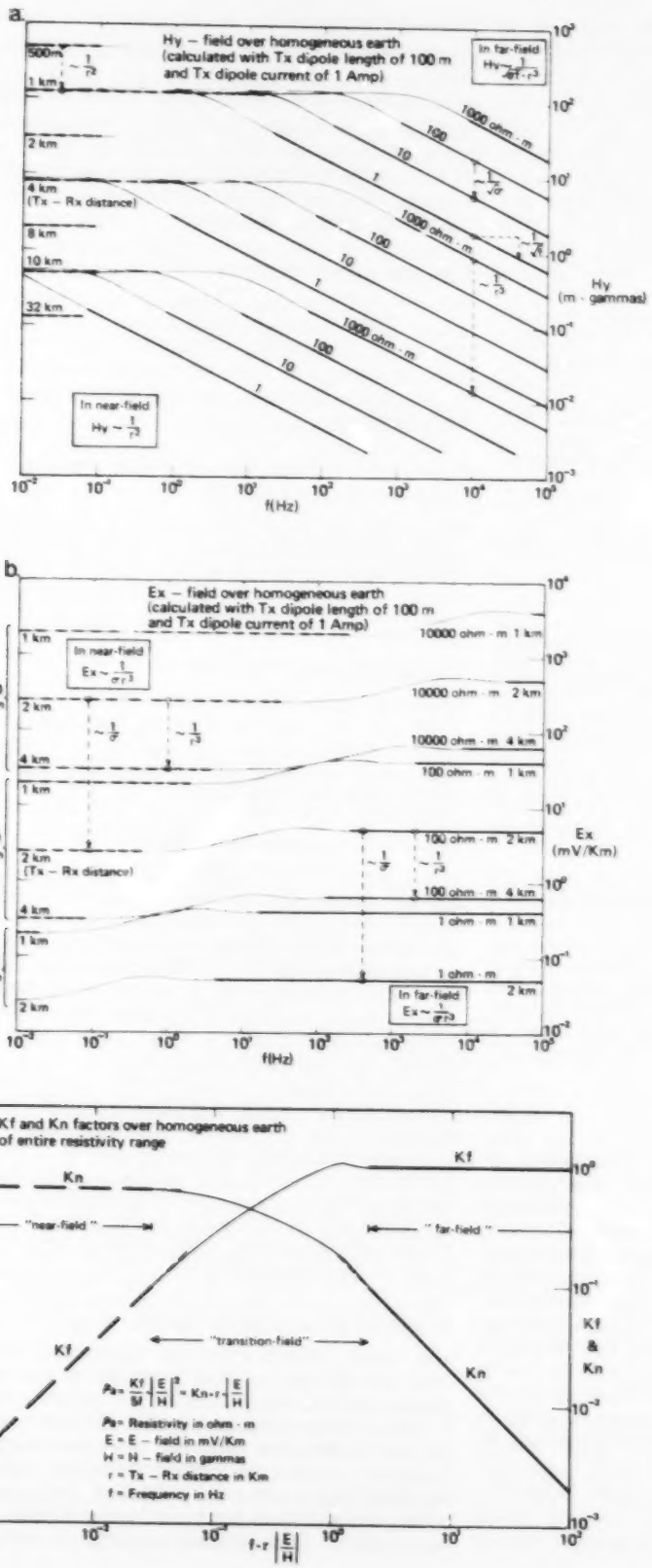

Figure 093.4 *(a) Hy-field and (b) Ex-field versus frequency over homogeneous earth of various resistivity, for various distances between transmitter and receiver, and (c) Kf and Kn factors over homogeneous earth of entire range of resistivity, Tx-Rx distance, and frequency.*

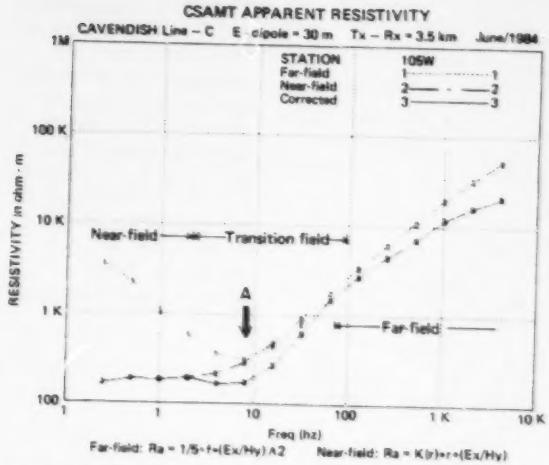

Figure 093.5 *Computer plot of three apparent resistivity profiles calculated by Cagniard equation, "near-field" equation, and the first order correction.*

resistivity pseudo-section plot or profile plot. Other parameters such as phase, or E and H field magnitude, can also be presented in the same form.

This immediate data processing and presentation permits the geophysicist to modify the survey plan and also to verify data in the field. A 1-D inversion program has also been developed for a microcomputer to use in the field base camp or in the office. Some examples will be shown with discussions for case histories.

ADVANTAGES OF CSAMT AND PHOENIX SYSTEM

There is no geophysical exploration method and/or system that can be said to be superior to any other system and method, in respect to all situations. However, the following list describes some advantages of CSAMT in general, and of the Phoenix System V-4 CSAMT in particular.

Depth of Detection

The depth of detection in geophysical exploration is not easy to express in simple terms. It is related to many factors such as earth resistivity, frequency, size of target, resistivity constrast, electrical noise, geological noise, and system sensitivity. The effective depth of penetration in CSAMT is a function of frequency and earth resistivity, and not the length of the receiver dipole or the distance between transmitter and receiver. The frequency range of 0.25 Hz to 8192 Hz permits sounding depths that vary from very shallow to very deep. The effective depth of detection of CSAMT, therefore, may be several hundred m to several km, depending upon the characteristics of the conductor at depth.

Lateral Resolution

CSAMT offers excellent lateral resolution, dependent only upon the length of the receive dipole, independent of the distance between the transmitter and receiver. The length of the receiver dipole can be adjusted to the size of the exploration target, with no loss in depth of penetration. A reconnaissance mode survey can often be completed using a large receiver dipole typically 100 to 200 m.

Flexible Survey Design

Normally a large survey area can be covered using a single grounded transmitter dipole. The location of this dipole, relative to the survey area, is generally flexible enough to allow utilization of existing roads to lay out the dipole wire and to position the transmitter equipment.

Insensitive to Topographic Effects Between Receiver and Transmitter

Since the measured value is normalized at the receiver, the topographic relation between the transmitter and receiver is not an important factor. This fact makes CSAMT particularly useful in mountainous or remote regions, as well as with limited land holdings.

Ease of Set-up of Transmitter

The single grounded transmitter dipole is much easier to set-up and maintain, than the large rectangular or square loops generally utilized by time-domain EM system. These loops must typically be several hundred m to a few km square.

Effects of Transmitter Location

The location of a large loop transmitter for time-domain EM is often critical to anomaly response. A second conductor can be easily masked by a first conductor located closer to the transmitter. Therefore, in time-domain EM, it is frequently necessary to repeat measurements with a second transmitter set-up at a different location to the first set-up. The limitations are discussed by Spies and Parker (1984). CSAMT, on the other hand, is much more independent of transmitter location with a reasonable distance between transmitter and receiver. This is so because CSAMT measures relative phase shift and amplitude ratio between the E and H fields. These parameters are controlled by local resistivity around the measuring point. Intervening conductors (between Tx dipole and Rx measuring point) affect the absolute phase shift/amplitude ratio between Rx - Tx, which is not of interest in CSAMT.

Effective Measurement Points

With other EM and resistivity methods, to obtain satisfactory anomaly shape information, the measurements have to be performed on either side of the anomaly. Also, especially in the Schlumberger method, the survey line must be extended to permit the transmitter dipole to extend to either side of the sounding point, requiring extra line cutting beyond a survey area. This is not the case for CSAMT because each station is essentially a point sounding. Fewer

receiver dipole measurements are required to represent an anomaly and no extra line cutting is required.

Apparent Resistivity Measurements in Real-time

With other EM techniques, it is generally necessary to do data processing and interpretation after a survey is completed, in order to calculate the resistivity of the conductor and the host media. CSAMT provides real-time calculation of apparent resistivity, which helps the geophysicist to understand the situation immediately, and permits him to re-configure the survey if needed.

High Productivity Through Simultaneous Multi-station Measurements

Six (or optionally seven) E-field measurements and one H-field measurement are made simultaneously. Resistivity changes are predominantly reflected by changes in the E-field magnitude. Only one H-field measurement per group of E-measurements is needed because the H-field is essentially constant over significant distances along a line parallel to the transmitter dipole, even for very strong conductive features. Although dependent upon topography of an area, seven receiver set-ups can be easily performed in a field day. This produces data from 42 stations, with 16 frequencies from 0.25 Hz to 8192 Hz at each station.

Wide Frequency Range

The wide frequency range from 0.25 Hz to 8192 Hz in binary steps provides very shallow to very deep soundings, thus making the interpretation, especially with inversion, more effective.

CASE HISTORIES

The following section discusses results of some CSAMT surveys carried out during the first year of this ETDF (April 1984 to March 1985).

CAVENDISH TEST RANGE, ONTARIO

The test range is located in Cavendish Township, situated about 200 km northeast of Toronto, on the southern side of the Salmon Lake Road, approximately 2 km west of Highway 507 and approximately 11 km south of Gooderham. There are two main shallow conductors, delineated by drilling and known from previous geophysical surveys. The bedrock at the test site consists of gneisses and crystalline limestones with foliation generally dipping steeply east. The two conductive zones contain high concentrations of sulphides. The detailed geology and interpreted cross section have been published by the Geological Survey of Canada (Williams *et al.* 1975).

The test survey covered Line C and Line B with different E-dipole lengths. This survey was the first test survey, during the CSAMT development stage. Distances of 3.5 km and 8.6 km between the transmitter and receiver were used in this survey. Because the Model AC3003 of the IPT-1 transmitter employed was not designed for a high inductance load (at high frequency with a long wire), the E-field was generally weak. The reader should note that the IPT-1 transmitter was later improved to take high inductance loads and the Model AC3004 has been developed.

Figure 093.6 shows examples of the CSAMT data obtained by the surveys as well as gravity and AMT data for comparison with the station lines. Figures 093.6b and 093.6c show the CSAMT apparent resistivity pseudo-section plots on Line B and Line C, both after near-field correction. The E-dipole length is 20 m. The CSAMT data indicate distinct features of very low resistivity and general zones of low resistivity under high resistivity zones. Such deep studies have not been made a great deal at the Cavendish test site because the test range has been utilized rather as a very shallow geophysical target. With conventional methods, such as IP and Slingram EM, it was actually difficult to make deep investigations, even if desired, without losing lateral resolution.

Figure 093.6a shows a profile of residual Bouguer gravity anomaly along Line B (re-drawn after Sobczak and Jacoby 1967). The gravity anomaly, >0.7 mgal at the peak, agrees with the amphibolite zone. In the paper, the excess mass, assuming ore near the surface, of 100 000 metric tons was estimated. Figure (d) shows an AMT apparent resistivity pseudo-section along Line B (re-scaled from Strangway, Ilkisik, and Redman 1983). Although the frequency range was from 10 Hz to 10 000 Hz and an E-dipole length of 30 m was employed, the agreement between the AMT results and CSAMT results is excellent, especially since both indicate the distinct zones of very low resistivity.

Further study about the distinct low resistivity zones will be especially interesting.

NIGHTHAWK LAKE TEST RANGE, ONTARIO

The tast range is located in the northern quadrant of Thomas Township, approximately 12 km south of Highway 101, on the Gibson Lake Road. The Gibson Lake Road turn-off is located approximately 40 km east of Timmins, Ontario, on Highway 101. There is a conductive graphite zone in the bedrock under about 90 m of glacial overburden. The surveys were carried out on Line 1E, Line 0, and Line 1W in July and October, 1984.

Figure 093.7a shows examples of the CSAMT results presented as grey-scale contoured apparent resistivity versus frequency pseudo-sections. The higher intensity indicates lower resistivity. The E-dipole length was 25 m and the distance between the transmitter and receiver was 4 km. Because of high resistivity (>10 000 ohm-m) basement rock, strong "near-field" effects were encountered. Figure 093.7a shows apparent resistivity on Line 1E without the "near-field" correction. The "near-field" effects are typically characterized by a doubling of apparent resistivity as frequency is halved. Figure 093.7b shows apparent resistivity from the same data after the "near-field" correction.

If a proper "near-field" correction is applied on CSAMT data, the result should correlate well with AMT data, which is guaranteed to be measured in the "far-field" "plane-wave" situation. Figure 093.7c shows a contoured AMT apparent resistivity pseudo-section (re-scaled after Strangway, Ilkisik, and Red-

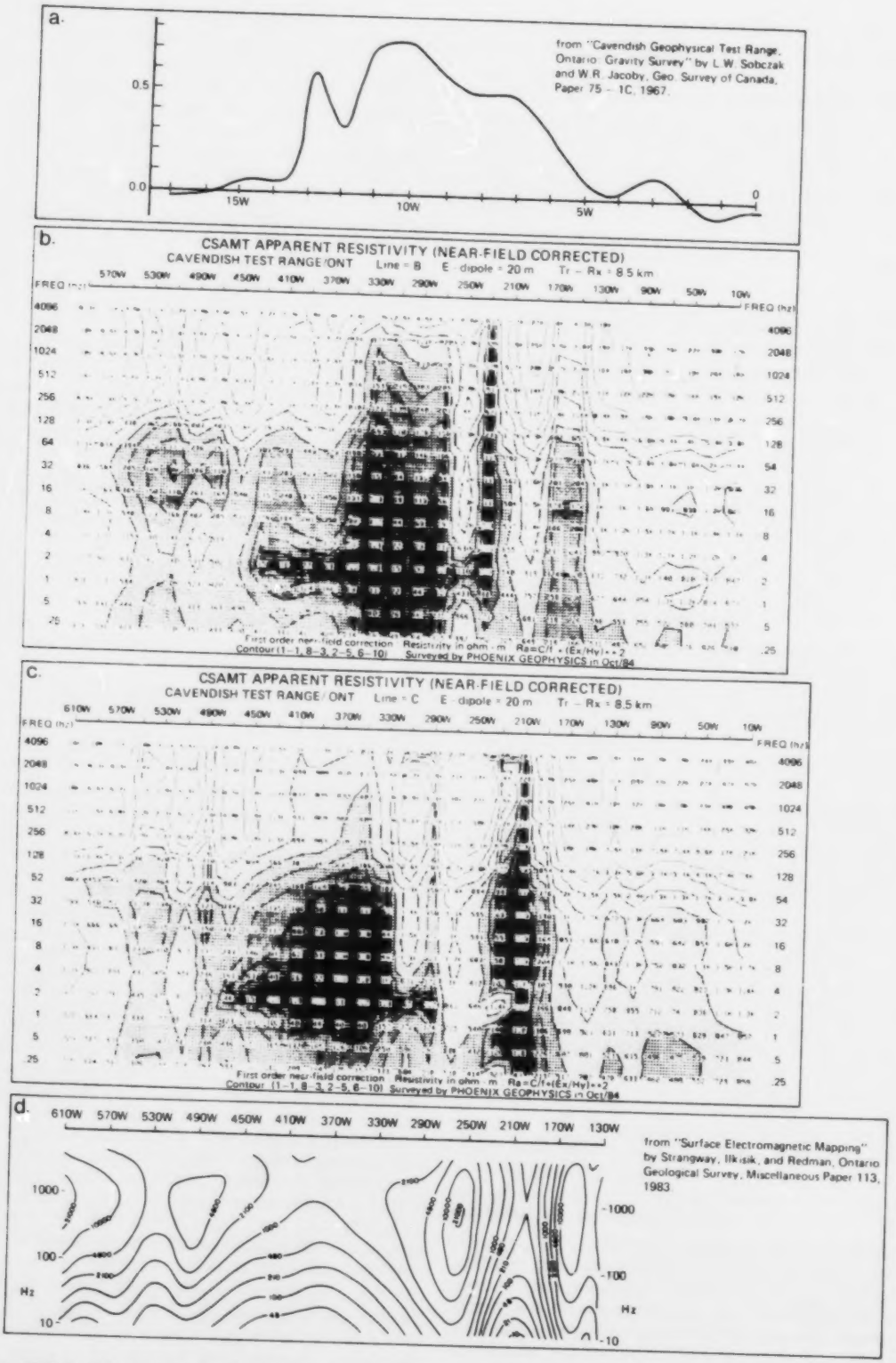

Figure 093.6 *CSAMT apparent resistivity pseudo-section on Line B(b) and Line B(c), residual Bouguer anomaly on Line B(a), and AMT apparent resistivity pseudo-section on Line B(d), Cavendish Test Range, Ontario.*

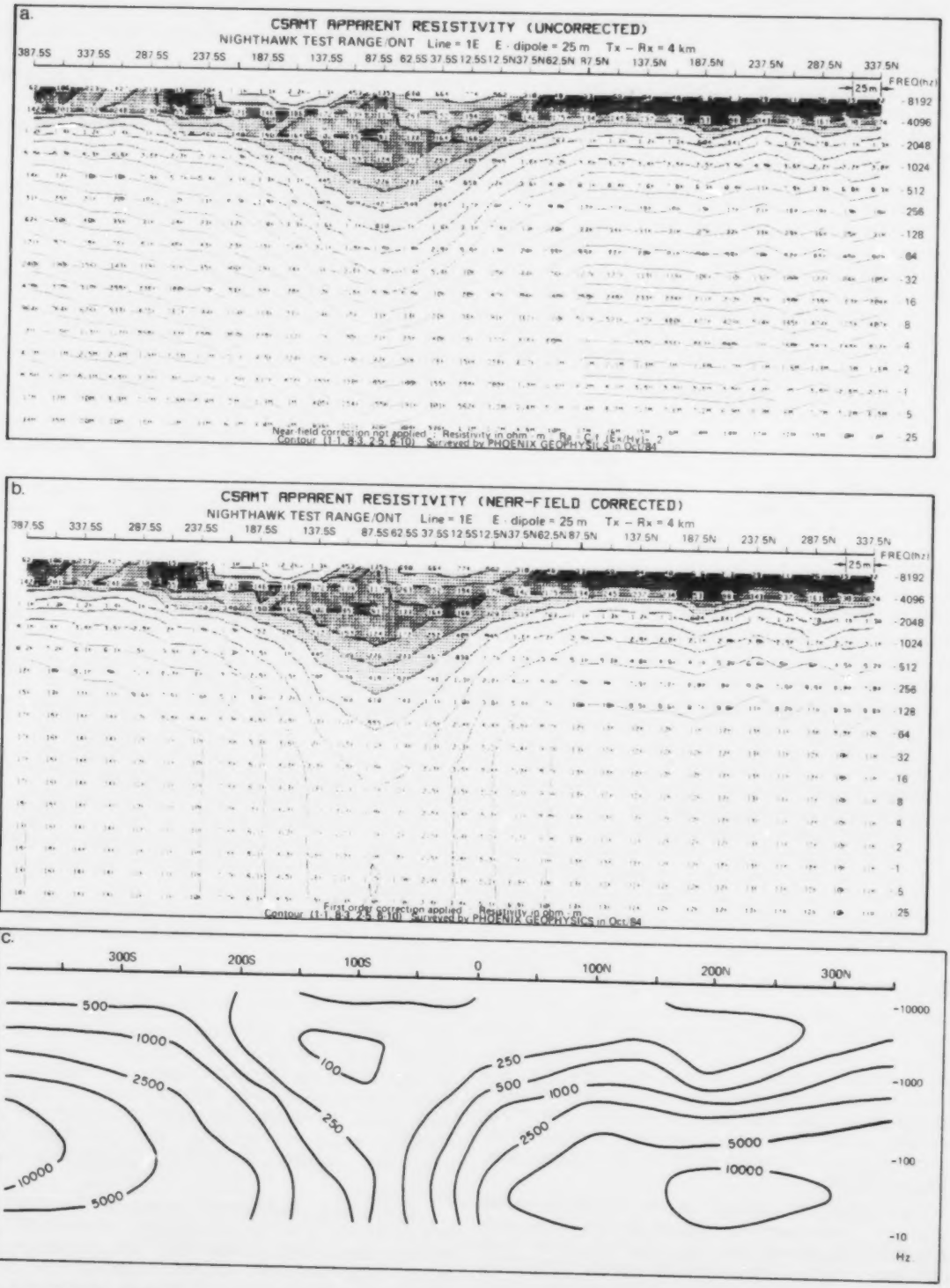

Figure 093.7 *CSAMT apparent resistivity pseudo-sections, "near-field" uncorrected (a) and "near-field" corrected (b) on Line 1E, and AMT apparent resistivity pseudo-section (c), Nighthawk Lake Test Range, Ontario. Note: Figure (c) is from Strangway, Ilkisik, and Redman (1983).*

man 1983) on the same line. The agreement between the "near-field" corrected CSAMT data, Figure 093.7b. and AMT data is excellent, although the AMT data seems to be more averaged because of the E-dipole length of 50 m and 100 m employed for the AMT survey instead of 25 m used for the CSAMT survey.

HATCHOBARU GEOTHERMAL AREA, OHITA, JAPAN

The CSAMT survey was carried out by Phoenix and personnel from West Japan Engineering Consultants for Kyushu Electric Power Co., in January 1985. The purpose of this survey was to evaluate CSAMT suitability in geothermal exploration. The survey area is located in the Hatchobaru geothermal area in Aso National Park in Ohita prefecture. The adjacent area is called the Roof of Kyushu and the terrain is very rough. There are two geothermal electric power stations, 12MW and 55MW, operating in the area.

Six lines were surveyed using a 100 m E-dipole because the size of the target structure is known to be considerably larger than 100 m. Figure 093.8a shows the CSAMT apparent resistivity pseudo-section plot on one of the lines, Line E. It should be noted that the vertical scale of the pseudo-section may be a function of depth at an individual station, since the lower frequency penetrates deeper; however, it is not linearly related.

All the data was then inverted to provide a layered resistivity versus depth pseudo-section. Figure 093.8b shows the results of the inversion.

In the same area, other geophysical methods were previously applied, permitting the joint inversion of Phoenix MT data and Schlumberger data along with the CSAMT inversion. The agreement between the CSAMT and MT/Schlumberger inversions in general is excellent. However, note that when MT and Schlumberger soundings are situated atop a resistivity discontinuity as indicated by the CSAMT apparent pseudo-section, the agreement between the CSAMT and MT/Schlumberger inversions is not as good as when these soundings are made atop smooth CSAMT resistivity structures.

ABUTA MINE, HOKKAIDO, JAPAN

CSAMT and Spectral I.P. surveys were conducted using a Phoenix V4 SIP/CSAMT system in the Abuta Mine area, Hokkaido, Japan, in March 1985. The mine stopped operation some time ago. For the CSAMT operation, the transmitter dipole was situated approximately 2 km from the survey line. The motor generator used was an MG-2 with <2 KW output power. The location of a massive pyrite zone is indicated in Figure 093.9a.

The CSAMT results are shown in the apparent resistivity pseudo-section (Figure 093.9b). The sulphide body is outlined well by a low resistivity zone of around 1 ohm-m approximately below 250E. The low resistivity zone is situated between two local high resistivity bodies at 375E and 75E. Data at frequencies from 256 Hz to 1024 Hz, and at stations from 625E to 875E, appears to be severely contaminated by a 50 Hz power line which was situated a few m away from the CSAMT magnetic sensor coil. As the general resistivity of the site is quite low, 10 ohm-m or lower, the "near-field" effects were not strong and some "transition-zone" effects were observed at 0.25 Hz to 1 Hz even with a Tx-Rx distance of only approximately 2 km.

The spectral I.P. survey was performed using 15 binary-stepped frequencies from 0.0625 Hz to 1024 Hz, N equal to 1 to 6, and X equal to 50 m. Figure 093.9c shows a pseudo-section of apparent resistivity at 1 Hz obtained by the dipole-dipole spectral I.P. survey. At the first inspection of the contoured resistivity plot, the authors wondered why the centre of the low resistivity zone is located below 350E, not 250E where the sulphide body is, although the authors know that an anomaly pattern is not simple with a dipole-dipole configuration. Exactly the same results were obtained with a conventional I.P. The general patterns and values of the apparent resistivity compare well with that of CSAMT.

A model simulation was performed using a finite-element forward program on a desktop computer. The simple model, shown in Figure 093.10c was based on the CSAMT apparent resistivity pseudo-section. Figure 093.10d shows the apparent resistivity from the model. The model results indicate an approximately 100 m lateral shift of the low resistivity pattern, in good agreement with the survey results (Figure 093.10b). Responses from the high resistivity bodies also demonstrate good agreement between the model and the survey results.

It took less than three hours to finish the CSAMT survey which comprised the 18 stations or soundings. From the survey results, the following may be concluded:

1. The CSAMT-derived resistivity structure is much more economical to obtain and easier to understand than that of the dipole-dipole resistivity mapping method.
2. Careful attention is necessary when interpreting dipole-dipole resistivity data. A simple orebody model may not be enough.
3. A convenient and portable 2-D modelling program, which can be run on a desktop computer, is highly desirable.

CONCLUSIONS AND FUTURE PLANS

The completion of the development of the CSAMT system was achieved with joint ETDF support and additional efforts funded solely by Phoenix. The Phoenix CSAMT system, based on the Phoenix V4 multi-channel universal receiver, proved to be economical, easy to operate, and to have wide application - in short, an effective geophysical instrument.

During the development stage of the hardware and software, the four test surveys were performed: in various locations domestically and abroad; in geological situations with simple to complicated structures; and in applications of mineral, geothermal, and geological mapping.

The new "near-field" correction was developed and compared with AMT data. In some cases, the

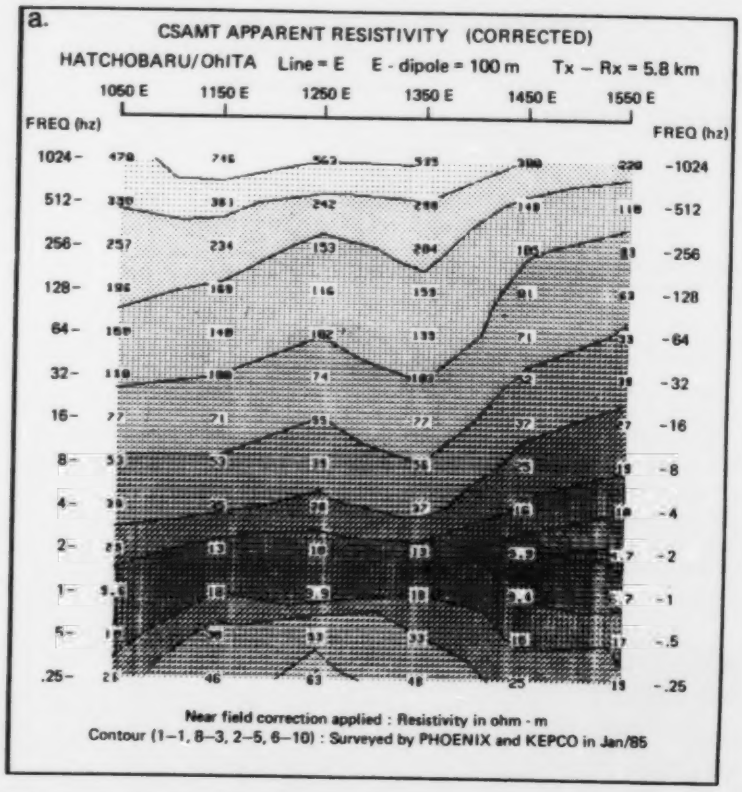

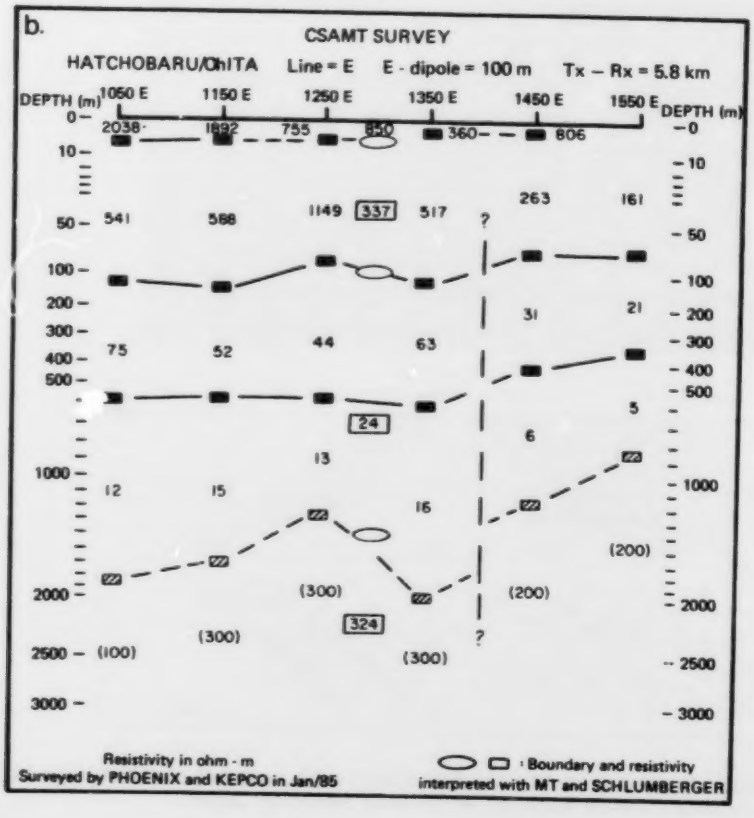

Figure 093.8 *CSAMT apparent resistivity pseudo-section (a) and the inverted resistivity structure (b) on Line-E, Hatchobaru, Japan. Figure (b) indicates also the interpretation of MT/Schlumberger data.*

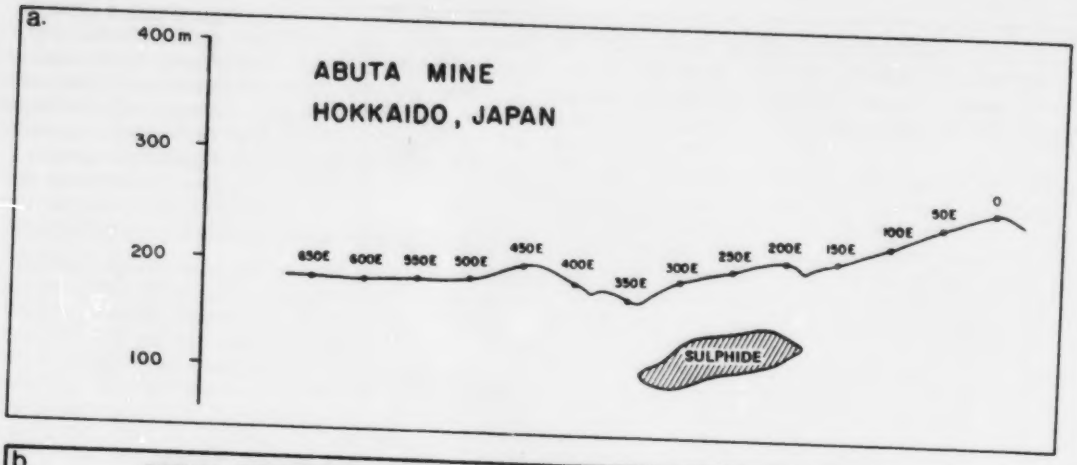

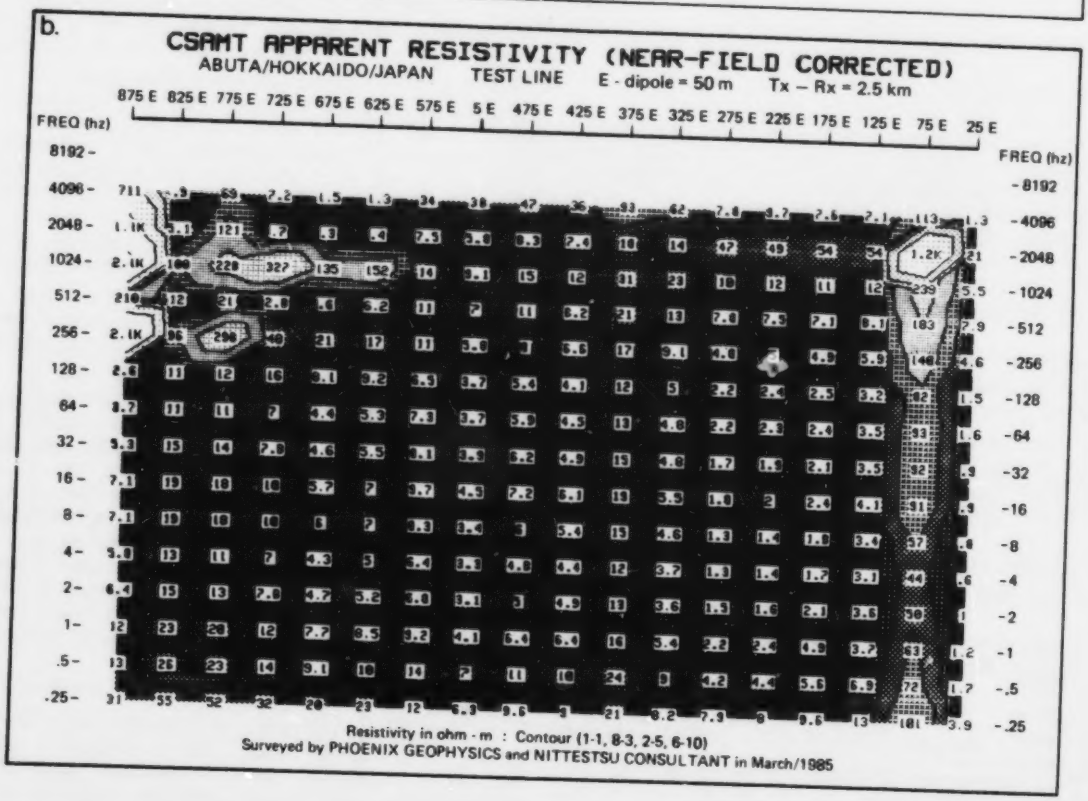
b.
CSAMT APPARENT RESISTIVITY (NEAR-FIELD CORRECTED)
ABUTA/HOKKAIDO/JAPAN TEST LINE E - dipole = 50 m Tx – Rx = 2.5 km
875 E 825 E 775 E 725 E 675 E 625 E 575 E 5 E 475 E 425 E 375 E 325 E 275 E 225 E 175 E 125 E 75 E 25 E
FREQ (hz)
8192
4096
2048
1024
512
256
128
64
32
16
8
4
2
1
.5
.25
Resistivity in ohm - m : Contour (1-1, 8-3, 2-5, 6-10)
Surveyed by PHOENIX GEOPHYSICS and NITTESTSU CONSULTANT in March/1985

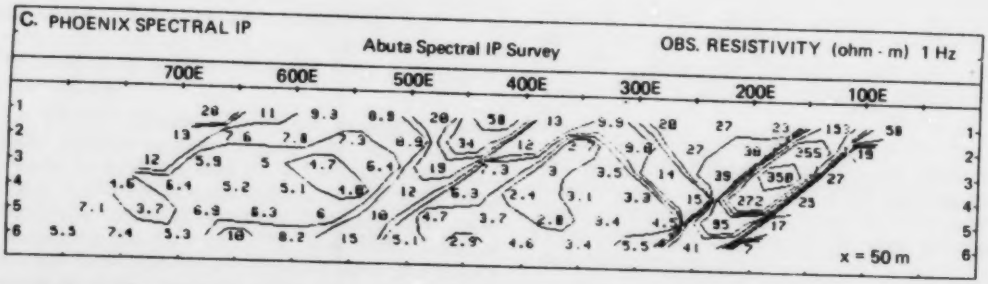

Figure 093.9 *CSAMT apparent resistivity pseudo-section (b) and Spectral I.P. apparent resistivity pseudo-section (c) with cross-section showing sulphide body (a), Abuta Mine, Hokkaido, Japan.*

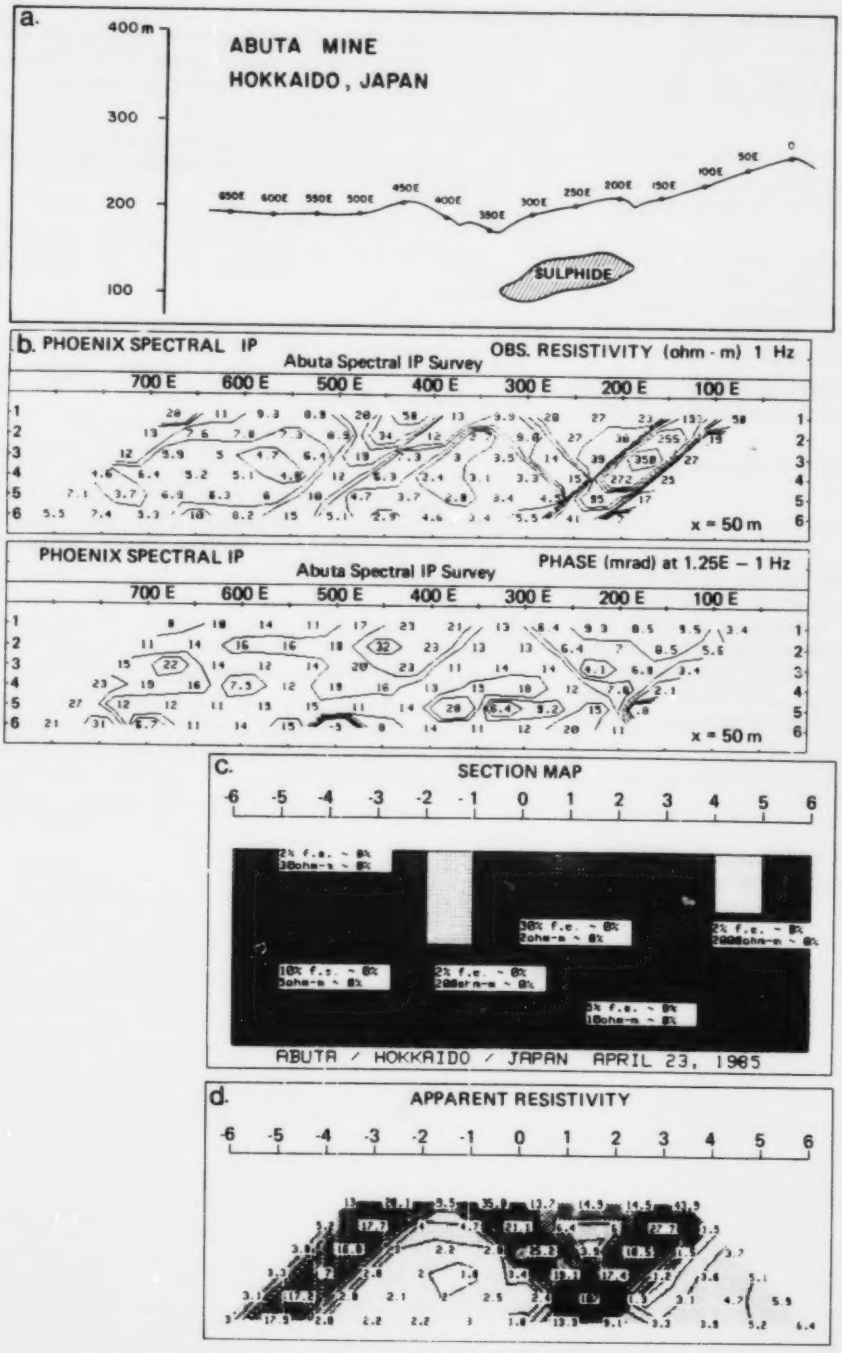

Figure 093.10 *Simulated model (c), the calculated apparent resistivity pseudo-section (d) and spectral I.P. apparent resistivity pseudo-section and Phase pseudo-section (b) with cross-section (a) showing the sulphide body, Abutu Mine, Hokkaido, Japan.*

CSAMT results were compared with MT and Schlumberger results as well as Spectral I.P. results.

One CSAMT/Spectral I.P. system was sold early in the fiscal year and another just after the end of the year.

Technical sales trips were made to Japan, Taiwan, China, Thailand, Indonesia, Australia, Turkey, and other countries, resulting in a number of serious enquiries.

In the following fiscal year, numerous test surveys are planned of which some are supported by ETDF. The purpose of the planned test surveys will be to widen the applications, to obtain more case histories, and to test the "near-field" correction.

Even more efforts on marketing will be put along customary lines which involve international agents and advertising.

More software development is planned especially on 2-D modelling.

ACKNOWLEDGMENTS

This development project was funded by an Exploration Technology Development Fund Grant from the Ontario Ministry of Natural Resources in 1984 and 1985. The author thanks the personnel of the Ontario Geological Survey for various advice and assistance, and Kyushu Electric Power Co., and Nittetsu Mining Co., for giving their permission to use the survey data.

REFERENCES

Cagniard, L.
1953: Basic Theory of the Magnetotelluric Method of Geophysical Prospecting; Geophysics, Volume 18, p.605-635.

Goldstein, M.A.
1971: Magnetotelluric Experiments Employing An Artificial Dipole Source; Unpublished Ph.D. Thesis, Department of Physics, University of Toronto.

Goldstein, M.A., and Strangway, D.W.
1975: Audio Frequency Magnetotelluric with a Grounded Dipole Source; Geophysics, Volume 40, p.669-683.

Sobczak, LW., and Jacoby, W.R.
1967: Cavendish Geophysical Test Range, Ontario: Gravity Survey; Geological Survey of Canada, Paper 75-1C.

Spies, B.R., and Parker, P.D.
1984: Limitations of Large-loop Transient Electromagnetic Surveys in Conductive Terrains; Geophysics, Volume 49, Number 7, p.902-912.

Strangway, D.W., Ilkisik, O.M., and Redman, J.D.
1983: Surface Electromagnetic Mapping in Selected Portions of Northern Ontario; Grant 118, p.159-173 *in* Geoscience Research Grant Program, Summary of Research, 1982-1983, edited by E.G. Pye, Ontario Geological Survey, Miscellaneous Paper 113, 199p.

Strangway, D.W., and Koziar, A.
1979: Audio-Frequency Magnetotelluric Sounding: A Case History at Cavendish Geophysical Test Range; Geophysics, Volume 44, p.1429-1446.

Williams, D.A., Scott, W.J., and Dyick, A.V.
1975: Cavendish Township Geophysical Test Range: 1973 Diamond Drilling; Geological Survey of Canada, Paper 74-62.